NIST GCR 12-917-21

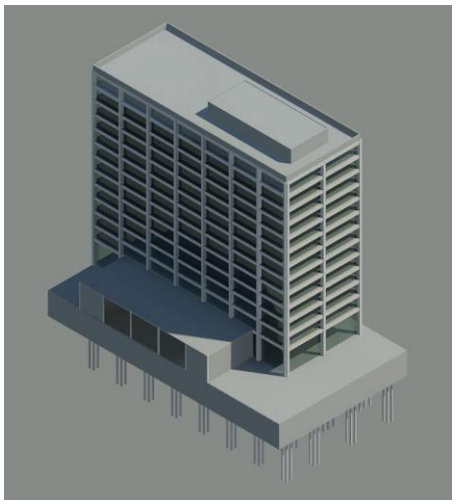

Soil-Structure Interaction for Building Structures

NEHRP Consultants Joint Venture
A partnership of the Applied Technology Council and the Consortium of Universities for Research in Earthquake Engineering

nehrp

NIST
National Institute of Standards and Technology
U.S. Department of Commerce

Disclaimers

This report was prepared for the Engineering Laboratory of the National Institute of Standards and Technology (NIST) under the National Earthquake Hazards Reduction Program (NEHRP) Earthquake Structural and Engineering Research Contract SB134107CQ0019, Task Order 69221. The contents of this publication do not necessarily reflect the views and policies of NIST or the U.S. Government.

This report was produced by the NEHRP Consultants Joint Venture, a joint venture of the Applied Technology Council (ATC) and the Consortium of Universities for Research in Earthquake Engineering (CUREE). While endeavoring to provide practical and accurate information, the NEHRP Consultants Joint Venture, the authors, and the reviewers assume no liability for, nor express or imply any warranty with regard to, the information contained herein. Users of information contained in this report assume all liability arising from such use.

Unless otherwise noted, photos, figures, and data presented in this report have been developed or provided by NEHRP Consultants Joint Venture staff or consultants engaged under contract to provide information as works for hire. Any similarity with other published information is coincidental. Photos and figures cited from outside sources have been reproduced in this report with permission. Any other use requires additional permission from the copyright holders.

Certain commercial software, equipment, instruments, or materials may have been used in the preparation of information contributing to this report. Identification in this report is not intended to imply recommendation or endorsement by NIST, nor is it intended to imply that such software, equipment, instruments, or materials are necessarily the best available for the purpose.

NIST policy is to use the International System of Units (metric units) in all its publications. In this report, information is presented in both metric units and U.S. Customary Units (inch-pound), as the inch-pound system is the preferred system of units in the U.S. earthquake engineering industry.

Cover illustration – Rendering of the Sherman Oaks building structural and foundation system, used in an example application of soil-structure interaction principles (courtesy of C. Haselton).

NIST GCR 12-917-21

Soil-Structure Interaction for Building Structures

Prepared for
U.S. Department of Commerce
National Institute of Standards and Technology
Engineering Laboratory
Gaithersburg, MD 20899

By
NEHRP Consultants Joint Venture
A partnership of the Applied Technology Council and the Consortium of Universities for Research in Earthquake Engineering

September 2012

U.S. Department of Commerce
Rebecca M. Blank, Acting Secretary

National Institute of Standards and Technology
Patrick D. Gallagher, Under Secretary of Commerce for Standards and Technology and Director

Participants

National Institute of Standards and Technology

John (Jack) R. Hayes, Jr., Director, National Earthquake Hazards Reduction Program
Steven L. McCabe, Deputy Director, National Earthquake Hazards Reduction Program
John (Jay) L. Harris III, Project Manager

NEHRP Consultants Joint Venture

Applied Technology Council
201 Redwood Shores Parkway, Suite 240
Redwood City, California 94065
www.ATCouncil.org

Consortium of Universities for
Research in Earthquake Engineering
1301 S. 46th Street, Building 420
Richmond, California 94804
www.CUREE.org

Joint Venture Management Committee

James R. Harris
Robert Reitherman
Christopher Rojahn
Andrew Whittaker

Joint Venture Program Committee

Jon A. Heintz (Program Manager)
Michael Constantinou
C.B. Crouse
James R. Harris
William T. Holmes
Jack Moehle
Andrew Whittaker

Project Technical Committee

Jonathan P. Stewart (Project Director)
C.B. Crouse
Tara Hutchinson
Bret Lizundia
Farzad Naeim
Farhang Ostadan

Project Review Panel

Craig Comartin
Yousef Hashash
Annie Kammerer
Gyimah Kasali
George Mylonakis
Graham Powell

Working Group Members

Fortunato Enriquez
Michael Givens
Curt Haselton
Silvia Mazzoni
Erik Okstad
Andreas Schellenberg

Project Manager

David Hutchinson

Preface

The NEHRP Consultants Joint Venture is a partnership between the Applied Technology Council (ATC) and the Consortium of Universities for Research in Earthquake Engineering (CUREE). In 2007, the National Institute of Standards and Technology (NIST) awarded the NEHRP Consultants Joint Venture a National Earthquake Hazards Reduction Program (NEHRP) "Earthquake Structural and Engineering Research" task order contract (SB1341-07-CQ-0019) to conduct a variety of tasks. In 2009, NIST initiated Task Order 69221 entitled "Improved Procedures for Characterizing and Modeling Soil-Structure Interaction for Performance-Based Seismic Engineering." The purpose of this project was to develop consensus guidance for implementing soil-structure interaction in response history analyses, and to identify areas of further research that were needed. The starting point for this work was decades of available soil-structure interaction research, and recently published engineering guidance for static analysis procedures.

Soil-structure interaction (SSI) analysis evaluates the collective response of three linked systems: the structure, the foundation, and the soil underlying and surrounding the foundation. Problems associated with practical application of SSI for building structures are rooted in a poor understanding of fundamental SSI principles. Implementation in practice is hindered by a literature that is difficult to understand, and codes and standards that contain limited guidance. This report represents an advancement in the state of SSI knowledge for practicing engineers. It provides a synthesis of the body of SSI literature, distilled into a concise narrative, and harmonized under a consistent set of variables and units. Techniques are described by which SSI phenomena can be simulated in engineering practice, and specific recommendations for modeling seismic soil-structure interaction effects on building structures are provided. The resulting recommendations are illustrated and tested, in detail, on realistic example buildings.

This work is the result of an extensive literature search and collection of available information on soil-structure interaction, discussions with researchers and practitioners on the state of SSI knowledge and practice, conduct of problem-focused investigations, and analytical parametric studies. A workshop of invited experts and other stakeholders was convened to receive feedback on the developing report and preliminary recommendations. Input from this group was instrumental in shaping the final product.

The NEHRP Consultants Joint Venture is indebted to the leadership of Jonathan Stewart, Project Director, and to the members of the Project Technical Committee, consisting of C.B. Crouse, Tara Hutchinson, Bret Lizundia, Farzad Naeim, and Farhang Ostadan, for their significant contributions in the development of this report and the resulting recommendations. Focused analytical studies were conducted by Curt Haselton, Fortunato Enriquez, Michael Givens, Silvia Mazzoni, Erik Okstad and Andreas Schellenberg. Technical review and comment at key developmental stages on the project were provided by the Project Review Panel consisting of Craig Comartin, Yousef Hashash, Annie Kammerer, Gyimah Kasali, George Mylonakis, and Graham Powell. The names and affiliations of all who contributed to this project are included in the list of Project Participants at the end of this report.

NEHRP Consultants Joint Venture also gratefully acknowledges Jack Hayes (Director, NEHRP), Steve McCabe (Deputy Director, NEHRP), and Jay Harris (NIST Project Manager) for their input and guidance in the preparation of this report, Dave Hutchinson for ATC project management, and Peter N. Mork and Bernadette Hadnagy for ATC report production services.

Jon A. Heintz
Program Manager

Table of Contents

List of Figures

List of Tables

Chapter 1
Introduction

The response of a structure to earthquake shaking is affected by interactions between three linked systems: the structure, the foundation, and the soil underlying and surrounding the foundation (FEMA, 2009). Soil-structure interaction analysis evaluates the collective response of these systems to a specified ground motion. The terms *Soil-Structure Interaction* (SSI) and *Soil-Foundation-Structure Interaction* (SFSI) are both used to describe this effect in the literature. In this report, the foundation is considered part of the structure, and the term SSI has been adopted.

This report presents a synthesis of the body of knowledge contained in SSI literature, which has been distilled into a concise narrative and harmonized under a consistent set of variables and units. Specific techniques are described by which SSI phenomena can be simulated in engineering practice, and recommendations for modeling seismic soil-structure interaction effects on building structures are provided.

1.1 Background and Objectives

Problems associated with the practical application of SSI for building structures are rooted in a poor understanding of fundamental SSI principles. Soil-structure interaction topics are generally not taught in graduate earthquake engineering courses, so most engineers attempting SSI in practice must learn the subject on their own. Unfortunately, practice is hindered by a literature that is often difficult to understand, and codes and standards that contain limited guidance. Most articles rely heavily on the use of wave equations in several dimensions and complex arithmetic to formulate solutions and express results. Moreover, nomenclature is often inconsistent, and practical examples of SSI applications are sparse. This gives rise to the present situation in which soil-structure interaction is seldom applied, and when it is, modeling protocols vary widely and are not always well conceived.

Although the *NEHRP Recommended Provisions for Seismic Regulations for New Buildings and Other Structures* has provided guidance for consideration of SSI effects in forced-based procedures for several decades, these procedures have not found significant use in practice. Practical application of SSI gained momentum following publication of FEMA 440, *Improvement of Inelastic Seismic Analysis Procedures* (FEMA, 2005), which provided the design community with procedures for incorporating the effects of soil-structure interaction in nonlinear static pushover-type analyses. These procedures were eventually adopted into ASCE/SEI 41-06,

Seismic Rehabilitation of Existing Buildings (ASCE, 2007). Because they were developed for nonlinear static analysis, however, they were not directly applicable to response history analysis, which requires more careful consideration of specific components of soil-foundation interaction and the manner by which input ground motions should be applied to structural models.

In 2009, the National Institute of Standards and Technology (NIST) initiated the Task Order 69221 Project entitled "Improved Procedures for Characterizing and Modeling Soil-Structure Interaction for Performance-Based Seismic Engineering." The purpose of this project was to develop consensus guidance for implementing soil-structure interaction in response history analyses, such that input ground motions accurately reflect the input at the base of structures, and that structural models include elements that account for the geotechnical and foundation conditions associated with the building under consideration. Work also included an extensive review of available research on soil-structure interaction, evaluation of existing SSI guidelines for static-type analyses, and development of recommendations for improvement where necessary.

This report is intended to provide background for addressing three fundamental questions that arise when contemplating the use of SSI in the seismic analysis of building structures:

1. *When is the use of foundation springs and dashpots important, and which structural response parameters are affected?*
2. *Under what conditions is consideration of the differences between foundation input motions and free-field ground motions important?*
3. *What field and laboratory investigations are necessary to develop foundation springs and dashpots for SSI analysis?*

Once the decision to implement SSI has been made, a basic level of understanding of the physical phenomenon and a practical analysis methodology for simulating its effects are needed. This report describes the principal components of SSI in a clear and concise way, and consistent nomenclature is used throughout. Explicit computational tools that can be used in engineering practice are provided, and applications of SSI to force-based analysis procedures, pushover (displacement-based) procedures, and response history analysis procedures are described.

As part of the work, soil-structure interaction procedures were applied to detailed example applications that investigate the influence of various SSI components on response history analysis results. The resulting recommendations are drawn from these studies, along with the results of other studies in recent literature.

Implementation of SSI within a design setting requires close collaboration between structural and geotechnical engineers. Neither discipline alone is likely to have sufficient knowledge of structural, foundation, and site considerations necessary to properly complete a meaningful analysis considering SSI effects. As such, the intended audience for this work is expected to be structural and geotechnical engineers experienced in earthquake engineering with a working knowledge of structural and soil dynamics principles. The mathematical complexities are kept to a minimum to make the content as accessible as possible to non-experts in structural dynamics and the mathematics of wave propagation. Detailed guidance on communication between structural and geotechnical engineers is also provided.

1.2 Overview of Soil-Structure Interaction

A seismic soil-structure interaction analysis evaluates the collective response of the structure, the foundation, and the geologic media underlying and surrounding the foundation, to a specified free-field ground motion. The term *free-field* refers to motions that are not affected by structural vibrations or the scattering of waves at, and around, the foundation. SSI effects are absent for the theoretical condition of a rigid foundation supported on rigid soil. Accordingly, SSI accounts for the difference between the actual response of the structure and the response of the theoretical, rigid base condition.

In Part 2 of FEMA P-750, *NEHRP Recommended Seismic Provisions for New Buildings and Other Structures* (FEMA, 2009), SSI effects are categorized as inertial interaction effects, kinematic interaction effects, and soil-foundation flexibility effects. The terms kinematic and inertial interaction were introduced in 1975 by Robert Whitman (Kausel, 2010). In the context of engineering analysis and design, these effects are related to:

- **Foundation stiffness and damping.** Inertia developed in a vibrating structure gives rise to base shear, moment, and torsion. These forces generate displacements and rotations at the soil-foundation interface. These displacements and rotations are only possible because of flexibility in the soil-foundation system, which significantly contributes to overall structural flexibility (and increases the building period). Moreover, these displacements give rise to energy dissipation via radiation damping and hysteretic soil damping, which can significantly affect overall system damping. Since these effects are rooted in structural inertia, they are referred to as *inertial interaction* effects.
- **Variations between foundation input motions and free-field ground motions.** Foundation input motions and free-field motions can differ because of: (i) *kinematic interaction*, in which stiff foundation elements placed at or below the ground surface cause foundation motions to deviate from free-field motions due to base slab averaging, wave scattering, and embedment effects in the absence of

structure and foundation inertia; and (ii) relative displacements and rotations between the foundation and the free-field associated with structure and foundation inertia.

- **Foundation Deformations.** Flexural, axial, and shear deformations of structural foundation elements occur as a result of forces and displacements applied by the superstructure and the soil medium. These represent the seismic demands for which foundation components should be designed, and they could be significant, especially for flexible foundations such as rafts and piles.

Methods that can be used to evaluate the above effects can be categorized as direct and substructure approaches. In a *direct analysis*, the soil and structure are included within the same model and analyzed as a complete system. In a *substructure approach*, the SSI problem is partitioned into distinct parts that are combined to formulate the complete solution.

Direct Analysis. As schematically depicted in Figure 1-1, the soil is often represented as a continuum (e.g., finite elements) along with foundation and structural elements, transmitting boundaries at the limits of the soil mesh, and interface elements at the edges of the foundation.

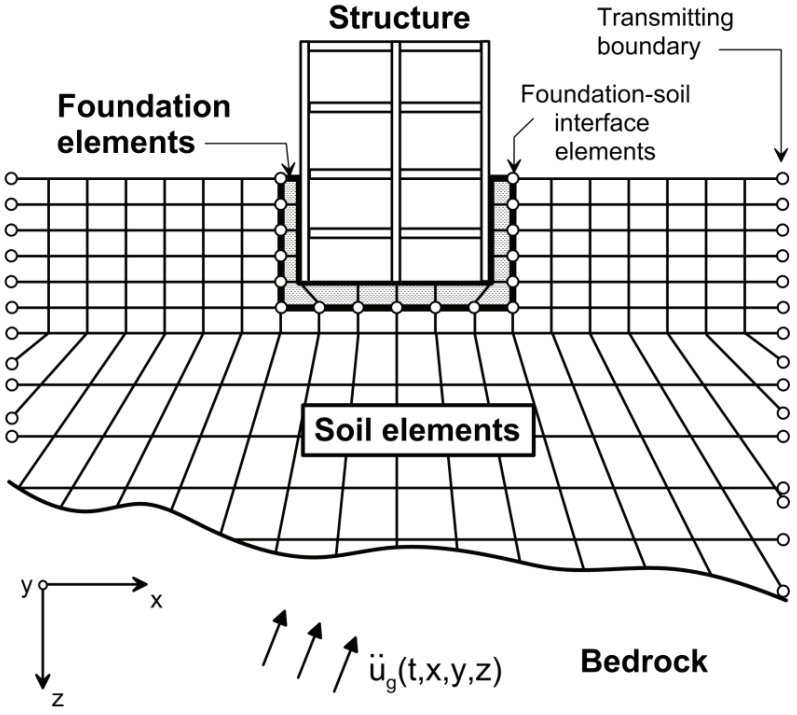

Figure 1-1 Schematic illustration of a direct analysis of soil-structure interaction using continuum modeling by finite elements.

Evaluation of site response using wave propagation analysis through the soil is important to this approach. Such analyses are most often performed using an equivalent linear representation of soil properties in finite element, finite difference,

or boundary element numerical formulations (Wolf, 1985; Lysmer et al., 1999). Direct analyses can address all of the SSI effects described above, but incorporation of kinematic interaction is challenging because it requires specification of spatially variable input motions in three dimensions.

Because direct solution of the SSI problem is difficult from a computational standpoint, especially when the system is geometrically complex or contains significant nonlinearities in the soil or structural materials, it is rarely used in practice.

Substructure Approach. Proper consideration of SSI effects in a substructure approach requires: (i) an evaluation of free-field soil motions and corresponding soil material properties; (ii) an evaluation of transfer functions to convert free-field motions to foundation input motions; (iii) incorporation of springs and dashpots (or more complex nonlinear elements) to represent the stiffness and damping at the soil-foundation interface; and (iv) a response analysis of the combined structure-spring/dashpot system with the foundation input motion applied.

The superposition inherent in a substructure approach requires an assumption of linear soil and structure behavior, although in practice this requirement is often followed only in an equivalent-linear sense. As depicted in Figure 1-2, the steps in a substructure approach are as follows:

- Specification of a *foundation input motion* (FIM), which is the motion of the base-slab that accounts for the stiffness and geometry of the foundation. Because inertia is dealt with separately, the FIM applies for the theoretical condition of the base-slab and structure having no mass (Figure 1-2b). This motion generally differs from the free-field motion, involves both translational and rotational components, and represents the seismic demand applied to the foundation and structural system. The variation between free-field and foundation input motions is expressed by a transfer function that represents the ratio of foundation/free-field motion in the frequency domain. Since inertial effects are neglected, the transfer function represents the effects of kinematic interaction only.

  An essential first step in defining the FIM is to evaluate the free-field response of the site, which is the spatial and temporal variation of ground motion in the absence of the structure and foundation. This task requires that the earthquake input motion in the free field is known, either at a specific point (e.g., ground surface, rock-outcrop) or in the form of incident waves (e.g., oblique shear waves) propagating up from a reference depth.

  Having established the free-field motion, wave-propagation analyses are performed to estimate the foundation input motion along the planned soil-foundation interface, as depicted in Figure 1-2d. Equivalent linear properties for

the soil (e.g., shear modulus, material damping) can be evaluated as part of this analysis.

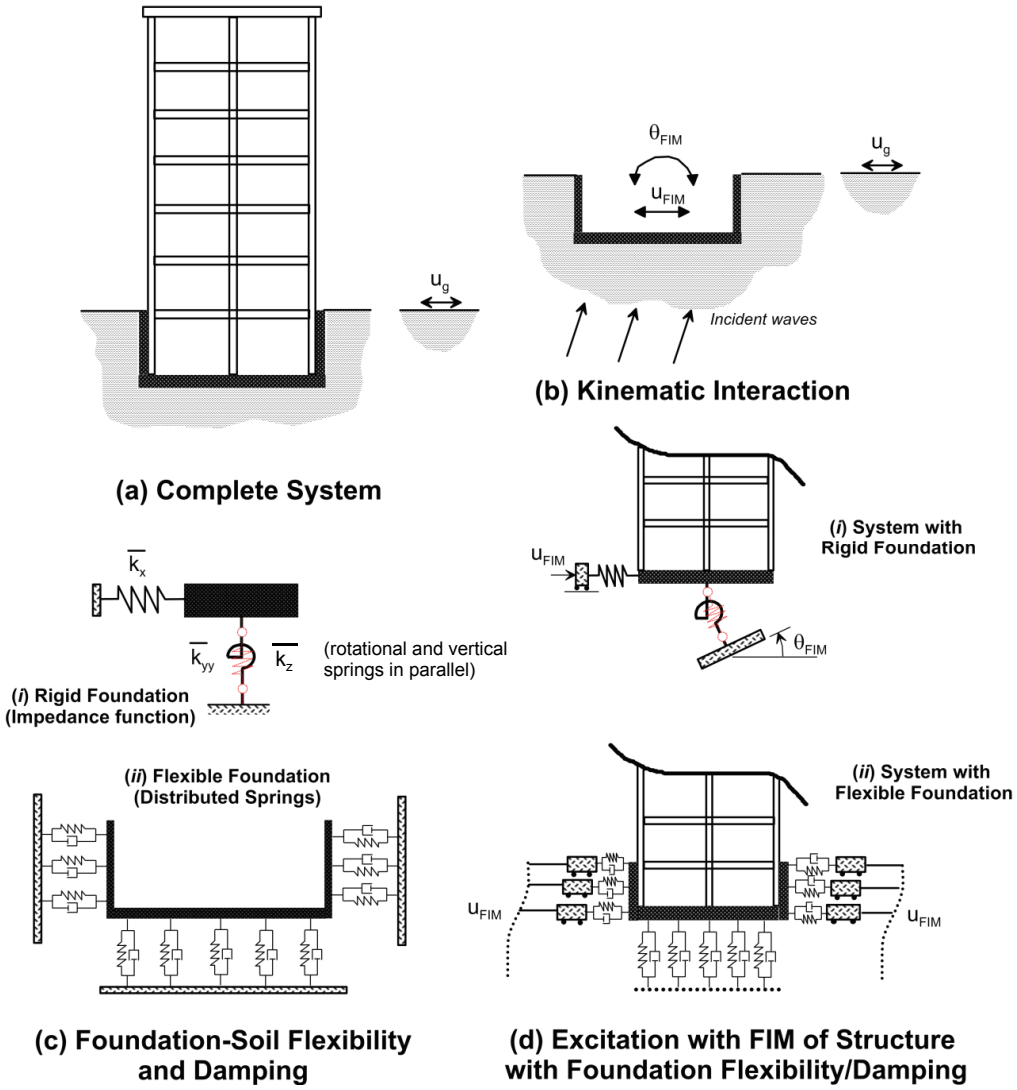

Figure 1-2 Schematic illustration of a substructure approach to analysis of soil-structure interaction using either: (i) rigid foundation; or (ii) flexible foundation assumptions.

- The stiffness and damping characteristics of the soil-foundation interaction are characterized using relatively simple impedance function models or a series of distributed springs and dashpots. *Impedance functions* represent the frequency-dependent stiffness and damping characteristics of soil-foundation interaction. Use of impedance function models for rigid foundations is illustrated in Figure 1-2c(i). Use of a series of distributed springs and dashpots acting around the foundation is illustrated in Figure 1-2c(ii). The latter case of distributed springs and dashpots is needed when foundation elements are non-rigid, or when internal

demands (e.g., moments, shears, deformations) are required outcomes of the analysis.

- The superstructure is modeled above the foundation and the system is excited through the foundation by displacing the ends of the springs and dashpots using the rocking and translational components of the FIM. It should be noted that FIM varies with depth. In the case of the distributed spring and dashpot model, differential ground displacements should be applied over the depth of embedment. This application of spatially variable displacements introduces a rotational component to the FIM, which is why a rotational component does not specifically appear in Figure 1-2d(ii).

1.3 Report Organization and Content

This report summarizes the body of knowledge on soil-structure interaction, and provides specific recommendations for modeling seismic soil-structure interaction effects on building structures in engineering practice.

Chapter 2 describes inertial SSI effects, beginning with the behavior of simple structure-soil systems to provide insight into the conditions for which inertial SSI effects are most critical. Also presented are detailed procedures for computing foundation stiffness and damping, both for idealized conditions in classical solutions and for more realistic conditions that may include flexible foundation systems, non-uniform soil, and material nonlinearity. Both shallow foundation systems (e.g., footings, mats) and deep foundation systems (e.g., piles) are discussed.

Chapter 3 describes the manner by which transfer functions can be computed for various foundation configurations considering kinematic interaction effects, and how transfer function amplitudes can be used to modify response spectral ordinates.

Chapter 4 describes how SSI procedures described in Chapter 2 and Chapter 3 are implemented in seismic design provisions contained in currently available consensus standards and design guidelines.

Chapter 5 describes the relatively limited number of SSI experiments and case history studies available in the literature, and summarizes some of the lessons learned from that work. Efforts to calibrate or verify analysis procedures against laboratory data or field performance data are noted, where applicable.

Chapter 6 presents a summary of the state-of-practice in SSI analysis, along with recommendations for improving communications between geotechnical and structural engineers.

Chapter 7 provides detailed example applications of the substructure analysis approach and procedures described in this report. Studies are performed on two

buildings with available earthquake recordings and varying degrees of SSI modeling sophistication. Recommendations for implementing SSI in response history analyses are provided, taking into consideration the capabilities of currently available structural engineering software.

Chapter 8 answers three fundamental questions that arise when contemplating the use of SSI in the seismic analysis of a building structure, summarizes SSI analysis procedures that would be followed on typical project in a step-by-step manner, and provides short-term and long-term research needs.

Appendices A, B, and C provide additional, more detailed information on the development of, and results from, analytical models used in the example applications of Chapter 7.

A list of Symbols defining key notation, and a list of References cited from the body of SSI literature are provided at the end of this report.

Chapter 2
Inertial Interaction

Inertial interaction refers to displacements and rotations at the foundation level of a structure that result from inertia-driven forces such as base shear and moment. This chapter describes inertial soil-structure interaction effects. Inertial displacements and rotations can be a significant source of flexibility and energy dissipation in the soil-structure system.

Section 2.1 discusses system behavior and highlights some of the principal effects of inertial interaction and the conditions for which its effects are significant. The methods focus on single degree-of-freedom systems, but they can be extrapolated to multi-degree-of-freedom systems with a dominant first mode. Section 2.2 provides a relatively detailed description of how foundation springs and dashpots can be specified to represent the flexibility and damping associated with soil-foundation interaction in translational and rotational vibration modes for shallow foundations (e.g., footings and mats). Section 2.3 provides corresponding solutions for the stiffness and damping characteristics of deep foundations (e.g., piles and drilled shafts). Some of the procedures given in Section 2.2 are coded into available computer programs such as DYNA6 (Western Engineering, 2011). This program can also be used for pile foundations, although the results are relatively approximate. Section 2.4 presents several models that can be used to evaluate shallow foundation response for conditions involving nonlinear material behavior or geometric nonlinearities (i.e. gapping).

2.1 Soil-Structure System Behavior

A *rigid base* refers to soil supports with infinite stiffness (i.e., without soil springs). A *rigid foundation* refers to foundation elements with infinite stiffness (i.e., not deformable). A *fixed base* refers to a combination of a rigid foundation elements on a rigid base. A *flexible base* analysis considers the compliance (i.e., deformability) of both the foundation elements and the soil.

Consider a single degree-of-freedom structure with stiffness, k, and mass, m, resting on a fixed base, as depicted in Figure 2-1a. A static force, F, causes deflection, Δ:

$$\Delta = \frac{F}{k} \tag{2-1}$$

From structural dynamics, the undamped natural vibration frequency, ω, and period, T, of the structure are given by Clough and Penzien (1993) as:

$$\omega = \sqrt{\frac{k}{m}}, \quad T = \frac{2\pi}{\omega} = 2\pi\sqrt{\frac{m}{k}} \tag{2-2}$$

By substituting Equation 2-1 into Equation 2-2, an expression for the square of period is obtained as:

$$T^2 = (2\pi)^2 \frac{m}{(F/\Delta)} = (2\pi)^2 \frac{m\Delta}{F} \tag{2-3}$$

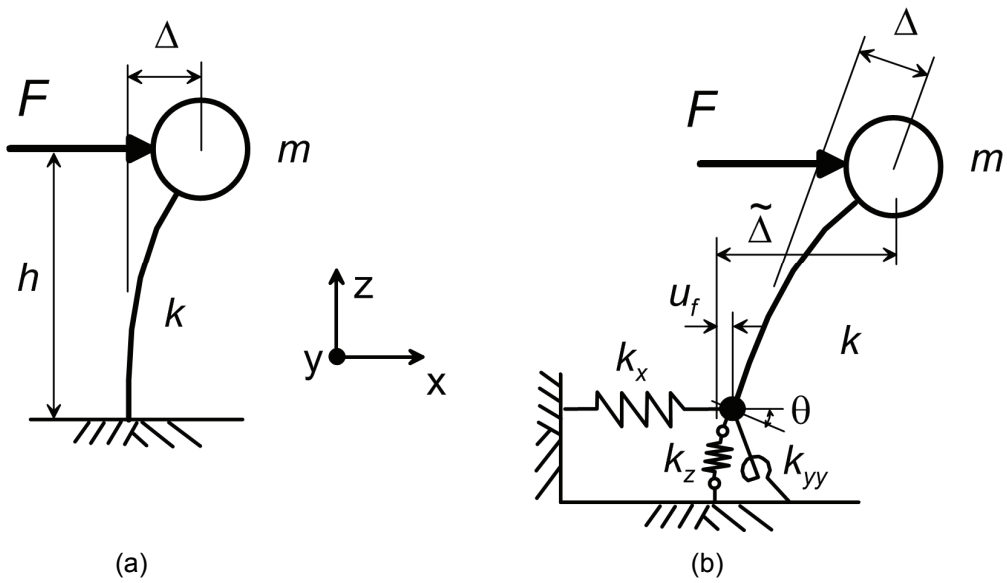

Figure 2-1 Schematic illustration of deflections caused by force applied to: (a) fixed-base structure; and (b) structure with vertical, horizontal, and rotational flexibility at its base.

Now consider the same structure with vertical, horizontal, and rotational springs at its base, representing the effects of soil flexibility against a rigid foundation, as depicted in Figure 2-1b. The vertical spring stiffness in the z direction is denoted k_z, the horizontal spring stiffness in the x direction is denoted k_x, and the rotational spring is denoted k_{yy}, representing rotation in the x-z plane (about the y-y axis). If a force, F, is applied to the mass in the x direction, the structure deflects, as it does in the fixed-base system, but the base shear (F) deflects the horizontal spring by u_f, and the base moment $(F \times h)$ deflects the rotational spring by θ. Accordingly, the total deflection with respect to the free-field at the top of the structure, $\tilde{\Delta}$, is:

$$\begin{aligned} \tilde{\Delta} &= \frac{F}{k} + u_f + \theta \cdot h \\ \tilde{\Delta} &= \frac{F}{k} + \frac{F}{k_x} + \left(\frac{F \cdot h}{k_{yy}}\right) h \end{aligned} \tag{2-4}$$

If Equation 2-4 is substituted into Equation 2-3, an expression for flexible base period, $\tilde{T}$, is obtained as:

$$\tilde{T}^2 = (2\pi)^2 \frac{m\tilde{\Delta}}{F} = (2\pi)^2 m\left(\frac{1}{k} + \frac{1}{k_x} + \frac{h^2}{k_{yy}}\right) \tag{2-5}$$

Combining expressions in Equation 2-5 and Equation 2-2 results in:

$$\left(\frac{\tilde{T}}{T}\right)^2 = \frac{k}{m} \cdot m \cdot \left(\frac{1}{k} + \frac{1}{k_x} + \frac{h^2}{k_{yy}}\right) \tag{2-6}$$

Equation 2-6 simplifies into a classical period lengthening expression (Veletsos and Meek, 1974):

$$\frac{\tilde{T}}{T} = \sqrt{1 + \frac{k}{k_x} + \frac{kh^2}{k_{yy}}} \tag{2-7}$$

Equation 2-7 can be applied to multi-degree-of-freedom structures by taking the height, h, as the height of the center of mass for the first-mode shape. This is commonly referred to as the effective modal height, which is approximately two-thirds of the overall structure height, and taken as 0.7 times the height in ASCE/SEI 7-10 (ASCE, 2010). In such cases, period lengthening applies to only the first-mode period.

In previous work by Veletsos and Nair (1975) and Bielak (1975), it has been shown that the dimensionless parameters controlling period lengthening are:

$$\frac{h}{V_s T}, \quad \frac{h}{B}, \quad \frac{B}{L}, \quad \frac{m}{\rho_s 4BLh}, \quad \text{and} \quad \nu \tag{2-8}$$

where h is the structure height (or height to the center of mass of the first mode shape), B and L refer to the half-width and half-length of the foundation, m is the mass (or effective modal mass), ρ_s is the soil mass density, and ν is the Poisson's ratio of the soil. Previous work was applicable to circular foundations, and has been adapted here for rectangular shapes considering the ratio, B/L.

To the extent that h/T quantifies the stiffness of the superstructure, the term $h/(V_s T)$ in Equation 2-8 represents the *structure-to-soil stiffness ratio*. The term h/T has units of velocity, and will be larger for stiff lateral force resisting systems, such as shear walls, and smaller for flexible systems, such as moment frames. The shear wave velocity, V_s, is closely related to soil shear modulus, G, computed as:

$$V_s = \sqrt{G/\rho_s} \tag{2-9}$$

For typical building structures on soil and weathered rock sites, $h/(V_s T)$ is less than 0.1 for moment frame structures, and between approximately 0.1 and 0.5 for shear wall and braced frame structures (Stewart et al., 1999b). Period lengthening

increases markedly with structure-to-soil stiffness ratio, which is the most important parameter controlling inertial SSI effects.

The *structure-height-to-foundation-width ratio*, *h/B*, and *foundation-width-to-length ratio*, *B/L*, in Equation 2-8 are aspect ratios describing the geometry of the soil-structure system. The *mass ratio*, $m/\rho_s 4BLh$, is the ratio of structure mass to the mass of soil in a volume extending to a depth equal to the structure height, *h*, below the foundation. In Equation 2-7, it can be seen that period lengthening has no fundamental dependence on mass. The mass ratio term was introduced so that period lengthening could be related to easily recognizable characteristics such as structural first mode period, *T*, and soil shear wave velocity, V_s, rather than structural stiffness, *k*, and soil shear modulus, *G*. The effect of mass ratio is modest, and it is commonly taken as 0.15 (Veletsos and Meek, 1974). The Poisson's ratio of the soil, ν, affects the stiffness and damping characteristics of the foundation.

Using models for the stiffness of rectangular foundations (of half-width, *B*; half-length, *L*; and $L \geq B$) resting on a homogeneous isotropic half-space with shear wave velocity, V_s, period lengthening ratios can be calculated with the results shown in Figure 2-2a, which is plotted for the special case of a square footing ($L = B$).

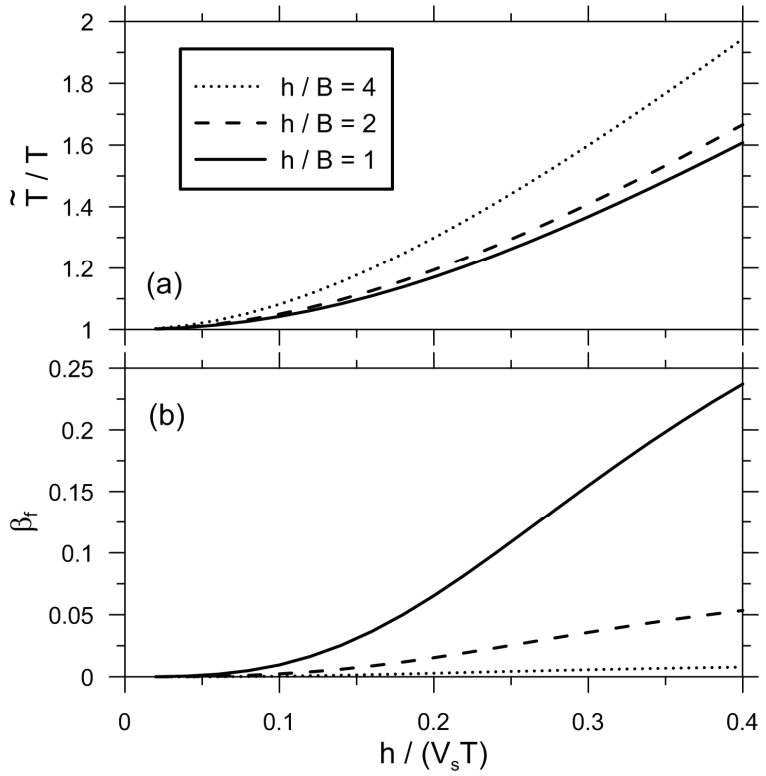

Figure 2-2 Plot of period lengthening ratio ($\widetilde{T}/T$) and foundation damping (β_f) versus structure-to-soil-stiffness ratio for square foundations ($L = B$) and varying ratios of *h*/*B*. In this plot, $\nu = 0.33$, *B/L* = 1.0, hysteretic soil damping $\beta_s = 0$, mass ratio = 0.15, and exponent $n = 2$.

All other factors being equal, period lengthening increases with the structure-height-to-foundation-width ratio, h/B, due to increased overturning moment and foundation rotation, θ. This implies that inertial SSI effects would be more significant in tall buildings, but this is not the case. Tall buildings typically have low $h/(V_sT)$ ratios, which is more important for controlling inertial SSI effects. Hence period lengthening in tall buildings is near unity (i.e., little or no period lengthening). For a fixed ratio of h/B, period lengthening is observed to decrease modestly with foundation-width-to-length ratio, B/L, due to increased foundation size (and therefore stiffness) normal to the direction of loading.

In addition to period lengthening, system behavior is also affected by damping associated with soil-foundation interaction, referred to as foundation damping, β_f. This damping is composed of two parts: (1) contributions from soil hysteresis (hysteretic damping); and (2) radiation of energy away, in the form of stress waves, from the foundation (radiation damping). Foundation damping is a direct contributor to the flexible-base system damping, β_0:

$$\beta_0 = \beta_f + \frac{1}{\left(\tilde{T}/T\right)^n}\beta_i \tag{2-10}$$

where β_i is the structural damping in the superstructure assuming a fixed base, which is generally taken as 5% for typical structural systems. More refined estimates of β_i are possible based on structural system type and configuration, as described in PEER/ATC-72-1, *Modeling and Acceptance Criteria for Seismic Design and Analysis of Tall Buildings* (ATC, 2010). Observations from case studies (Stewart et al., 1999b) have shown that β_f ranges from approximately 0% to 25%. The exponent, n, on the period lengthening term in Equation 2-10 is taken as 3 for linearly viscous structural damping, and 2 otherwise (e.g., for hysteretic damping) (Givens, 2013).

Analytical models for foundation damping have been presented by Veletsos and Nair (1975), Bielak (1975 and 1976), Roesset (1980), Wolf (1985), Aviles and Perez-Rocha (1996), Maravas et al. (2007), and Givens (2013), among others. The classical solution of Veletsos and Nair accounts for the frequency dependence of foundation damping terms. It assumes structural damping to be purely viscous, and applies for a circular foundation resting on a half-space. The equation for β_f provided by Veletsos and others is complex-valued (i.e., composed of real plus imaginary values), which complicates the interpretation of its physical meaning. Bielak's work utilizes the same conditions except that the foundation is assumed to be a cylinder penetrating a half-space to an embedment depth, D, and the resulting expressions are real-valued. The value of exponent n in Equation 2-10 is taken as 3 for the Veletsos and Bielak solutions because structural damping is assumed to be viscous.

The procedure given by Wolf (1985) neglects the frequency dependence of foundation stiffness terms, and assumes foundation radiation damping to be linearly viscous (i.e., constant dashpot coefficients for translation and rotation, c_x and c_{yy}), and applies for a circular foundation resting on a half-space. Considering frequency dependence, the form of Wolf's damping expression (similar to Roesset, 1980) can be re-written as:

$$\beta_f = \left[\frac{\left(\tilde{T}/T\right)^{n_s} - 1}{\left(\tilde{T}/T\right)^{n_s}}\right]\beta_s + \frac{1}{\left(\tilde{T}/T_x\right)^{n_x}}\beta_x + \frac{1}{\left(\tilde{T}/T_{yy}\right)^{n_{yy}}}\beta_{yy} \qquad \text{(2-11a)}$$

Where β_s is soil hysteretic damping, β_x and β_{yy} are damping ratios related to radiation damping from translational and rotational modes (described further in Section 2.2), and T_x and T_{yy} are fictitious vibration periods, calculated as if the only source of the vibration was foundation translation or rotation, as follows:

$$T_x = 2\pi\sqrt{\frac{m}{k_x}} \quad T_{yy} = 2\pi\sqrt{\frac{mh^2}{k_{yy}}} \qquad \text{(2-11b)}$$

Exponents n_s, n_x, and n_{yy} depend on the specific form of damping associated with the respective components of the foundation damping, and all other terms are as previously defined. However, because none of these terms would be expected to be linearly viscous, it is recommended to take these exponents as 2 (Givens, 2013). Note that for $n = n_s$, the period lengthening terms in front of the β_i term in Equation 2-10 and the β_s term in Equation 2-11a are weight factors that together sum to unity. Accordingly, Equation 2-11a can be viewed as a "mixing rule" for damping in different vibration modes and sources. Because Wolf's results were produced neglecting the frequency dependence of foundation stiffness terms, Equation 2-11a can provide more accurate results if those effects are included in the period lengthening calculation.

Soil hysteretic damping, β_s, is strain-dependent, and can typically be evaluated from information in the literature. Classical models are summarized in Kramer (1996). More contemporary empirical models by Darendeli (2001) and Menq (2003) account for overburden pressure and shear strain in a consistent manner across multiple soil types.

The Wolf solution for foundation damping in Equation 2-11a, along with the classical Veletsos, Bielak, and Roesset solutions, neglect contributions from terms involving the product of two damping ratios. Maravas et al. (2007) presents exact solutions in which those terms are included. Like Wolf, Maravas et al. (2007) utilizes hysteretic damping so exponents $n = 2$, and if terms involving the product of two damping ratios are excluded, Equation 2-11a is recovered.

As was the case for period lengthening shown in Figure 2-2a, Figure 2-2b shows that foundation damping β_f increases strongly with structure-to-soil-stiffness ratio, $h/(V_sT)$. In Figure 2-2b, all exponents were taken as 2. Damping β_f decreases with increasing values of h/B, indicating that lateral movements of the foundation (which dominate at low h/B ratios) dissipate energy into soil more efficiently than foundation rocking (which dominates at high h/B ratios). Radiation damping terms (β_x and β_{yy}) are reduced significantly when a stiff bedrock layer is encountered at moderate or shallow depths, as described further in Section 2.2.2.

Analysis procedures for $\tilde{T}/T$ and β_f similar to those described above have been validated relative to observations from instrumented buildings shaken by earthquakes (Stewart et al., 1999a; 1999b). These studies show that the single most important parameter controlling the significance of inertial interaction is $h/(V_sT)$, and that inertial SSI effects are generally negligible for $h/(V_sT) < 0.1$, which occurs in flexible structures (e.g., moment frame buildings) located on competent soil or rock. Conversely, inertial SSI effects tend to be significant for stiff structures, such as shear wall or braced frame buildings, located on softer soils.

The effect of inertial SSI on the base shear of a building is illustrated in Figure 2-3. Because base shear for elastic response is commonly computed based on pseudo-spectral acceleration in the first mode, the figure depicts the variation in pseudo-spectral acceleration versus period in both linear and log scales. The pseudo-spectral acceleration for a flexible-base structure, $\tilde{S}_a$, is obtained by entering the spectrum drawn for effective damping ratio, β_0, at the corresponding elongated period, $\tilde{T}$.

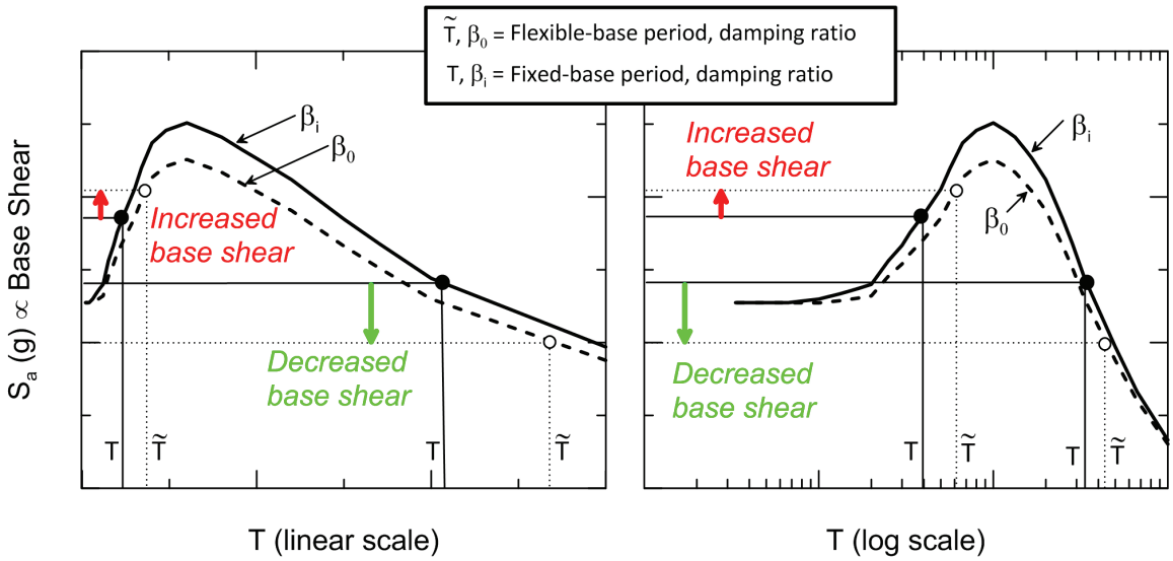

Figure 2-3 Illustration of inertial SSI effects on spectral acceleration (base shear) associated with period lengthening and change in damping.

The effect of SSI on base shear is related to the slope of the spectrum. Base shear tends to increase when the slope is positive and decrease when the slope is negative.

For the common case of buildings with relatively long periods on the descending portion of the spectrum, use of $\tilde{S}_a$ (flexible base) in lieu of S_a (fixed base) typically results in reduced base shear demand. Conversely, inertial SSI can increase the base shear in relatively short-period structures.

The period at which the spectral peak occurs, referred to as the predominant period of ground motion, T_p, is generally controlled by the tectonic regime, earthquake magnitude, and site-source distance (Rathje et al., 2004), and will only match the site period in certain cases involving large impedance contrasts due to soil layering. In the absence of unusual site effects, typical values of T_p range from approximately 0.2 to 0.5 seconds for shallow crustal earthquakes in tectonically active regions, such as California.

2.2 Equations for Shallow Foundation Stiffness and Damping

2.2.1 Models for Rigid Foundations and Uniform Soils

Impedance functions represent the frequency-dependent stiffness and damping characteristics of soil-foundation interaction. Classical solutions for the complex-valued impedance function can be written as (Luco and Westman, 1971; Veletsos and Wei, 1971):

$$\bar{k}_j = k_j + i\omega c_j \tag{2-12a}$$

where $\bar{k}_j$ denotes the complex-valued impedance function; j is an index denoting modes of translational displacement or rotation; k_j and c_j denote the frequency-dependent foundation stiffness and dashpot coefficients, respectively, for mode j; and ω is the circular frequency (rad/s). A dashpot with coefficient c_j represents the effects of damping associated with soil-foundation interaction. An alternative form for Equation 2-12a is:

$$\bar{k}_j = k_j \left(1 + 2i\beta_j\right) \tag{2-12b}$$

where:

$$\beta_j = \frac{\omega c_j}{2k_j} \text{ (defined for } k_j > 0) \tag{2-13a}$$

An advantage of the expression for β_j in terms of c_j in Equation 2-13a is that, at resonance of the SSI system, β_j can be interpreted as a fraction of critical damping in the classical sense (Clough and Penzien, 1993). A drawback of Equation 2-13a is that, as k_j approaches zero, β_j goes to infinity.

The imaginary part of the complex impedance represents a phase difference between harmonic excitation and response at a given frequency. The phase difference, ϕ_j, between force and (lagged) displacement is (Clough and Penzien 1993; Wolf 1985):

$$\phi_j = \tan^{-1}\left(2\beta_j\right) \tag{2-13b}$$

Angle ϕ_j is also known as a loss angle. For example, if β_j is 10%, peak harmonic displacement will lag peak force by 0.197 radians (11.3 degrees). When β_j goes to infinity, ϕ_j is bounded by $\pi/2$.

Many impedance function solutions are available for rigid circular or rectangular foundations located on the surface of, or embedded within, a uniform, elastic, or visco-elastic half-space. In the case of a rigid rectangular foundation resting on the surface of a half-space with shear wave velocity V_s, Pais and Kausel (1988), Gazetas (1991), and Mylonakis et al. (2006) review impedance solutions in the literature and present equations for computing the stiffness and damping terms in Equation 2-12.

Solutions describe translational stiffness and damping along axes *x*, *y*, and *z*, and rotational stiffness and damping about those axes (denoted *xx*, *yy*, and *zz*). Stiffness is denoted k_j, and is a function of foundation dimensions, soil shear modulus, G, Poisson's ratio of the soil, ν, dynamic stiffness modifiers, α_j, and embedment modifiers, η_j:

$$k_j = K_j \times \alpha_j \times \eta_j \tag{2-14a}$$

$$K_j = GB^m f\left(B/L, \nu\right), \quad \alpha_j = f\left(B/L, a_0\right) \tag{2-14b}$$

$$\eta_j = f\left(B/L, D/B, d_w/B, A_w/BL\right) \tag{2-14c}$$

where K_j is the static foundation stiffness at zero frequency for mode j, and $m = 1$ for translation, and $m = 3$ for rotation. Shear modulus, G, should reflect the effects of modulus reduction with increasing shear strain amplitude. ASCE/SEI 7-10, *Minimum Design Loads for Buildings and Other Structures* (ASCE, 2010), and FEMA P-750, *NEHRP Recommended Seismic Provisions for New Buildings and Other Structures* (FEMA, 2009), provide the information presented in Table 2-1 for adjusting the shear modulus and shear wave velocity for large strain levels.

Maximum (or small strain) shear modulus, G_0, can be calculated from Equation 2-9 as $G_0 = V_s^2 \rho_s$, where V_s is based on geophysical measurements in the field, and ρ_s is the soil mass density. An average effective value of V_s is generally computed across an effective profile depth, z_p, as described in Section 2.2.2. Dynamic stiffness modifiers, α_j, are related to the dimensionless frequency a_0:

$$a_0 = \frac{\omega B}{V_s} \tag{2-15}$$

which has the physical interpretation of being the ratio of B to approximately one-sixth of the seismic wavelength for frequency ω. This frequency parameter is essentially unique for half-space conditions, but may not be so in presence of a stiff

stratum at shallow depth (Anoyatis and Mylonakis, 2012). For time domain analysis, a single frequency ω is usually selected for the purpose of evaluating foundation spring and dashpot coefficients that depend on a_0. This can be taken as the frequency corresponding to the period associated with the dominant response of the structure. In most cases, this will be the first-mode, flexible-base period.

Table 2-1 Values of Shear Wave Velocity and Shear Modulus Reduction for Various Site Classes and Shaking Amplitudes (ASCE, 2010; FEMA, 2009)

	Reduction Factor (V_s)			Reduction Factor (G/G_0)		
	$S_{DS}/2.5$ [1]			$S_{DS}/2.5$ [1]		
Site Class	*≤0.1*	*0.4*	*≥0.8*	*≤0.1*	*0.4*	*≥0.8*
A	1.00	1.00	1.00	1.00	1.00	1.00
B	1.00	0.97	0.95	1.00	0.95	0.90
C	0.97	0.87	0.77	0.95	0.75	0.60
D	0.95	0.71	0.32	0.90	0.50	0.10
E	0.77	0.22	[2]	0.60	0.05	[2]
F	[2]	[2]	[2]	[2]	[2]	[2]

Notes: [1] S_{DS} is the short period spectral response acceleration parameter defined in ASCE/SEI 7-10; use straight line interpolation for intermediate values of $S_{DS}/2.5$.

[2] Value should be evaluated from site-specific analysis.

Table 2-2a lists expressions for static foundation stiffness, K_j, for three translational and three rotational degrees of freedom for a rigid rectangular footing located at the ground surface. These equations are similar for Pais and Kausel (1988), Gazetas (1991), and Mylonakis et al. (2006).

Embedment of foundations below the ground surface increases static foundation stiffness. Factors, η_j, to increase K_j for the effects of embedment are provided in Table 2-2b. The Pais and Kausel (1988) equations are most often used in practice. The equations by Gazetas (1991) and Mylonakis et al. (2006) are more general, accounting for embedment effects resulting from gapping between the soil and foundation side walls.

Equations for dynamic stiffness modifiers, α_j, and radiation damping ratios, β_j, for rigid footings located at the ground surface are provided in Table 2-3a. Dynamic stiffness modifiers and radiation damping ratios for embedded footings are provided in Table 2-3b.

Table 2-2a Elastic Solutions for Static Stiffness of Rigid Footings at the Ground Surface

Degree of Freedom	Pais and Kausel (1988)	Gazetas (1991); Mylonakis et al. (2006)
Translation along z-axis	$K_{z,sur} = \frac{GB}{1-\nu}\left[3.1\left(\frac{L}{B}\right)^{0.75} + 1.6\right]$	$K_{z,sur} = \frac{2GL}{1-\nu}\left[0.73 + 1.54\left(\frac{B}{L}\right)^{0.75}\right]$
Translation along y-axis	$K_{y,sur} = \frac{GB}{2-\nu}\left[6.8\left(\frac{L}{B}\right)^{0.65} + 0.8\left(\frac{L}{B}\right) + 1.6\right]$	$K_{y,sur} = \frac{2GL}{2-\nu}\left[2 + 2.5\left(\frac{B}{L}\right)^{0.85}\right]$
Translation along x-axis	$K_{x,sur} = \frac{GB}{2-\nu}\left[6.8\left(\frac{L}{B}\right)^{0.65} + 2.4\right]$	$K_{x,sur} = K_{y,sur} - \frac{0.2}{0.75-\nu}GL\left(1-\frac{B}{L}\right)$
Torsion about z-axis	$K_{zz,sur} = GB^3\left[4.25\left(\frac{L}{B}\right)^{2.45} + 4.06\right]$	$K_{zz,sur} = GJ_t^{0.75}\left[4 + 11\left(1-\frac{B}{L}\right)^{10}\right]$
Rocking about y-axis	$K_{yy,sur} = \frac{GB^3}{1-\nu}\left[3.73\left(\frac{L}{B}\right)^{2.4} + 0.27\right]$	$K_{yy,sur} = \frac{G}{1-\nu}\left(I_y\right)^{0.75}\left[3\left(\frac{L}{B}\right)^{0.15}\right]$
Rocking about x-axis	$K_{xx,sur} = \frac{GB^3}{1-\nu}\left[3.2\left(\frac{L}{B}\right) + 0.8\right]$	$K_{xx,sur} = \frac{G}{1-\nu}\left(I_x\right)^{0.75}\left(\frac{L}{B}\right)^{0.25}\left[2.4 + 0.5\left(\frac{B}{L}\right)\right]$

Notes:

Axes should be oriented such that $L \geq B$.

I_i = area moment of inertia of soil-foundation contact, i denotes which axis to take the surface around.

$J_t = I_x + I_y$ polar moment of inertia of soil-foundation contact surface.

G = shear modulus (reduced for large strain effects, e.g., Table 2-1).

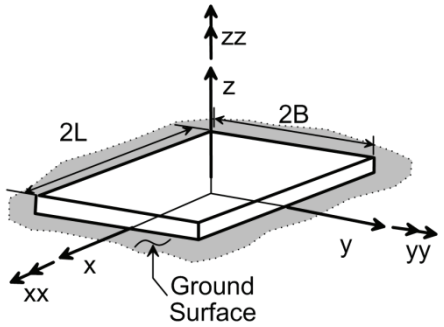

Table 2-2b Embedment Correction Factors for Static Stiffness of Rigid Footings

Degree of Freedom	Pais and Kausel (1988)	Gazetas (1991); Mylonakis et al. (2006)
Translation along z-axis	$\eta_z = \left[1.0 + \left(0.25 + \frac{0.25}{L/B}\right)\left(\frac{D}{B}\right)^{0.8}\right]$	$\eta_z = \left[1 + \frac{D}{21B}\left(1 + 1.3\frac{B}{L}\right)\right]\left[1 + 0.2\left(\frac{A_w}{4BL}\right)^{2/3}\right]$
Translation along y-axis	$\eta_y = \left[1.0 + \left(0.33 + \frac{1.34}{1 + L/B}\right)\left(\frac{D}{B}\right)^{0.8}\right]$	$\eta_y = \left(1 + 0.15\sqrt{\frac{D}{B}}\right)\left[1 + 0.52\left(\frac{z_w A_w}{BL^2}\right)^{0.4}\right]$
Translation along x-axis	$\eta_x \approx \eta_y$	Same equation as for η_y, but A_w term changes for $B \neq L$
Torsion about z-axis	$\eta_{zz} = \left[1 + \left(1.3 + \frac{1.32}{L/B}\right)\left(\frac{D}{B}\right)^{0.9}\right]$	$\eta_{zz} = 1 + 1.4\left(1 + \frac{B}{L}\right)\left(\frac{d_w}{B}\right)^{0.9}$
Rocking about y-axis	$\eta_{yy} = \left[1.0 + \frac{D}{B} + \left(\frac{1.6}{0.35 + (L/B)^4}\right)\left(\frac{D}{B}\right)^2\right]$	$\eta_{yy} = 1 + 0.92\left(\frac{d_w}{B}\right)^{0.6}\left[1.5 + \left(\frac{d_w}{D}\right)^{1.9}\left(\frac{B}{L}\right)^{-0.6}\right]$
Rocking about x-axis	$\eta_{xx} = \left[1.0 + \frac{D}{B} + \left(\frac{1.6}{0.35 + L/B}\right)\left(\frac{D}{B}\right)^2\right]$	$\eta_{xx} = 1 + 1.26\frac{d_w}{B}\left[1 + \frac{d_w}{B}\left(\frac{d_w}{D}\right)^{-0.2}\sqrt{\frac{B}{L}}\right]$

Notes:

d_w = height of effective side wall contact (may be less than total foundation height)

z_w = depth to centroid of effective sidewall contact

A_w = sidewall-solid contact area, for constant effective contact height, d_w, along perimeter.

For each degree of freedom, calculate $K_{emb} = \eta K_{sur}$

Coupling Terms: $K_{emb,rx} = \left(\frac{D}{3}\right) K_{emb,x}$

$$K_{emb,ry} = \left(\frac{D}{3}\right) K_{emb,y}$$

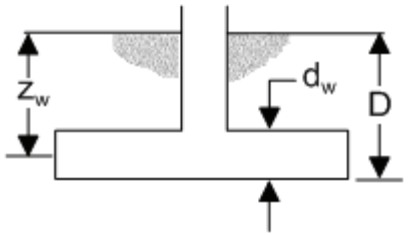

Table 2-3a Dynamic Stiffness Modifiers and Radiation Damping Ratios for Rigid Footings (adapted from Pais and Kausel, 1988)

Degree of Freedom	Surface Stiffness Modifiers	Radiation Damping
Translation along z-axis	$\alpha_z = 1.0 - \left[\dfrac{\left(0.4 + \dfrac{0.2}{L/B}\right)a_0^2}{\left(\dfrac{10}{1+3(L/B-1)}\right)+a_0^2}\right]$	$\beta_z = \left[\dfrac{4\psi(L/B)}{(K_{z,sur}/GB)}\right]\left[\dfrac{a_0}{2\alpha_z}\right]$
Translation along y-axis	$\alpha_y = 1.0$	$\beta_y = \left[\dfrac{4(L/B)}{(K_{y,sur}/GB)}\right]\left[\dfrac{a_0}{2\alpha_y}\right]$
Translation along x-axis	$\alpha_x = 1.0$	$\beta_x = \left[\dfrac{4(L/B)}{(K_{x,sur}/GB)}\right]\left[\dfrac{a_0}{2\alpha_x}\right]$
Torsion about z-axis	$\alpha_{zz} = 1.0 - \left[\dfrac{\left(0.33 - 0.03\sqrt{L/B-1}\right)a_0^2}{\left(\dfrac{0.8}{1+0.33(L/B-1)}\right)+a_0^2}\right]$	$\beta_{zz} = \left[\dfrac{(4/3)\left[(L/B)^3+(L/B)\right]a_0^2}{(K_{zz,sur}/GB^3)\left[\left(\dfrac{1.4}{1+3(L/B-1)^{0.7}}\right)+a_0^2\right]}\right]\left[\dfrac{a_0}{2\alpha_{zz}}\right]$
Rocking about y-axis	$\alpha_{yy} = 1.0 - \left[\dfrac{0.55a_0^2}{\left(0.6+\dfrac{1.4}{(L/B)^3}\right)+a_0^2}\right]$	$\beta_{yy} = \left[\dfrac{(4\psi/3)(L/B)^3 a_0^2}{\left(\dfrac{K_{yy,sur}}{GB^3}\right)\left[\left(\dfrac{1.8}{1+1.75(L/B-1)}\right)+a_0^2\right]}\right]\left[\dfrac{a_0}{2\alpha_{yy}}\right]$
Rocking about x-axis	$\alpha_{xx} = 1.0 - \left[\dfrac{\left(0.55+0.01\sqrt{L/B-1}\right)a_0^2}{\left(2.4-\dfrac{0.4}{(L/B)^3}\right)+a_0^2}\right]$	$\beta_{xx} = \left[\dfrac{(4\psi/3)(L/B)a_0^2}{(K_{xx,sur}/GB^3)\left[\left(2.2-\dfrac{0.4}{(L/B)^3}\right)+a_0^2\right]}\right]\left[\dfrac{a_0}{2\alpha_{xx}}\right]$

Notes:

Orient axes such that $L \geq B$.

Soil hysteretic damping, β_s, is additive to foundation radiation damping, β_f.

$a_0 = \omega B / V_s$; $\psi = \sqrt{2(1-\nu)/(1-2\nu)}$; $\psi \leq 2.5$

Table 2-3b Dynamic Stiffness Modifiers and Radiation Damping Ratios for Embedded Footings (adapted from Pais and Kausel, 1988)

Degree of Freedom	Radiation Damping
Translation along z-axis	$\beta_z = \left[\frac{4\left[\psi\left(L/B\right)+\left(D/B\right)\left(1+L/B\right)\right]}{\left(K_{z,emb}/GB\right)}\right]\left[\frac{a_0}{2\alpha_z}\right]$
Translation along y-axis	$\beta_y = \left[\frac{4\left[L/B+\left(D/B\right)\left(1+\psi L/B\right)\right]}{\left(K_{y,emb}/GB\right)}\right]\left[\frac{a_0}{2\alpha_y}\right]$
Translation along x-axis	$\beta_x = \left[\frac{4\left[L/B+\left(D/B\right)\left(\psi+L/B\right)\right]}{\left(K_{x,emb}/GB\right)}\right]\left[\frac{a_0}{2\alpha_x}\right]$
Torsion about z-axis	$\beta_{zz} = \left[\frac{\left(4/3\right)\left[3\left(L/B\right)\left(D/B\right)+\psi\left(L/B\right)^3\left(D/B\right)+3\left(L/B\right)^2\left(D/B\right)+\psi\left(D/B\right)+\left(L/B\right)^3+\left(L/B\right)\right]a_0^2}{\left(\frac{K_{zz,emb}}{GB^3}\right)\left[\left(\frac{1.4}{1+3\left(L/B-1\right)^{0.7}}\right)+a_0^2\right]}\right]\left[\frac{a_0}{2\alpha_{zz}}\right]$
Rocking about y-axis	$\beta_{yy} = \left[\frac{\left(4/3\right)\left[\left(\frac{L}{B}\right)^3\left(\frac{D}{B}\right)+\psi\left(\frac{D}{B}\right)^3\left(\frac{L}{B}\right)+\left(\frac{D}{B}\right)^3+3\left(\frac{D}{B}\right)\left(\frac{L}{B}\right)^2+\psi\left(\frac{L}{B}\right)^3\right]a_0^2}{\left(\frac{K_{yy,emb}}{GB^3}\right)\left[\left(\frac{1.8}{1+1.75\left(L/B-1\right)}\right)+a_0^2\right]}+\frac{\left(\frac{4}{3}\right)\left(\frac{L}{B}+\psi\right)\left(\frac{D}{B}\right)^3}{\left(\frac{K_{yy,emb}}{GB^3}\right)}\right]\left[\frac{a_0}{2\alpha_{yy}}\right]$
Rocking about x-axis	$\beta_{xx} = \left[\frac{\left(4/3\right)\left[\left(\frac{D}{B}\right)+\left(\frac{D}{B}\right)^3+\psi\left(\frac{L}{B}\right)\left(\frac{D}{B}\right)^3+3\left(\frac{D}{B}\right)\left(\frac{L}{B}\right)+\psi\left(\frac{L}{B}\right)\right]a_0^2}{\left(\frac{K_{xx,emb}}{GB^3}\right)\left[\left(\frac{1.8}{1+1.75\left(L/B-1\right)}\right)+a_0^2\right]}+\frac{\left(\frac{4}{3}\right)\left(\psi\frac{L}{B}+1\right)\left(\frac{D}{B}\right)^3}{\left(\frac{K_{xx,emb}}{GB^3}\right)}\right]\left[\frac{a_0}{2\alpha_{xx}}\right]$

Notes:

Soil hysteretic damping, β_s, is additive to foundation radiation damping, β_f.

$\alpha_{emb} = \alpha_{sur}$; from Table 2-3a

$a_0 = \omega B / V_s$; $\psi = \sqrt{2\left(1-\nu\right)/\left(1-2\nu\right)}$; $\psi \le 2.5$

The frequency dependence of quantities provided in Table 2-3a reflects the effect of condensation of infinite degrees of freedom in soil having mass and associated dynamic effects (i.e., hidden mass effect). Frequency dependence would disappear for massless soil, as a_0 would become zero (because $V_s = \sqrt{G_{\max}/\rho} \to \infty$ in Equation 2-15), causing $\alpha_j = 1$, and $\beta_j = 0$. Dynamic stiffness modifiers provided in Table 2-3b are insensitive to embedment, so values for embedded foundations are the same as values given in Table 2-3a for footings located at the ground surface (i.e., $\alpha_{j,\,emb} = \alpha_{j,\,sur}$).

Figure 2-4 shows the variation in dynamic stiffness modifiers versus frequency for rigid footings located at the ground surface. In the case of translational stiffness, dynamic stiffness modifiers (α_x, α_y) are essentially unity, regardless of frequency or foundation aspect ratio. For rotational stiffness, however, dynamic stiffness modifiers for rocking (α_{xx}, α_{yy}) degrade markedly with frequency, but are relatively insensitive to aspect ratio.

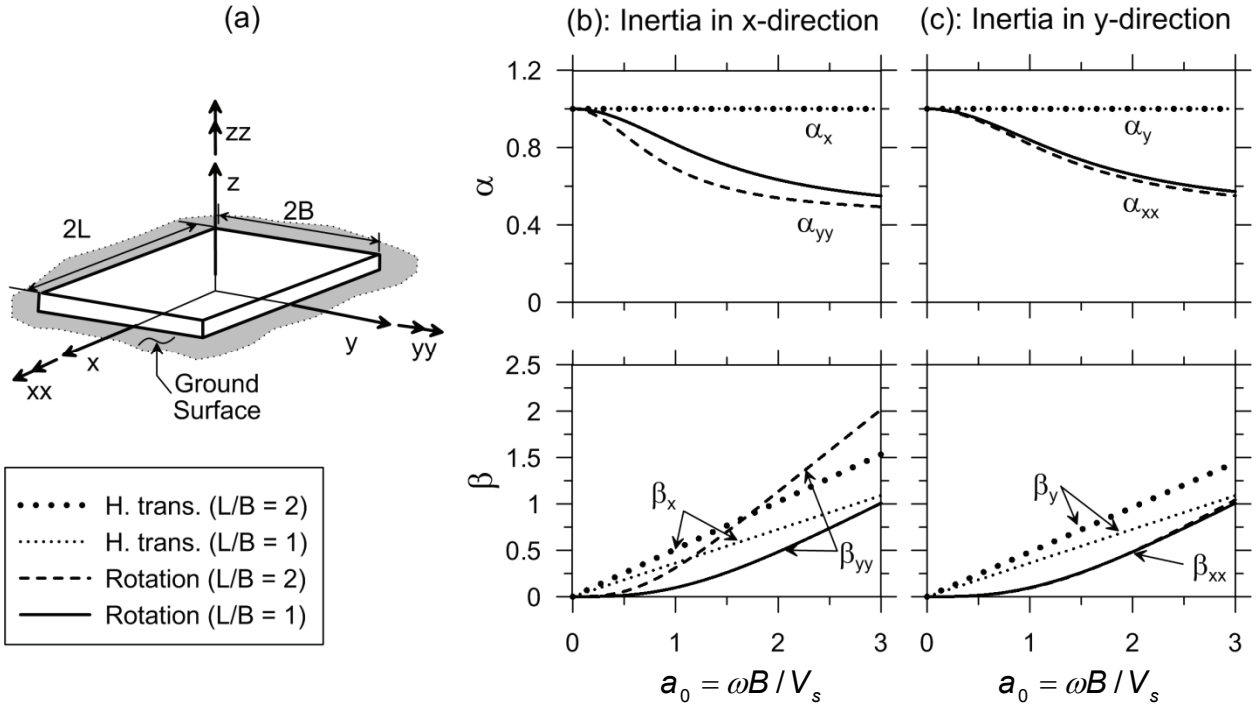

Figure 2-4 Plot of dynamic stiffness modifiers and damping ratios versus dimensionless frequency, for rectangular footings resting on the surface of a homogeneous half-space, with zero hysteretic damping, and ν=0.33: (a) geometry; (b) *x*-direction; and (c) *y*-direction.

Because soil hysteretic damping, β_s, is taken as zero, Figure 2-4 also shows the variation in radiation damping ratios for translation (β_x, β_y) and rotation (β_{xx}, β_{yy}) versus frequency. Translational radiation damping is only modestly affected by the direction of shaking or the aspect ratio of the foundation. The modest increase of translational damping with aspect ratio is a result of the increased foundation size (i.e., larger wave source).

In contrast, rotational radiation damping is strongly sensitive to the direction of shaking and the aspect ratio of the foundation. Rotational damping is largely controlled by vertical cyclic displacements at the edges of the foundation (without separation between soil and footing). As aspect ratio increases, the ends of the foundation are located further apart, and energy radiating into the soil from each end of the foundation experiences less destructive interference, thus increasing damping. At low frequencies ($a_0 < 1$ to 2), damping from rotation is generally smaller than damping from translation, although the trend reverses as frequency increases and foundations become relatively oblong. The practical significance of this effect is that translational deformation modes in the foundation, while often relatively unimportant from the perspective of overall structural system flexibility, can be the dominant source of foundation damping. When used to calculate the dashpot coefficient, c_j, the β_j term should be taken as the sum of radiation damping for the appropriate vibration mode (from Equation 2-13a and Table 2-3) and soil hysteretic damping, β_s, provided by a geotechnical engineer.

Figure 2-5 shows the variation in dynamic stiffness modifiers and radiation damping ratios versus frequency for embedded foundations. In equations provided by Pais and Kausel (1988), dynamic stiffness modifiers are unaffected by embedment, and this

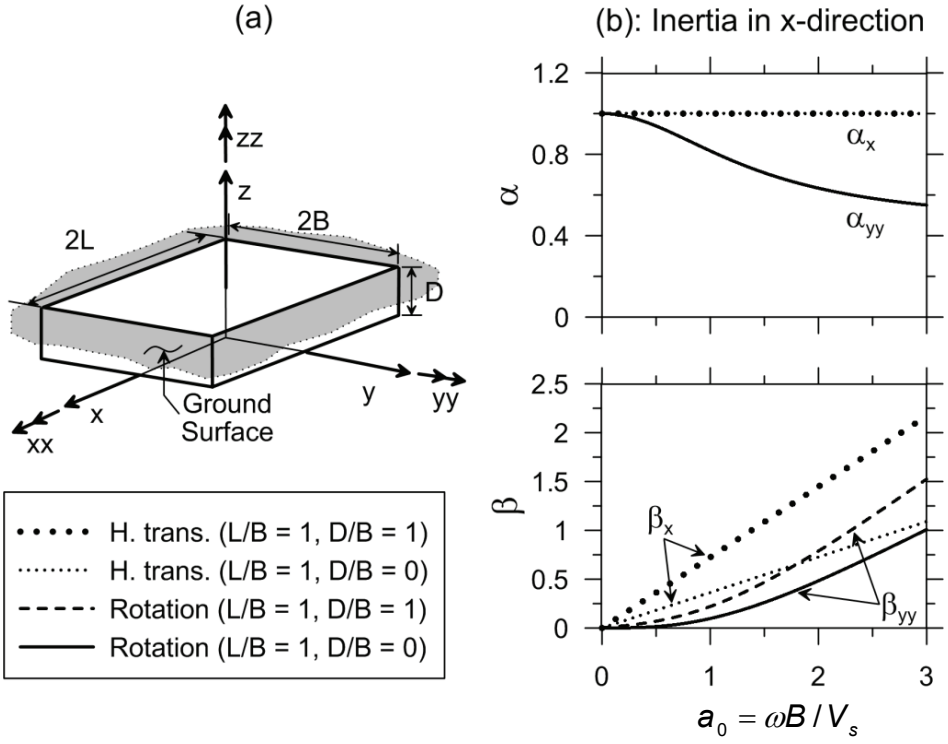

Figure 2-5 Plot of dynamic stiffness modifiers and damping ratios versus dimensionless frequency, for square footings embedded in a homogeneous half-space, with zero hysteretic damping, and ν=0.33: (a) geometry; and (b) *x*-direction (*y*-direction similar).

result is shown in Figure 2-5b. Apsel and Luco (1987), however, found a somewhat different result, indicating some sensitivity to embedment. Apsel and Luco observed a more rapid decay of stiffness with frequency for embedded foundations, which is not reflected in the figure.

The elasto-dynamic analyses upon which Figure 2-5 is based assume perfect contact between soil and basement walls. Accordingly, the solutions indicate much higher damping levels than those for shallow foundations (Gazetas, 1991). These damping levels may not be reliable when gaps form between foundations and the adjacent soil, which reduces the potential for radiation damping from basement walls. In studies performed by Stewart et al. (1999b), buildings shaken by earthquakes generally do not exhibit damping levels consistent with such models. As a result, the impedance of embedded foundations can be conservatively estimated from the equations for static stiffness in Table 2-2a and adjusted by dynamic stiffness modifiers for surface foundations from Table 2-3b.

2.2.2 Effect of Non-Uniform Soil Profiles

In most cases, V_s profiles are evaluated away from foundations (i.e., in the free-field) and reflect a variation of shear modulus with depth. Variation in soil shear modulus with depth, and the presence of additional weight from a structure, complicates the selection of an appropriate shear wave velocity in the calculation of static foundation stiffnesses. To evaluate a single effective V_s value for use in computations, it is necessary to: (1) correct V_s values measured in the free-field to account for overburden pressures associated with the added weight of the structure; and (2) calculate an average effective V_s value over an appropriate depth range.

Soil shear modulus, G_0, is known to increase with mean effective confining stress, σ'_m, as follows:

$$G_0 = G_a \left(\frac{\sigma'_m}{p_a} \right)^n \tag{2-16}$$

where G_a is the shear modulus at atmospheric pressure, σ_m' is the effective confining stress, p_a is taken as approximately 100 kPa, and n varies from approximately 0.5 for granular soils (Hardin and Black, 1968; Marcuson and Wahls, 1972) to 1.0 for cohesive soils with plasticity index (PI) greater than 6.5 (Yamada et al., 2008). Recognizing that V_s is proportional to the square root of shear modulus, free-field measurements of shear wave velocity (at depth) can be corrected to account for overburden pressures due to the added weight of the structure as follows:

$$V_{s,F}(z) \approx V_s(z) \left(\frac{\sigma'_v(z) + \Delta\sigma'_v(z)}{\sigma'_v(z)} \right)^{n/2} \tag{2-17}$$

where $V_{s,F}(z)$ is the overburden-corrected shear wave velocity at depth z, $V_s(z)$ denotes the shear wave velocity measured in the free-field at depth z, $\sigma'_v(z)$ is the effective stress from the self-weight of the soil at depth z, and $\Delta\sigma_v(z)$ is the increment of vertical stress due to the weight of the structure at depth z, which can be computed using classical Boussinesq stress distribution theory (e.g., Fadum, 1948). The overburden correction in Equation 2-17 is typically significant only at shallow depths (i.e., 50% to 100% of the foundation dimension).

Using overburden-corrected values of shear wave velocity, an average effective profile velocity must be calculated over an appropriate depth interval. The depth interval necessary for computing an average effective profile velocity was investigated by Stewart et al. (2003). By matching the static stiffnesses for a uniform half-space to those for computed for a non-uniform profile using the solutions of Wong and Luco (1985), this work determined that shear wave velocities should be averaged over an effective profile depth, z_p, below the foundation bearing level. The profile depth is discretized into layers having thickness Δz_i and velocity $V_{s,F}(z)_i$. Designated as $V_{s,\,avg}$, the average effective profile velocity should be calculated as the ratio of the profile depth, z_p, to the summation of shear wave travel time through each depth interval (Equation 2-18a). The depth interval, z_p, necessary for computing an average effective profile velocity can be taken as the half-dimension of an equivalent square foundation matching the area of the actual foundation, B_e^A, or the half-dimension of an equivalent square foundation matching the moment of inertia of the actual foundation, B_e^I, computed as follows:

$$V_{s,\,avg} = \frac{z_p}{\sum_{i=1}^{n}\left(\Delta z_i \Big/ \left(V_{s,F}(z)\right)_i\right)} \tag{2-18a}$$

$$Horizontal\left(x \text{ and } y\right): \quad z_p = B_e^A, \quad B_e^A = \sqrt{A/4} = \sqrt{BL} \tag{2-18b}$$

$$Rocking(xx): \quad z_p \approx B_e^I, \;\; xx: B_e^I = \sqrt[4]{0.75 I_x} = \sqrt[4]{B^3 L} \tag{2-18c}$$

$$Rocking(yy): \quad z_p \approx B_e^I, \;\; yy: B_e^I = \sqrt[4]{0.75 I_y} = \sqrt[4]{B L^3} \tag{2-18d}$$

This approach can, in principle, be applied to effectively rigid foundation systems by considering B and L as the half-dimensions of the entire foundation plan. This requires consideration of foundation flexibility and connectivity of the discrete elements comprising the foundation system. Guidance for non-rigid (i.e., flexible) foundation elements is provided in Section 2.2.3.

When soil shear modulus increases with depth, some of the seismic energy radiating from the foundation reflects upward towards the foundation, hence it is not "lost" as occurs in a uniform half-space. Impedance solutions for this phenomenon are

available for circular foundations (vertical translation: Guzina and Pak, 1998; horizontal translation and rotation, approximate cone solution: Gazetas, 1991) and rectangular foundations (vertical translation, rocking: Vrettos, 1999) for different types of heterogeneity.

Figure 2-6 shows a plot of dynamic stiffness modifiers and radiation damping ratios comparing results for a uniform half-space and non-uniform profiles in which G varies with depth, as shown. The effect on radiation damping is more pronounced in rotation (Figure 2-6b) than in translation (Figure 2-6a). Also, the effect on the rotational stiffness modifier, α_{yy}, for square foundations (Figure 2-6b) is modest. Hence, the effect of variation in soil shear modulus with depth is most critical for static stiffness and radiation damping associated with foundation rocking. Because rocking is often an insignificant contributor to overall foundation damping, the practical impact of soil non-homogeneity is primarily related to its effect on static stiffness.

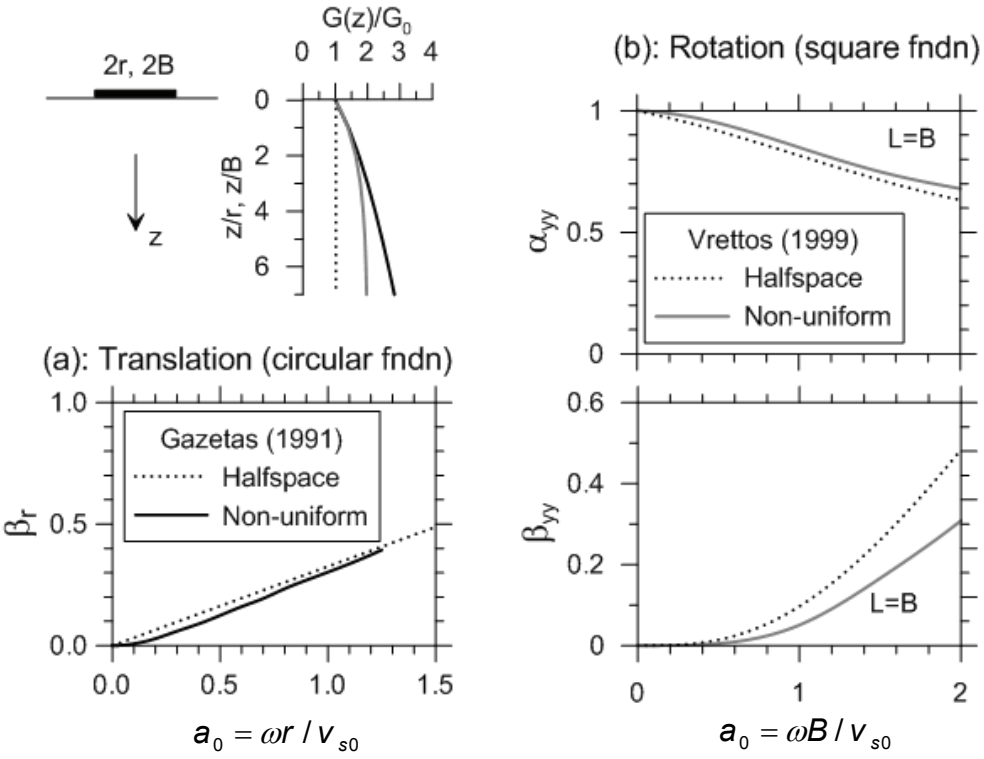

Figure 2-6 Plot of dynamic stiffness modifiers and radiation damping ratios versus dimensionless frequency comparing uniform half-space and non-uniform profiles in which G varies with depth: (a) translation for circular foundations (from Gazetas, 1991); and (b) rotation for square foundations (from Vrettos, 1999).

In the extreme case of a rigid material at depth in a soil profile, radiation damping from body wave propagation disappears at frequencies lower than the fundamental frequency of the soil column. While no geologic materials are actually rigid, this can

be of concern when the ratio of the shear wave velocity of the firm layer to that of the soil exceeds approximately two. In such cases, the static stiffness of foundations is increased (solutions available in Mylonakis et al., 2006).

2.2.3 Effect of Flexible Structural Foundation Elements

Classical impedance function solutions, such as those presented in Table 2-2 and Table 2-3, strictly apply for rigid foundations. As illustrated in Figure 2-1, soil-foundation interaction for rigid foundations can be represented by individual springs for each foundation degree of freedom. Actual foundation slabs and basement walls, however, are non-rigid structural elements. The few theoretical solutions that exist apply to circular foundations supporting a rigid core (Iguchi and Luco, 1982), flexible perimeter walls (Liou and Huang, 1994), or rigid concentric walls (Riggs and Waas, 1985). Figure 2-7 shows the effect of flexible foundation elements on rotational stiffness, k_{rr}, and rotational radiation damping ratio, β_{rr}, for the cases of a circular foundation supporting a rigid core or flexible perimeter wall.

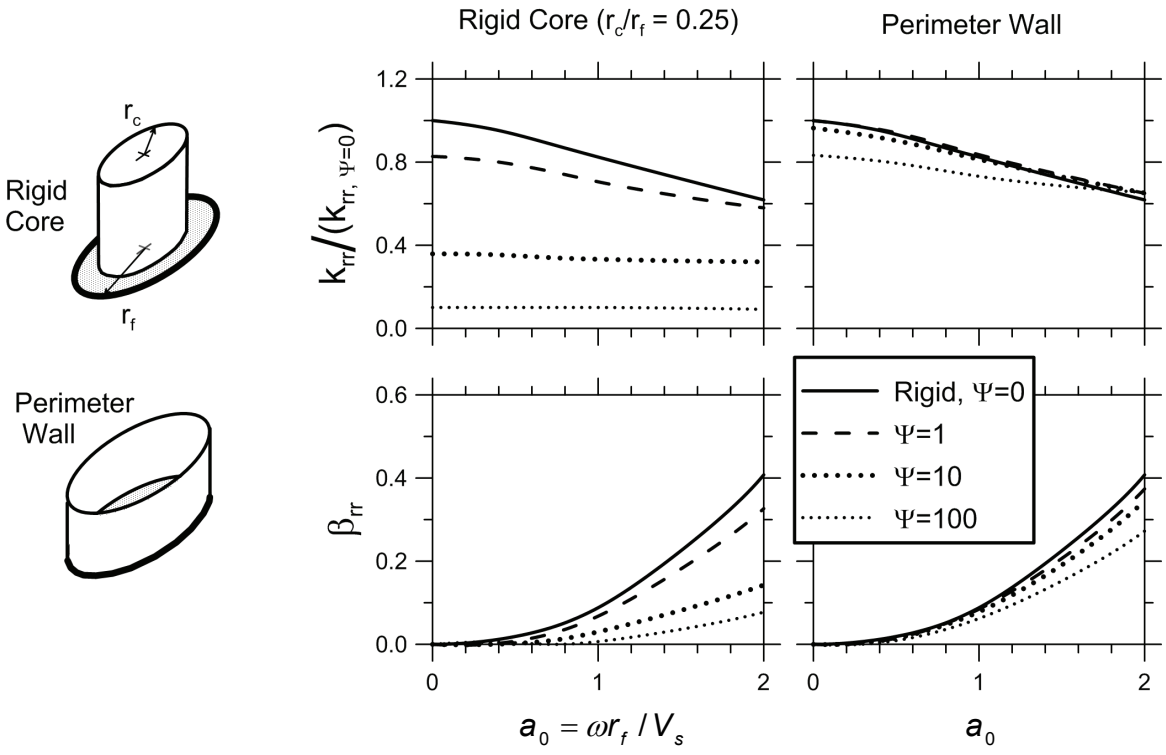

Figure 2-7 Effect of flexible foundation elements on rotational stiffness (k_{rr}) and rotational radiation damping ratio (β_{rr}) for circular foundations supporting a rigid core (Iguchi and Luco, 1982) and flexible perimeter walls (Liou and Huang, 1994).

The flexibility of the foundation is represented by a relative soil-to-foundation stiffness ratio, Ψ, taken from plate theory as:

$$\Psi = \frac{G r_f^3}{\left(E_f t_f^3 / \left(12(1-\nu_f^2) \right) \right)} \tag{2-19}$$

where r_f is the foundation radius, t_f is the foundation thickness, and E_f and ν_f are the Young's modulus and Poisson's ratio of the foundation concrete. The case of $\Psi = 0$ corresponds to a rigid foundation slab.

Liou and Huang (1994) showed that foundation flexibility does not significantly affect translational stiffness and damping terms for the case of flexible perimeter walls. For rotational stiffness and radiation damping, Figure 2-7 shows that foundation flexibility effects are relatively modest for the case of flexible perimeter walls, and most significant for the case of a rigid core.

Typical practice does not adjust the impedance function for non-rigid foundations as shown in Figure 2-7. Instead, foundations springs are distributed across the extent of the foundation, as illustrated in Figure 1-2c. Distributed springs allow the foundation to deform in a natural manner given the loads imposed by the superstructure and the spring reactions. For vertical springs, this can be accomplished by calculating the vertical translational impedance, as described above, and normalizing it by the foundation area to compute stiffness intensity, k_z^i (also known as coefficient of subgrade reaction), with dimensions of force per cubic length:

$$k_z^i = \frac{k_z}{4BL} \tag{2-20a}$$

A dashpot intensity can be similarly calculated as:

$$c_z^i = \frac{c_z}{4BL} \tag{2-20b}$$

As illustrated in Figure 2-8, the stiffness of an individual vertical spring in the interior portion of the foundation can be taken as the product of k_z^i and the spring's tributary area dA. If this approach were used across the entire length, the vertical stiffness of the foundation would be reproduced, but the rotational stiffness would generally be underestimated. This occurs because the vertical soil reaction is not uniform, and tends to increase near the edges of the foundation. Using a similar process with c_z^i would overestimate radiation damping from rocking. This occurs because translational vibration modes (including vertical translation) are much more effective radiation damping sources than rocking modes.

To correct for underestimation of rotational stiffness, strips along the foundation edge (of length $R_e L$) are assigned stiffer springs. When combined with springs in the interior, the total rotational stiffness of the foundation is reproduced. Harden and Hutchinson (2009) present expressions for end length ratios and spring stiffness increases as a function of L/B using static stiffnesses from Gazetas (1991).

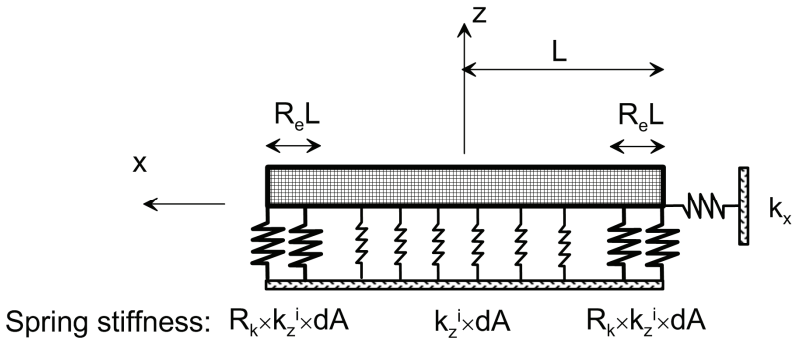

Figure 2-8 Vertical spring distribution used to reproduce total rotational stiffness k_{yy}. A comparable geometry can be shown in the y-z plane (using foundation dimension 2B) to reproduce k_{xx}.

More generally, the increase in spring stiffness, R_k, can be calculated as a function of foundation end length ratio, R_e, as:

$$Rocking(yy): \quad R_{k,yy} = \frac{\left(\frac{3k_{yy}}{4k_z^i BL^3}\right) - \left(1-R_e\right)^3}{1-\left(1-R_e\right)^3} \tag{2-21a}$$

$$Rocking(xx): \quad R_{k,xx} = \frac{\left(\frac{3k_{xx}}{4k_z^i B^3 L}\right) - \left(1-R_e\right)^3}{1-\left(1-R_e\right)^3} \tag{2-21b}$$

Equations 2-21 were derived by matching the moment produced by the springs for a unit foundation rotation to the rotational stiffness k_{yy} or k_{xx}. In these equations, a value of R_e can be selected (typically in the range of 0.3 to 0.5), which then provides a unique R_k. This correction for rotational stiffness, however, does not preserve the original vertical stiffness k_z. This is considered an acceptable approximation, in general, because rocking is the more critical foundation vibration mode in most structures.

To correct for overestimation of rotational damping, the relative stiffness intensities and distribution are used (based on the stiffness factor R_k and end length ratio R_e), but dashpot intensities over the full length and width of the foundation are scaled down by a factor, R_c, computed as:

$$Rocking(yy): \quad R_{c,yy} = \frac{\frac{3c_{yy}}{4c_z^i BL^3}}{R_{k,yy}\left(1-\left(1-R_e\right)^3\right)+\left(1-R_e\right)^3} \tag{2-21c}$$

$$Rocking(xx): \quad R_{c,xx} = \frac{\dfrac{3c_{xx}}{4c_z^i B^3 L}}{R_{k,xx}\left(1-\left(1-R_e\right)^3\right)+\left(1-R_e\right)^3} \qquad \text{(2-21d)}$$

Use of the above procedures for modifying vertical spring impedances will reproduce the theoretical rotational stiffness and damping through distributed vertical springs and dashpots. While this allows foundation flexibility to be accounted for, in the sense that foundation structural elements connected to springs and dashpots are non-rigid, a question that remains is whether or not the rotational impedance computed using a rigid foundation impedance function is an appropriate target for calibration. For the case of a rigid core illustrated in Figure 2-7 it is not, but solutions for more practical situations are not available.

In the horizontal direction, the use of a vertical distribution of horizontal springs depends largely on whether the analysis is two-dimensional or three-dimensional, and whether or not the foundation is embedded. Current recommendations are as follows:

- For two-dimensional analysis of a foundation on the ground surface, the horizontal spring from the impedance function is directly applied to the foundation, as shown in Figure 2-8 (i.e., no distributed springs).
- For two-dimensional analysis of an embedded foundation, the component of the embedded stiffness attributable to the base slab (i.e., the stiffness without the embedment modifier, k_x/η_x) can be applied to the spring at the base slab level. Distributed springs are then positioned along the height of the basement walls with a cumulative stiffness equal to $k_x(1–1/\eta_x)$.
- For three-dimensional analysis, springs are distributed in both horizontal directions uniformly around the perimeter of the foundation. The sum of the spring stiffnesses in a given direction should match the total stiffness from the impedance function.

2.2.4 Limiting Spring Forces

Previous sections have discussed linear spring stiffness, but have not addressed foundation capacity. Pushover procedures for SSI analysis typically utilize elastic-perfectly-plastic force-deflection relationships for springs. Hence, limiting spring forces (i.e., capacities) are needed for vertical and horizontal springs.

In the case of vertical springs, the capacity is the unfactored bearing capacity of the foundation distributed over the tributary area of the spring (dA). Bearing capacity should be calculated considering the foundation geometry, drained or undrained shear strength parameters as appropriate, soil unit weight, and simultaneous presence of both horizontal and vertical loads on the foundations. These concepts are discussed

at length in foundation engineering textbooks (e.g., Coduto, 1994; Salgado, 2008), and are not reviewed here. Bearing capacity solutions provided by Soubra (1999) are commonly used in the nuclear industry. Limiting spring forces should not be calculated using allowable bearing pressures that have been derived based on long-term foundation settlement limitations, nor should factors of safety be applied.

In the case of horizontal springs, the capacity of springs located at the level of a footing or mat should reflect the unfactored sliding resistance at the slab-soil interface. The capacity of springs along basement walls should reflect the unfactored passive earth pressure.

Shear strength parameters used for computation of bearing capacity, sliding resistance, and passive earth pressure should be selected with due consideration of soil type, level of soil saturation, possible cyclic degradation effects, and the rapid loading rate applied during earthquakes. Selection of appropriate strength parameters is beyond the scope of this report, but good general guidelines can be found in soil mechanics textbooks, and in SCEC (2002).

Limiting lateral and vertical capacities of foundations are usually not simultaneously realizable. This is especially important in the presence of geometric nonlinearities such as soil-foundation gapping, described further in Section 2.4.

2.3 Impedance of Vertical Pile Foundations

Buildings founded on soft soils may have pile-supported footings or mats, especially when the foundation is not embedded (i.e., no basement levels). This section discusses the effective stiffness and damping of pile-supported foundations. Only the case of vertical piles is considered, as battered piles are seldom used in building structures.

Impedance of single pile foundations in the translational and vertical modes of vibration using elasto-dynamic solutions is covered. Rotational (or cross rotational-translational) impedance of single piles is omitted because rotational stiffness is typically derived from groups of piles supporting a footing or mat, which is based on vertical response parameters.

The impedance of pile groups for lateral and rotational vibration modes using elasto-dynamic solutions is also covered. Pile-to-pile interaction effects are considered and the manner by which vertical responses of piles are combined to develop rotational impedance is discussed. Pile stiffnesses from elasto-dynamic solutions are contrasted with the discrete element modeling typically performed in practice.

An important consideration when piles are combined with shallow spread footings or a mat foundation is whether or not lateral resistance is provided by the shallow foundation elements in combination with the piles. Soil might be expected to settle

away from shallow foundation elements in cases involving clayey foundation soils and end-bearing piles, particularly when there are surface fills at the site. In such cases, lateral load resistance would derive solely from the piles and basement walls. On the other hand, when soil settlement is not expected, a hybrid impedance model can be used in which lateral load resistance is provided by both shallow and deep foundation elements (e.g., in the case of sandy soils and friction piles).

2.3.1 Impedance of Single Piles

Springs and dashpots effectively replace a single pile in the numerical modeling of a pile-supported foundation, as schematically illustrated in Figure 2-9. The impedance of single piles, represented by k_j^p and c_j^p, can be described in the notation used for shallow foundations (Equations 2-12 to 2-14a). The dynamic stiffness for a particular vibration mode is denoted k_j^p, and the corresponding dashpot, representing the effects of damping, is denoted c_j^p. Subscript *j* represents the vibration mode, which is taken as *x* (horizontal) and *z* (vertical).

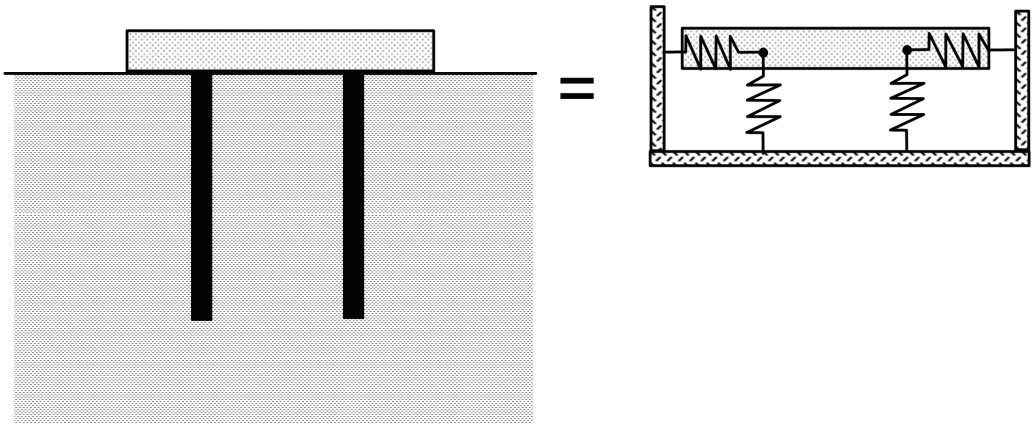

Figure 2-9 Schematic illustration showing replacement of piles with equivalent springs for translational and vertical (rotational) impedance.

The dynamic stiffness of a single pile can be represented as the product of static stiffness K_j^p and a dynamic modifier α_j^p:

$$k_j^p = K_j^p \times \alpha_j^p \tag{2-22a}$$

where:

$$\begin{aligned} K_j^p &= \chi_j E_s d \\ \chi_j &= \left(w_{pj} + w_{sj} + w_{bj}\right) f\left(E_p/E_s, L_p/d\right) \\ \alpha_j^p &= f\left(E_p/E_s, \rho_p/\rho_s, w_{sj}, \nu, a_0^p\right) \end{aligned} \tag{2-22b}$$

In Equation 2-22b, χ_j is a dimensionless constant for vibration mode *j*; *d* is pile diameter; E_s and E_p are the Young's moduli for soil and pile materials, respectively; ρ_s and ρ_p are the mass densities for soil and pile materials, respectively; ν is the

Poisson's ratio of the soil; w_{pj}, w_{sj}, and w_{bj} represent weight factors that together sum to unity for pile, soil, and pile tip stiffness contributions, respectively, for vibration mode j (details below); and a_0^p is a dimensionless frequency for piles (Kaynia and Kausel, 1982):

$$a_0^p = \frac{\omega d}{V_s} \tag{2-23}$$

Because a_0^p uses pile diameter in lieu of foundation half-width B, it is typically more than an order of magnitude smaller than a_0 (Equation 2-15) under the same cyclic frequency ω. A fundamental aspect of pile response to lateral head loading is that a long pile does not deflect over its entire length, but only to a certain depth, termed the active pile length, L_a (shown in Figure 2-10).

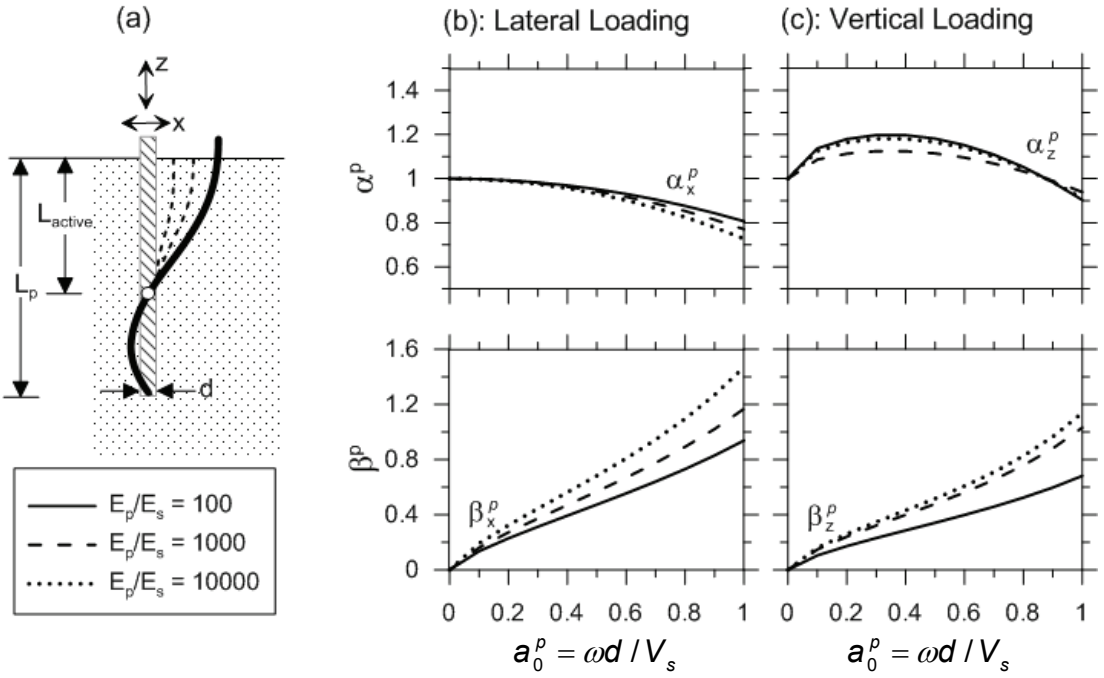

Figure 2-10 Plot of dynamic stiffness modifiers and damping ratios versus dimensionless frequency, for single piles in a homogeneous half-space, with ν=0.4 and ρ_p/ρ_s=1.3: (a) geometric parameters; (b) lateral loading; and (c) vertical loading.

The active pile length is on the order of 10 to 20 pile diameters, depending on pile-soil stiffness contrast, soil non-homogeneity, and fixity conditions at the pile head (Randolph, 1981; Gazetas, 1991; Pender 1993; Syngros 2004; Karatzia and Mylonakis 2012). Piles with lengths $L_p > L_a$ essentially behave as infinitely long beams, and the actual length does not affect flexural response. Active lengths tend to be greater for dynamic loading than for static loading, due to the ability of elastic waves to travel further down the pile than a static stress field.

Axially loaded piles tend to respond to much greater depths (in excess of 50 pile diameters), and tip reaction is almost always mobilized. Accordingly, an axially-loaded pile cannot usually be approximated by an infinite rod.

Expressions for active pile length for lateral deformations can be cast in the form:

$$L_a = \Lambda \left(\frac{E_p}{E_s} \right)^{\mu} d \tag{2-24}$$

where Λ and μ are dimensionless constants, and all other terms are as previously defined. For fixed-head piles in homogeneous soil under static loading, Randolph (1981) and Fleming et al. (1992) recommend $\Lambda = 1.8$ and $\mu = 0.25$. For dynamic loading, Gazetas (1991) recommends $\Lambda = 2$ and $\mu = 0.25$. Based on a more accurate set of finite-element analyses, Syngros (2004) recommends $\Lambda = 2.4$ and $\mu = 0.25$. A discussion about the differences in the various formulas for active length can be found in Karatzia and Mylonakis (2012). Approximate values of active pile lengths, L_a, are $10d$ to $20d$ for lateral loading, and the actual pile length, L_p, for axial loading.

Once an appropriate active length, L_a, is selected, an average effective profile velocity between the ground surface and depth, L_a, can be computed. These guidelines are approximate, and further research is needed to better define effective values of V_s for use in the analysis of pile impedance. Small-strain shear modulus, G_0, is then evaluated from shear wave velocity, V_s, as $G_0 = \rho_s V_s^2$ (from Equation 2-9). Soil shear modulus, G, should be reduced relative to G_0 for large strain effects (e.g., Table 2-1). Young's modulus for soil can then be related to shear modulus as:

$$E_s = 2(1+\nu)G \tag{2-25}$$

As an alternative to the use of Table 2-1 for evaluating modulus reduction effects, soil strains adjacent to a horizontally loaded pile can be evaluated as (Kagawa and Kraft, 1981):

$$\gamma(z) \approx \frac{(1+\nu)u(z)}{2.5d} \tag{2-26}$$

where $\gamma(z)$ denotes an average soil shear strain at depth z, and $u(z)$ the corresponding horizontal pile displacement. On the basis of this equation, a strain-compatible soil shear modulus can be obtained through conventional modulus reduction curves (e.g., Darendeli, 2001;Vucetic and Dobry, 1991).

Weight factors in Equation 2-22b (w_{pj}, w_{sj}, and w_{bj}) represent the relative contributions of the pile structural stiffness, pile-soil interaction through side-load transfer, and pile-soil interaction through toe resistance for vibration mode j. These weight factors always sum to unity (i.e., $w_{pj} + w_{sj} + w_{bj} = 1.0$), and are not required

for analysis of static stiffness. Individual weight factors are used, however, for dynamic modifiers and damping coefficients, as described below.

Equations related to the static stiffness of single piles are provided in Table 2-4a. The equations are used to determine dimensionless parameters χ_j and weight factors (w_{pj}, w_{sj}, and w_{bj}). Note that the equations for χ_j depend, in turn, on a series of additional dimensionless parameters. For lateral vibration ($j=x$), the additional variable is the dimensionless modulus of subgrade reaction, δ_x, which is related to E_p/E_s as indicated in the table. For vertical vibration ($j=z$), the additional variables are Ω and λL_p (both related to E_p/E_s), and the corresponding modulus, δ_z. Equations for dynamic stiffness modifiers (α_j^p terms) and damping ratios (β_j^p terms) for single piles are provided in Table 2-4b.

Damping ratios reflect material damping in the pile and soil materials (β_p and β_s, respectively) as well as radiation damping (β_{rj} terms). The dynamic stiffness modifiers and radiation damping ratios for single piles obtained from these expressions are plotted in Figure 2-10.

2.3.2 Impedance of Grouped Piles

When piles are used as part of a building foundation system, they are usually configured in groups to support continuous mat foundations or discrete pile caps for individual load-bearing elements. The impedance of a pile group cannot be determined by simple addition of individual pile impedances because grouped piles interact through the soil by "pushing" or "pulling" each other through waves emitted from their periphery. This is called a *group effect*, and it can significantly affect the impedance of a pile group as well as the distribution of head loads among individual piles in the group. Group effects depend primarily on pile spacing, frequency, and number of piles. They are more pronounced in the elastic range, and dynamic group effects decrease in the presence of material nonlinearity.

The ratio of the pile group impedance in any oscillation mode, k_j^G, to the sum of the individual static pile impedances in the same oscillation mode, $N_{piles} \times k_{j,static}^P$, is the *efficiency factor* of the pile group (Kaynia and Kausel, 1982). Efficiency factors are generally less than unity for low frequencies, but can increase significantly at higher frequencies under low strain conditions. Negative efficiency factors are also possible, which suggests a phase difference of over 90 degrees between oscillations of a single pile and oscillations of the pile group at the same frequency. Note that these factors strictly refer to dynamic compliance of the group and are different from the familiar efficiency factors for group bearing capacities in foundation engineering.

Table 2-4a Equations for Static Stiffness of Single Piles

Degree of Freedom	Surface Stiffness Modifiers	Reference
Translation along x-axis	$\chi_x = \frac{1}{2}\pi^{1/4}\delta_x^{3/4}\left(\frac{E_p}{E_s}\right)^{1/4}$	Poulos and Davis (1980) Scott (1981), Mylonakis (1995)
	$\delta_x = 2\left(\frac{E_p}{E_s}\right)^{-3/40}$	Dobry et al. (1982) Syngros (2004)
	$\left.\begin{array}{l} w_{px} = 1/4 \\ w_{sx} = 3/4 \\ w_{bx} = 0 \end{array}\right\}$ *Long pile* $(L_p / d > L_{active})$	Dobry et al. (1982) Mylonakis (1995) Mylonakis and Roumbas (2001)
Translation along z-axis	$\chi_z = \left(\frac{\pi\delta_z}{2}\right)^{1/2}\left(\frac{E_p}{E_s}\right)^{1/2}\frac{\Omega + \tanh(\lambda L_p)}{1+\Omega\tanh(\lambda L_p)}$	Randolph and Wroth (1978) Scott (1981)
	$\Omega = \frac{2}{\left(\sqrt{\pi\delta_z}\right)\left(1-\nu^2\right)}\left(\frac{E_p}{E_s}\right)^{-1/2}$	Mylonakis and Gatezas (1998), Randolph (2003), Salgado (2008)
	$\lambda L_p = \left(\frac{4\delta_z}{\pi}\right)^{\frac{1}{2}}\left(\frac{E_p}{E_s}\right)^{-\frac{1}{2}}\left(\frac{L_p}{d}\right)$	
	$\delta_z = 0.6 \;\; ; \;\; \left(L_p / d > 10,\ E_p / E_s > 100\right)$	Blaney et al. (1975) Roesset (1980) Thomas (1980)
	$w_{pz} = 1-\left(w_{sz} + w_{bz}\right)$	
	$w_{sz} = \frac{-2\left[\left(\lambda L_p\right)\left(\Omega^2-1\right)+\Omega\right]+2\Omega\cosh\left(2\lambda L_p\right)+\left(1+\Omega^2\right)\sinh\left(2\lambda L_p\right)}{4\cosh^2\left(\lambda L_p\right)\left[\Omega+\tanh\left(\lambda L_p\right)\right]\left[1+\Omega\tanh\left(\lambda L_p\right)\right]}$	
	$w_{bz} = \frac{2\Omega}{2\Omega\cosh\left(\lambda L_p\right)\left(1+\Omega^2\right)\sinh\left(\lambda L_p\right)}$	

Table 2-4b Equations for Dynamic Stiffness Modifiers and Damping Ratios for Single Piles

Degree of Freedom	Static Stiffness Modifier	Reference
Translation along x-axis	$\alpha_x^p = 1 - \frac{3\pi}{32\delta_x}\left(\frac{\rho_p/\rho_s}{1+\nu}\right)\left(a_o^p\right)^2$	Mylonakis and Roumbas (2001)
Translation along z-axis	$\alpha_z^p = 1 - w_{sz}\left[\left(\frac{\pi}{8\delta_x}\right)\left(\frac{\rho_p/\rho_s}{1+\nu}\right)\left(a_o^p\right)^2 - \frac{1}{2}\left(a_o^p\right)^{1/2}\right]$	Mylonakis (2011)

Degree of Freedom	Damping Ratio	Reference
Translation along x-axis	$\beta_x^p = \frac{1}{4}\beta_p + \frac{3}{4}\beta_s + \frac{3}{4}\beta_{rx}$	Dobry et al. (1982) Mylonakis and Roumbas (2001)
	$\beta_{rx} = \left[\frac{3}{2\alpha_x(1+\nu)\delta_x}\right]\left(a_o^p\right)^{3/4}$	Gazetas and Dobry (1984a,b)
Translation along z-axis	$\beta_z^p = w_{pz}\beta_p + \left(w_{sz} + w_{pz}\right)\beta_s + \beta_{rz}$	Mylonakis (2011)
	$\beta_{rz} = \frac{1}{\alpha_z^p}\left[w_{sz}\frac{1.2\pi}{4(1+\nu)\delta_z}\left(a_o^p\right)^{3/4} + w_{bz}0.21a_o^p\right]$	Gazetas and Dobry (1984b)

Results for horizontal and rocking oscillations are provided in Figure 2-11 for pile groups in square configurations computed using the solution by Mylonakis and Gazetas (1999). Peaks and valleys observed in the plots are due to destructive and constructive interference of the waves between piles, which tend to increase and decrease in dynamic impedance, as first identified by Wolf and Von Arx (1978), and explained by Kaynia and Kausel (1982), Nogami (1983), and Dobry and Gazetas (1988).

The above effects tend to decrease with non-homogeneity and nonlinearity in the soil, as the waves emitted from the periphery of the piles become less coherent (El-Naggar and Novak, 1994 and 1995; Michaelides et al., 1998). At the low normalized frequencies of interest in most practical problems ($a_0^p \le 0.4$), efficiency factors are less than one and saturate as the number of piles, N_{piles}, increases. Hence, for large piles groups, low-frequency efficiencies would not be significantly lower than those shown for the 4×4 pile group in Figure 2-11. Efficiency factors above unity for the rocking mode are due to the intrinsic out-of-phase movement of the piles located on opposite sides of the rocking axis.

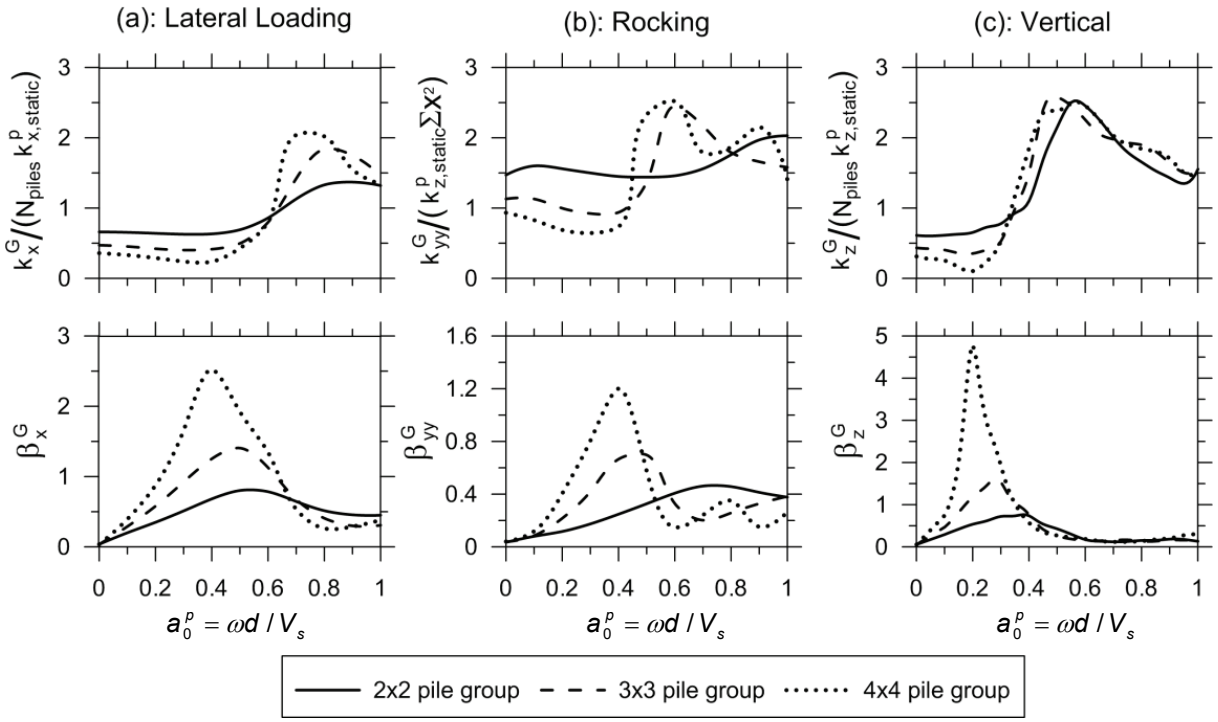

Figure 2-11 Plots of pile group efficiency factors and damping ratios versus dimensionless frequency for square pile groups for: (a) lateral loading at head of pile group under zero cap rotation; (b) moment at head of pile group, introducing rocking under zero cap translation; and (c) vertical loading at head of pile group. Lateral and rocking results are for E_p/E_s = 1000, L_p/d = 20, ρ_p/ρ_s = 1.3, ν =0.4, (pile spacing)/d = 5, β_p = 0, and β_s = 0.05. Vertical resutls are for E_p/E_s = 100, L_p/d = 15, ρ_p/ρ_s = 1.4, ν = 0.4, (pile spacing)/d = 5, β_p = 0, and β_s = 0.05.

In Figure 2-12, the group impedance of a 3×3 pile group is compared to that of a footing of equivalent dimensions. Results are presented relative to a common normalized frequency using the conversion:

$$a_0 = a_0^P \frac{B}{d} \tag{2-27}$$

Results show that the effect of the piles is dramatic for rotational stiffness, increasing k_{yy} by factors up to 50 relative to a shallow footing alone. Translational stiffness is also increased, but to a lesser degree. Interestingly, damping ratios are on the same order of magnitude, with somewhat greater variation with frequency caused by pile-to-pile interaction effects.

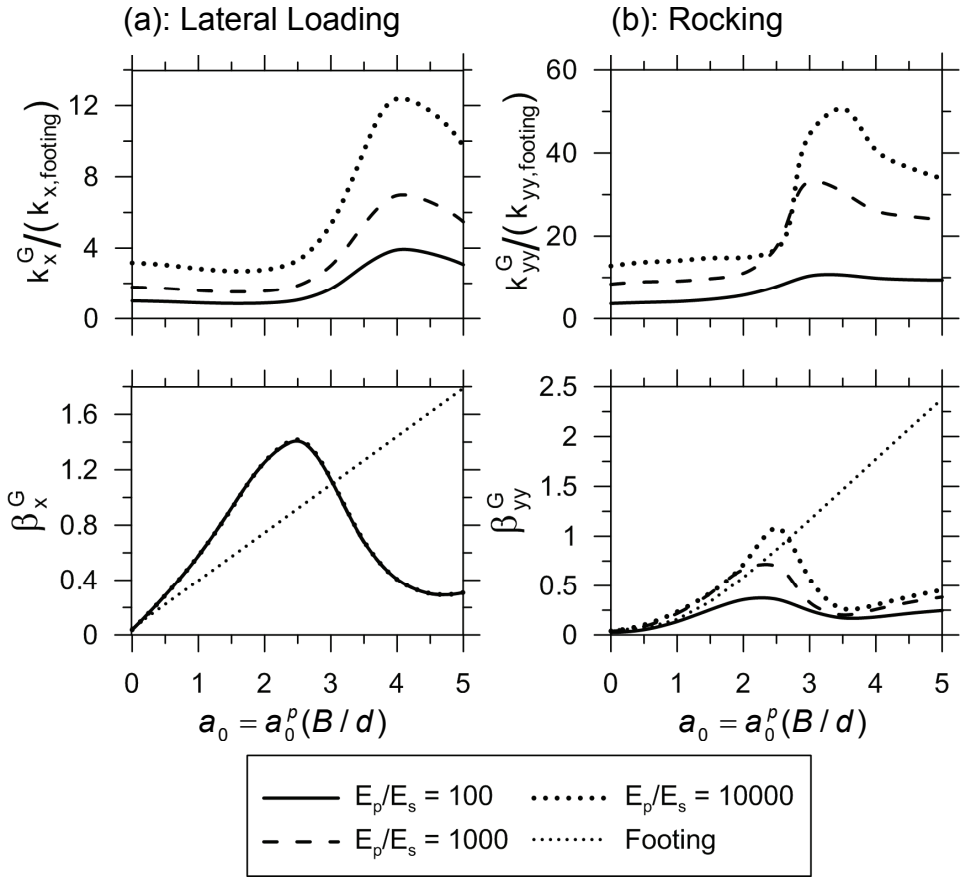

Figure 2-12 Comparison between the impedance (stiffness and damping ratio) of a 3x3 pile group and the impedance of a footing with equivalent dimensions for: (a) lateral loading at head of pile group; and (b) moment at head of pile group, introducing rocking. Results are for L_p/d = 20, ρ_p/ρ_s = 1.3, ν =0.4, (pile spacing)/d = 5, β_p = 0, and β_s = 0.05.

2.3.3 Discrete Element Methods (p-y and t-z Curves)

In engineering practice, piles are typically modeled using discrete element methods, as prepared in common commercial computer programs such as APILE (Ensoft, Inc. program for analysis of axial capacity of piles) and LPILE (Ensoft, Inc. program for analysis of piles under lateral loads). In such programs, it is straightforward to extract head load-deflection relationships from the analysis, which are often used in lieu of elasto-dynamic solutions described above.

Unfortunately, the *p-y* (nonlinear lateral spring) and *t-z* (nonlinear vertical spring) relations used in these programs were developed to represent large-deformation response in static or cyclic loading, and they do not accurately capture stiffness or damping. In fact, many spring formulations have an initial stiffness that is infinite (i.e., the backbone curve is vertical at the origin). When the pile-soil system is not expected to yield, the elasto-dynamic solutions presented above provide a superior

representation of stiffness and damping. Research is needed to develop next-generation *p-y* and *t-z* curves that capture these stiffness formulations at small displacements and soil nonlinearity.

2.4 Nonlinear Soil-Structure Interaction Models for Response History Analysis

Nonlinear soil-structure interaction phenomena can involve geometric and material nonlinearities in the superstructure, foundation, and soil. Specific sources of nonlinearity may include: (1) yielding of seismic-force-resisting elements in the superstructure; (2) yielding of soil, potentially exacerbated by strength loss induced by pore-pressure (e.g., liquefaction, cyclic softening); (3) gapping between the foundation and the soil, such as base uplift or separation of foundation sidewalls from the surrounding material; and (4) yielding of foundation structural elements. These nonlinear effects must be computed with response history analyses (RHA) performed in the time domain. Addressing all these issues in RHA is a formidable task, even with modern computational capabilities. Despite recent progress, knowledge in the area is incomplete and the subject is evolving.

Most of the research performed on nonlinear SSI has been related to structural yielding with linear, or equivalent-linear, soil (Case 1, above) or soil yielding/gapping with a linear structure (Case 2/Case 3, above). A brief overview of this work is presented in the following sections.

2.4.1 Nonlinear Structure and Equivalent-Linear Soil

Because of difficulties associated with modeling the constitutive behavior of soil in three dimensions and wave propagation in a finite volume of geologic material under the structure, without spurious wave reflections at fictitious model boundaries, most studies focus on nonlinearities in the superstructure. If structural yielding develops at relatively low intensity input motions, or if the foundation is over-designed, significant material nonlinearities in the foundation and soil may not occur. This justifies the use of equivalent-linear representations of subsurface material properties in such analyses.

In a series of studies involving response of yielding simple oscillators, supported on foundations resting on linear or equivalent-linear soil, subjected to strong earthquake excitations, Ciampoli and Pinto (1995), Mylonakis and Gazetas (2000), Perez-Rocha and Aviles (2003) among others, concluded that nonlinear SSI generally reduces ductility demand in the superstructure. This effect can be rationalized using principles for linear SSI presented in Figure 2-3. When the period is lengthened on the descending branch of the spectrum (i.e., $T/T_p > 1$), the seismic demand is reduced, regardless of whether the structure yields or not.

In the case of long-period input motions that potentially place the structure on the ascending branch of the spectrum (i.e., $T/T_p < 1$), SSI-induced period lengthening may lead to an increase in ductility demand. This can be viewed as progressive resonance, when the effective fundamental period of the yielding structure, T, approaches the predominant period of the foundation input motion, T_p. Evaluation of the damping effects is more complex as nonlinearity tends to reduce radiation damping and increase material damping in both the soil and the structure.

The performance of yielding structures is typically represented in terms of: (1) the global or system ductility demand, μ_s; or (2) the conventional member ductility demand, μ (Priestley and Park, 1987; Paulay and Priestley, 1992). For the structure in Figure 2-1, these factors are defined as:

$$\mu_s = \frac{\tilde{\Delta}_{\max}}{\tilde{\Delta}_y} \tag{2-28}$$

$$\mu = \frac{\Delta_{\max}}{\Delta_y} \tag{2-29}$$

where $\tilde{\Delta}_{\max}$, $\tilde{\Delta}_y$, $\Delta_{\max}$, Δ_y are the maximum earthquake-induced displacement at the top of a structure, the corresponding displacement at yield, the maximum earthquake-induced column displacement relative to a rotated foundation, and the corresponding column displacement at yield, respectively.

A key difference between these factors is that member ductility demand, μ, refers exclusively to structural deformations, whereas global or system ductility demand, μ_s, encompasses rigid body movements associated with translation and rotation of the foundation, which do not reflect strains in the superstructure. Equation 2-28 and Equation 2-29 are geometric relations, and the former always provides smaller numerical values than the latter for a given set of structural response values (Ciampoli and Pinto, 1995; Mylonakis and Gazetas, 2000). Because of this, the use of Equation 2-28 for assessing SSI effects on structural response might be of limited value.

2.4.2 Nonlinearity in the Foundation and Soil

There is mounting analytical and experimental evidence that material and geometric nonlinearities in the soil may be beneficial to the seismic response of a structure. This has led some authors (e.g., Gazetas, 2006; Gajan and Kutter, 2008) to propose revising the foundation design philosophy by allowing significant yielding in the soil close to the foundation, or the foundation itself, to dissipate energy and protect the superstructure. This requires control of settlement and tilting of the structure. Hence, the analysis and design process considering soil nonlinearity involves optimization of the trade-offs between the potentially beneficial effects of soil

yielding (especially with regard to energy dissipation) and the detrimental effects of settlement or residual tilt. In this section, several methods are described by which calculations of this type can be carried out.

Soil-structure interaction studies with nonlinear soil and foundation behavior can be classified into three approaches: (1) continuum models, (2) beam-on-nonlinear winkler foundation (BNWF) models, and (3) plasticity-based macro-models. The first approach is by far the most computationally demanding, and has been employed to a limited extent (Borja and Wu, 1994; Jeremic et al., 2009). Available findings suggest the creation of stress-induced inhomogeneities under the foundation, which may limit wave radiation away from the structure and cause wave reflections leading to resonance effects.

The second and third approaches for nonlinear soil modeling are briefly described below. Although both approaches can consider material nonlinearities, only macro-element approaches are currently configured for material nonlinearities (gapping). The basic description of the models, their input parameters, and a brief comparison with experimental data are provided. The reader is referred to related literature for additional information. The emphasis in the following discussion is on two specific models that are implemented in OpenSees, *Open System for Earthquake Engineering Simulation* (McKenna, 1997; OpenSees, 2011). Their implementation could be reasonably extended to other computational platforms in the future. Much of the content is adapted from Gajan et al. (2010).

Beam-on-Nonlinear Winkler Foundation (BNWF) Models

Starting with the pioneering work of McClelland and Focht (1958), beam-on-nonlinear winkler foundation (BNWF) models have been used for many years for analyzing the response of foundations, most notably piles, for static loads (Matlock, 1970; Cox et al., 1974) and dynamic loads (Penzien, 1970; Nogami et al., 1992; Boulanger et al., 1999). Key advantages of these models over continuum formulations lies in their ability to describe soil-structure interaction phenomena by one-dimensional nonlinear springs distributed along the soil-foundation interface. It is well-known that the modulus of the springs (also known as modulus of sub-grade reaction) is not uniquely a soil property, but also depends on foundation stiffness, geometry, frequency, response mode, and level of strain. A limitation of the approach relates to its one-dimensional nature. A spring responds only to loads acting parallel to its axis, so loads acting in a perpendicular direction have no effect on the response of the spring. Accordingly, the concept of plastic potential and flow rule cannot be explicitly incorporated. Nevertheless, the BNWF approach is popular because of its simplicity and predictive abilities on a variety of problems.

The impedance models described in Section 2.2 are associated with linear springs that can be coupled with gapping and damper elements (e.g., implemented by Chopra and Yim, 1985). Nonlinear springs for shallow foundations have been used in conjunction with gapping and damper elements by Allotey and Naggar (2003 and 2007) as well as Raychowdhury and Hutchinson (2009).

The BNWF model implemented into OpenSees by Raychowdhury and Hutchinson (2009) consists of elastic beam-column elements that capture the structural footing behavior with independent zero-length soil elements that model the soil-footing behavior. Currently it is developed for two-dimensional analysis only. Therefore, the one-dimensional elastic beam-column elements used for the footing have three degrees-of-freedom per node (i.e., horizontal, vertical, and rotation). As illustrated in Figure 2-13, one-dimensional uniaxial springs are used to simulate the vertical load-displacement behavior (*q*-*z*), horizontal passive load-displacement behavior against the side of a footing (*p*-*x*), and horizontal shear-sliding behavior at the base of a footing (*t*-*x*). Moment-rotation behavior is captured by distributing vertical springs along the base of the footing.

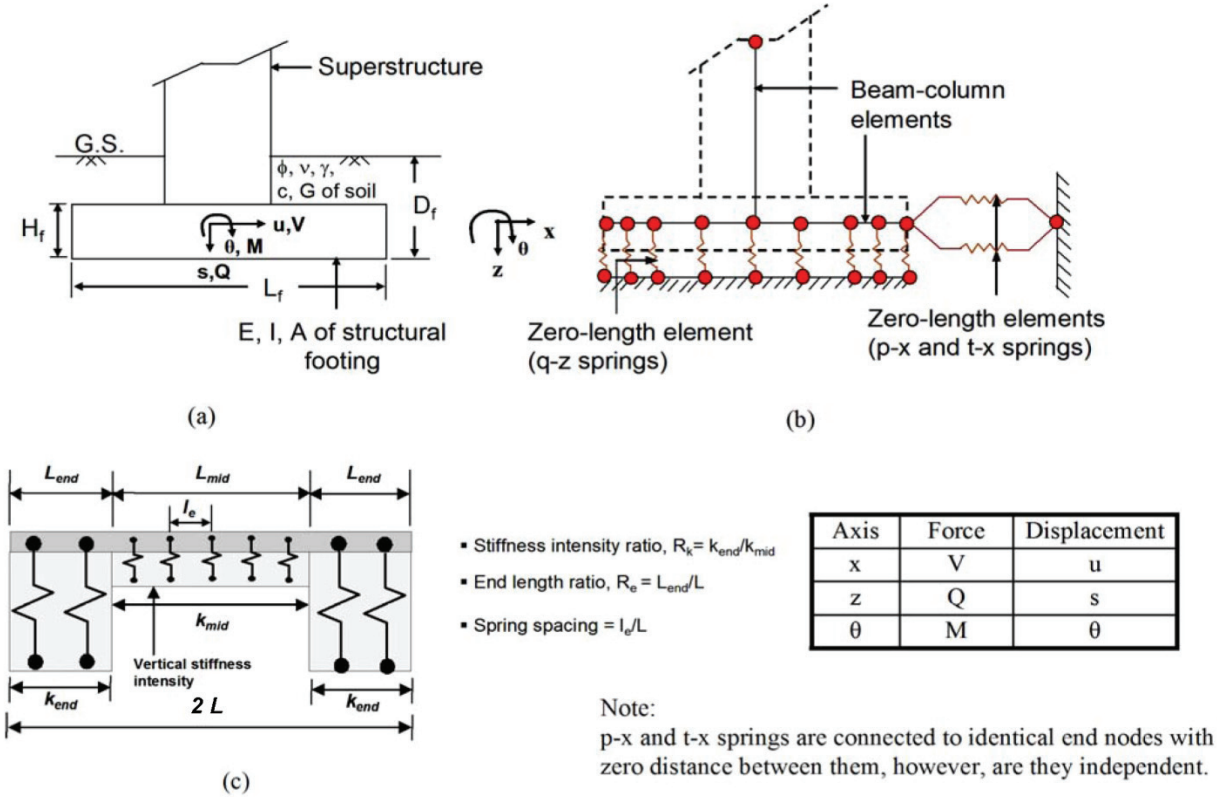

Figure 2-13 Schematic illustration of a Beam-on-Nonlinear Winkler Foundation (BNWF) model: (a) hypothesized foundation-superstructure system; (b) idealized model; and (c) variable vertical stiffness distribution (Raychowdhury and Hutchinson, 2009, with permission).

The mathematical model of the *q-z, p-x,* and *t-x* nonlinear springs in Figure 2-13 was adapted from a model for pile foundations by Boulanger et al. (1999). Within the OpenSees framework, the materials describing these springs are the *QzSimple2*, *PxSimple1*, and *TxSimple1* material models, respectively. The *QzSimple2*, *PxSimple1*and *TxSimple1* material models differ from their parent (pile-calibrated) models (*QzSimple1*, *PySimple1*, and *TzSimple1*) only in the backbone shape parameters. Each material captures the "far-field" elastic behavior and "near-field" permanent displacements.

The material models are mechanistic, based on an arrangement of various linear and nonlinear springs, gap elements, and dashpots. Radiation damping can be accounted for using a dashpot that is placed in parallel with the far-field elastic component. The backbone curves are thus characterized by a linear-elastic region, followed by an increasingly growing nonlinear region. The *QzSimple2* material has an asymmetric hysteretic response, with a backbone curve defined by an ultimate load on the compression side and a reduced strength in tension to account for the low strength of soil in tension. The *PxSimple1* material is envisioned to capture the passive resistance, associated stiffness, and potential gapping of embedded shallow footings subjected to lateral loads. This material model is characterized by a pinched hysteretic behavior, which can more suitably account for the phenomena of gapping during unloading on the opposite side of a footing. The *TxSimple1* material is intended to capture the frictional resistance along the base of a shallow foundation. This material is characterized by a large initial stiffness and a broad hysteresis, as anticipated for frictional behavior associated with foundation sliding.

The functional forms and parameters describing the *p-x*, *t-x*, and *q-z* springs are similar, so only the *q-z* model is described here. The backbone curve has linear and nonlinear regions. The linear-elastic portion of the backbone curve is described by the initial stiffness k_z:

$$q = k_z s \tag{2-30}$$

where q represents the spring force, and s represents the spring deflection. The upper limit of the linear-elastic region, defined as q_0, is taken as a fraction of the ultimate load q_{ult} as follows:

$$q_0 = C_r q_{ult} \tag{2-31}$$

where C_r is a parameter specified in OpenSees. The nonlinear (post-yield) portion of the backbone is described by:

$$q = q_{ult} - \left(q_{ult} - q_0\right)\left[\frac{cs_{50}}{cs_{50} + \left|s - s_0\right|}\right]^n \text{ (for } |s| > s_0\text{)} \tag{2-32}$$

where s_{50} is the displacement at which 50% of the ultimate load is mobilized, s_0 is the displacement at load q_0, and both c and n are constitutive parameters controlling the shape of the post-yield portion of the backbone curve.

The unload-reload rules that operate with the backbone curve are relatively simple, generally consisting of the familiar Masing rules (i.e., the shape of the unload and reload portion of the cyclic loop matches twice the backbone curve). The drag and gap component is parameterized by a bilinear closure spring in parallel with a nonlinear drag spring. The cyclic response of each of the material models, when subjected to a sinusoidal displacement, is demonstrated in Figure 2-14.

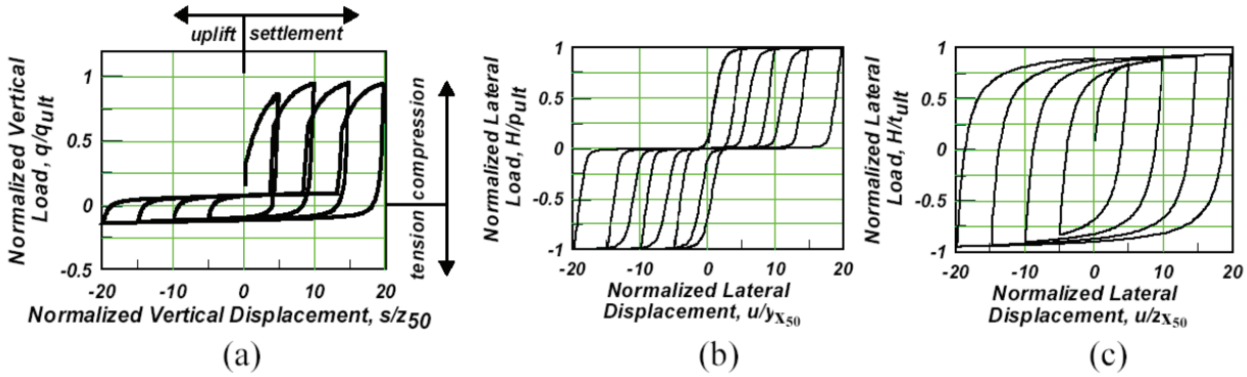

Figure 2-14 Cyclic response of OpenSees BNWF springs subjected to a sinusoidal displacement: (a) *q–z* spring (*Qzsimple2* material model); (b) *p–x* spring (*Pxsimple1* material model); and (c) *t–x* spring (*Txsimple1* material model) (Raychowdhury and Hutchinson, 2009, with permission).

User-defined parameters for the *q-z* element can be synthesized based on two physical parameters obtained from the results of a typical high-quality geotechnical site investigation (i.e., bearing capacity, q_{ult}, and elastic stiffness, k_z) and several relatively subtle parameters defining the details of the elements described above. The need for several relatively unfamiliar parameters presents a barrier to implementation of this type of model in practice. These parameters include:

- **Radiation damping (c_z).** This dashpot coefficient is considered to be a physical parameter that is well documented in the literature (e.g., Section 2.2). The parameter is sensitive to soil stiffness, footing shape, aspect ratio and embedment.
- **Tension capacity (*TP*).** The tension capacity parameter, *TP*, determines the maximum magnitude of the drag force in Component 1 of the nonlinear springs. It is the ratio of tension capacity to bearing capacity with typical selected values of 0 to 0.10 (as suggested in Boulanger et al., 1999), although, more recently some experts (e.g., Kutter) have recommended using a *TP* value of zero.
- **Distribution and magnitude of vertical stiffness.** As illustrated in Figure 2-8 and Figure 2-13, two parameters are necessary to account for the distribution and

magnitude of the vertical stiffness along the length of a footing: (1) the stiffness intensity ratio, R_k (where, $R_k=K_{end}/K_{mid}$); and (2) the end length ratio, R_e (where, $R_e=L_{end}/2L$). A variable stiffness distribution along the length is used to force the distributed BNWF spring model to match the overall rotational stiffness (Equations 2-21). The end region, L_{end}, is defined as the length of the edge region over which the stiffness is increased. ATC-40, *Seismic Evaluation and Retrofit of Concrete Buildings* (ATC, 1996) suggests the use of $L_{end} = B/6$ from each end of the footing. This expression of end length ratio is independent of the footing aspect ratio. Harden and Hutchinson (2009) suggest an expression that is a function of the footing aspect ratio.

- **Spring spacing (*S*).** The spring spacing is input by the user as a fraction of the footing half-length L ($S = l_e/L$), where l_e is the non-normalized spring spacing. A maximum element length equal to 8% of the footing half-length (i.e., a minimum number of 25 springs along the full length of the footing) is recommended to provide numerical stability and reasonable accuracy.
- **Shape parameters (C_r, c, n).** These parameters are hard-wired into the OpenSees implementation of the material models, meaning that they are not specified by users. The recommended values are soil-type dependent, and were developed based on comparisons of model predictions to test data as described by Raychowdhury and Hutchinson (2008).

Figure 2-15 shows a comparison of the BNWF model of Raychowdhury and Hutchinson (2009) to results from centrifuge test SSG04–06 conducted at the University of California at Davis (summarized in Thomas et al., 2005). This test was a slow, cyclic test conducted on a medium aspect ratio ($M / (V \times L) = 2.4$) shearwall building, with a vertical factor of safety, $FS_v = 2.3$, resting on dense sand with $D_r =$ 80%. In these tests, M is the moment applied by the horizontal force, V, at the level of the soil-foundation interface. Figures 2-15a through 2-15d show moment versus rotation, settlement versus rotation, shear force versus sliding, and settlement versus sliding histories, as predicted by the model and compared with the experiment. The model compares reasonably well with the experimental results in terms of capturing the shapes of the hysteresis loops and rotational and lateral stiffnesses. Additional comparisons are provided in Raychowdhury (2008).

Plasticity Based Macro-Element (PBM) Models

Plasticity Based Macro-Element (PBM) theory is a recent development (Nova and Montrasio, 1991) with application to nonlinear response of rigid foundations. This family of models combines elements from both continuum and BNWF formulations. Hence, it aims at bridging the gap between the two approaches. The models are based on the following main assumptions: (1) the foundation is considered sufficiently rigid, so its response can be described by three or six degrees of freedom

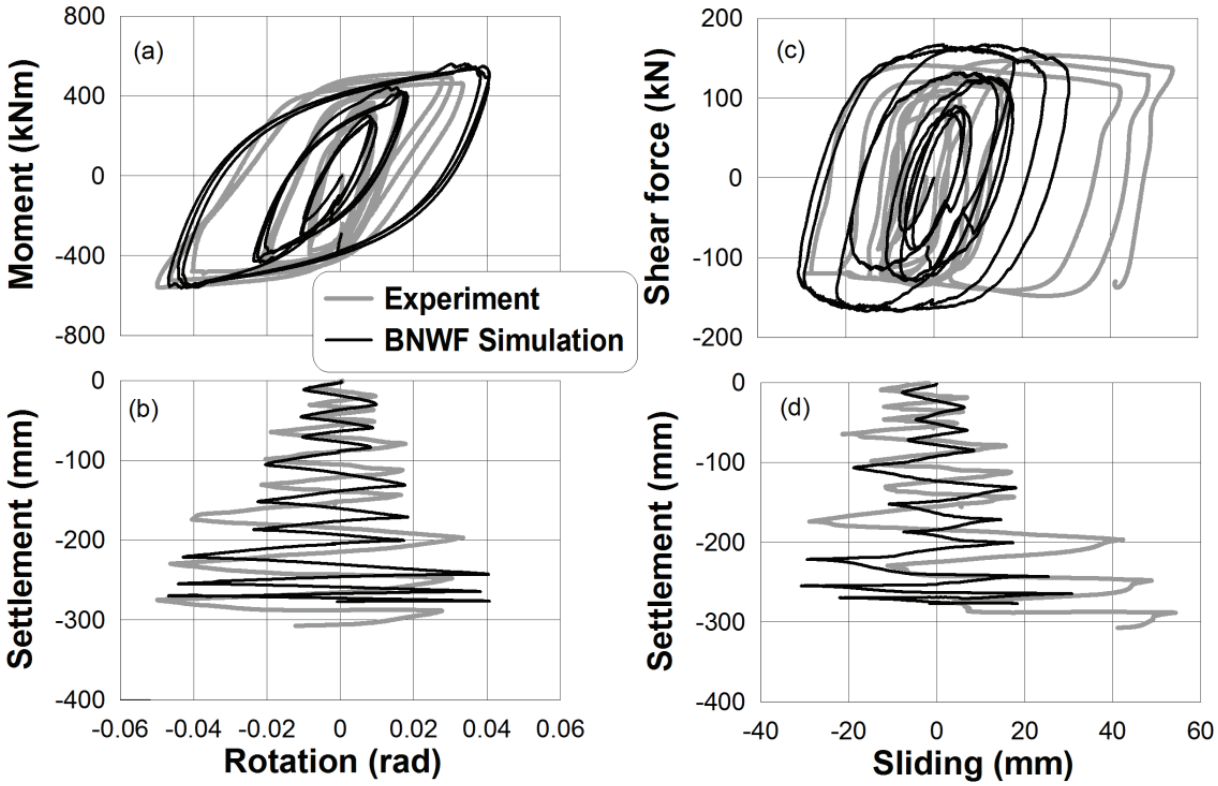

Figure 2-15 Comparison of BNWF model response to centrifuge tests for a medium aspect ratio building on dense sand, with D_r = 80%, and FS_v = 2.3: (a) moment-rotation; (b) settlement-rotation; (c) shear-sliding; and (d) settlement-sliding (Raychowdhury and Hutchinson, 2009, with permission).

in two and three dimensions, respectively; (2) an ultimate surface, corresponding to a general bearing capacity failure in vertical force–shear force–moment (Q-V-M) space, exists corresponding to the state of stress beyond which plastic flow occurs; (3) a mechanism for describing plastic flow is incorporated in the form of a hypo-plastic approach or a simple G-γ and β_s-γ correction based on a characteristic shear strain; and (4) uplift behavior can be modeled by means of a nonlinear model allowing for separation between the footing and soil (Pecker and Chatzigogos, 2010).

While PBM models are rational and can capture plastic effects, available formulations possess a number of drawbacks, notably an inability to incorporate flexible foundation behavior, the effects of stress-induced inhomogeneity on radiation damping, and failure modes other than general shear failure. In addition, there is limited experimental validation of the models. More details are given in Cremer et al. (2001), Houlsby and Cassidy (2002), Chatzigogos et al. (2009) and Pecker and Chatzigogos (2010). A variant of these models, focusing on uplift phenomena in compliant soil, is examined in some detail below.

Macro-element models describe a single element placed at the interface between a rigid foundation and free-field soil to represent the flexibility and energy dissipation

associated with soil-structure interaction. From a numerical modeling standpoint, the macro-element is directly located at the footing-soil interface, replacing the rigid foundation and surrounding soil. When incremental displacements are given to the macro-element as input, it returns the corresponding incremental loads, and vice versa. Figure 2-16 shows an example of a contact interface model (CIM) developed by Gajan and Kutter (2009).

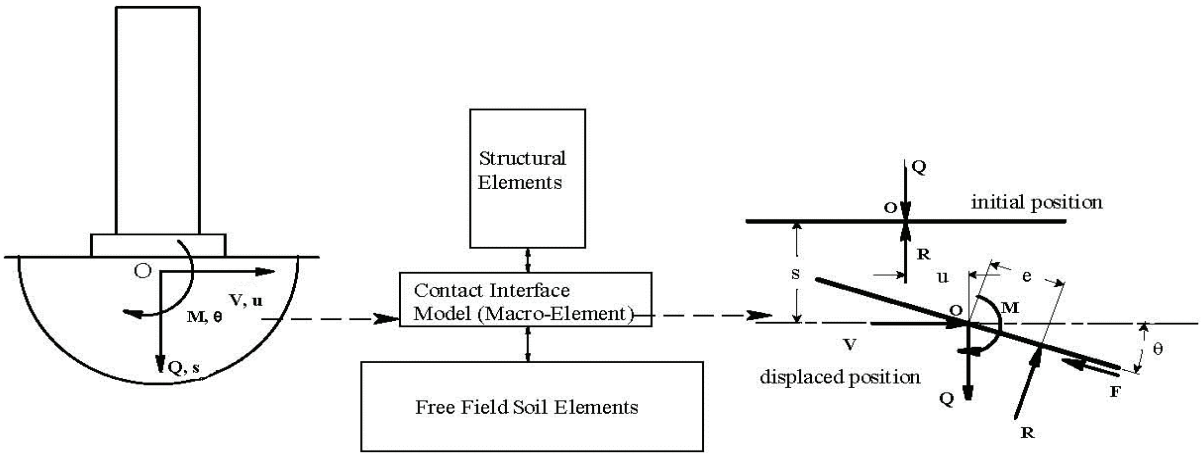

Figure 2-16 Conceptual illustration of a macro-element contact interface model (CIM) (Gajan and Kutter, 2009, with permission from ASCE).

The model differs from other macro-element models in that its constitutive relations are obtained by tracking the geometry of gaps and contacts of the soil-foundation interface. To this end, the CIM provides nonlinear relations between cyclic loads and displacements of the soil-foundation system during combined cyclic loading (i.e., vertical, shear, and moment).

Soil-foundation contact is tracked in the CIM using a parameter called the critical contact area ratio, A/A_c, where A is the area of the footing, and A_c is the area of the footing required to have contact with the soil to support the vertical and shear loads. The ratio A/A_c can be considered to be an alternate definition of the factor of safety with respect to bearing capacity. For a two-dimensional shear wall structure loaded in the plane of the wall, the ratio A/A_c equals the footing length ratio $2L/L_c$, as shown in Figure 2-17a. In Figure 2-17b, the foundation position is tracked relative to the underlying soil surface, which is pushed as far as the "soil_max" surface, but which rebounds to the "soil_min" surface when unloaded. Zero stress transfer between the soil and foundation occurs in the gap region.

With seven user-defined input parameters, the CIM is intended to capture the essential features (load capacities, stiffness degradation, energy dissipation, and permanent deformations) of the cyclic load-deformation behavior of shallow foundations. One advantage of the CIM relative to the BNWF model is that the

moment, shear, and vertical load capacities are coupled. Coupling between the vertical and moment capacities is caused by gap formation (i.e., the moment capacity typically occurs after a gap has formed, causing the vertical capacity to drop). The coupling between shear and moment capacity is accounted for using an interaction diagram as described by Gajan and Kutter (2009).

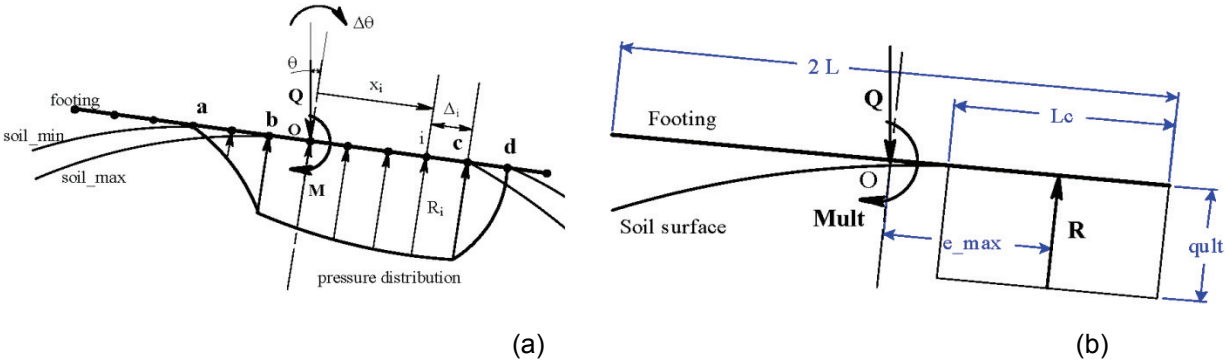

Figure 2-17 Contact interface model (CIM): (a) definition of critical contact length; and (b) tracking of foundation position relative to soil pressures (Gajan and Kutter, 2009, with permission from ASCE).

Input parameters for the CIM are the ultimate vertical load, Q_{ULT}, the length of footing, $2L$, the initial vertical stiffness, K_v, the initial horizontal stiffness, K_h, the elastic rotation limit, $\theta_{elastic}$, the rebound ratio, R_v, and the internal node spacing, D_L. The initial rotation stiffness is calculated by the CIM based on the specified vertical stiffness and footing geometry. Of those parameters, $\theta_{elastic}$, R_v, and D_L are relatively subtle, and are briefly described below:

- **Elastic rotation limit ($\theta_{elastic}$).** The elastic rotation limit is defined as the maximum amplitude of rotation for which no settlement occurs. A value of 0.001 radians is recommended based on comparisons with centrifuge experiments (Gajan et al., 2008).
- **Rebound ratio (R_v).** The rebound ratio, R_v, is an empirical factor that accounts for the elastic rebound and bulging of soil into the gap below an uplifted footing. It is the ratio of the soil uplift displacement (from rebound) to the total soil settlement, and significantly affects the length of the transition zone between the gap and the full foundation pressure zone shown in Figure 2-17b. The default value is 0.1, which reasonably fits data from available centrifuge model tests. Increasing R_v reduces cyclic foundation settlement, and improves numerical convergence in most cases.
- **Footing node spacing (D_L).** The node spacing, D_L, specifies the distance between footing nodes internally created within the model. This user-defined parameter affects numerical stability and accuracy as well as computation time. Node spacing should be selected based on the vertical factor of safety, FS_v;

foundations with large FS_v require small node spacing, D_L. The suggested range for D_L varies from 1.0% of the half-length, L, of the footing (for $FS_v \approx 2$) to 0.1% (for $FS_v \approx 40$).

A number of additional parameters describing the shape of the moment-shear interaction diagram and the shape of transition curves between elastic and yielding states are hard-wired into the OpenSees source code for this element, as described in Gajan and Kutter (2009).

Figure 2-18 shows a comparison of the CIM model to results from centrifuge test SSG02–05 conducted at the University of California at Davis (summarized in Gajan et al., 2003). This test was a static cyclic test conducted on a medium aspect ratio ($M / (V \times L) = 3.44$) shearwall building, with a vertical factor of safety, $FS_v = 2.6$, resting on dense sand with $D_r = 80\%$. Figures 2-18a through 2-18d show moment versus rotation, settlement versus rotation, shear force versus sliding, and settlement versus sliding histories, as predicted by the model and compared with the experiment. The CIM demonstrates good comparison with the experimental results in terms of capturing the shapes of the hysteresis loops and rotational and lateral stiffnesses. Additional comparisons are presented in Gajan (2006) and Gajan et al. (2008).

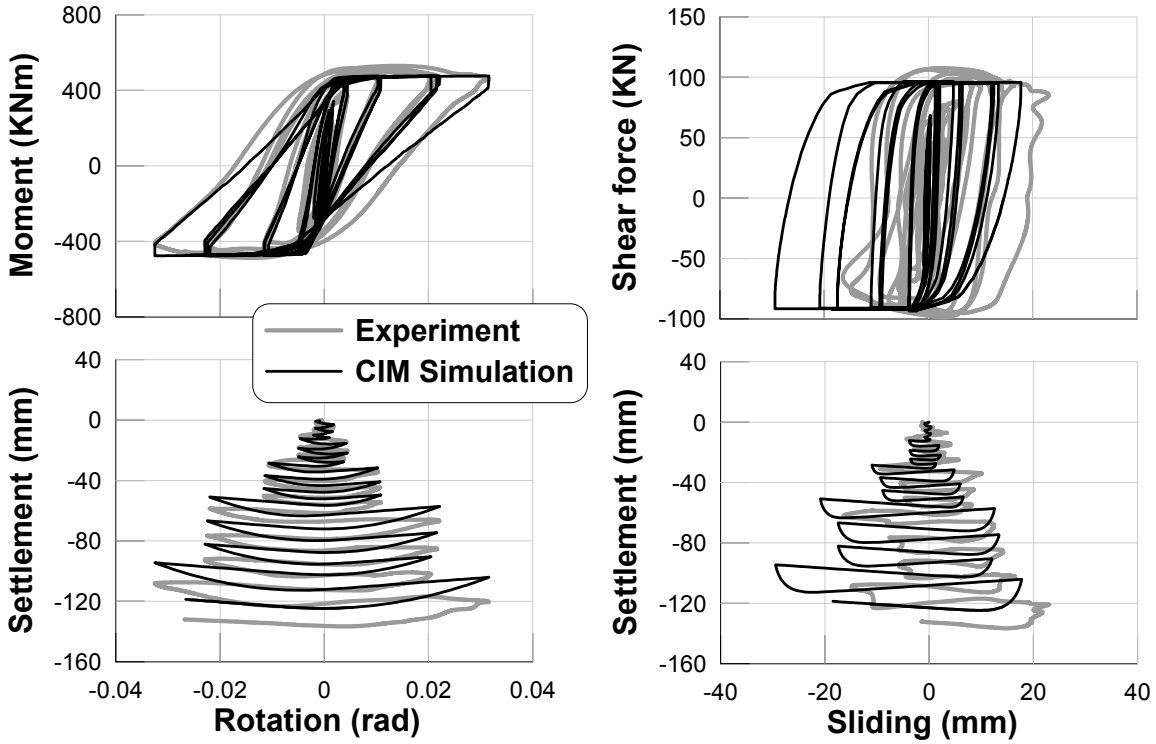

Figure 2-18 Comparison of CIM simulation to centrifuge tests for a medium aspect ratio building on dense sand, with $D_r = 80\%$, and $FS_v = 2.6$: (a) moment-rotation; (b) settlement-rotation; (c) shear-sliding; and (d) settlement-sliding (Gajan and Kutter, 2009, with permission from ASCE).

2.4.3 Model Comparisons and Recommendations for Response History Analysis

Gajan et al. (2010) compared the performance of the BNWF and CIM nonlinear SSI models for hypothetical site conditions and experimental datasets. Based on those comparisons, recommendations for model selection are as follows:

- If the simulations are to be used for structural design of footing elements, or the footing flexibility is anticipated to contribute to the foundation response, the BNWF model should be chosen. This model can be used to more directly evaluate internal moments and shears used for section design.
- If the normalized moment to shear ratio $M/(V \times L)$ is less than approximately 3.0, and sliding is not restrained by slabs and grade beams, then the moment capacity of the footing will be sensitive to shear load, and vice versa. In this case, the CIM model is preferred because of its ability to account for coupling between the moment, shear, and axial responses. For cases with $M/(V \times L)$ greater than 3.0, rocking will tend to dominate, and both models should produce similar results if the parameter selection protocols herein are followed. Coupling may also be neglected for very small $M/(V \times L)$ ratios where sliding is known to dominate. Note: *M*, *V*, and *L* are as defined previously.
- In other analytical platforms (other than OpenSees), implementation of the BNWF model will be more easily accomplished if bilinear spring, gap, and damping elements are available. Although feasible, implementation of the CIM in another platform would require implementation of a new element, and access to the source code for the host platform.

Chapter 3
Kinematic Interaction

Kinematic interaction results from the presence of stiff foundation elements on or in soil, which causes motions at the foundation to deviate from free-field motions. One cause of these deviations is *base-slab averaging*, in which spatially variable ground motions within the building envelope are averaged within the foundation footprint due to the stiffness and strength of the foundation system. Another cause of deviation is *embedment effects*, in which foundation-level motions are reduced as a result of ground motion reduction with depth below the free surface. If the foundation is pile-supported, the piles interact with wave propagation below the base slab, which can further modify foundation-level motions at the base of a structure.

This chapter describes the phenomena of base-slab averaging, embedment effects, and kinematic pile response, and presents available models for analysis of these effects. Models for kinematic interaction effects are expressed as frequency-dependent ratios of the Fourier amplitudes (i.e., transfer functions) of foundation input motion (FIM) to free-field motion. The FIM is the theoretical motion of the base slab if the near-surface foundation elements (i.e., base slabs, basement walls) and the structure had no mass, and is used for seismic response analysis in the substructure approach described in Section 1.2.

3.1 Shallow Foundations at the Ground Surface

Base-slab averaging results from adjustment of spatially variable ground motions that would be present within the envelope of the foundation, which are averaged within the foundation footprint due to the stiffness and strength of the foundation system. Base-slab averaging can be understood by recognizing that the motion that would have occurred in the absence of the structure is spatially variable. Placement of a foundation slab across these variations produces an averaging effect in which the foundation motion is less than the localized maxima that would have occurred in the free-field. Torsional rotations, referred to as the "tau effect" (Newmark, 1969), can also be introduced.

Motions of surface foundations are modified relative to the free-field when seismic waves are incoherent. *Incoherence* of the incident waves at two different points means that they have variations in their phase angle. Some incoherence is deterministic (i.e., predictable), because it results from wave passage. For example, as illustrated in Figure 3-1a, the presence of a non-zero vertical angle causes waves to arrive at different points along the foundation of a building at different times. This is

referred to as the *wave passage effect*. Investigation of wave passage effects in dense seismic arrays at soil sites indicates apparent propagation velocities, V_{app}, of approximately 2.0 km/sec to 3.5 km/sec, which appears to be controlled by wave propagation in crustal rock beneath the soil column (Ancheta et al., 2011).

Incoherence that remains when waves are aligned to have common arrival times is stochastic, and is quantified by *lagged coherency* models. Stochastic incoherence results from source-to-site heterogeneities in the seismic path of travel, which scatters seismic waves. Lagged coherency is also well-documented in array studies (e.g., Abrahamson et al., 1991; Ancheta et al., 2011). As a practical matter, incoherence from wave passage and lagged coherency is always present in earthquake ground motions to some degree.

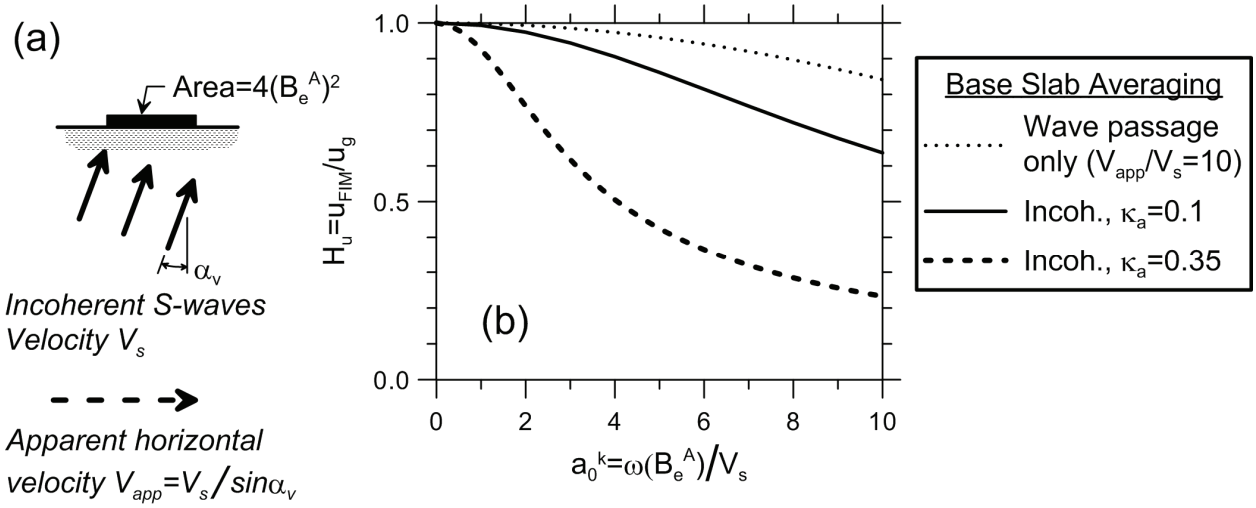

Figure 3-1 Illustration of foundation subjected to inclined shear waves: (a) schematic geometry; (b) transfer functions between FIM and free-field motion for wave passage using a semi-empirical model for incoherent waves (parameter κ_a is defined in Equation 3-5).

In the presence of incoherent wave fields, translational base-slab motions are reduced relative to the free-field, and rotational motions are introduced. The reduction in translational motion is generally the more important result. Reductions of base-slab translation and the introduction of torsion and rotation in the vertical plane are effects that tend to become more significant with increasing frequency. The frequency-dependence of these effects is primarily associated with: (1) the increased effective size of the foundation relative to the seismic wavelengths at high frequencies; and (2) significant reductions in lagged coherency with increasing frequency (Abrahamson et al., 1991).

There are numerous theoretical models for predicting the relationship between foundation input and free field ground motions in the presence of inclined, but

otherwise coherent, shear waves (i.e., wave passage effects). Mylonakis et al. (2006) synthesized these models with the following expressions:

$$u_{FIM} = H_u u_g \tag{3-1a}$$

$$H_u = \frac{\sin\left(a_0^k \left(\frac{V_s}{V_{app}}\right)\right)}{a_0^k \left(\frac{V_s}{V_{app}}\right)}, \quad a_0^k \le \frac{\pi}{2}\frac{V_{app}}{V_s} \tag{3-1b}$$

$$H_u = \frac{2}{\pi}, \quad a_0^k > \frac{\pi}{2}\frac{V_{app}}{V_s} \tag{3-1c}$$

In the above expressions, a_0^k is similar to a_0 defined in Equation 2-15, except that the foundation dimension is related to base contact area, as follows:

$$a_0^k = \frac{\omega B_e^A}{V_s} \tag{3-2}$$

where B_e^A is related to foundation area, as defined in Equation 2-18b. At $a_0^k = 0$, the expression in Equation 3-1b becomes indeterminate, and H_u should be taken as unity.

If, as indicated in array studies, V_{app} ranges from approximately 2.0 km/s to 3.5 km/s, then for a typical soil site, a reasonable estimate of the velocity ratio, V_{app}/V_s, is approximately 10. In Figure 3-1b, the result labeled "wave passage only" shows the transfer function between u_{FIM} and u_g based on Equations 3-1. Using this model, wave passage alone causes relatively modest base-slab reductions in ground motion across the frequency range of engineering interest.

Transfer functions of recorded foundation input and free-field motions are generally significantly lower at high frequencies than predicted by wave passage models. This occurs because wave passage is a relatively modest contributor to the spatial variation in ground motion that drives base-slab averaging. Additional sources of variability include stochastic phase variability (quantified by lagged coherency) and stochastic variations in Fourier amplitudes. Two approaches for capturing these effects in the analysis of transfer functions are: (1) continuum modeling of the soil and foundation system subject to input motions with a defined coherency function (*Computer Program SASSI2000*, Lysmer et al., 1999; Ostadan et al., 2005); and (2) application of a semi-empirical simplified model (Veletsos et al., 1997; Kim and Stewart, 2003).

In SASSI, a site-specific and foundation-specific model is generated in three dimensions. The foundation and soil material properties are equivalent-linear without iteration on strain-dependent properties. Empirical coherency models can be

used that include wave passage and lagged coherency (e.g., Ancheta et al., 2011, for soil sites; EPRI, 2007, for hard rock sites).

The semi-empirical model is based on a theoretical formulation of the kinematic interaction problem by Veletsos and Prasad (1989) and Veletsos et al. (1997), who apply spatially variable ground motions to a rigid foundation perfectly bonded to the soil. Models evaluate the response of rigid, massless, circular and rectangular foundations on the surface of an elastic half-space to incoherent S-waves propagating either vertically or at an angle α_v to the vertical, as shown in Figure 3-1a. The results are a relationship between transfer function amplitude and a_0^k. This relationship is essentially independent of foundation shape, but is strongly dependent upon a parameter, κ_a, related to lagged coherency and wave inclination that scales the frequency axis of the theoretical transfer function. For vertically propagating waves this transfer function (adapted from Veletsos and Prasad, 1989) can be written as:

$$H_u = \left\{ \frac{1}{b_0^{\,2}} \left[1 - \exp\left(-2b_0^{\,2}\right) \left(I_0(2b_0^{\,2}) + I_1(2b_0^{\,2}) \right) \right] \right\}^{1/2} \tag{3-3}$$

where $b_0 = \left(\sqrt{4/\pi}\right)\kappa_a a_0^k$ and I_0 and I_1 are modified Bessel functions, zero and first order, respectively. Equation 3-3 was developed for circular foundations. The $\sqrt{4/\pi}$ term adapts a_0^k (for rectangles) to a_0 defined for an equivalent radius that preserves foundation area. For small and large values of the argument ($2b_0^2$), the Bessel function summation in Equation 3-3 can be written in terms of power series and exponential functions, respectively (Watson, 1995); for routine application, these approximations can be expressed as:

$$\left(I_0(2b_0^{\,2}) + I_1(2b_0^{\,2}) \right) = \begin{cases} 1 + b_0^{\,2} + b_0^{\,4} + \dfrac{b_0^{\,6}}{2} + \dfrac{b_0^{\,8}}{4} + \dfrac{b_0^{\,10}}{12} & \text{for } b_0 \le 1 \\ \exp\left(2b_0^2\right) \left[\dfrac{1}{\sqrt{\pi} b_0} \left(1 - \dfrac{1}{16 b_0^2} \right) \right] & \text{for } b_0 > 1 \end{cases} \tag{3-4}$$

Note that the exponential terms in Equation 3-3 and Equation 3-4 cancel for $b_0 > 1$. The two functions in Equation 3-4 have a misfit of 0.0073 at $b_0 = 1$, which is accurate enough for practical purposes.

By matching model predictions to observed variations between foundation input and free-field ground motions from instrumented buildings, Kim and Stewart (2003) developed a semi-empirical model for κ_a that can be written as:

$$\kappa_a = 0.00065 \times V_s, \quad 200 < V_s < 500 m/s \tag{3-5}$$

where V_s is a representative small-strain shear wave velocity for the soil beneath the foundation, which can be calculated as described in Section 2.2.2.

Values of κ_a identified through calibration reflect the combined effects of incoherence from wave passage and stochastic processes, as well as Fourier amplitude variability. Figure 3-1b shows transfer function H_u calculated using the semi-empirical approach near the upper and lower limits of κ_a. Two key observations from this figure are: (1) as κ_a increases (indicating increasingly spatially variable motions), H_u decreases significantly; and (2) for the range of κ_a supported by case history data, H_u from the semi-empirical procedure is much lower than from wave passage models. This can be attributed to significant contributions of stochastic phase and amplitude variability to base-slab averaging.

The data set considered by Kim and Stewart (2003) consists of buildings with mat foundations, footing and grade beam foundations, and grade beam and friction pile foundations, generally with base dimensions, B_e^A, in the range of 15 m to 40 m. Although the Veletsos models strictly apply to rigid foundations, the semi-empirical model applies to the more realistic foundation conditions present in the calibration data set.

Errors could occur, however, when the model is applied to conditions beyond the calibration data set. In particular, the effects of incoherence in the Veletsos models is taken as proportional to wavelength, thus implying strong scaling with frequency and distance. Array data indicate that distance scaling is much weaker than the frequency scaling (Abrahamson et al., 1991; Ancheta et al., 2011), so the model would be expected to over-predict the effects of incoherence (under-predict H_u) for very large foundations. The opposite would be true for small foundations. Even within the parameter range of the calibration data set, it should be recognized that the empirical model fits the data in an average sense, and should not be expected to match any particular observation.

3.2 Embedded Shallow Foundations

If the base slab of a building is embedded below the ground surface (i.e., the structure has a basement), foundation-level motions are further reduced as a result of ground motion reduction with depth below the free surface. The available solutions apply to rigid cylinders embedded in a uniform soil of finite or infinite thickness (half-space). Analytical solutions by Kausel et al. (1978) and Day (1978) describe foundation input motions at the base of embedded cylinders as a function of free-field surface ground motion u_g. When subjected to vertically propagating coherent shear waves, embedded cylinders experience a reduction in base translational motion, relative to u_g, due to ground motion reductions with depth and wave scattering effects. Rotations in the vertical plane are also introduced as a result of differential displacements imposed upon the cylinders over their embedded depth. These transfer functions can be adapted to rectangular foundation shapes as:

$$H_u = \frac{u_{FIM}}{u_g} = \cos\left(\frac{D}{B_e} a_0^k\right) = \cos\left(\frac{D\omega}{V_s}\right), \quad \frac{D\omega}{V_s} < 1.1 \tag{3-6a}$$

$$H_u = 0.45, \quad \frac{D\omega}{V_s} > 1.1 \tag{3-6b}$$

$$H_{yy}(\omega) = \frac{\theta L}{u_g} = 0.26\left[1 - \cos\left(\frac{D\omega}{V_s}\right)\right], \quad \frac{D\omega}{V_s} < \frac{\pi}{2} \tag{3-6c}$$

$$H_{yy}(\omega) = 0.26, \quad \frac{D\omega}{V_s} > \frac{\pi}{2} \tag{3-6d}$$

where D is the embedment depth, as shown in Figure 3-2a. Velocity, V_s, in this case should be interpreted as the average effective profile velocity, $V_{s,\,avg}$, defined in Section 2.2.2. The transfer functions for rotation in the *xx* direction have the same form as Equation 3-6(c) and Equation 3-6(d), except that it expresses the rotation $\theta B/u_g$.

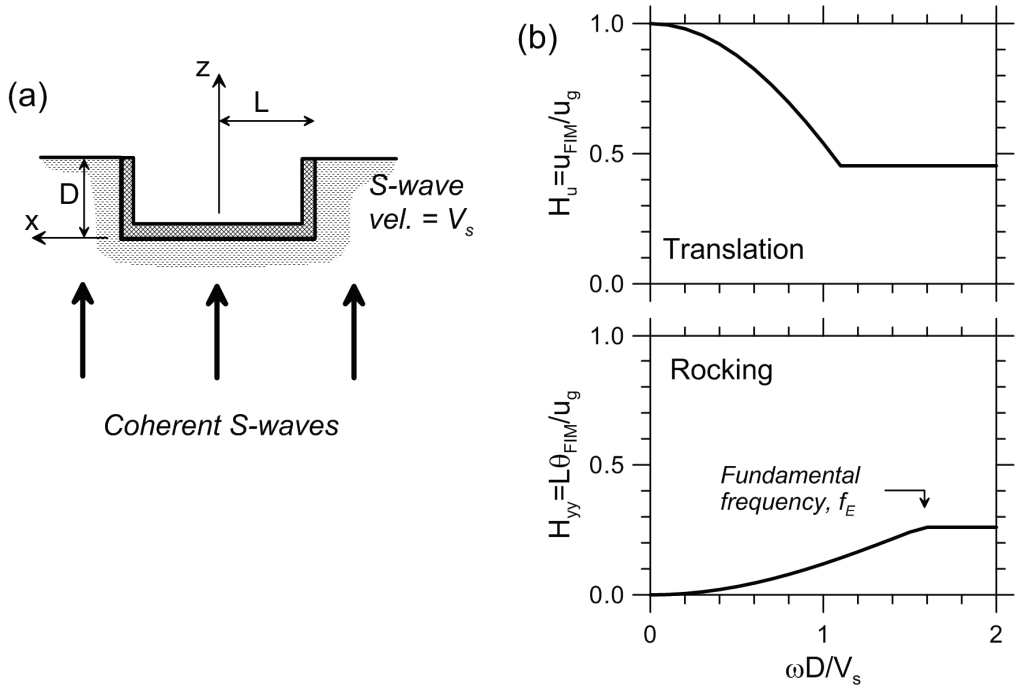

Figure 3-2 Illustration of foundation subjected to vertically incident shear waves: (a) schematic geometry; and (b) transfer functions for horizontal foundation translation and rocking.

Figure 3-2b plots the transfer functions for translation and rotation. The reduction of translation is substantial at high frequencies, saturating at about 70% of f_E, which is the fundamental frequency of the soil column between the surface and depth, D. With a high-frequency de-amplification level of 0.45, the embedment effect is often more important than the base-slab averaging effect for building structures.

Conversely, foundation rotation increases with frequency and saturates at f_E. Stewart and Tileylioglu (2007) checked the predictions of rigid cylinder models against records from nuclear reactor structures and embedded buildings. Away from frequencies strongly influenced by inertial interaction, the comparison was favorable, indicating that these functions can be applied to realistic conditions encountered in engineering practice.

To illustrate the significance of kinematic interaction from base-slab averaging and embedment effects, transfer functions were computed using motions recorded from the 1987 Whittier earthquake at the Ranch Cucamonga Law and Justice Center building (California Strong Motion Instrumentation Program, CSMIP, Station Number 23497). Results are shown in Figure 3-3.

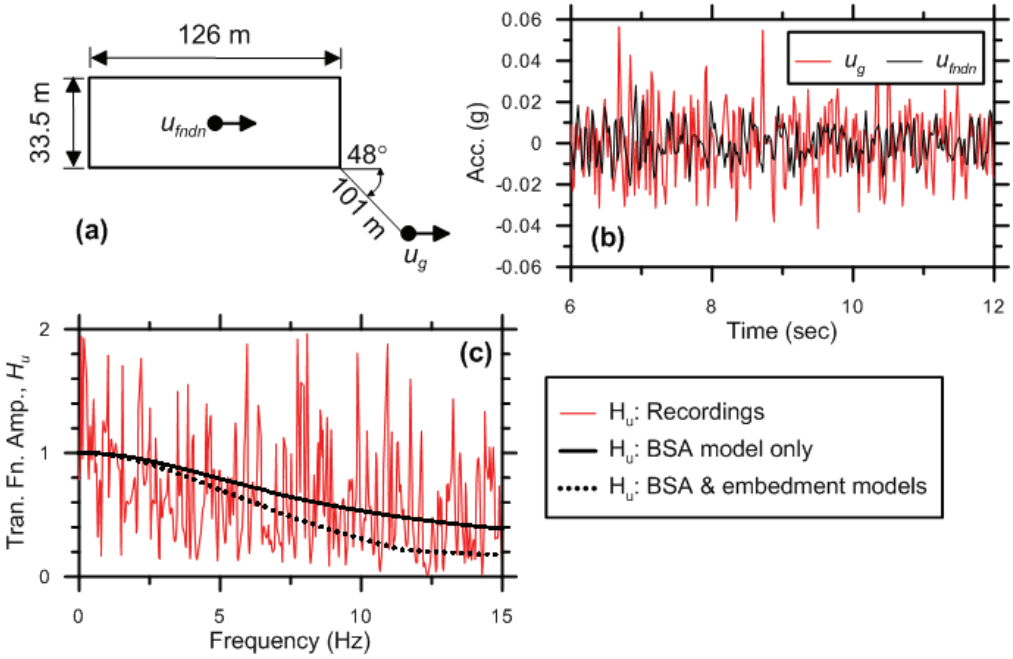

Figure 3-3 Illustration of base-slab averaging and embedment effects at CSMIP Station 23497 during the 1987 Whittier Earthquake: (a) foundation and sensor location plan; (b) acceleration time histories; and (c) observed and model-based transfer functions.

Reference recording locations in the east-west (E-W) direction, at an embedment depth of 5.9 m below the foundation, and in the free-field, are shown in Figure 3-3a. Acceleration histories shown in Figure 3-3b illustrate the general reduction of ground motions at the foundation, u_{fndn}, relative to the free field, u_g. Figure 3-3c compares the transfer function of recordings, u_{fndn}/u_g, computed using procedures given in Mikami et al. (2008) to model predictions for base-slab averaging alone and base-slab averaging combined with embedment. Model predictions are based on Equations 3-3 to 3-6, using V_s = 390 m/sec, B = 16.8 m, L = 63.1 m, and D = 5.9 m. The data have significant scatter, but trend from unity at zero frequency to about 0.2

to 0.4 at high frequencies. The models capture these general trends, but are clearly not a perfect fit to the data.

3.3 Pile Foundations

When building foundations are pile-supported, the kinematic interaction problem is complicated by the influence of the piles on wave propagation below the foundation, and also by the potential for the soil to settle away from the pile-supported base of the structure, forming a gap. This is a complex kinematic soil-structure interaction problem for which there are no well-calibrated engineering models.

Flores-Berones and Whitman (1982), Fan et al. (1991), and Nikolaou et al. (2001) describe the kinematic response of vertical piles and pile groups in elastic soil subjected to vertically propagating coherent shear waves. Similar solutions for inclined (coherent) waves have been presented by Barghouthi (1984), Mamoon and Banerjee (1990), and Kaynia and Novak (1992). Because the incident motions assumed in the development of these models were coherent, these models do not adequately incorporate base-slab averaging effects. Consequently, model predictions do not compare favorably to data (Kim and Stewart, 2003). In particular, transfer function ordinates, H_u, are significantly over-predicted by the Fan et al. (1991) models at high frequencies.

Kim and Stewart (2003) found that observed variations between foundation input and free-field ground motions at building sites in California could be adequately represented with the models for shallow foundations in Section 3.1 and Section 3.2. The pile-supported buildings considered were generally founded on alluvial soils, and the piles were not end-bearing. At building sites in Japan, however, Mikami et al. (2006) found that model predictions for base-slab averaging (SASSI, and the semi-empirical method in Section 3.1) overestimated H_u relative to data. The pile foundations in the Japanese data set have relatively high flexural stiffness, and were more nearly end-bearing, in comparison to the California data set. Development of analytical solutions for the kinematic interaction problem for pile-supported foundations of varying flexural rigidity subjected to realistic (incoherent) input motion remains an important research need.

3.4 Application of Transfer Functions

Design-basis response spectra generally apply to free-field ground motion conditions. Suites of acceleration time histories are also developed when response history analyses are to be performed. This section discusses how the transfer function from a kinematic interaction analysis should be used to modify free-field ground motions represented by a response spectrum, or ground motion suite, to account for the interaction effects described above.

The response spectrum for u_{FIM} ($S_{a\text{-}FIM}$) differs from the spectrum for u_g (S_a) because of a reduction in high frequency ground motion components due to kinematic interaction. For moderate to low frequencies, the ratio of spectral ordinates can be estimated as:

$$\frac{S_{a-FIM}(f)}{S_a(f)} \approx H_u(f), \quad f < f_L \tag{3-7a}$$

At higher frequencies, the approximation from Equation 3-7 does not hold because high frequency spectral ordinates and PGA are controlled by lower-frequency components of the ground motion. At high frequencies, a conservative approximation of spectral ordinates can generally be obtained from:

$$\frac{S_{a-FIM}(f)}{S_a(f)} \approx H_u(f_L), \quad f > f_L \tag{3-7b}$$

The limiting frequency, f_L, depends on the frequency content of u_g. For typical stiff soil or rock ground motions having mean periods in the range of 0.2 sec to 0.5 sec, f_L has been found to be approximately 5 Hz, as documented in Appendix E of FEMA 440, *Improvement of Nonlinear Static Seismic Analysis Procedures* (FEMA, 2005). Long-period ground motions resulting from near-fault directivity pulses or soft soil effects, however, can have much lower limiting frequencies, f_L, such that no significant spectral ordinate reductions from kinematic interaction are realizable. Further research is needed to identify factors controlling f_L, and to develop more reliable recommendations for engineering application.

Differences between transfer functions and ratios of response spectra are illustrated in Figure 3-4 using the Rancho Cucamonga data presented in Figure 3-3. East-west (E-W) response spectra are shown in Figure 3-4a. Reductions in foundation motions relative to free-field motions are apparent for periods less than approximately 0.7 sec (of frequencies greater than 1.4 Hz). Figure 3-4b shows the ratio of response spectra (RRS) for the E-W direction along with: (1) the transfer function model, H_u, for both base-slab averaging and embedment effects; and (2) the RRS model derived from H_u using Equation 3-7. The RRS model captures the general trends of the data, although there are significant period-to-period variations in the data (and even some RRS ordinates greater than unity). The RRS data does not show the strong decrease in spectral ratios with decreasing period that is evident in the H_u function, which illustrates the saturation effect described above.

Acceleration histories representing the FIM can be modified from free-field motions using the following procedure:

1. Calculate the Fourier transforms of u_g.

2. Multiply the amplitude of u_g by H_u. As an optional step, the phase of u_{FIM} could be randomized from that of u_g using the procedures in Chapter 3 of Ancheta (2010). If the phase is not randomized, then u_g and u_{FIM} will be coherent.

3. Perform a reverse Fourier transform to estimate $u_{FIM}(t)$.

For most practical situations, this procedure could be avoided by merely selecting and modifying ground motions for compatibility with $S_{a\text{-}FIM}$ in lieu of S_a, in which case no further modification is needed.

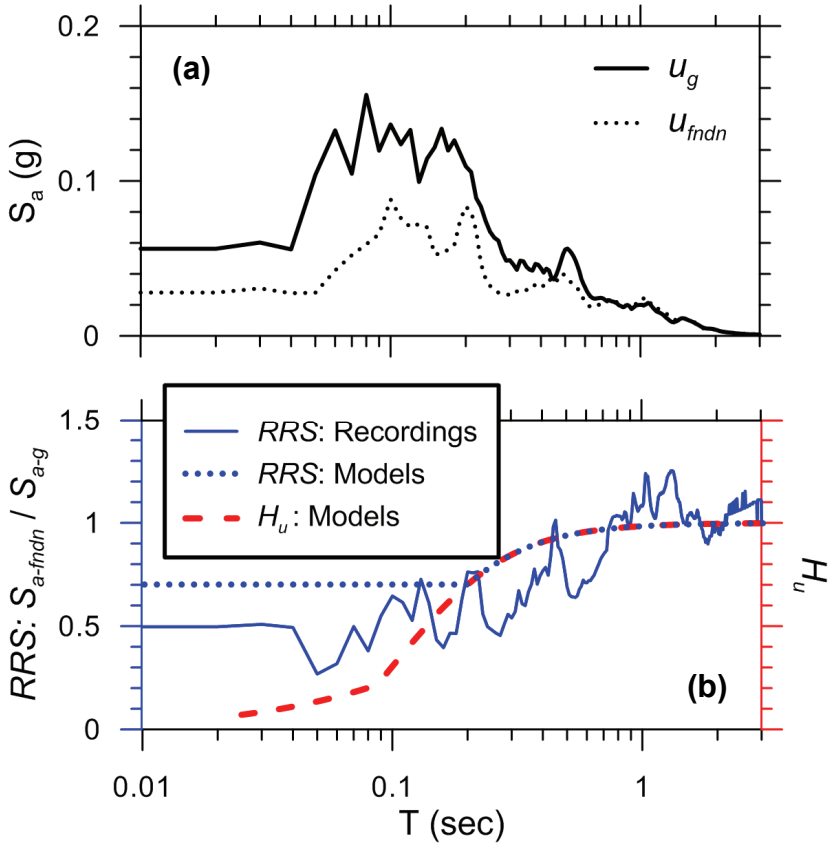

Figure 3-4 Illustration of differences between transfer functions and ratios of response spectra using data from CSMIP Station 23497 during the 1987 Whittier Earthquake: (a) E-W response spectra recorded at the site; and (b) ratio of response spectra from recordings compared to model prediction for RRS and transfer function, H_u.

Chapter 4
Implementation in Standards and Design Guidelines

Soil-structure interaction provisions exist in the following engineering standards and design guidelines:

- ATC-40, *Seismic Evaluation and Retrofit of Concrete Buildings* (ATC, 1996).
- ASCE 4-98, *Seismic Analysis of Safety-Related Nuclear Structures and Commentary* (ASCE, 1998).
- FEMA 440, *Improvement of Nonlinear Static Seismic Analysis Procedures* (FEMA, 2005).
- ASCE/SEI 41-06, *Seismic Rehabilitation of Existing Buildings* (ASCE, 2007)
- FEMA P-750, *NEHRP Recommended Seismic Provisions for New Buildings and Other Structures* (FEMA, 2009).
- ASCE/SEI 7-10, *Minimum Design Loads for Buildings and Other Structures* (ASCE, 2010).
- PEER Report No. 2010/05, *Guidelines for Performance-Based Seismic Design of Tall Buildings* (PEER, 2010).

Despite the availability of these resources, soil-structure interaction is seldom considered in typical U.S. design practice. This is driven in part by challenges in understanding, learning, and implementing fundamental SSI principles, but also in the way that SSI provisions are characterized in seismic design provisions. In general, accounting for SSI is handled through optional procedures, some of which can only reduce base shear demands. Under such conditions, ignoring SSI is not only easier, it is conservative.

However, trends in practice are tending toward increased use of SSI. This has been driven principally by seismic retrofit projects in which SSI analysis is used to gain better insight into structural performance and to improve accuracy in the analytical simulation of important structural response quantities. This chapter describes the implementation of SSI procedures in currently available engineering standards and guidelines. Limitations of those procedures are also briefly discussed.

4.1 Force-Based Procedures

Implementation of soil-structure interaction into the equivalent lateral force procedure for seismic design is specified in Chapter 19 of ASCE/SEI 7-10, which was developed based on information contained in the *NEHRP Recommended Provisions* (FEMA, 2009). The seismic base shear considering SSI effects is defined as:

$$V = C_s \bar{W} \tag{4-1}$$

where C_s is a seismic coefficient, taken as the design response spectral ordinate, at building period T, normalized by the acceleration of gravity, g, and $\bar{W}$ is the effective seismic weight of the structure (taken as 70% of the total weight). The shape of the design response spectrum is schematically illustrated in Figure 4-1.

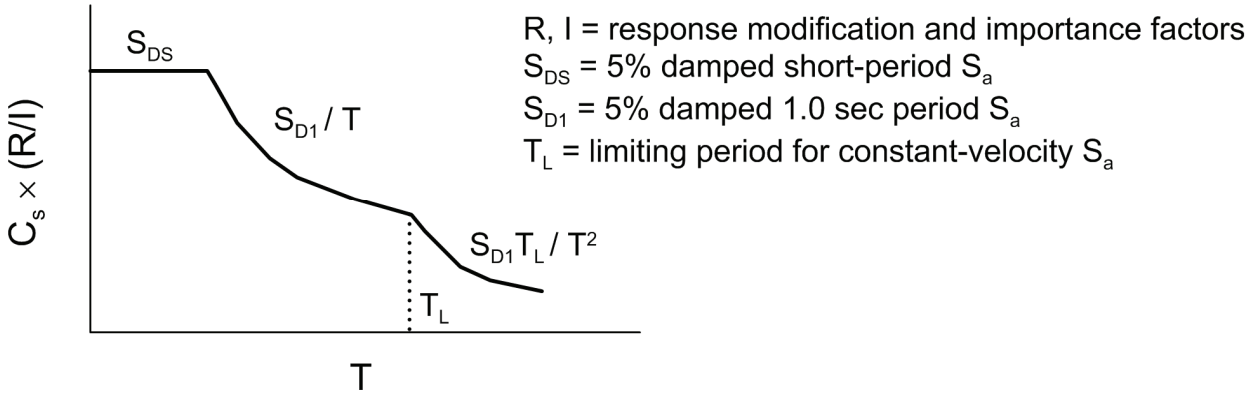

Figure 4-1 Schematic illustration of the shape of the design response spectrum in the *NEHRP Recommended Provisions*.

ASCE/SEI 7-10 (and the *NEHRP Recommended Provisions*) neglect kinematic interaction effects but account for inertial interaction effects related to period lengthening and damping ratio. The change in base shear is calculated as:

$$\Delta V = \left[C_s - \tilde{C}_s \left(\frac{0.05}{\beta_0} \right)^{0.4} \right] \bar{W} \tag{4-2}$$

The change in base shear is related to the change in seismic coefficient (or spectral acceleration). The $\tilde{C}_s$ term in Equation 4-2 represents the seismic coefficient obtained from the design spectrum at an elongated period, $\tilde{T}$. The term $\left(0.05/\beta_0\right)^{0.4}$ represents the reduction in spectral ordinate associated with a change in damping from the fixed-base structural damping value of $\beta_i = 0.05$, to the flexible-base value of β_0.

It is important to note that the shape of the design spectrum is flat, or has a negative slope with respect to period. Coupled with the requirement that β_0 must exceed β_i

(discussed further below), this ensures that utilizing SSI provisions will always reduce base shear.

Modification of design base shear for SSI effects in equivalent lateral force procedures has a potentially significant shortcoming. There is no link between base shear reduction factors intended to represent structural ductility (i.e., *R* factors) and soil-structure interaction. Crouse (2001) noted that existing *R* factors may already reflect the beneficial effects of soil-structure interaction, and modifying the base shear to account for both SSI and ductility may be unconservative in some cases. Accordingly, there is a need to revisit the definition of *R* factors with respect to SSI effects, and define values that represent structural ductility effects alone.

Period lengthening is calculated using an equation similar to Equation 4-3 (originally presented as Equation 2-7 in Chapter 2 of this report):

$$\frac{\tilde{T}}{T} = \sqrt{1 + \frac{k}{k_x} + \frac{kh^2}{k_{yy}}} \tag{4-3}$$

however, ASCE/SEI 7-10 does not specify how lateral stiffness, k_x, or rotational stiffness, k_{yy}, are to be evaluated. The *Commentary* to the *NEHRP Recommended Provisions* provides some guidance related to circular foundations, but the rectangular foundation models contained in Chapter 2, Section 2.2 are more useful for practical engineering applications.

The shear modulus, *G*, used in conjunction with equations for static foundation stiffness, must be reduced from the shear modulus at small strain levels, G_0, to account for large strain effects. ASCE/SEI 7-10 (and the *NEHRP Recommended Provisions*) provides values for adjusting the shear modulus and shear wave velocity for large strain levels based on site class and spectral response acceleration levels. These values are provided in Table 2-1.

Foundation damping is calculated using an equation similar to Equation 4-4 (originally presented as Equation 2-10 in Chapter 2 of this report):

$$\beta_0 = \beta_f + \frac{1}{\left(\tilde{T}/T\right)^n}\beta_i \tag{4-4}$$

with fixed-base structural damping, $\beta_i = 0.05$, and exponent, $n = 3$ (for ideally viscous material damping). In ASCE/SEI 7-10 (and the *NEHRP Recommended Provisions*), the foundation damping factor, β_f, is not evaluated directly from controlling variables as in Equation 2-11a (Chapter 2 of this report), but is taken from a plot like the one shown in Figure 4-2, in which the period lengthening ratio is related to β_f as a function of structure aspect ratio, h/r. Note that *r* is an equivalent foundation radius, which is calculated to match the foundation area for squat structures and the

foundation moment of inertia for slender structures. The relationship in Figure 4-2 is calculated from Veletsos and Nair (1975), using the absolute value of the complex-valued damping relationship, and including both radiation damping and hysteretic soil damping.

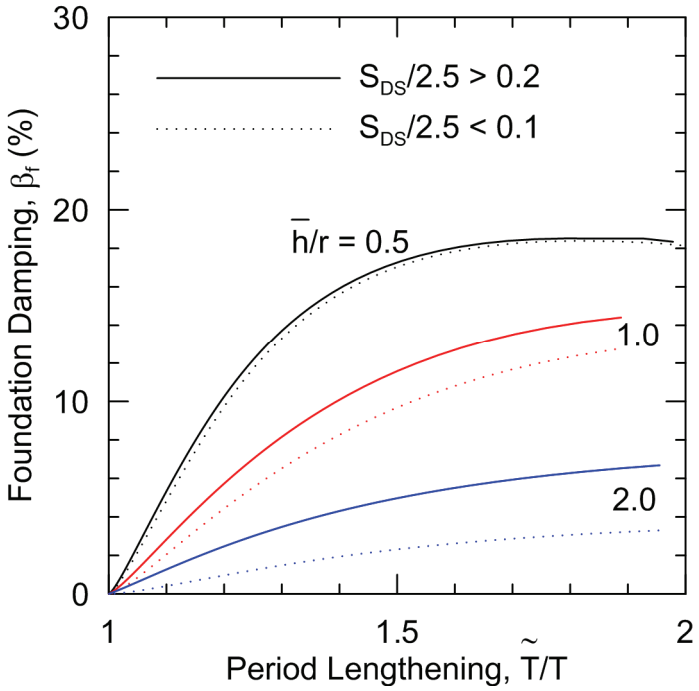

Figure 4-2 Plot of relationship between period lengthening and foundation damping (FEMA, 2009; ASCE, 2010).

Soil-structure interaction provisions for the equivalent lateral force procedure in ASCE/SEI 7-10 (and the *NEHRP Recommended Provisions*) are written such that base shear demand is only reduced through consideration of SSI. Therefore, ignoring SSI effects in the design process is analytically conservative. In practice, the beneficial effects of period lengthening and foundation damping are negligible for tall, flexible structures. Use of SSI procedures yields the most benefit for short-period, stiff structures with stiff, interconnected foundation systems (i.e., mats or interconnected footings) founded on soil.

Consideration of soil-structure interaction is also permitted when modal response spectrum analysis is used for seismic design. Implementation of SSI in modal response spectrum analysis is similar to the implementation for equivalent lateral force analysis. Period lengthening and modification of damping, however, are only applied in the fundamental lateral mode of response. Higher mode vibration periods and damping ratios are not modified for the effects of SSI.

The principal limitations of force-based procedures in ASCE/SEI 7-10 are: (1) use of simplified spectra that can only result in a decrease in base shear as period lengthens;

(2) use of relatively simplified models, applicable to circular foundation geometries, for soil-foundation springs and foundation damping; and (3) lack of consideration of kinematic interaction effects on foundation-level ground motions. These limitations were considered necessary to make the procedures sufficiently simple for broad use in practice.

A potentially important consideration associated with the use of the SSI procedures in Chapter 19 of ASCE/SEI 7-10 is the value of the fixed-base fundamental period, T. Chapter 12 of ASCE/SEI 7-10 contains approximate methods for evaluation of T, and limiting values (i.e., $C_u T_a$), which bias the estimate of T to intentionally produce conservative values of design base shear. In SSI procedures, T should be taken as the best estimate value of period, without deliberate bias.

Chapter 12 of ASCE/SEI 7-10 (Section 12.13) also contains procedures for incorporation of foundation flexibility (i.e., soil springs) into structural models for linear analysis. The use of an elongated period from Chapter 19 with a structural model containing foundation springs (per Section 12.13) would overestimate the effects of foundation flexibility, so the simultaneous use of both sets of procedures is not permitted in ASCE/SEI 7-10.

4.2 Displacement-Based Procedures

In displacement-based procedures, system behavior is represented by a force versus displacement relationship that is calculated through nonlinear static (i.e., pushover) analyses. A pushover analysis involves the application of static lateral loads distributed over the height of the structure, and calculation of the resulting displacements in a model of the SSI system. A pushover analysis of a structure with a flexible base is schematically illustrated in Figure 4-3.

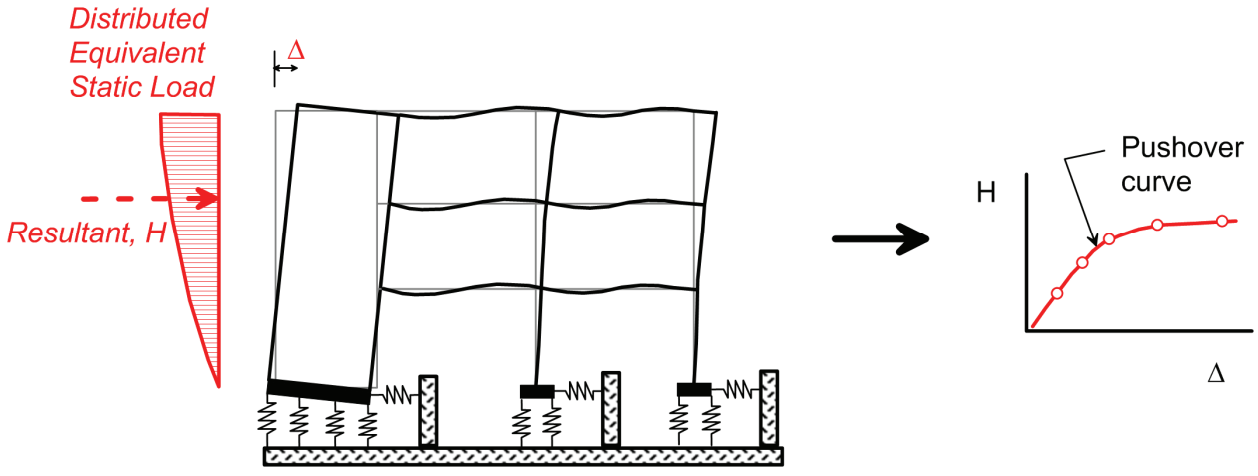

Figure 4-3 Schematic illustration of a pushover analysis and development of a pushover curve for a structure with a flexible base.

The cumulative lateral load resultant, H, is related to a reference displacement, Δ, forming the nonlinear pushover curve. In some applications, the pushover curve is modified to an acceleration-displacement response spectrum (ADRS) by converting H to an equivalent spectral acceleration, and converting Δ to an equivalent spectral displacement (e.g, Chopra and Goel, 1999; Powell, 2006). At each point on the pushover curve, the deformations of all components in the structural system are related to the reference displacement.

Powell (2006) describes common ways by which the pushover curve is combined with a design response spectrum to estimate the seismic displacement in a structure. Three such methods are known as the Capacity Spectrum Method (ATC, 1996), the Coefficient Method (FEMA, 1997; FEMA, 2000; and ASCE, 2007), and Equivalent Linearization (FEMA, 2005). These methods are illustrated in Figure 4-4.

Soil-structure interaction is considered in displacement-based analysis procedures through: (1) foundation springs used in the pushover model; (2) reduction of the free-field response spectrum for kinematic interaction effects; and (3) reduction of the response spectrum for flexible-base damping ratios, β_0, that are greater than the fixed-base structural damping ratio, β_i. The manner by which these components are evaluated in displacement-based analysis procedures is described below. Slight modifications to the notation contained in reference engineering standards and guidelines have been made for consistency with the notation adopted in this report.

In general, soil-foundation springs used in pushover analyses are similar to those described in Chapter 2, Section 2.2, except that dynamic stiffness modifiers are neglected. The Pais and Kausel (1988) static stiffness equations listed in Table 2-2 are used. Distributed vertical springs are evaluated in a manner similar to that described in Chapter 2, Section 2.2.3. Horizontal springs are not distributed but are concentrated at the end of the foundation as shown in Figure 2-8 (in Chapter 2).

Kinematic interaction effects are represented in terms of ratios of response spectra (RRS) between the foundation and free-field motions. Equations for RRS as a function of period are given for the effects of base slab averaging and embedment are adapted from FEMA 440 as follows:

$$RRS_{bsa} = 1 - \frac{1}{14100}\left(\frac{2\left(B_e^{A} \div 0.3048\right)}{T}\right)^{1.2} \quad T > \frac{1}{f_L} \tag{4-5a}$$

$$RRS_{bsa} = 1 - \frac{1}{14100}\left(2\left(B_e^{A} \div 0.3048\right) f_L\right)^{1.2} \quad T \le \frac{1}{f_L} \tag{4-5b}$$

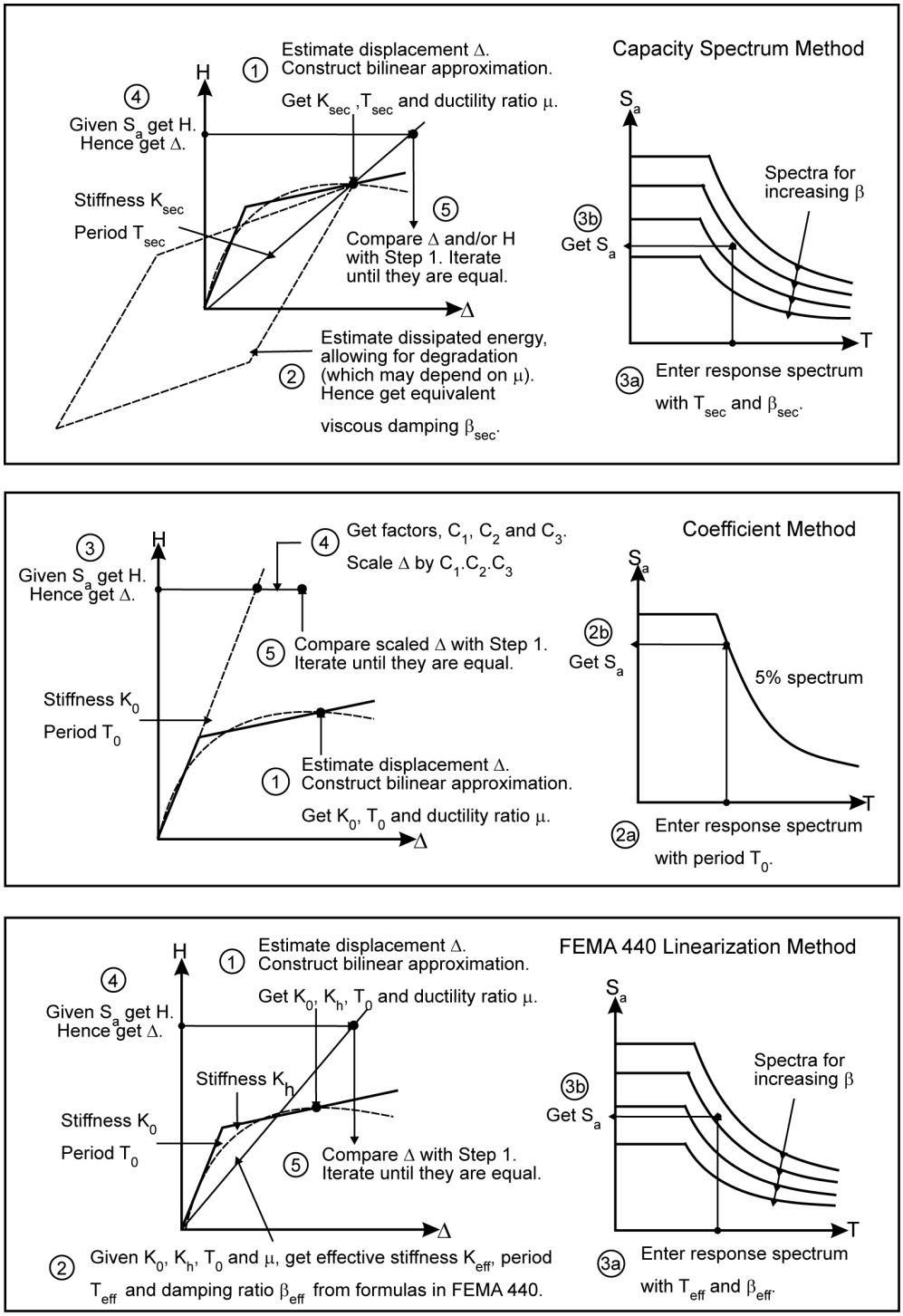

Figure 4-4 Schematic illustration of procedures used to combine pushover curves with design response spectra to estimate seismic displacements in a structure (Powell, 2006, with permission).

$$RRS_{emb} = \cos\left(\frac{2\pi D}{TV_{sr}}\right) \quad T > \frac{1}{f_L} \tag{4-6a}$$

$$RRS_{emb} = \cos\left(\frac{2\pi D f_L}{V_{sr}}\right) \quad T \le \frac{1}{f_L} \tag{4-6b}$$

where V_{sr} is the strain-reduced shear wave velocity evaluated using the reduction factors in Table 2-1. In Equations 4-5, the equivalent foundation dimension B_e^A is expressed in units of meters. These equations are a curve-fit of the semi-empirical base-slab averaging transfer function described in Equation 3-3 (in Chapter 3). A shear wave velocity term does not appear in Equations 4-5 because the V_s terms cancel in the expression for b_0 in Equation 3-3. The resulting RRS curves for base-slab averaging are shown in Figure 4-5.

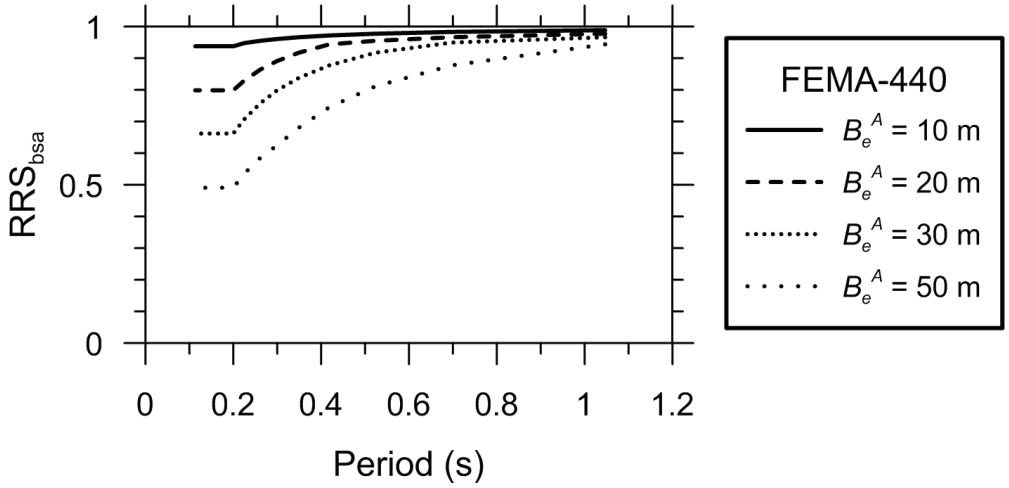

Figure 4-5 Ratios of response spectra (u_{FIM}/u_g) for base slab averaging using the semi-empirical formulation adopted in FEMA 440.

For embedment, the RRS in Equations 4-6 match Equation 3-4 (in Chapter 3) after re-writing in terms of period, T, instead of angular frequency, ω. In FEMA 440, the limiting period, f_L, is taken as 5 Hz (0.2 sec). As of this writing, these equations are in the process of being revised in the next version of ASCE/SEI 41 (ASCE, 2013) to reflect the recommendations contained in Chapter 3 of this report.

In FEMA 440, the objective of the damping analysis is to estimate the foundation damping ratio, β_f, which is then combined with the fixed-base structural damping ratio, β_i, to estimate β_0 using Equation 4-4 (with $n = 3$). The principal challenge is to extract β_f from the results of the pushover analysis of the structure in both its fixed-base and flexible-base condition. As described in Chapter 2, Section 2.2.3, foundation flexibility can significantly reduce radiation damping (β_{yy}) from rotational vibration modes, which is considered in the FEMA 440 procedures.

First, the period lengthening ratio at small displacements is estimated using the initial stiffness of capacity diagrams for the fixed-base and flexible-base structures. Assuming shaking in the *x*-direction, stiffness K_x is then evaluated using equations in Table 2-2 (the dynamic stiffness modifier, α_x, is assumed as unity). The effective rotational stiffness of the foundation system is then evaluated from a manipulation of Equation 2-7 as follows:

$$K_{yy} = \frac{K^*_{fixed} h^2}{\left(\frac{\tilde{T}}{T}\right)^2 - 1 - \frac{K^*_{fixed}}{K_x}} \tag{4-7}$$

where K^*_{fixed} is the equivalent fixed-base stiffness of the structure evaluated from:

$$K^*_{fixed} = \bar{M}\left(\frac{2\pi}{T}\right)^2 \tag{4-8}$$

Note that dynamic stiffness modifier, α_{yy}, is also taken as unity. The value of K_{yy} estimated from Equation 4-7 reflects the stiffness of the foundation structural elements as implemented in the pushover analysis, so no assumptions of foundation rigidity are required.

The next step is to reduce the period lengthening ratio from the small-displacement condition to the large-displacement (i.e., post-yield) condition (with elongated periods). Taking μ as the expected ductility demand for the system (including structure and soil effects), the effective period lengthening in the post-yield state is computed as:

$$\left(\frac{\tilde{T}}{T}\right)_{eff} = \left\{1 + \frac{1}{\mu}\left[\left(\frac{\tilde{T}}{T}\right)^2 - 1\right]\right\}^{0.5} \tag{4-9}$$

This effective period lengthening ratio can then be used with Figure 4-2 to estimate the foundation damping ratio, β_f.

4.3 Response History Procedures

Most of the resources listed at the beginning of this chapter (e.g., ATC-40, FEMA 440, FEMA P-750, ASCE/SEI 41-06, and ASCE/SEI 7-10) are silent on the implementation of SSI effects in response history analyses. Similar to ASCE/SEI 7-10 (Section 12.13), they permit the use of soil springs in principal, but offer no specific guidance on how the springs should be selected or utilized in a response history analysis.

The Pacific Earthquake Engineering Research Center (PEER) *Guidelines for Performance-Based Seismic Design of Tall Buildings* (PEER, 2010) recommends a

response history substructure analysis procedure similar to the approach described in this report. However, the specification of input motions and the distribution of springs and dashpots, as depicted in Figure 1-2 (in Chapter 1), are simplified to streamline response history analysis, as shown in Figure 4-6. Two idealizations of the SSI system are recommended in the PEER *Guidelines*, depending on the level of earthquake shaking intensity, identified as the: (1) service level earthquake (SLE); and (2) maximum considered earthquake (MCE).

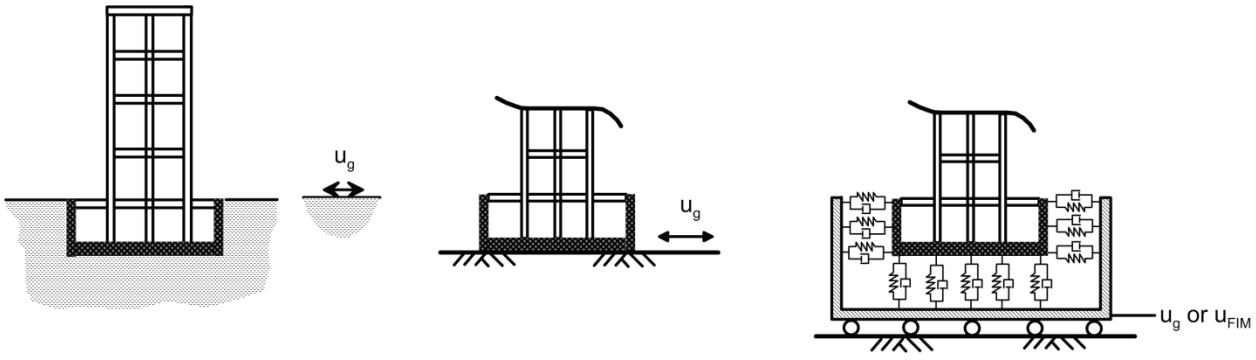

Figure 4-6 Schematic illustration of a tall building with subterranean levels: (a) complete system; (b) simplified model for service-level earthquake intensity; and (c) simplified foundation model for maximum considered earthquake intensity.

Subterranean levels are modeled in both the SLE and MCE analyses, including the mass, stiffness, and structural capacities of structural elements such as walls, columns, and slabs. Response history analysis for the SLE (Figure 4-6b), is performed with a relatively simple model that omits the surrounding soil and does not include soil springs. Response history analysis for the MCE (Figure 4-6c), is performed with springs and dashpots representing soil-foundation interaction along basement walls and below the base slab. In this case, ground motions are applied to a rigid "bathtub" surrounding the subterranean portions of the structure. In both the SLE and MCE analyses, the motion applied at the base of the model can be either the free-field motion (u_g) or the foundation input motion (u_{FIM}). These recommendations are derived largely from the recommendations of Naeim et al. (2008).

Procedures for calculating spring stiffnesses and capacities are not specified in the PEER *Guidelines*, but can be taken as those from Chapter 2 of this report. Similarly, foundation input motions can be modified from free-field motions using the procedures in Chapter 3 of this report.

4.4 Nuclear Structures

Guidance for the seismic analysis of nuclear safety-related facilities in the United States is provided in ASCE 4-98, *Seismic Analysis of Safety-Related Nuclear*

Structures and Commentary (ASCE, 2000). This standard was developed mainly for non-reactor nuclear structures, and at the time of this writing, is currently under revision. ASCE 4-98 is a companion to ASCE/SEI 43-05, *Seismic Design Criteria for Structures, Systems, and Components in Nuclear Facilities* (ASCE, 2005), which is used as a reference standard for submittal of combined operating license applications (COLAs) for new reactors.

Both the direct analysis and substructure approaches for SSI described in Chapter 1 are permitted under ASCE 4-98. Provisions related to response history analyses as well as equivalent lateral force-based analyses are included. Referring to Figure 1-2 (in Chapter 1), consideration of kinematic interaction effects, foundation flexibility, and damping are included. ASCE 4-98 does not consider base slab averaging effects, but it does consider embedment effects. The foundation input motion adjusted for embedment effects is referred to as the *Foundation Input Response Spectra* (FIRS), which is computed for the free-field conditions at the foundation level using wave propagation analysis (de-convolution). The procedure in the upcoming version of ASCE 4 (ASCE, in preparation) will also allow for base-slab averaging through response history analysis, in which the input motion is specified with a defined coherency function, as described in Section 3.1, using software such as SASSI (Ostadan et al., 2005).

Soil-foundation flexibility is represented using spring-based solutions (CLASSI, Wong, 1979) or equivalent-linear elastic solid finite elements (SASSI, Lysmer et al., 1999). As such, the procedures for nuclear structures have generally been based on elasto-dynamic solutions of the soil-structure interaction problem.

Chapter 5
Experiments and Case Studies

Testing has played a relatively minor role in the research and evolution of soil-structure interaction. For the most part, research has been dominated by numerical analysis exercises. The models developed from numerical and theoretical studies, however, apply for idealized conditions, so testing and seismic monitoring play a vital role in guiding the implementation of idealized models in practice.

This chapter identifies and reviews experiments and case studies available in the literature. Information is separated into field-scale and laboratory-scale tests, which typically have different objectives and different applications. Tests involving shallow foundations and dynamic loading are emphasized. Results from tests identified in this chapter, where applicable, have been interpreted for use in SSI modeling in other chapters of this report.

5.1 Seismic Monitoring and Field Tests

Seismic monitoring and field testing of structures is generally performed with one of two objectives: (1) evaluation of system properties such as the fundamental mode period and damping of an SSI system; or (2) estimation of foundation impedance ordinates representing the stiffness and damping characteristics of soil-foundation interaction.

5.1.1 System Studies

In system studies, seismic data from well-instrumented buildings are used in system identification analyses to estimate modal vibration parameters. To evaluate SSI effects, input-output pairs must be selected that isolate the system behavior associated with the structure alone (fixed-base properties) and the full system (flexible-base properties), as described in Stewart and Fenves (1998). Results can then be compared to period lengthening and foundation damping models of the type described in Section 2.1. Stewart et al. (1999a; 1999b), for example, describe the results of such analyses and lessons learned regarding the practical application of impedance functions for rigid circular foundations.

System studies can also be undertaken using forced-vibration tests (e.g., Yu et al., 2005). The input-output pairs that should be used for evaluation of fixed- and flexible-base properties are given by Tileylioglu (2008). No major study applying these techniques to evaluate period lengthening and foundation damping has been completed to date.

5.1.2 Field Experiments for Foundation Impedance

Experimental investigations of impedance functions typically seek to evaluate stiffness and damping terms for horizontal translation ($j = x$ or y) and rotation within the vertical plane ($j = xx$ or yy). Cyclic excitation is generally provided by a shaker installed on the roof or foundation of a structure. Table 5-1 summarizes field forced-vibration experiments of this type. Analysis procedures for evaluation of foundation impedance from recordings of structural vibrations are provided in Tileylioglu et al. (2011).

Table 5-1 Summary of Field Forced-Vibration Tests Used to Evaluate Foundation Impedance Functions

				Excitation		Results			
Foundation Dimensions	*Embed. (m)* [1]	*f_1 (Hz)* [2]	*V_s (m/s)* [3]	*Source*	*Freq. Range (Hz)* [4]	*$\tilde{T} / T$* [5]	*Impedance Obtained*	*Freq. Range (Hz)* [4]	*Reference*
3×3m	0 to 1.5	17.5	305	shaker on ground	7 to 70	1.3 (D=1.5); 1.5 (D = 0)	k_x, c_x, k_{yy}, c_{yy}	modal freq. only	Lin and Jennings (1984)
25×25m	4 to 5.5	NS: 2.16; EW: 1.26	300	shaker on roof	NS: 0.8 to 2.5; EW: 0.8 to 1.75	NS: 1.06; EW: 1.1	k_x, c_x, k_{yy}, c_{yy}	NS: 0.8-2.5; EW: 0.8-1.75	Luco et al. (1988); Wong et al. (1988)
1.3×1.3m; 1.2×1.1m	0	n/a	120; 75	shaker on fndn.	10 to 60	n/a	k_x, c_x, k_{yy}, c_{yy}	0 to 60	Crouse et al. (1990)
diam. = 10.8m	5.2	9.37	300	shaker on roof and fndn.	2 to 20	2	k_x, c_x, k_{yy}, c_{yy}, $k_{x\text{-}yy}$, $c_{x\text{-}yy}$, k_z, c_z	5 to 14	de Barros and Luco (1995)
4.1×4.1m	0	6.0, 13	198	shaker on roof	5 to 15	1.15, 1.29	k_x, c_x, k_{yy}, c_{yy}	5 to 15	Tileylioglu et al. (2011)

Notes: [1] Foundation embedment depth; [2] Fundamental mode, fixed-base frequency; [3] Vs=Shear wave velocity of soil; [4] Frequency range; and [5] Period lengthening.

Symbols: D=embedment depth; n/a=not available; NS=North-South building axis; EW=East-West building axis; diam=diameter; and fndn=foundation.

The first field investigations of foundation impedance provided results over a limited range of frequencies (Lin and Jennings, 1984; Luco et al., 1988; Wong et al., 1988) or for very small structures representative of strong motion instrument huts (Crouse et al., 1990). More recently, de Barros and Luco (1995) tested a relatively large model structure (of a nuclear reactor) and provided impedance ordinates over a relatively wide frequency range (approximately 4 Hz to 20 Hz). Figure 5-1 shows impedance ordinates evaluated by de Barros and Luco. Results are shown in non-normalized form due to uncertainty in the shear modulus of the foundation soils, and illustrate the noisy character of the data, especially at frequencies under 4 Hz or greater than 14 Hz. Also shown in Figure 5-1 are three model predictions for

stiffness and damping, caused by uncertainty in the appropriate value for shear wave velocity, V_s.

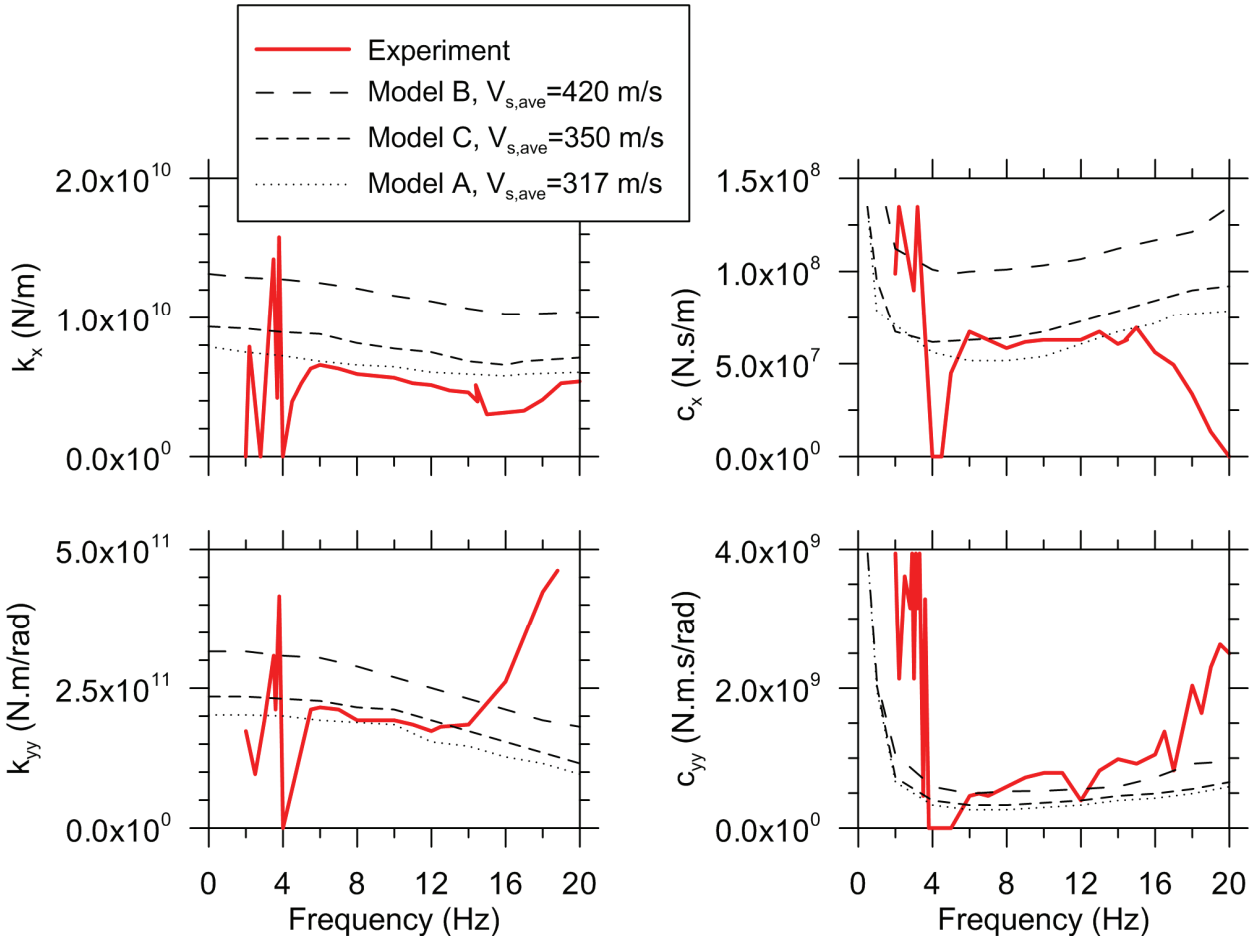

Figure 5-1 Non-normalized impedance values from experimental data compared with theoretical predictions for a nuclear containment structure at Hualien, Taiwan for translational (top) and rotational (bottom) modes (adapted from de Barros and Luco, 1995).

Two practical difficulties associated with field testing for impedance ordinates and comparison to model predictions have been encountered in the previous work. First, limited resolution of the data acquisition system with respect to analogue-to-digital signal conversion and time-stamping contribute significantly to noise in the results. Most previous studies have not formally evaluated noise effects, which can lead to spurious results (e.g., impedance ordinates in Figure 5-1 for frequencies outside the 4 Hz to 14 Hz range). Second, shear wave velocity profiles have generally been established using downhole or suspension logging methods in the free-field.

Use of downhole or suspension logging methods can have limited resolution very near the ground surface (e.g., Andrus et al., 2004). Because the soil materials immediately below the foundation exert the greatest influence on foundation stiffness, this introduces uncertainty in the selection of an appropriate value of V_s for

use with numerical solutions. Also, seismic velocities measured in the free field neglect the effect of confinement provided by the weight of the structure. Although this can be corrected using the procedures given in Section 2.2.2, this has seldom been done in prior field experiments.

The final study listed in Table 5-1 overcame many of the practical difficulties encountered in previous work through the use of high-fidelity, modern sensors and data acquisition equipment available through the NEES@UCSB equipment site (http://nees.ucsb.edu/). Seismic velocities were measured immediately adjacent to the foundation so that they incorporated overburden effects. Sample results are shown in Figure 5-2, and the data are observed to be numerically stable across the range of tested frequencies. Stronger damping was evident in the translational versus the rotational vibration modes, and radiation damping was a significant contributor in each case.

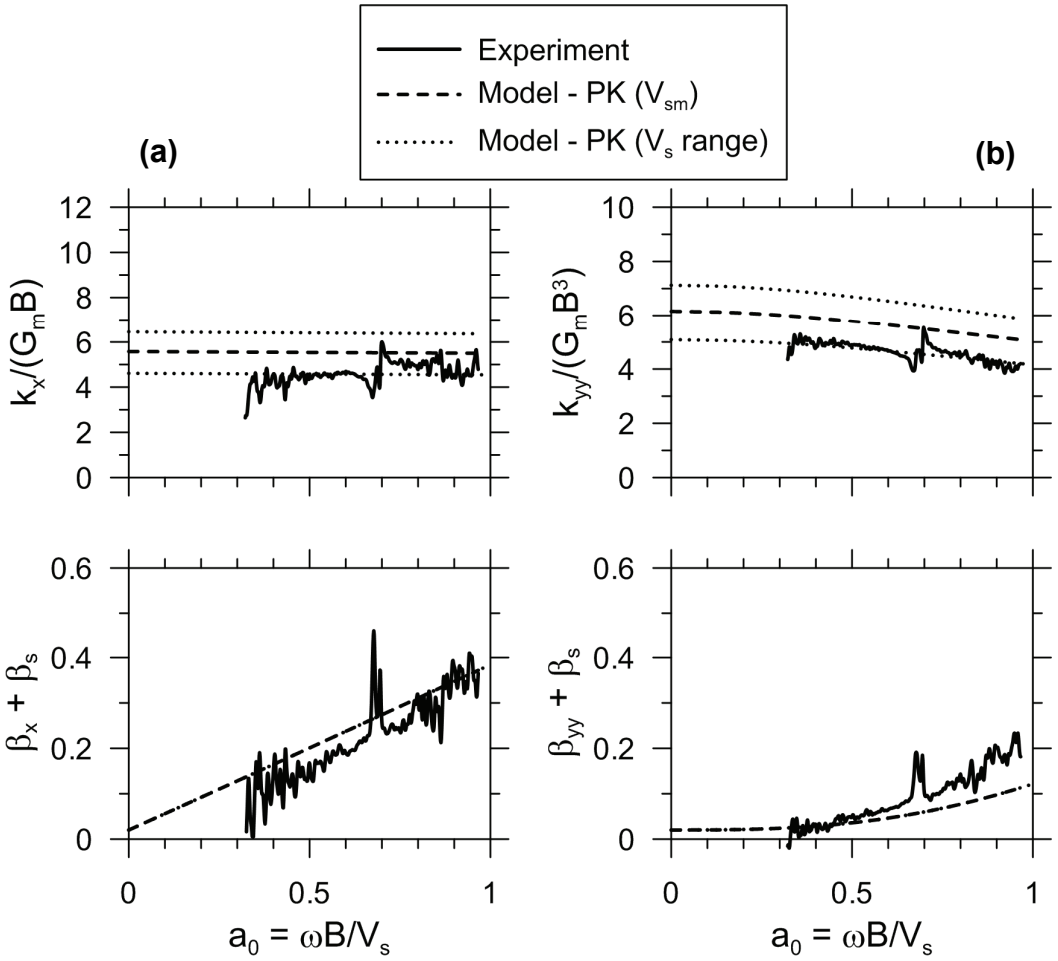

Figure 5-2 Normalized impedance values from experimental data compared with theoretical predictions for the Garner Valley site for: (a) translational; and (b) rotational modes (adapted from Tileylioglu et al., 2011). Velocity, V_{sm}, and modulus, G_m, denote median values from test data.

5.1.3 Field Experiments for Nuclear Applications

Field tests have been supported by nuclear regulatory agencies in the United States and abroad to provide data that can be used to validate analysis procedures, such as CLASSI (Wong, 1979) and SASSI (Lysmer et al, 1999), commonly used for nuclear reactor structures. In one case (Hualien site in Taiwan), these experiments can be used to infer impedance functions. Such cases were presented above and are not repeated here (de Barros and Luco, 1995). Following is a discussion of three similar experiments:

- **Lotung, Taiwan.** This experiment utilized a ¼-scale containment model constructed in Lotung, Taiwan. The objective of the study was to validate SSI analysis methodologies. The Lotung model was a cylindrical structure with a total height of 15 m and embedment depth of 4.5 m. The free-field, structure, and internal components were instrumented to record motions and pressures at the soil-foundation interface. Earthquakes recorded in 1986 were used for subsequent analyses. The model reactor was installed in a soft soil site with measured shear wave velocities, shear moduli, and damping curves with shear strain. The data were used in a blind prediction exercise (Ostadan et al., 1991). Because the data consisted of earthquake recordings and not controlled experiments, it was not practical to directly identify impedance functions across a significant frequency range, as described in Section 5.1.2.

  Findings from the Lotung experiments included information on the relative accuracy of different software packages (SASSI provided favorable results), the effects of soil nonlinearity as manifested in the fundamental frequency of the structure (which is dominated by rocking), and the application of one-dimensional wave propagation analyses to evaluate the free-field motions at the foundation depth through de-convolution.

- **Aomori, Japan.** In 1994, the Nuclear Power Engineering Corporation (NUPEC) initiated a multi-year test program in Aomori Prefecture in northern Japan. This experiment investigated the effects of foundation-soil-foundation interaction of proximate structures. The test consisted of three building conditions: (1) a single reactor building as a reference for comparison; (2) closely spaced twin reactor buildings; and (3) a reactor and turbine building in close proximity. With due consideration of soil property uncertainty, SASSI was able to replicate the principal test results (Xu et al., 2003).

- **Blast Testing at Gillette, Wyoming.** In 2004 and 2005, the Japan Nuclear Safety Organization (JNES) performed a series of blast tests in the Black Thunder mines in Gillette, Wyoming (Nie et al., 2008). The experiments included a model of a 3-story concrete structure in close proximity to the mine. Recorded motions at the site ranged from peak ground acceleration (PGA) of less

than 0.1g to more than 1.0g. Analyses were conducted by JNES using the soil spring approach, SASSI, and LS-DYNA (Livermore Software Technology Corporation). The objective of the study was to create uplift and study the effect of uplift on SSI results. The main findings were as follows:

a. Uplift was initiated with a horizontal PGA of about 0.15g and vertical PGA of about 0.12g.

b. The contact ratio (the foundation area in contact with soil over the total foundation area) dropped to 65% at a horizontal PGA of 0.45g and vertical PGA of 0.41g.

c. Linear analysis over-predicted the extent of the uplift.

d. Analyses that included soil nonlinearity resulted in lesser uplift than linear analyses.

A number of additional tests have been performed with information relevant to seismic earth pressures on retaining walls. Further reports on this topic are presented in Ostadan and White (1998) and Ostadan (2005).

5.2 Laboratory-Scale Tests

Laboratory-scale investigations of soil-foundation interaction have been performed on various configurations using shake-table, free vibration, and centrifuge excitation. Several of these tests are summarized in Table 5-2. Laboratory-scale tests are useful for examining frequency-dependent foundation stiffness terms and nonlinear soil-foundation interaction. In recent years centrifuge tests have been used to guide the development of macro-element models for nonlinear soil-foundation interaction of the type described in Section 2.4.

However, laboratory tests are limited in their ability to reproduce certain field conditions (e.g., Novak, 1987). For example, the finite size of a laboratory test container precludes radiation damping of waves with quarter-wavelengths on the order of the container dimension. This is illustrated in Figure 5-3, which shows theoretical model-based damping ratios increasing with foundation size, whereas the experimental data show essentially constant damping ratio at the hysteretic (material) damping level. The difference is due to radiation damping that is present in the theoretical model, but not in the experiments, due to the small size of the laboratory container.

Table 5-2 Summary of Laboratory-Scale Tests of Dynamic Response of Footings

Parameters and Details						Excitation	Testing Information		
Foundation Dimensions (model scale)	*Structure Description*	*Emb. Depth (cm)*	*g-Level*	*Soil Parameters*	*Soil Depth and Container Dimensions (cm)*	*Source*	*Motion Analyzed*	*Data Availability*	*Reference*
h=45.7cm square/rec. B=5.6 to 13.3 cm L=B-6B circle radius=14.9cm	concrete block	0	1	moist sand; ν=0.33; γ=121 pcf; β_s=0.025	level ground D=152.4 2B=304.8 2L=304.8	applied static force at top of block and suddenly released	vertical, torsion, coupled swaying-rocking	Report	Dobry et al. (1986) Erden (1974) Stokoe and Erden (1985)
h=45.9 to 46.7cm square/rec. B=5.6-13.3 cm L=B-6B circle radius=14.9cm	concrete block	~7.5 to 18.8	1	moist sand; ν=0.33; γ=121 pcf; β_s=0.025	level ground D=152.4 2B=304.8 2L=304.8	applied static force at top of block and suddenly released	vertical, coupled swaying-rocking	Report	Gazetas and Stokoe (1991) Erden (1974) Stokoe and Erden (1985)
h=2.8cm B=1.9cm L=1.9cm	aluminum block 1cm below surface	3.8	30	Dry, No. 120 Nevada sand D_r=75%	level ground D=35.6 2B=61.0 2L=91.4	base/sidewall shear and passive/active force	vertical, torsion, coupled swaying-rocking	Downloadable data; report	Gadre and Dobry (1998)
h=50.8cm B=1.73cm L=6.68cm	double aluminum shear walls	0 to 1.5	20	Nevada sand D_r=60 to 80% and bay mud C_u=100 kPa	level ground D=53.0 2B=90.0 2L=175.0	applied slow sinusoidal cyclic force and dynamic base shaking	rocking	Downloadable data; report	Rosebrook and Kutter (2001a, 2001b, 2001c)
h=48.6cm B=2.5 to 1.73cm L=2.5 to 7.1cm	single wall with frame	2.5	20	Nevada sand D_r=80%	level ground D=53.0 2B=90.0 2L=175.0	applied slow sinusoidal cyclic force and dynamic base shaking	rocking	Downloadable data; report	Chang et al. (2007)
h=276.4cm B=13.5 to 17.75cm L=13.5 to 17.75cm	bridge pier	8.6	20	Nevada sand D_r=80%	level ground D=53.0 2B=90.0 2L=175.0	applied slow sinusoidal cyclic force and dynamic base shaking	rocking	Downloadable data; report	Ugalde (2007)
radius=1.5cm	steel base plate with dual dome	0	50	saturated; dense sand (D_r=85%) over loose sand (D_r=45%)	level ground D=22.0 2B=23.5 2L=56.0	applied sinusoidal cyclic force (freq=50Hz for 500ms)	vertical, torsion, coupled swaying-rocking	Report	Ghosh and Madabhushi (2007)
h=50.75cm B=1.63cm L=6.75 to 7.0cm	single and double rigid steel or aluminum shear wall	0 to 7	20	Nevada sand D_r=60 to 80% and bay mud C_u=100 kPa	level ground D=53.0 2B=90.0 2L=175.0	applied slow sinusoidal cyclic force and dynamic base shaking	rocking	Downloadable data; report	Gajan and Kutter (2008)

Symbols: 2L=total length; 2B=total width; h=height; g-level=gravity load multiplier applied while testing; D=embedment depth; ν=Poisson's ratio; γ=unit weight of soil; β_s=soil damping ratio; D_r = relative density of sand; and Cu = undrained shear strength of clay.

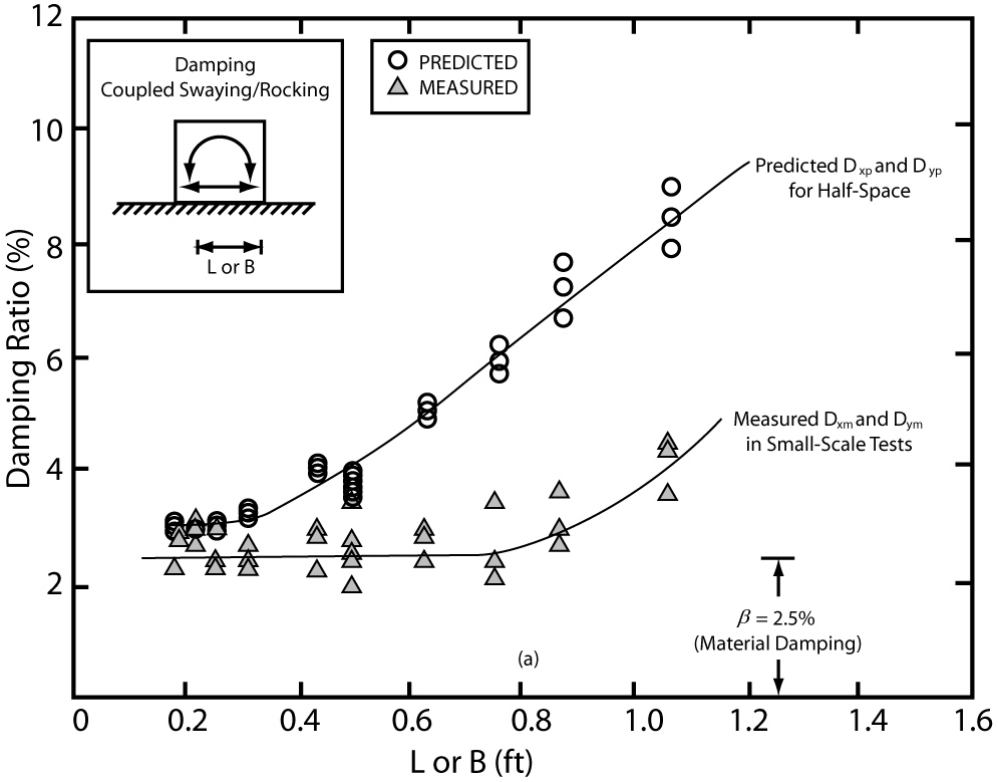

Figure 5-3 Comparison of damping ratio of vibrating blocks of various sizes predicted using impedance models for a half-space and measured from free-vibration tests on laboratory-scale models (Dobry et al.,1986, with permission from ASCE).

Chapter 6
State of Practice

Substantial research has been available for many years, yet there is relatively limited implementation of soil-structure interaction in engineering practice. There is often a lag between the state of knowledge and the state of practice, and this has proven to be particularly true in the case of soil-structure interaction. Even among relatively experienced practitioners, it is clear that there is room for improvement in the technical approaches used in SSI modeling, as well as the manner in which structural engineers, geotechnical engineers, engineering seismologists, and other design and construction professionals interact with each other on projects involving soil-structure interaction.

This chapter summarizes general observations on the state of the practice with regard to modeling soil-structure interaction effects on building structures, and makes specific recommendations for the process of communication and collaboration between design professionals. As a result, the intended audience for this chapter is wider than it is for other chapters in this report, and includes owners, project managers, architects, construction managers, and others who are involved in managing, designing, and constructing the built environment.

6.1 Overview

The state of the practice with regard to SSI was discussed informally and anecdotally with selected structural engineers, geotechnical engineers, and members of the project team. Design professionals engaged in these discussions represented small and large firms with different backgrounds, levels of experience, and geographic locations. Collectively their experience covered a wide range of building sizes, occupancy types, and structural materials. Comments attributed to geotechnical engineers may also be related to engineering seismologists that are providing recommendations as part of the geotechnical engineering scope of services, either as a member of the geotechnical engineering firm, as a subconsultant, or as an independent consultant on projects.

6.2 Observations

This section synthesizes observations of the state of practice related to general issues, collaboration between design professionals, information needed and shared, understanding of SSI principles, and implementation in terms of SSI analyses, soil springs, and common approaches to design problems.

6.2.1 General Observations

Key general observations include:

- The dialogue between structural and geotechnical engineers varies widely, both in extent and sophistication. It appears that an increase in the amount of collaboration would be beneficial, as would better understanding of what each discipline does, and needs, and why. Many geotechnical engineers, for example, are not sure how their recommendations are ultimately being used, and often do not know whether or not their recommendations are being properly implemented.
- In many cases, static and dynamic springs for modeling soil properties are not being consistently or properly developed by geotechnical engineers, nor are they being consistently or properly implemented by structural engineers.
- Understanding of SSI principles is fairly limited among structural engineers, and is usually limited to application of vertical foundation springs. A broader implementation of SSI techniques is rare, and there is virtually no use of foundation damping in any explicit way.
- For typical foundation situations, there is no consensus among structural engineers on the best modeling approaches to use.
- SSI has been used in design of new buildings and in seismic retrofit of existing buildings, although there appears to be greater implementation of SSI in projects involving existing buildings, often as part of performance-based designs or assessments.

6.2.2 Collaboration Between Design Professionals

There is significant variation in the amount of communication and collaboration between structural engineers and geotechnical engineers on typical projects. On some projects, there are few, if any, meetings or direct conversations. On other projects, there is substantial discussion, with several meetings to explore issues and possible approaches and solutions. Some geotechnical engineers express frustration that they provide information and recommendations, but they do not have any role in confirming how their work is used, or whether the final approaches implemented by the design team are appropriate.

On most projects, structural engineers are engaged by the architect, but geotechnical engineers are engaged by the building owner. This arrangement is primarily the result of a perceived increase in liability for geotechnical engineering, and the reluctance of architects, and their professional liability insurers, to engage geotechnical engineers as subconsultants. As a result, geotechnical engineers are not directly managed by the architect as lead design professional, and geotechnical

engineers are typically not part of formal design team meetings arranged by the architect.

There is also an issue of timing. In some cases, geotechnical engineering work is substantially complete by the time design work begins in earnest. Most importantly, however, is an issue related to cost. The fee structure on a typical design project does not allow for multiple design iterations or the use of unfamiliar analytical techniques. This discourages the use of SSI because of a potential increases in design time, even when it could result in significant savings in construction costs.

A need for increased communication and collaboration between engineering disciplines seems particularly important in light of limited experience in SSI implementation, and lack of clear standards of practice.

6.2.3 Information Needed by the Structural Engineer

Structural engineers routinely seek a common set of information from geotechnical engineers on most projects. This includes a description of the soil and rock characteristics at the site, geotechnical hazards that need to be mitigated, and recommendations on appropriate foundation systems. Specific information requested often includes: design bearing pressures under footings; estimates of predicted settlements; at rest, active and passive lateral pressures; coefficients for sliding; vertical and lateral capacities for deep foundations; expected site seismicity; and soil profile type. Depending on the size, nature and sophistication of the project, additional information is often needed, including shoring and underpinning recommendations, force-displacement relationships or springs to represent vertical and horizontal soil properties, site specific spectra, and response histories.

Traditionally, base-slab averaging and embedment effects have not been considered, and this information is not regularly requested. With the publication of FEMA 440, *Improvement of Nonlinear Static Seismic Analysis Procedures* (FEMA, 2005) and other subsequent engineering resources, structural engineers are beginning to take advantage of these effects on new projects, and are beginning to request related design information.

Although there are consistent needs on many projects, few structural engineers report the availability of checklists, or other standardized lists, to assist in organizing and requesting the geotechnical information necessary for foundation design or SSI modeling. A sample checklist of geotechnical information needed by the structural engineer would be considered a useful aid.

6.2.4 Information Needed by the Geotechnical Engineer

Geotechnical engineers can provide better recommendations when they have more detailed information on which to base them. In addition to information from soil

borings and other critical soil data, necessary basic information includes structural design information such as the location of the building on the site, the governing building code, the anticipated height and footprint, the presence of a basement, and the potential structural and foundation systems being considered. A plan of column locations along with anticipated column loading, if available, is useful. Tolerances for differential settlement in the superstructure are valuable, and it is important to know if uplift on foundations is anticipated. The need for site-specific spectra versus response histories must be communicated so the geotechnical scope of work can include their preparation.

If consideration of SSI effects is anticipated, necessary additional information includes details on what type of springs will be used and the approximate building fundamental period. To assist in preparing an appropriate scope of work and in improving dialogue between disciplines, a sample checklist of structural design information needed by the geotechnical engineer is considered a valuable aid.

6.2.5 Understanding of Soil-Structure Interaction Principles

Understanding of SSI principles varies widely across both the structural and geotechnical engineering disciplines. Most structural engineers can appreciate that SSI effects are more pronounced in soft soils, and many are aware that foundation input motions can differ from free-field ground motions. Although SSI effects are known to be significant on stiff, squat, shorter-period buildings, many practitioners mistakenly believe that SSI would have a larger effect on taller, flexible, longer-period buildings.

Structural engineers associate several benefits with modeling of SSI effects. By including the soil in the modeling process, engineers can gain a better understanding of the distribution of forces and displacements in the structure, and additional insight into the foundation design. Some structural engineers are taking advantage of the potential for lowering structural design forces through period lengthening, base-slab averaging, and embedment effects, however, use of foundation damping, and the corresponding reduction in design forces, is typically not being considered.

6.2.6 Analysis Procedures

Analysis procedures used to address seismic loading include equivalent lateral force procedures, modal response spectrum analysis procedures, nonlinear static (pushover) procedures, and nonlinear response history procedures. Although there is increasing use of nonlinear procedures in design, response history analyses are performed by a minority of structural engineers, and among that minority, response history analyses are performed on a relatively small percentage of projects. Currently available codes, standards, and guidelines provide SSI provisions for force-based procedures (e.g., equivalent lateral force and response spectrum analysis) and

displacement-based procedures (e.g., static pushover-type analyses), however, little or no guidance is provided for implementing SSI in response history analysis procedures (see Chapter 4).

Typically, SSI is limited to implementing springs as boundary conditions representing flexibility of the soil-foundation interface in the model. Finite element modeling of the soil continuum is almost never performed in routine building design practice.

Most software packages commonly used in building design have the ability to include uniaxial springs representing support flexibility. However, some are not able to model compression-only properties that might be appropriate for non-embedded (i.e., surface) foundations. More sophisticated programs can vary the compression and tension properties of the springs, and permit bilinear or tri-linear force-displacement relationships. Multi-support excitation is difficult to implement and is not widely available in commonly used structural engineering software, though it is available in programs such as OpenSees (McKenna, 1997).

6.2.7 Implementation of Foundation Springs

Vertical springs are almost always used in the design of mat foundations in order to properly understand the distribution of design forces in the mat. This is typically done with a single modulus of subgrade reaction representing long-term settlement properties of the supporting soil. Use of springs under gravity load-carrying grade beams is also relatively frequent. Springs are occasionally placed beneath spread footings, strip footings, grade beams, piles, and piers. To a lesser extent, they are used to model the combination of soil and foundation vertical flexibility (e.g., individual piles or pile groups).

In comparison, horizontal springs are much less frequently used. In rare cases, they are used on piers and piles to understand the distribution of lateral forces to the foundation elements, particularly if the foundation consists of different systems with different stiffnesses. Horizontal springs are infrequently used to represent the passive pressure developed on the sides of pile caps, grade beams, or retaining walls.

Most structural engineers rely on geotechnical engineers to provide soil spring properties. When values are not provided, or when structural engineers to confirm values that are provided, they refer to engineering resources such as FEMA 356, *Prestandard and Commentary for the Seismic Rehabilitation of Buildings* (FEMA, 2000) or its successor document, ASCE/SEI 41-06, *Seismic Rehabilitation of Existing Buildings* (ASCE, 2007), which provide guidance on default soil properties and equations for static spring stiffnesses. A few structural engineers also use rule-of-thumb checks based on practical experience. Most structural engineers, however,

do not know the basis of spring values provided by the geotechnical engineer, and the basis is often not stated in the geotechnical report.

Often the modulus of subgrade reaction, given for long-term gravity loading, is used as the basis for dynamic loading conditions. This can lead to significant underestimation of soil stiffness during dynamic loading, and significant overestimation of the amount of displacement and rotation caused by the deflecting soil. The cause for this appears to be a lack of understanding about the differences between long-term and short-term loading effects on soil, a lack of clarity on what is needed by the structural engineer, and a lack of understanding of the limits of the information the geotechnical engineer is providing.

When foundation springs are used, practice varies on the extent to which uncertainty is used to bound expected soil properties. Resources like FEMA 356 and ASCE/SEI 41-06 specify a range of two times the expected values to one-half of the expected values, but this is dependent on the variability in site conditions and scatter of material properties. Some structural engineers use a simple, conservative upper bound assuming a fixed base (or an essentially infinitely rigid spring). Others modify the spring values provided by the geotechnical engineer in some way. The best result is obtained when the geotechnical engineer provides upper- and lower-bounds around expected values. This usually narrows the bounds recommended by FEMA 356 and ASCE/SEI 41-06, but is dependent on the variability in site conditions and scatter present in measured soil properties.

When force-displacement relationships are provided for dynamic loading conditions, a maximum or ultimate capacity is frequently provided, allowing an elasto-plastic relationship to be developed. When this is not directly provided, safety factors are occasionally given, permitting back-calculation of the plateau value. Some geotechnical reports, however, remain fully in the allowable stress design format in which safety factors are used but not reported. This situation prevents a rational investigation of SSI effects at higher seismic force levels.

For deep foundations such as piles or piers, different stiffnesses are occasionally provided for tension and for compression. Lateral springs are typically developed using common commercial software programs that provide the displacement, shear, and moment profile considering the variation in soil properties over the depth of the element.

6.2.8 Modeling Approaches for Common Design Situations

Modeling approaches vary depending on the configuration of the building, the presence of a basement, and the level of the supporting grade.

Embedded Buildings

Figure 6-1 illustrates a common situation of a building with a basement that is surrounded by soil with a level grade on all sides. Several potential modeling strategies that can be used to analyze such a building are shown in Figure 6-2.

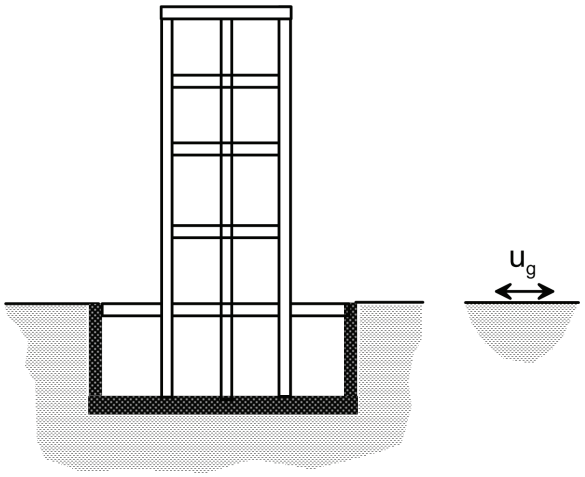

Figure 6-1 Illustration of an embedded building configuration with a basement surrounded by soil and a level grade on all sides.

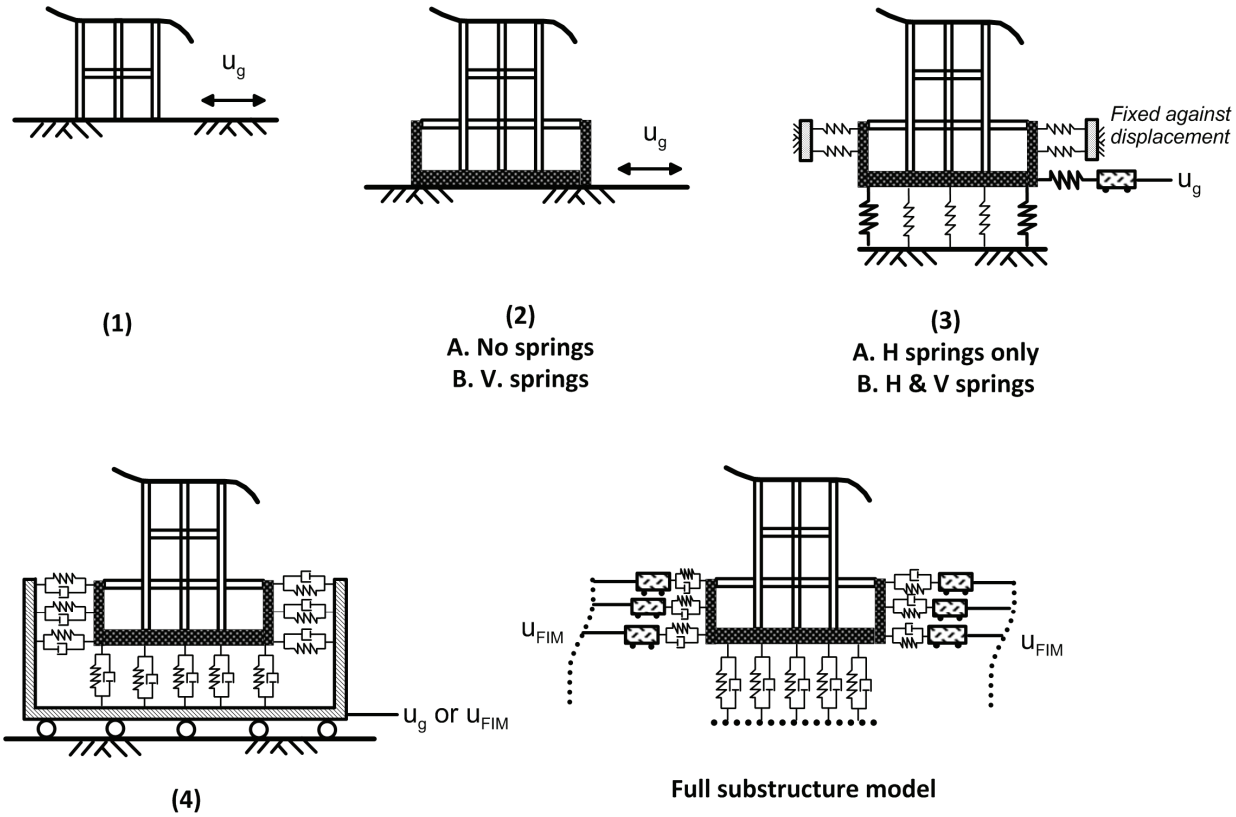

Figure 6-2 Modeling approaches for embedded foundations.

Of the modeling approaches illustrated in Figure 6-2, there was no consensus on the best approach, or even the most common approach in design practice. Observations include the following:

- **Model 1.** In this approach, the building is assumed to be fixed at the ground level, and no SSI effects are considered. Reactions are calculated at the base of the model at grade, and then applied to the foundation in a separate model. This approach is used occasionally by some engineers, and frequently by others. Some believe this model is more appropriate for moment frame and braced frame buildings, and less appropriate for shear wall buildings. Others would only use this model if there were no "back-stay effects." Back-stay effects occur when the lateral system of the superstructure does not align with the full footprint of the foundation. An example of such a configuration is a superstructure with a concrete shear wall core system founded on a wider basement podium structure with perimeter walls. Backstay effects involve the transfer of lateral forces in the superstructure into additional elements that exist within the basement, typically through one or more floor diaphragms. This force transfer helps tall buildings resist overturning effects, and is referred to as the backstay effect because of its similarity to the back-span of a cantilever beam.

  The added stiffness of the retaining walls, and the relative rigidity of the walls and diaphragms comprising the basement, can lead to larger shear forces in the basement levels than in the superstructure. Modeling of the in-plane flexibility of the basement diaphragms can provide more rational results for this effect. When the lateral force-resisting system of the superstructure covers the full footprint of the basement, the backstay effect is reduced or eliminated.

- **Model 2.** In this approach, the soil on the sides of the retaining walls is ignored, but the basement structure is explicitly included in the model. The lowest basement level is taken as the base of the model. It is argued that the amount of movement required to develop passive pressure of any significance far exceeds the amount of movement anticipated in the basement retaining walls, so the retained earth can be conservatively ignored. One variation of this model (Model 2A) has a fixed base. A second variation of this model (Model 2B) has vertical springs under the foundation. Model 2A is occasionally used, though limited by some to the preliminary design phases of their projects. Model 2B is used more frequently, though some use both Model 1 and Model 2B to bound their analyses for design.

- **Model 3.** In this approach, horizontal springs are used to capture the effect of the surrounding soil. The ends of the springs are fixed against translation, and ground motion is input at the base of the model. When this modeling approach is used, it is used in pushover analyses. One variation of this model (Model 3A) is fixed vertically. A second variation of this model (Model 3B) includes vertical

springs. Model 3A is used occasionally by some, while Model 3B is used more frequently. Some engineers never use either version of this modeling approach.

- **Model 4.** In this approach, horizontal springs are attached to rigid walls (referred to as a "bathtub"), and the ground motion is applied to the bathtub so that the ends of the horizontal springs all move together with the input motion. This modeling approach is rarely used, although it is recommended in the recent *Guidelines for Performance-Based Seismic Design of Tall Buildings* (PEER, 2010).
- **Full Substructure Model (MB).** This modeling approach is designated the Baseline Model (or MB). It represents a comprehensive modeling approach in which dashpots are used to address soil damping variation, foundation rotation is considered, and multi-support excitation is applied through the horizontal springs so that the inputs vary up the height of the basement walls. This model is not currently used in practice.

Partially Embedded Buildings with Unbalanced Loading

Figure 6-3 illustrates a building with a basement that does not have retained earth on one or more sides. In this situation, the loading caused by the soil pressure on one side of the building is typically analyzed separately and added to the building inertial loading by linear superposition. Structural engineers report the use of Models 2A, 2B, 3A, and 3B, as shown in Figure 6-2, for modeling partially embedded buildings.

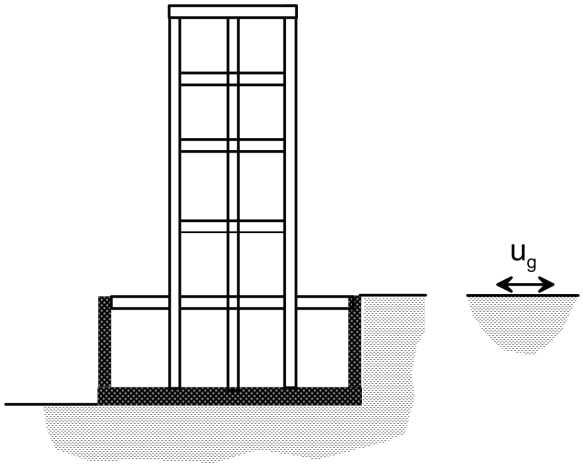

Figure 6-3 Illustration of a partially embedded building configuration with unbalanced loading.

Buildings without a Basement

Figure 6-4 shows a building without a basement. Structural engineers report the use of different modeling approaches for buildings without a basement, depending on the type of foundation system:

- For mat foundations, Model 2B is typically used. Note that Model 4 is equivalent to Model 2B when the foundation is not embedded.
- For spread footings, both Models 1 and 2B (equivalent to Model 4) are used.
- For grade beams, both Models 1 and 2B (equivalent to Model 4) are used.
- For drilled piers or piles, Model 2B (equivalent to Model 4) is frequently used.

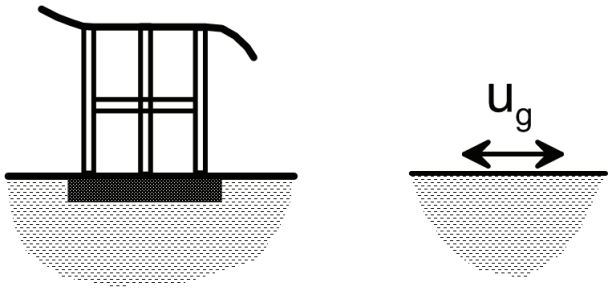

Figure 6-4 Illustration of a building configuration without a basement.

6.3 Recommendations

Based on the above observations, recommendations for improving the implementation of SSI include:

- Enhanced techniques for improving dialogue and collaboration between structural engineers and geotechnical engineers.
- A sample checklist of information that the structural engineer should consider providing to the geotechnical engineer.
- A sample checklist of information needed by the structural engineer, which should be requested from the geotechnical engineer.
- Sample formats for presentation of static and dynamic spring parameters.
- Guidance on modeling approaches applied to typical foundation design situations, with recommendations for practice.
- Example applications showing the benefits and drawbacks associated with simplified SSI modeling approaches.

6.3.1 Improved Collaboration Between Structural and Geotechnical Engineers

Better clarity on the part of structural engineers with regard to the modeling approach for the soil and foundation will help geotechnical engineers provide better recommendations. Having a defined number of meetings between the geotechnical and structural engineers will improve communication and help ensure proper development and implementation of foundation recommendations.

Some owners require geotechnical reports to be written in stages, including an initial draft to help foster communication, and then later drafts or a final report after the design is further along and needs are better defined. For example, an initial draft memo might broadly define the various possible foundation systems, and give preliminary design values. Once the final system is selected (or narrowed down to final candidates), then detailed recommendations can be presented.

Owners can level the playing field in the competitive market place by clearly requesting these additional scope items in the proposal. Owners can also coordinate the timing of consultant selection and engagement so that geotechnical and structural engineers are on a concurrent project delivery schedule. Some projects might benefit from a foundation design charrette involving a foundation contractor to discuss project specific installation issues that can help in refining and improving the design.

6.3.2 Checklist of Information That Should be Provided to Geotechnical Engineers

Certain information is needed by the geotechnical engineer to develop foundation design recommendation and provide the necessary information for modeling SSI effects. This information is often provided by the structural engineer, though other members of the design team (e.g., architect or owner's representative) can supply much of the information. A sample checklist of items includes the following:

1. *Location*. Identify the site and the proposed location of the building on the site.
2. *Building Code*. Identify the building code, standard, or design guideline that will be used on the project.
3. *Performance Objectives*. If performance-based design will be used, identify the guidelines that are proposed and the specific performance objectives, acceptance criteria, and hazard levels that are being considered.
4. *Description of the Building*. Provide a description of the building, including the number of stories, anticipated height, footprint size, overall square footage, occupancies, and basement depth. Describe the potential structural and foundation systems under consideration. Provide drawings if they are available, particularly a foundation plan or floor plan showing column locations, and a building section.
5. *Differential Settlement Tolerance*. Provide special restrictions on differential settlement, if any, as these can impact foundation system selection.
6. *Approximate Fundamental Building Period*. If potential structural systems are known, provide the approximate fundamental building period in each direction. This is useful in developing recommendations for SSI modeling parameters.

7. *Loads to Foundation*. If preliminary loads are known, provide values, or a range of potential values for the following load cases (assuming earthquake governs over wind). The load combinations listed below are an example list; others should be provided as relevant for the particular project. Consistent with historic practice, and much of current practice, allowable stress design combinations are shown; however, factored loads should be provided when performance-based design and SSI will be used. Associated capacities are needed, particularly at the maximum or ultimate load level. Note that both factored level load combinations and "ultimate" level load combinations are listed, as the associated capacities will be different at each level.

    a. Allowable stress design:

        i. D: average and maximum.

        ii. $D + L$: average and maximum.

        iii. $D + 0.75L + 0.75(0.7E)$: average and maximum compression.

        iv. $0.6D + 0.7E$: average and maximum tension.

    b. Strength design:

        i. $1.2D + 1.6L$: average and maximum.

        ii. $1.2D + E + L$: average and maximum compression.

        iii. $1.2D + E_m + L$: maximum ultimate compression.

        iv. $0.9D + E$: average and maximum tension.

        v. $0.9D + E_m$: maximum ultimate tension.

8. *Soil-Structure Interaction*. Indicate if SSI is likely to be included in the design process, along with the level of sophistication of modeling that is anticipated. Indicate if recommendations on ground motion modification for foundation embedment and base-slab averaging are needed. Indicate if recommendations for foundation damping are needed.

9. *Site Specific Spectra.* Indicate if site specific spectra are needed. Indicate whether uniform hazard spectra or conditional mean spectra are desired. If the site is in a known near-fault region, clarify if spectra are needed for fault normal and fault parallel orientations. If site is known to be on soft soil, particularly Site Class F, indicate whether ground response analysis of the soil/rock column is anticipated. If known, indicate whether shear wave velocity measurements for the site will be needed.

10. *Response History Analysis*. Indicate if response history analysis is anticipated, and, if so, how many ground motions are required or desired. Indicate the

preferred scaling technique, such as spectrally matched or amplitude scaled, where known.

6.3.3 Checklist of Information Needed by Structural Engineers

Certain information is needed by the structural engineer to develop preliminary and final foundation designs, to perform structural analysis, and to model SSI effects. Ideally, this information should be requested from the geotechnical engineer prior to commencement of the geotechnical site investigation. Some of the following items comprise basic information that is typically included as part of a geotechnical investigation report, while others will likely be excluded unless specifically requested. A sample checklist of items includes the following:

1. *Site Description.* Request a description of the soil and rock conditions at the site.
2. *Boring Reference Elevations*. Where boring logs summarizing the encountered soil conditions are presented in terms of depth from the ground surface, request the ground surface elevation at each boring location with respect to a common benchmark or datum. A plan of boring locations should also be requested, preferably showing the existing and new building footprint.
3. *Field and Laboratory Testing Results*. Request a summary and interpretation of field and laboratory testing, including shear wave velocities, if they were measured.
4. *Site Seismicity Information*. Request information needed for calculation of the code base shear and site specific response spectrum. Indicate the assumptions and methodology used to develop the response spectra, including uniform hazard versus conditional mean spectra, scaling requirements, geomean versus maximum rotated component assumptions, assumed shear wave velocities, whether or not site response analysis was conducted, and the type of hazard model used. Request spectra for fault-normal and fault-parallel orientations, as appropriate.
5. *Response Histories*. If response history analysis is required or desired, request appropriate ground motion acceleration histories. Indicate the assumptions and methodology used to develop the acceleration histories, such as the scaling technique (spectrally matched or amplitude scaled, for example), and fault normal/fault parallel orientation approaches.
6. *Seismic Site Hazards*. Request assessment of potential for liquefaction, lateral spreading, and other types of seismic hazard that would affect the structural design.
7. *Groundwater Table*. Request information on the design groundwater elevation.

8. *Foundation Type Recommendations*. Request recommendations for suitable foundation types given the geotechnical conditions at the site. The following information is needed for some of the most common foundation types:

    a. *Mat Foundation:*

        i. Bearing pressures. Allowable soil bearing pressures under dead, dead plus live, and dead plus live plus wind/seismic load cases. Request associated safety factors for each case. Note whether the weight of soil above the foundation and the equivalent weight of soil displaced by the concrete foundation can be neglected when evaluating soil bearing pressures.

        ii. Modulus of subgrade reaction. This information is needed in order to define vertical springs for computer analysis of a mat foundation. It will be used for long-term gravity load cases.

        iii. Vertical soil springs for earthquake loading. In addition to the modulus of subgrade reaction, request expected, upper-, and lower-bound force-displacement relationships for short-term dynamic loading for vertical springs. Request similar relationships for horizontal springs.

        iv. Coefficient of friction at the bottom of mat/soil interface, plus associated safety factor.

        v. Allowable passive lateral earth pressure on vertical faces of mat, plus the associated safety factor. Indicate how passive and sliding resistance can be combined.

        vi. Heave and settlement estimates.

    b. *Spread/Strip Footings/Grade Beams.* Request information similar to that required for the mat foundation, including an estimate of anticipated long-term differential settlement between adjacent footings. Request expected, upper-, and lower-bound force-displacement relationships for short-term dynamic loading for vertical springs. Request similar relationships for horizontal springs.

    c. *Drilled Piers or Piles:*

        i. Request skin friction and end bearing capacities at allowable levels and at ultimate levels, suitable for use with code overstrength load combinations for both tension and compression loading.

        ii. Force-deflection plots for axial loading. Request expected, upper-, and lower-bound force-displacement relationships for short-term dynamic loading for vertical springs.

iii. Plots of lateral load versus deflection and lateral load versus maximum moment for both fixed head and pinned head conditions. Request expected, upper-, and lower-bound force-displacement relationships.

iv. Request information on how group effects may control vertical or lateral capacity of piles.

v. Request estimates of long-term differential settlement between pile caps and spread footings when the two systems are mixed.

vi. Request recommendations on minimum depth of embedment.

vii. Request identification of special construction/inspection requirements.

9. *Miscellaneous Site Items*:

a. *Excavations:*

i. Maximum slope angles and soil treatment necessary to provide stable slopes during excavations.

ii. Underpinning and shoring recommendations if required.

iii. Underpinning settlement expectations.

iv. Tie back recommendations.

b. *Excavated material/engineered fill.* Request information on backfill and compaction requirements, and whether or not native soils will be acceptable as fill.

c. *Retaining wall recommendations*. Request design values for cantilevered and restrained site retaining walls, including allowable and ultimate bearing pressures, active and passive pressures, coefficient of friction, seismic and non-seismic surcharge criteria, appropriate combinations of resisting elements, and methods of surcharge loading. Request expected, upper-, and lower-bound force-displacement relationships for short-term dynamic loading for horizontal springs, if requested.

d. *Existing building considerations:*

i. Zone of influence of existing building foundations.

ii. Existing footing surcharge loads and other lateral earth pressures.

iii. Deflection requirements of existing foundations, soldier piles, secant piles, and monitoring recommendations.

e. *Recommendations for slabs-on-grade.*

f. *Assessment of soil corrosivity.*

10. *Additional SSI Recommendations*. In addition to the spring parameters noted above, request the following:

    a. *Base slab averaging.* Base slab averaging recommendations and limitations for spectral modifications, if needed.

    b. *Embedment effects.* Recommendations on embedment effects for spectral modifications, if needed.

    c. *Damping.* Recommendations on soil damping and dashpots if they will be used in SSI modeling.

6.3.4 Sample Format for Soil Spring Characterization

Soil springs are often not properly, or adequately, implemented in practice. In some cases, the modulus of subgrade reaction developed for long-term settlement is being used for dynamic loading situations. In other cases, a single value or single force-displacement relationship is being used for the soil properties. Figure 6-5 provides a sample format for presentation of soil spring data.

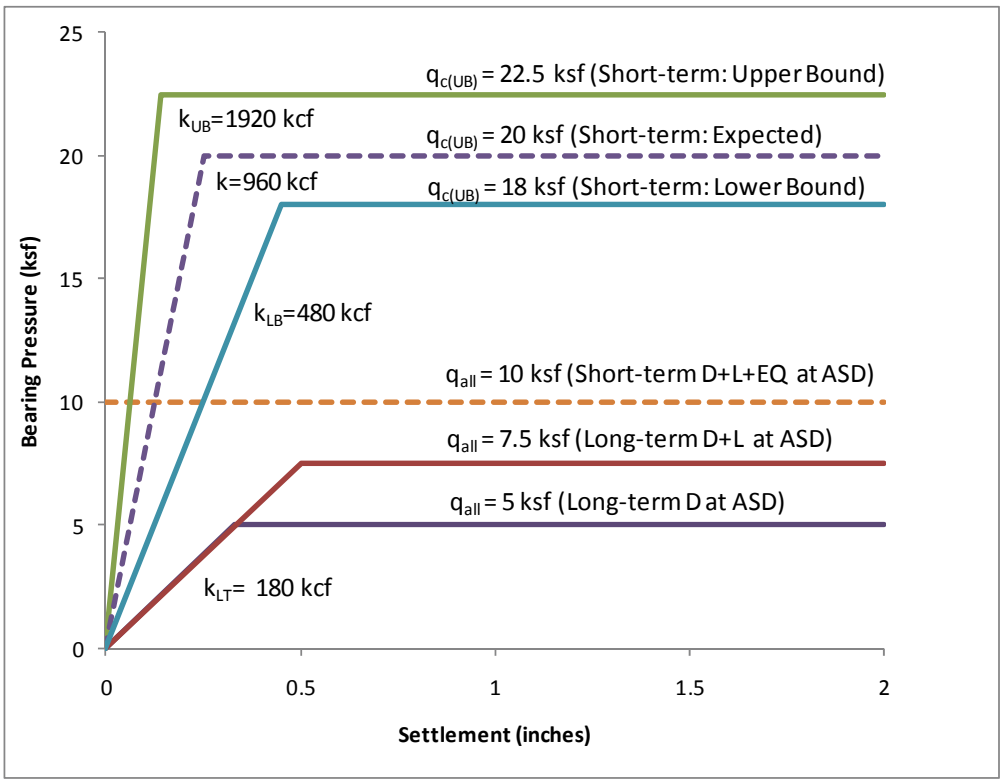

Figure 6-5 Sample format for presentation of force-displacement relationships for soil springs.

The sample format includes both the relationship for long-term settlement, which needs only a lower-bound, and recommendations for the expected (or target) properties under dynamic loading, including both an upper-bound and lower-bound.

Per ASCE/SEI 41-06 and other engineering resources, these bounds are typically two times and one-half times the target, unless narrower bounds are provided by the geotechnical engineer based on the variability of the site soil conditions. For simplicity, Figure 6-5 uses an elasto-plastic format. Actual properties would have a positive post-yield slope and a more rounded transition, which could be approximated by a tri-linear curve.

6.3.5 Guidance on Modeling Approaches for Typical Foundation Situations

Guidance on modeling approaches applied to typical foundation design situations, and recommendations for practice, is provided throughout this report. Examples are provided in Chapter 7, and recommended procedures are provided in Chapter 8.

6.3.6 Example Applications of Simplified Soil-Structure Interaction

Case studies illustrating the level of effort, relative benefits, and potential drawbacks associated with simplified SSI modeling approaches are provided in example applications presented in Chapter 7 for a variety of different building configurations.

Chapter 7
Example Applications

ΔBuilding seismic response analysis including soil-structure interaction involves characterization of the soil-foundation interface in the analytical model. Typical methods for idealizing the soil-foundation interface in current engineering practice are described in Chapter 6. While some of these models are simple, others require significant effort to capture linear or nonlinear SSI effects. Example applications in this chapter are used to demonstrate different foundation modeling techniques and investigate the relative accuracy of the resulting building response predictions.

Methods for developing soil springs and dashpots described in this report are implemented on case-study buildings using several models with different idealizations at the soil-foundation interface. Examples are used to illustrate the corresponding level of effort for different modeling approaches. Overall results and selected structural response quantities from the models are compared and contrasted. Analyses are performed in the context of a substructure approach to modeling SSI effects.

7.1 Overview of Example Applications

The overall approach for development of example applications involved: (1) the selection of suitable instrumented buildings that have experienced (and recorded) earthquake ground motions; (2) development of baseline models for comprehensive substructure-based analysis of seismic response; (3) calibration of baseline models to approximately match the recorded response of the buildings through variation of structural parameters; and (4) systematic variation in the idealization of the soil-foundation interface to evaluate the impact of different modeling approaches on the predicted response of the buildings.

Work included a review of the results from similar studies performed by others and published in the literature. Information from these studies was used to guide the example applications presented herein, and corroborate the resulting observations.

7.1.1 Summary of Results from Prior Studies

Prior studies reported by Naeim et al. (2008) and Tileylioglu et al. (2010) utilized typical structural engineering software packages, such as ETABS, *Extended Three Dimensional Analysis of Building Systems* (Computers and Structures, Inc.), and SAP2000, *Integrated Software for Structural Analysis and Design* (Computers and

Structures, Incorporated), to model the soil-foundation interface of two buildings in Los Angeles, California. One building is a 54-story building, and the second building is a 6-story building. Both buildings have embedded foundations, and both experienced earthquakes with recorded ground motions. Only the results of the 54-story building, however, have been published to date.

Analyses initially employed the full substructure modeling approach, designated the Baseline Model (or MB) as described in Chapter 6, except that kinematic base rocking was applied to the base of vertical foundation springs along with depth-variable ground motions. This results in double-counting of kinematic rotation effects. Fortunately, these effects were minor for the structures investigated, and double-counting did not have a significant impact on results.

Springs were elastic, with no compression capacity limit, and zero tension capacity. Kinematic effects were evaluated in a manner similar to that described in Chapter 3 (except that kinematic base rocking was applied). Significant difficulties were encountered in implementing multi-support excitation using typical engineering production software packages. Results were considered reliable for displacement response, but not reliable for forces. In general, however, good matches between computed and observed responses were reported using the baseline modeling (MB) approach.

Selected elements of the full substructure modeling approach were then omitted from the models to investigate their impact on the computed response. The following factors did not have a significant impact on the results: (1) consideration of multi-support excitation along basement walls; and (2) application of a zero-tension condition in the foundation springs. Consideration of kinematic interaction effects had a significant impact on the distribution of interstory drifts, particularly below grade. Consideration of foundation springs had a significant impact on building vibration periods and distribution of interstory drifts.

Two modeling approaches commonly used in practice were shown to provide poor results: (1) fixing the structure at the ground surface, truncating the embedded portions of the structure, and applying the free-field translation as the input motion (Chapter 6, Model 1); and (2) modeling the embedded base of the structure, using horizontal and vertical springs with ends fixed against translation, and applying free-field motions as input at the base slab level (Chapter 6, Model 3).

A fixed-base approach considering embedded portions of the structure (Chapter 6, Model 2) provided better results, while the “bathtub” approach (Chapter 6, Model 4) was not considered in this work.

7.1.2 Building Selection

The criteria considered in building selection included: (1) embedded foundations, so that kinematic effects associated with embedment and depth-variable ground motions could be considered; (2) recordings of rocking at the foundation level, which requires two vertical instruments; (3) relatively regular structural configurations, so that the results obtained are not peculiar to any one building in particular; and (4) structural configurations and site conditions that would tend to be conducive to significant inertial SSI effects.

Only buildings with seismic instrumentation and available earthquake recordings in California were considered, using archives provided by the Center for Engineering Strong Motion Data (CESMD). The CESMD provides strong-motion data for earthquake engineering applications. It was established by the United States Geological Survey (USGS) and the California Geological Survey (CGS) to integrate and disseminate earthquake strong-motion data from the CGS California Strong Motion Instrumentation Program (CSMIP), the USGS National Strong Motion Project, and the Advanced National Seismic System (CESMD, 2011).

Two case-study buildings were selected from CSMIP, consisting of: (1) a 13-story, reinforced concrete moment frame structure (designed in 1964; retrofitted in 1994), with two basement levels, located in Sherman Oaks, California; and (2) a 10-story, reinforced concrete shear wall core and perimeter moment frame structure (designed in 1970), without any basement levels, located in Walnut Creek, California. The exterior elevations of the buildings are shown in Figure 7-1.

(a) (b)

Figure 7-1 Exterior elevations of two case-study buildings: (a) 13-story Sherman Oaks building; and (b) 10-story Walnut Creek building (CESMD, 2011, with permission).

The Sherman Oaks building foundation consists of grade beams and friction pile foundations on alluvial sediments. The building was shaken strongly by the 1994 Northridge earthquake and less-strongly by other, more distant events. The Walnut Creek building foundation consists of a shallow concrete mat foundation below the shear wall core, and a combination of spread footings and belled caissons with shallow embedment, resting on weathered shale bedrock, below the perimeter moment frames. The Walnut Creek building was shaken by the 1989 Loma Prieta earthquake and other smaller events.

No single building was found to meet all of the selection criteria. The Sherman Oaks building satisfied criteria (1) and (3) above, while the Walnut Creek building satisfied criteria (2), (3), and (4) above.

7.1.3 Modeling Approaches

Modeling approaches considered in the example applications are shown in Figure 7-2. They are based on the approaches implemented in typical engineering practice, as described in Chapter 6. They include the Baseline Model (designated MB), and various simplified idealizations of the soil-foundation interface, designated Model 1, Model 2, Model 3, and Model 4.

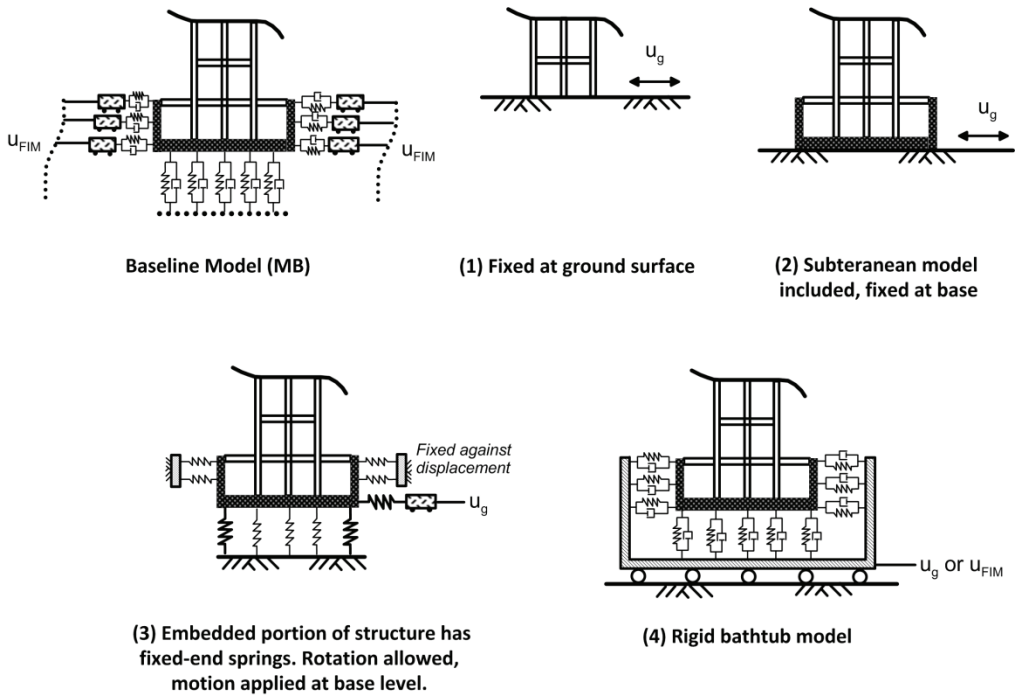

Figure 7-2 Modeling approaches considered in example applications.

- **Baseline Model (MB).** A baseline model (designated MB) is a three-dimensional model of the building, foundation, and soil-foundation interface. Baseline models are not intended to be the most accurate models that could be developed (a direct SSI analysis in a finite element platform could provide

improved results). Instead, they are intended to represent a comprehensive modeling approach that includes soil springs to consider translational and rotational degrees of freedom, dashpots to address soil damping effects, and multi-support excitation to capture variable input motions over the depth of embedment. Baseline models incorporate vertical translation, horizontal translation, and rocking degrees of freedom. A series of springs and dashpots are developed based on site-specific soil properties. Seismic input includes base translation, as well as kinematic loading of basement walls (simulated by displacement histories applied to the ends of horizontal springs attached to basement walls). Baseline models are calibrated to match building response quantities interpreted from available recorded data.

Once baseline models have been successfully calibrated to match recorded data, the soil-foundation interface is idealized using one of the following simplified modeling approaches from Chapter 6:

- **Model 1.** In Model 1, only the above-ground portion of the structure is modeled, the base is fixed at the ground surface, and the free-field ground motion, u_g, is applied at the base of the model.
- **Model 2.** In Model 2, the above-ground and subterranean portions of the structure are modeled, the based is fixed at the bottom of the embedded portion of the structure, the soil surrounding the embedded portion is ignored (i.e., no horizontal foundation springs are used), and the free-field ground motion, u_g, is applied at the base of the model.
- **Model 3.** In Model 3, the above-ground and subterranean portions of the structure are modeled, horizontal and vertical soil springs are included, the far end of each spring is fixed against translation, and the free-field ground motion, u_g, is applied at the base slab while horizontal springs at other levels remain fixed. In the example applications, Model 3 is investigated using response history analysis, although in practice, it is typically used in nonlinear static (pushover) analysis applications.
- **Model 4.** In Model 4, the above-ground and subterranean portions of the structure are modeled, horizontal and vertical soil springs are included, the far end of each spring is fixed against a rigid "bathtub" element, and the horizontal foundation input motion, u_{FIM}, or free-field motion, u_g, is applied to the rigid element. The key difference between Model 4 and Model MB is the manner in which the seismic demand is applied. In Model 4, the effect of kinematic loading on basement walls associated with depth-variable displacement histories is neglected. Further, the use of free-field motions in lieu of foundation input motions neglects kinematic interaction altogether by replacing the recorded

motions at the base of the building with equivalent free-field motions applied uniformly at the ends of all horizontal foundation springs.

Table 7-1 summarizes the properties of the modeling approaches considered in the example applications. Variations in Model MB (denoted MB.1 and MB.2) are considered as follows:

- In Model MB.1, the embedded portion of the building is assumed to be rigid. The specification of seismic demand is not modified. The objective of this model is to investigate the effects of flexibility in the subterranean structural elements.
- In Model MB.2, there is a change in the way that soil flexibility is modeled. In this model, springs are not allowed to develop tension to investigate the effects of nonlinearities in the foundation springs.

Table 7-1 Summary of Modeling Approaches Considered in Example Applications

	Model Variations						
Parameters	*No. 1*	*No. 2*	*No. 3*	*No. 4*	*MB*	*MB.1*	*MB.2*
Structural Foundation Elements	N/A	Flexible	Flexible	Flexible	Flexible	Rigid	Flexible
Input Motion	u_g	u_g	u_g	4a: u_{FIM} 4b: u_g	u_{FIM}	u_{FIM}	u_{FIM}
Depth-variable Ground Motion	No	No	No	No	Yes	Yes	Yes
Spring Tension	n/a	n/a	Permitted	Permitted	Permitted	Permitted	Not Permitted

All modeling schemes, except Model MB.2, permit tension to develop in the soil springs. The rationale for this approach is that, prior to an earthquake, actual basement wall-to-soil contact pressures range between 'at rest' and 'active' earth pressures. Springs have an initial condition of zero force. Since earthquake shaking will impose alternating cycles of increased and decreased pressures relative to the initial state, wall-to-soil contact can be represented by a spring that develops tension, provided that the level of deformation does not lead to gap formation. Given the modest levels of demand imposed on the Sherman Oaks and Walnut Creek buildings, this was expected to be a reasonable assumption, and this assumption was tested using Model MB.2 on the Sherman Oaks building.

7.2 Sherman Oaks Building

The Sherman Oaks building is a 13-story structure above grade with two basement levels below grade. The seismic force-resisting system consists of reinforced concrete moment-resisting frames that extend from the roof to the foundation, supplemented by perimeter concrete shear walls in the subterranean levels. The gravity system consists of cast-in-place concrete slabs supported on concrete beams

and columns. The building was originally designed in 1964, and later seismically upgraded with friction dampers following the 1994 Northridge earthquake.

Construction drawings of the Sherman Oaks building were made available for inspection through the auspices of the California Strong Motion Instrumentation Program. The building measures 50 m (164 ft) tall from the ground surface to the roof. The plan dimensions of the superstructure are 21.9 m (72 ft) wide by 57.6 m (189 ft) long, although it widens at the first floor to match the foundation dimensions. The height of the first story is 7.0 m (23 ft), and other above-grade stories are 3.6 m (11.75 ft). The basement levels are embedded approximately 6.2 m (20.5 ft) below the ground surface. The height of the first basement level is 3.5 m (11.5 ft), and the height of the second basement level is 2.7 m (9 ft). The characteristics of the foundation are described in Section 7.2.3 below.

7.2.1 Site Characterization

A plan view of the Sherman Oaks site is shown in Figure 7-3. The ground surface elevation is approximately 216 m (709 ft) above mean sea level. Boring information and geophysical logs were obtained from geotechnical investigations conducted in the vicinity of the site (LeRoy, Crandall and Associates, 1978 and 1982).

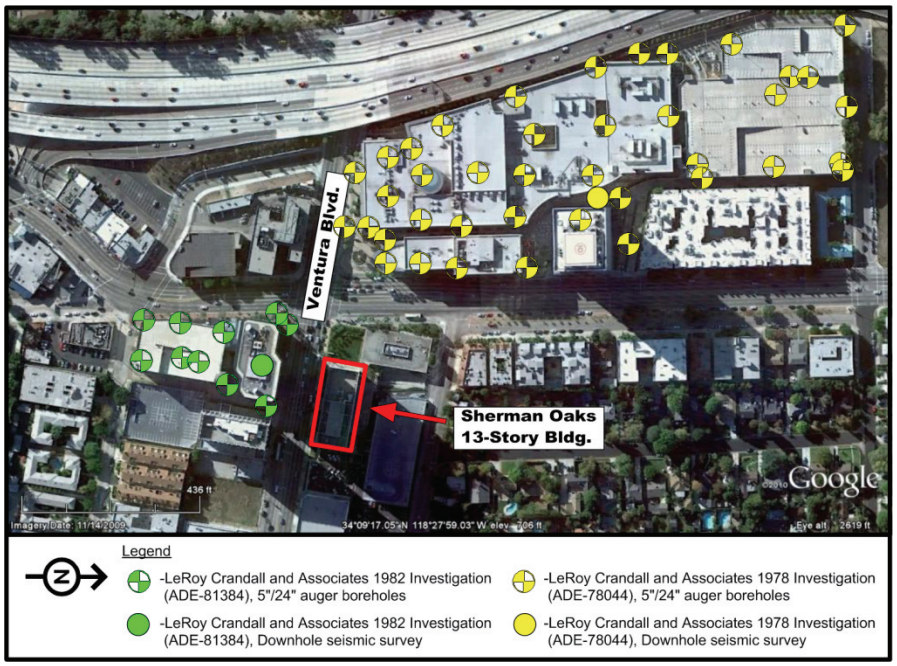

Figure 7-3 Plan view of the Sherman Oaks site showing locations of borehole and geophysical logs used for site characterization (adapted from LeRoy, Crandall and Associates, 1978 and 1982).

Information from a total of 47 borings ranging in depth from 15 m (50 ft) to 38 m (125 ft) was obtained. Borings indicated relatively consistent soil conditions, consisting of alluvial deposits composed of silt, with sand and clay overlying shale

bedrock at depths ranging from 21 m (70 ft) to 27 m (90 ft). The water table was measured at an approximate depth of 12 m (40 ft) below the ground surface. Geophysical data was developed from downhole seismic surveys. Based on available geotechnical information, an interpretation of the soil layering at the site, in terms of shear wave velocity profile and material profile, is shown in Figure 7-4.

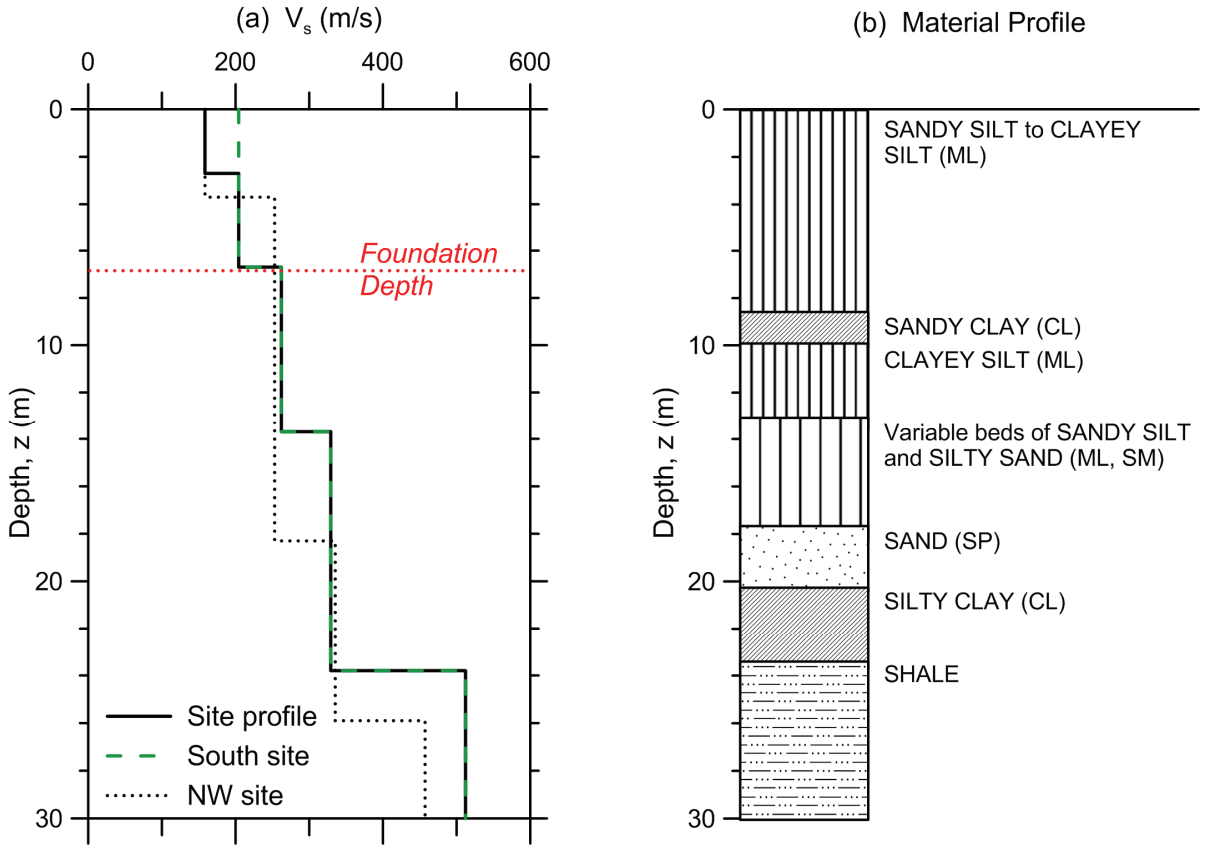

Figure 7-4 Subsurface characteristics of the Sherman Oaks site: (a) shear wave velocity profile; and (b) material profile (adapted from LeRoy, Crandall and Associates, 1978 and 1982).

The average moist unit weight was taken to be 20 kN/m^3 (124 lb/ft^3). To estimate strength properties of the foundation soils, direct shear test results from samples were utilized. In the shallow soils, where most of the soil-foundation load transfer will occur, the soil is unsaturated, so drained shear strengths were used. For the range of surcharge pressures over the soil profile extending to the bottom of piles at a depth of approximately 16.2 m (53 ft) below grade, the soil Mohr Coulomb strength parameters inferred from available data are: (1) $c' = 20.1$ kN/m^2, and $\phi' = 30°$, from 0.0 m to 6.1 m; and (2) $c' = 12.9$ kN/m^2, and $\phi' = 38°$, from 6.1 m to 16.2 m.

7.2.2 Ground Motion Recordings

The Sherman Oaks building was instrumented in 1977 by the California Strong Motion Instrumentation Program and designated CSMIP Station No. 24322.

Instrumentation includes 15 accelerometers at the locations shown in Figure 7-5, including the second basement (foundation level), ground floor, second floor, eighth floor, and roof levels. There is only one vertical sensor located at the foundation level, so base rocking effects cannot be measured, and there are no free-field instruments in the vicinity of the site.

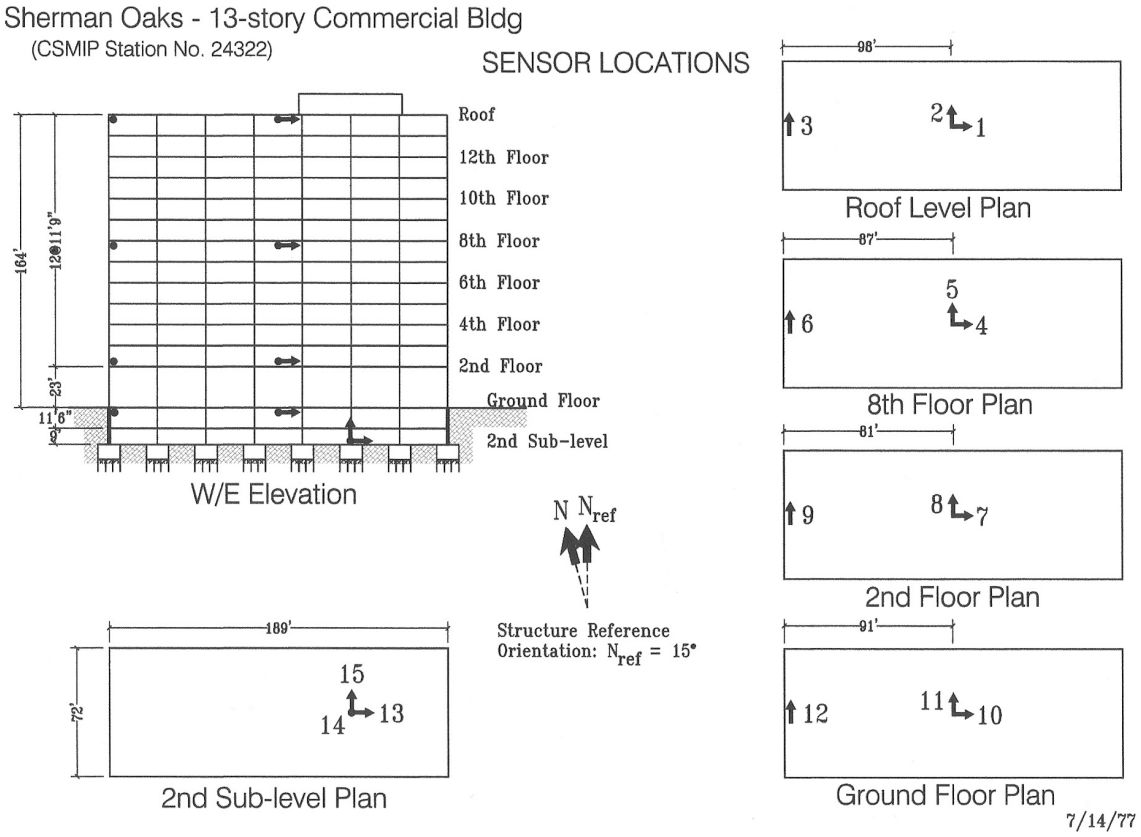

Figure 7-5 Sherman Oaks building (CSMIP Station No. 24322) instrument locations (CESMD, 2011, with permission).

Since 1977, six earthquake events have been recorded and processed by CSMIP at this station. The events, along with peak accelerations for the second basement level, ground floor, and roof are presented in Table 7-2. Note that in the 1987 Whittier and 1994 Northridge events, the peak accelerations followed an unusual pattern in which the largest recorded motions occurred at the ground floor (i.e., the recorded motions at the foundation and roof levels were smaller). As a result, subsequent calculations are based on peak accelerations measured at the foundation level.

Horizontal translations recorded at the second basement (foundation) level were used as foundation input motions, u_{FIM}. The foundation input motion, u_{FIM}, is the modified free-field, u_g, response due to base-slab averaging and embedment effects. Typically, u_g is known, and u_{FIM} must be calculated based on transfer functions. In this case, u_{FIM} was measured and u_g was inferred using transfer functions to remove the base-

slab averaging and embedment effects. The recorded u_{FIM} and inferred u_g response spectra for the 1994 Northridge earthquake are shown in Figure 7-6.

Table 7-2 Summary of Earthquake Events Recorded at the Sherman Oaks Building

Earthquake	Second Basement (Foundation), (g)			Ground Floor (g)			Roof (g)		
	N-S	*E-W*	*V*	*N-S*	*E-W*	*V*	*N-S*	*E-W*	*V*
1987 Whittier	0.100	0.148	0.038	0.250	0.169	----	0.140	0.140	----
1992 Landers	0.039	0.031	0.012	0.045	0.035	----	0.085	0.095	----
1994 Northridge	0.453	0.227	0.181	0.886	0.392	----	0.467	0.257	----
2007 Chatsworth	0.015	0.022	NR	0.045	0.058	----	0.025	0.036	----
2008 Chino Hills	0.049	0.037	0.010	0.073	0.045	----	0.082	0.067	----
2010 Calexico	0.004	0.004	0.003	0.004	0.005	----	0.049	0.022	----

Symbols: N-S=north-south; E-W=east-west; V=vertical; NR=no record available.

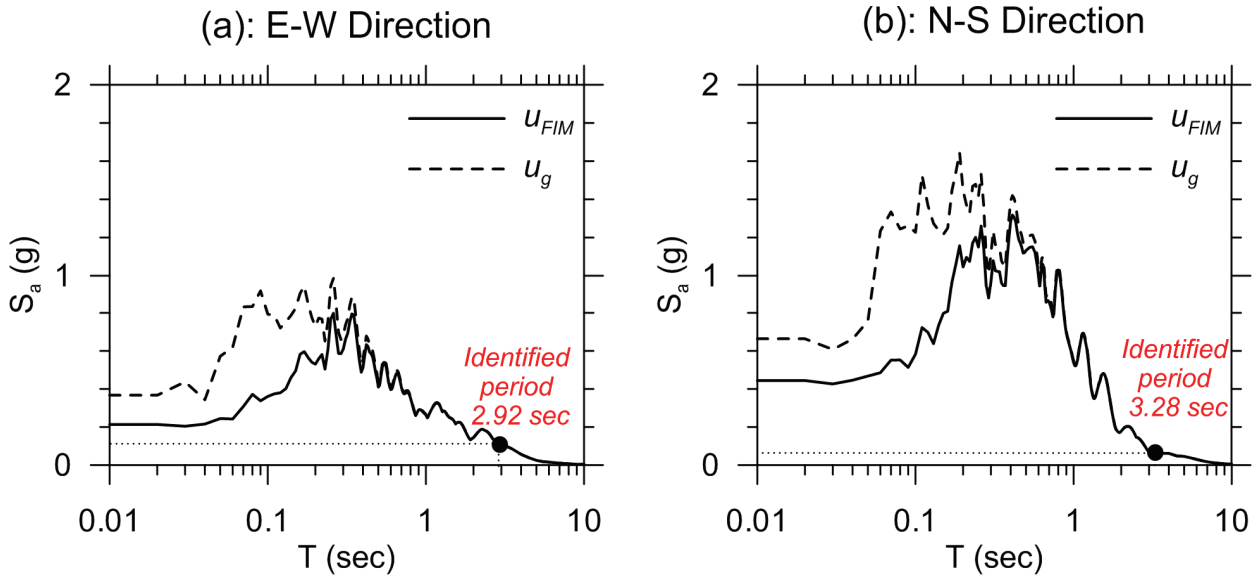

Figure 7-6 Response spectra for recorded foundation input motion, u_{FIM}, and inferred free-field motion, u_g, at the Sherman Oaks building, 1994 Northridge earthquake.

An equivalent linear ground response analysis was performed using DEEPSOIL v4.0 (University of Illinois, 2011) to estimate the depth-variable ground response adjacent to the embedded portion of the structure, taking the recording of u_{FIM} as input at 6.7 m with an elastic half-space. Input motions in ground response analyses can be specified as "outcropping" or "within," the former requiring an elastic half-space, and the latter requiring a rigid base (Kwok et al., 2007). For the Sherman Oaks building, the motion was recorded "within" the profile, but on a large foundation slab that could be interpreted as representing an outcropping condition. Analyses were performed for both conditions, with "outcropping" results appearing to be more realistic.

Dynamic soil properties consisted of the V_s profile shown in Figure 7-4 and modulus reduction and damping curves appropriate for the overburden pressures and soil types present at the site, as given by Darendeli (2001). DEEPSOIL does not update the shear modulus reduction of the elastic half-space during the analysis. Therefore, the elastic half-space parameter was updated through iterative runs until convergence was reached with the V_s of the deepest layer in the soil column. The computed variation of peak ground acceleration (PGA) and peak ground velocity (PGV) with depth is shown in Figure 7-7. Note that PGA changes significantly with depth (approximately 50%) whereas the change in PGV is comparatively minor.

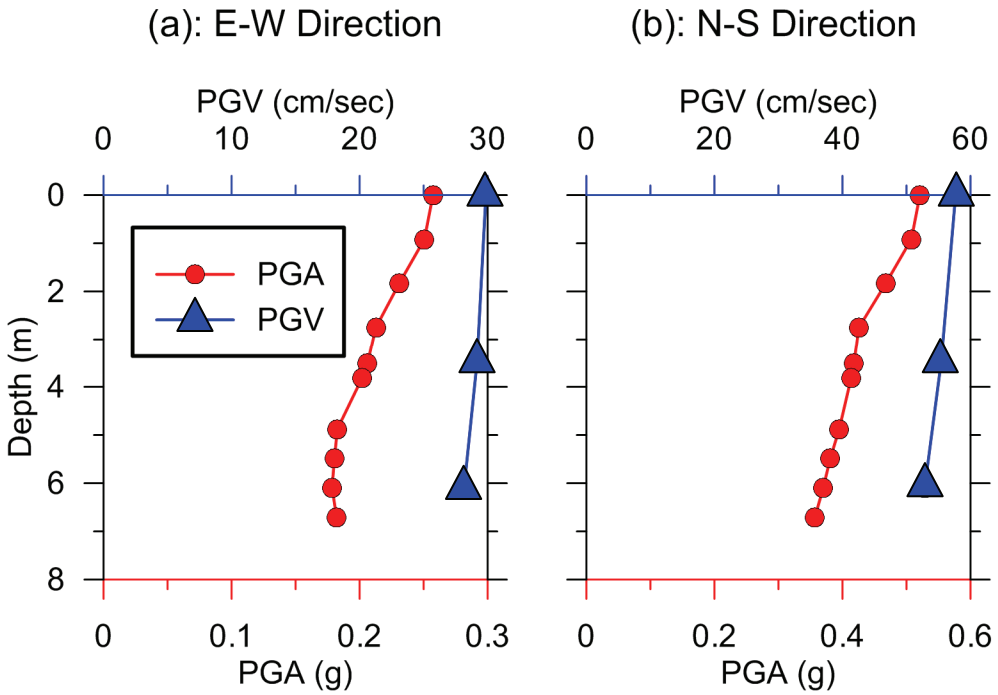

Figure 7-7 Computed variation of peak ground acceleration (PGA) and peak ground velocity (PGV) with depth at the Sherman Oaks site, 1994 Northridge earthquake.

7.2.3 Foundation Conditions

The foundation is rectangular in plan, measuring 36.3 m (119 ft) wide by 57.6 m (189 ft) long. The foundation consists of bored pile groups of varying configurations, interconnected by pile caps and grade beams. The cast-in-place (bored) concrete piles measure 51 cm (20 in) in diameter, and extend to a depth of approximately 9.9 m (32.5 ft) below the lowest basement level (i.e., approximately 16.2 m below grade). Typical pile spacing varies between 0.9 m (3 ft) to 1.2 m (4 ft), center to center. Concrete basement walls surround all embedded levels below grade. A foundation plan developed based on information contained in construction drawings provided by CSMIP is shown in Figure 7-8.

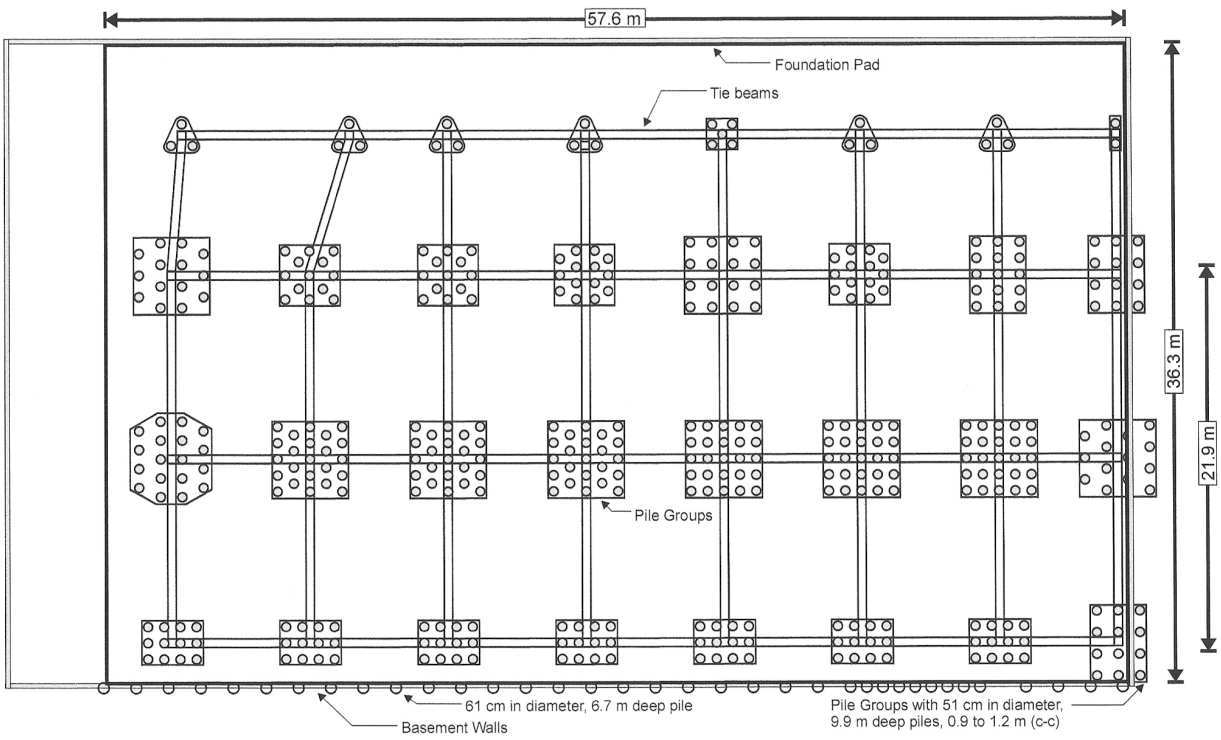

Figure 7-8 Sherman Oaks building foundation plan, based on construction drawings provided by CSMIP.

7.2.4 Development of Foundation Springs and Dashpots

For the Sherman Oaks building, resistance is provided by both shallow and deep foundation elements. It is assumed that the shallow foundation elements (principally grade beams) remain in contact with the soil, which is justified by the sandy nature of the soils at the site and the presence of friction piles rather than end-bearing piles.

The methodologies described in Chapter 2 were applied to the development of foundation springs and dashpots for the Sherman Oaks building. Critical input parameters included the foundation dimensions, fundamental vibration periods of the structure, soil properties, and the amplitude of the input motion. Modeling of the Sherman Oaks foundation and site conditions included the following:

- Determination of average effective profile velocity for shallow foundation elements, considering foundation dimensions, overburden pressures from the structure, and nonlinear effects.
- Determination of the structure-to-soil stiffness ratio for estimating the significance of soil-structure interaction effects.
- Calculation of shallow foundation horizontal stiffness and damping coefficients, and their separate contributions arising from base slab friction and passive pressure resistance against the basement walls.

- Calculation of vertical stiffness and damping coefficients for springs under the base slab, emphasizing the adjustment for rotational impedance for shallow foundation elements.
- Contribution of pile groups to the vertical and lateral stiffness of the foundation system.
- Distribution of shallow foundation springs and dashpots to the nodes in the analytical model.
- Calculation of limiting spring forces (i.e., capacities).

Static stiffnesses, dynamic stiffness modifiers, and embedment correction factors, were calculated for the Sherman Oaks building based on gross foundation dimensions (21.9 m by 57.6 m). The use of gross foundation dimensions assumes that stress bulbs below the pile caps and grade beams overlap at modest depth, so that the shallow foundation components effectively perform as a unified foundation system. This assumption does not require the relatively thin foundation slab between pile caps and grade beams to resist bearing pressures.

Average Effective Profile Velocity. For soil profiles that vary with depth, foundation stiffness and damping coefficients are based on an average effective profile velocity calculated over an effective profile depth, z_p. Table 7-3 summarizes the effective profile depth, z_p, the depth range, and the average effective profile velocity calculated using Equation 2-18 for each foundation vibration mode over the depth range considered.

Table 7-3 Summary of Effective Profile Depths and Average Effective Profile Velocities for the Sherman Oaks Building

Vibration Mode	Basis [1]	z_p (m)	Depth Range (m)	$V_{s,avg}$ (m/s)
Horizontal translation (x and y), overall	$\sqrt{BL}$	17.8	0 to 24.0	254.2
Horizontal translation (x and y), base spring	$\sqrt{BL}$	17.8	6.2 to 24.0	296.2
Vertical translation (z)	$\sqrt{BL}$	17.8	0 to 24.0	254.2
Rocking along x-axis (xx)	$\sqrt[4]{B^3L}$	14.0	0 to 20.2	243.0
Rocking along y-axis (yy)	$\sqrt[4]{BL^3}$	22.6	0 to 28.8	277.7

Notes: [1] Calculated using overall foundation half-width, B=11 m; half-length, L=28.8 m.

In Table 7-3, the maximum depth considered is greater than z_p by the amount of the foundation embedment, D (i.e., the depth range extends to $D + z_p$). For the specific case of the horizontal base spring, the depth interval begins at the base of the foundation.

Before averaging, measured free-field velocities, V_s, should be increased to account for the presence of overburden pressures caused by the added weight of the structure. For the Sherman Oaks building, the weight of the soil that was excavated for the basement levels was slightly greater than the estimated weight of the structure, so no net overburden pressure exists below the foundation, and no correction was applied.

Structure-to-Soil Stiffness Ratio. Taking the transverse (N-S) direction as critical, the structure-to-soil stiffness ratio, $h/(V_sT)$, for the Sherman Oaks building is approximately 0.06, calculated using two-thirds of the modeled building height from foundation to roof, h = 2/3(56.2 m) = 37.5 m, the fundamental period for the fixed base condition in the transverse direction, T = 2.71 sec, and the average effective profile velocity for rocking about the *xx*-axis, $V_{s,\,avg}$ = 243.0 m/s. Because this ratio is less than 0.1, strong inertial SSI effects would not be expected to occur (i.e., period lengthening near unity, foundation damping near zero). The building was further analyzed, however, to study potential kinematic interaction effects on higher mode responses. This study was used to determine if a building for which traditional first-mode SSI metrics indicated no significant effect, could, in fact, exhibit potentially significant impacts on the vertical distribution of structural response quantities used in design (e.g., drift ratios and story shears).

Horizontal Stiffness and Damping. Calculations for horizontal stiffness and damping ratios are shown in Table 7-4. For horizontal stiffness, contributions from both base friction and passive pressure resistance were considered. Because base friction mobilizes the soil below the embedment depth, D, the average effective profile velocity for the base spring is taken between depths D and $D+z_p$. The base spring stiffness was subtracted from the overall horizontal stiffness to determine the portion of horizontal stiffness attributed to passive pressure resistance against the basement walls.

In Table 7-4, shear modulus, G, was evaluated from Equation 2-9, using a soil mass density, ρ_s, of 20 kN/m^3/g, and values of average effective profile velocity, $V_{s,\,avg}$, determined using overburden-corrected shear wave velocities below the foundation, shown in Table 7-3. Values of shear modulus should be reduced to account for large strain effects associated with nonlinear behavior. Using Table 2-1, assuming Site Class D, and peak acceleration (at the foundation level) of about 0.45 g from the 1994 Northridge earthquake, the shear modulus reduction factor, G/G_0 = 0.5. A modulus reduction factor of 1.0 was used for the other smaller events. Other parameters were determined using the equations referenced in the table.

Table 7-4 Calculation of Shallow Foundation Stiffness and Damping Parameters for the Sherman Oaks Building

Spring/Dashpot	$G^{(1)}$ Eq. 2-9 (MPa)	$K_{sur}{}^{(2)}$ Table 2-2a (kN/m; kN-m/rad)	η Table 2-2b	$a_0{}^{(3)}$ Eq. 2-15	α Table 2-3a	β_{sur} Table 2-3a	β_{emb} Table 2-3b	Dynamic Stiffness Eq. 2-14a	Dashpot Coefficient Eq. 2-13a
Horizontal, overall x-direction $\left(k_{x,total}, c_{x,total}\right)$	65.2	6.48e6	1.45	0.13	1	0.076	0.114	$k_{x,total} = \alpha_x K_{x,sur} \eta_x$	$c_{x,total} = 2k_{x,total}\left(\frac{\beta_{emb} + \beta_s}{\omega}\right)$
Horizontal, overall y-direction $\left(k_{y,total}, c_{y,total}\right)$	65.2	7.04e6	1.45	0.13	1	0.070	0.106	$k_{y,total} = \alpha_y K_{y,sur} \eta_y$	$c_{y,total} = 2k_{y,total}\left(\frac{\beta_{emb} + \beta_s}{\omega}\right)$
Horizontal, base spring x-direction $\left(k_{x,base}, c_{x,base}\right)$	88.6	8.81e6	---	0.11	1	0.065	---	$k_{x,base} = \alpha_x K_{x,sur}$	$c_{x,base} = 2k_{x,base}\left(\frac{\beta_{sur} + \beta_s}{\omega}\right)$
Horizontal, base spring y-direction $\left(k_{y,base}, c_{y,base}\right)$	88.6	9.56e6	---	0.11	1	0.060	---	$k_{y,base} = \alpha_y K_{y,sur}$	$c_{y,base} = 2k_{y,base}\left(\frac{\beta_{sur} + \beta_s}{\omega}\right)$
Vertical, z $\left(k_z, c_z\right)$	65.2	8.55e6	1.22	0.13	1	---	0.132	$k_z = \alpha_z K_{z,sur} \eta_z$	$c_z = 2k_z\left(\frac{\beta_{emb} + \beta_s}{\omega}\right)$
Rocking about x-axis $\left(k_{xx}, c_{xx}\right)$	58.0	1.05e9	1.74	0.14	1	---	0.010	$k_{xx} = \alpha_{xx} K_{xx,sur} \eta_{xx}$	$c_{xx} = 2k_{xx}\left(\frac{\beta_{emb} + \beta_s}{\omega}\right)$
Rocking about y-axis $\left(k_{yy}, c_{yy}\right)$	73.9	5.55e9	1.58	0.12	0.99	---	0.003	$k_{yy} = \alpha_{yy} K_{yy,sur} \eta_{yy}$	$c_{yy} = 2k_{yy}\left(\frac{\beta_{emb} + \beta_s}{\omega}\right)$

Notes: (1) Calculated using a shear modulus reduction factor, G/G_0=0.5 for the Northridge earthquake; for other events G/G_0=1.0, and values would be doubled.
(2) Calculated using overall foundation half-width, B=11 m; half-length, L=28.8 m; and ν=0.33.
(3) Calculated at a frequency corresponding to the first-mode period of the flexible-base structure.

Dashpot coefficients were determined using Equation 2-13a and the total foundation damping ratio. The total foundation damping ratio is equal to the sum of the radiation damping ratio (determined using equations in Chapter 2) and the soil hysteretic damping ratio, β_s. For the Sherman Oaks site, the soil hysteretic damping ratio was evaluated using Darendeli (2001), and determined to be 0.088 for the Northridge earthquake, and 0.009 for the other events.

Vertical Stiffness and Damping. Calculations for overall vertical and rotational stiffness and damping ratios are shown in Table 7-4, using values of average effective profile velocity from Table 7-3. Vertical springs were distributed over the footprint of the foundation, as shown in Figure 7-9, using a vertical stiffness intensity that is normalized by area (Equation 2-20). Stiffness intensities were adjusted near the edges of the foundation to match the overall rocking stiffness values given in Table 7-4 (using Equation 2-21 and an end length ratio of $R_e = 0.4$). The stiffness of any individual spring in the model was then computed as the product of stiffness intensity and the tributary area for the spring.

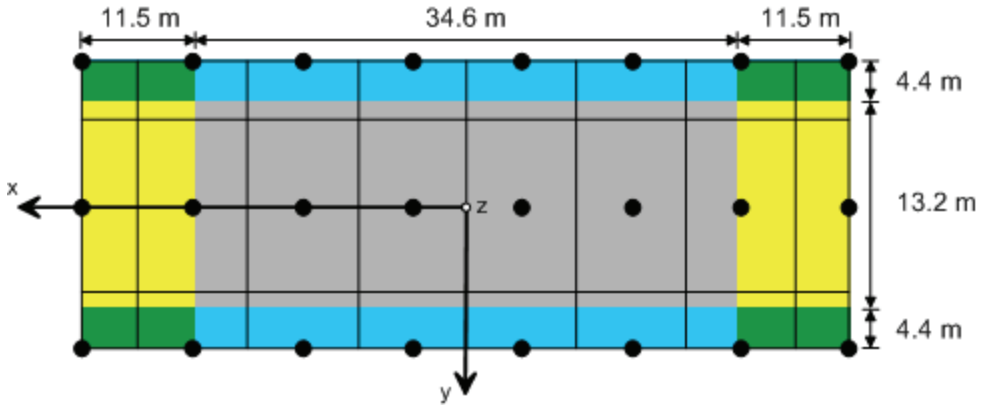

	$k_z^i\left(\text{kN/m}^3\right)$	$c_z^i\left(\text{kN-sec/m}^3\right)$
	8,202	715
	29,361	2,454
	36,524	3,209
	43,687	3,964

Figure 7-9 Vertical spring and dashpot intensities distributed over the footprint of the Sherman Oaks building. Solid lines represent tributary area boundaries and solid circles represent column nodes.

Vertical stiffness intensities in the central zone of the foundation were computed using Equation 2-20a. Edge intensities were increased by factors of $R_k = 5.33$ for the *xx*-direction and $R_k = 3.58$ for the *yy*-direction to correct for underestimation of rotational stiffness (Equations 2-21a, 2-21b). Corner intensities were evaluated as the average of the intensities in the *xx*- and *yy*-directions. Dashpot intensities were calculated based on stiffness intensities using Equation 2-20b, and reduced by R_c (Equations 2-21c, 2-21d), to correct for overestimation of rotational damping.

Contribution of Pile Groups. Pile group horizontal and vertical stiffness and damping ratios were evaluated in accordance with Section 2.3. Active pile length, L_a, was evaluated separately for the two vibration modes. It is approximately equal to the pile length, L_p, for vertical modes, and is less than L_p for horizontal modes. For the Sherman Oaks building, the active pile length for horizontal loading was evaluated using the results from Syngros (2004). Static pile stiffnesses, K_j^p, were calculated using the equations in Table 2-4a, modified for dynamic effects to calculate the single pile stiffness, k_j^p, and then modified for group effects. Calculations were based on average effective shear wave velocity calculated over an effective profile depth from D to $D+L_a$, and shear modulus reduced for large strain effects (G/G_0=0.5 for the Northridge earthquake; 1.0 for other events). Approximate dynamic pile group efficiency factors for the Sherman Oaks building were evaluated using Figure 2-11.

Results are shown in Table 7-5. Results are provided for 3x3 and 4x4 pile group configurations and applied to individual pile groups shown in Figure 7-8. Results for 3x3 pile groups were applied to groups with 12 piles, and results for 4x4 pile groups were applied to groups with more than 13 piles. The modeled stiffness for each pile group is the product of the individual pile stiffness, k_j^p, the pile group efficiency factor, k_j^G, and the number of piles, N_{pile}, in each group.

Table 7-5 Calculation of Pile Stiffness and Damping Parameters for the Sherman Oaks Building

Spring/ Dashpot	Active Pile Length, L_a (m)	$V_{s,avg}$ (m/s)	G[(1)] (MPa)	Static Pile Stiffness, K_j^p[(2)] (MN/m)	Pile Group Efficiency Factor, k_j^G[(3)]	Pile Group Damping Ratio, β_j[(3)]
Horizontal, x, y (3x3 group)	4.1	180.1	63.4	237.3	0.47	0.2
Vertical, z (3x3 group)	9.9	183.7	67.6	859.3	0.43	0.25
Horizontal, x, y (4x4 group)	4.1	180.1	63.4	237.3	0.36	0.05
Vertical, z (4x4 group)	9.9	183.7	67.6	859.3	0.30	0.29

Notes: [(1)] Calculated using a shear modulus reduction factor, G/G_0=0.5 for the Northridge earthquake.
[(2)] Calculated for E_p=474.8 MPa, and d=0.6 m.
[(3)] Approximated using Figure 2-11.

Distribution of Springs to Foundation Nodes. A total of 68 nodes were included in the Sherman Oaks foundation model. Horizontal springs and dashpots were distributed across nodes on the basement walls (representing passive pressures) and base slab (representing base shear). Vertical springs and dashpots were distributed

across nodes on the base slab. A plan view, transverse section, and longitudinal section of foundation nodes are shown in Figure 7-10.

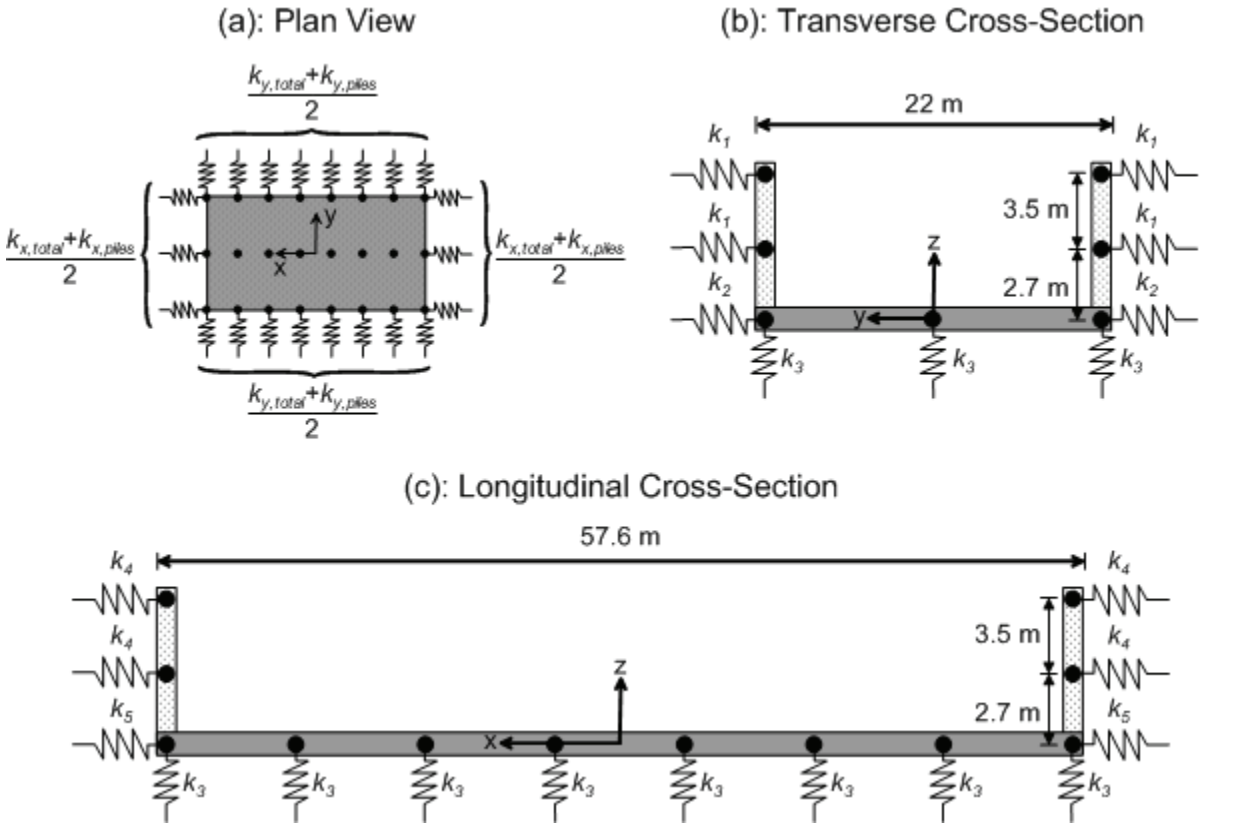

Pile Group Contribution	$k_{y,piles} = \sum k_y^G$	$k_{x,piles} = \sum k_x^G$
Translation in the y-direction	$k_1 = \frac{k_{y,total} - k_{y,base}}{48}$	$k_2 = k_1 + \frac{k_{y,base}}{16} + \frac{k_{y,piles}}{16}$
Translation in the x-direction	$k_4 = \frac{k_{x,total} - k_{x,base}}{27}$	$k_5 = k_4 + \frac{k_{x,base}}{6} + \frac{k_{x,piles}}{6}$
Translation in the z-direction	$k_3 = k_z^G + k_z$ Note: k_3 is not a constant value; k_z^G is a function of N_{piles}, and k_z is a function of spring intensities shown in Figure 7-9.	

Figure 7-10 Plan view, transverse section, and longitudinal section of foundation nodes for the Sherman Oaks building, and calculation of associated spring stiffnesses.

The overall horizontal stiffness, including contributions from base shear, passive pressure resistance against the basement walls, and pile groups, was distributed around the foundation perimeter (i.e., interior nodes have no horizontal springs).

Half of the horizontal stiffness was distributed to each edge of the foundation in each direction. Horizontal stiffness was partitioned between a base stiffness and a wall stiffness in each direction. Wall stiffnesses were distributed equally to each basement wall node, and base stiffnesses were distributed equally along each side of the foundation.

Vertical stiffness, including contributions from shallow foundation elements and piles, was modeled at all 24 foundation nodes. Shallow foundation stiffness contributions were based on stiffness intensity, and pile stiffness contributions were based on the vertical pile group stiffness calculations. Dashpots were distributed to the foundation nodes in an identical manner.

Limiting Spring Capacities. Capacities of individual springs were evaluated using conventional vertical and lateral pile group capacity analysis (e.g., Salgado, 2008). Pile group capacities were assigned to foundation nodes as described above for spring stiffness. Capacities are compared to spring force demands in the following section.

7.2.5 Analysis Results

The Sherman Oaks building was analyzed in OpenSees (McKenna, 1997), incorporating foundation springs and dashpots described above. Details for the development and calibration of the Baseline Model (MB) are described in Appendix A. Adjustments to the shear modulus for cracked concrete, Rayleigh damping, and structural mass and stiffness were used to produce a reasonably close match to recordings from the 1994 Northridge earthquake. Based on calibration studies, Model MB was considered a reasonable engineering approximation for the Sherman Oaks building. Using this model as a basis, alternative modeling configurations for the Sherman Oaks building were developed and studied, and the resulting response quantities were compared for the following variants:

- Model MB.1, which examined the importance of flexibility in subterranean structural elements (walls and slabs);
- Model MB.2, which examined the importance of nonlinearity in foundation springs by not allowing tension (allowing gap formation);
- Model 4, which removed the effects of depth-variable ground motions and considered the use of free-field motions (versus foundation input motions);
- Model 3, which fixed the far ends of foundation springs against displacement and applied input motions at the base slab level;
- Model 2, which ignored the effects of embedment by omitting the surrounding soil and assumed a fixed base at the foundation level; and

- Model 1, which ignored the response of the subterranean levels by assuming a rigid base at the ground level.

Fundamental periods of vibration for each of the model variants are shown in Table 7-6. The resulting modeled periods were only modestly affected by different idealizations of the soil-foundation interface.

Table 7-6 Comparison of Fundamental Periods for Alternative Foundation Modeling Configurations for the Sherman Oaks Building

	Fundamental Period (sec)	
Model	*Longitudinal*	*Transverse*
MB (Baseline Model)	2.67	2.72
MB.1 (rigid subterranean structure)	2.35	2.68
MB.2 (no tension in foundation springs)	2.65	2.73
Model 4 (bathtub)	2.67	2.72
Model 3 (fixed horizontal springs)	2.34	2.65
Model 2 (fixed at foundation)	2.67	2.71
Model 1 (fixed at grade)	2.34	2.67

Comparisons of computed displacement histories, maximum displacement, drift ratios, story shear coefficients, and peak floor accelerations between Model MB and the other models are shown in Figures 7-11 through 7-15. A summary of peak response quantities from all foundation modeling configurations is shown in Figure 7-16.

Model MB.1 and Model MB.2. Results for Model MB.1 in Figure 7-11 showed that rigid subterranean structural elements caused an increase structural response, particularly in the NS direction, likely due to the change in period. In the case of Model MB.2, results in Figure 7-11 showed that allowing geometric nonlinearities (i.e., gap formation) had no discernible impact on response. This suggests that gaps would not be expected to form in the foundation springs between the soil and the basement walls, and supports the equivalent-linear soil-foundation modeling assumptions suggested in Section 7.1.3.

Model 4. Results for Model 4 in Figure 7-12 showed that the bathtub model introduces negligible changes in displacement response over the height of the structure (i.e., less than 3.6% different at the roof level). Changes in story drift and story shear force profiles were also negligible. Peak floor accelerations were most sensitive to the change in modeling configuration. Values above the ground level were relatively unaffected, but values in the subterranean levels were sensitive to the

use of free field motions (results marked ‘4b’) versus foundation input motions (results marked ‘4a’).

Model 3. Results for Model 3 in Figure 7-13 showed the least agreement with Model MB. Fixing the upper-level foundation springs against displacement, and applying input motions to the base slab, caused large differences in all response quantities including building vibration periods, displacement histories, drift ratios, and story shears. Given the significant discrepancies observed, use of this modeling configuration is not recommended.

Model 2. Results for Model 2 in Figure 7-14 showed that modeling the subterranean levels, even while ignoring the effects of the surrounding soil, can provide good results for some response quantities. Model 2 exhibited good agreement for building vibration periods and displacement histories. Reasonable agreement was observed for maximum displacement and drift ratios, but story shears and peak floor accelerations differed more significantly, particularly in the subterranean levels.

Model 1. Results for Model 1 indicated that ignoring the subterranean levels significantly alters the period of vibration. As a result, displacement histories were more out-of-phase than most other modeling configurations, as shown in Figure 7-15. Differences in story drifts, story shears, and peak floor accelerations were relatively large (up to 50% different) in some cases.

In Figure 7-16, peak displacement, drift, and story shear response quantities from all modeling configurations were synthesized and plotted in a single figure. Results for Model 3 are clear outliers for each of the parameters considered. Results for Model 4 are closest to Model MB, followed by Model 2, and then Model 1. Differences in response quantities, when they occurred, were generally greater in the subterranean levels than in the levels above grade.

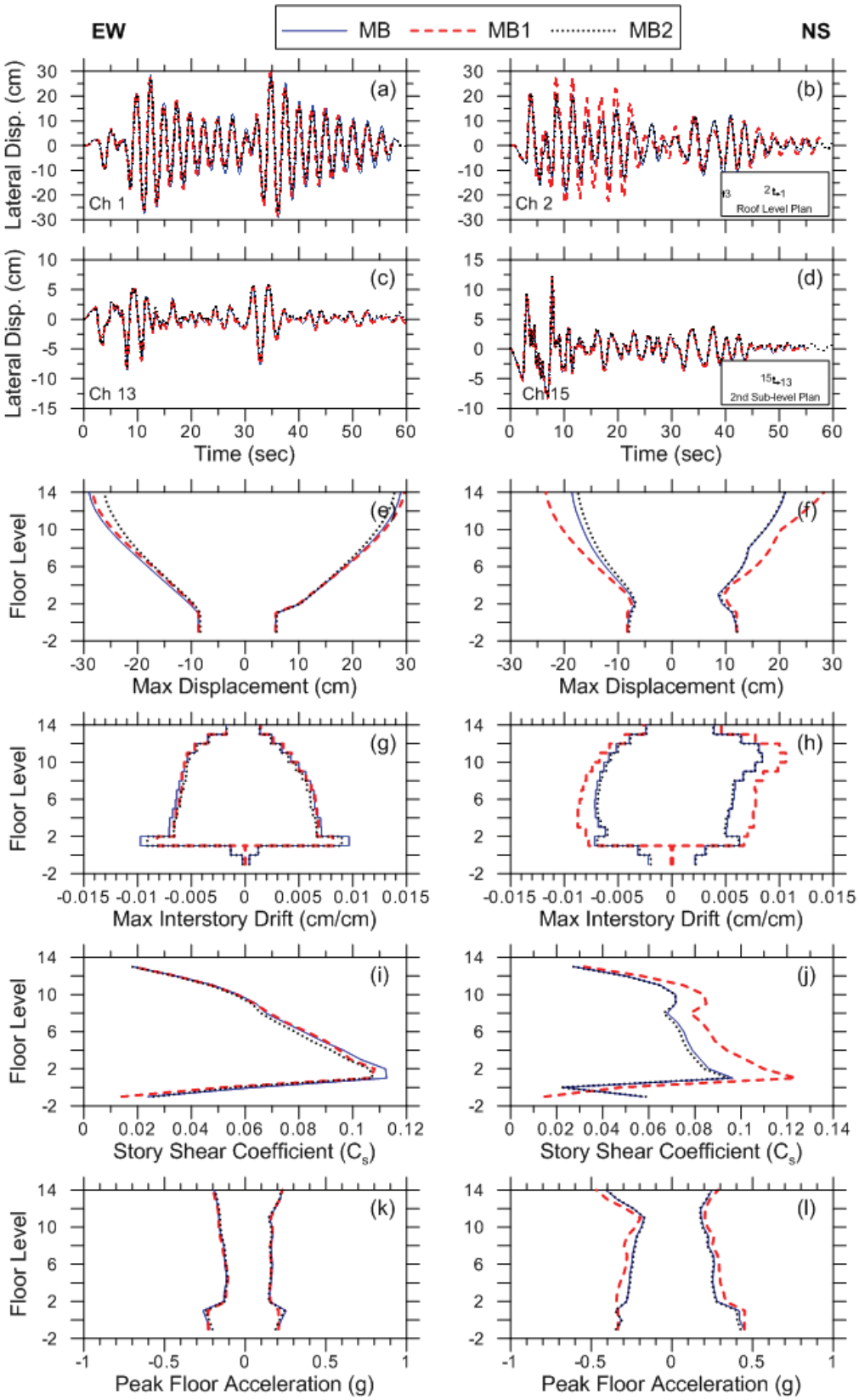

Figure 7-11 Comparison of displacements, drifts, story shears, and accelerations between Model MB, MB.1 and MB.2 for the Sherman Oaks building.

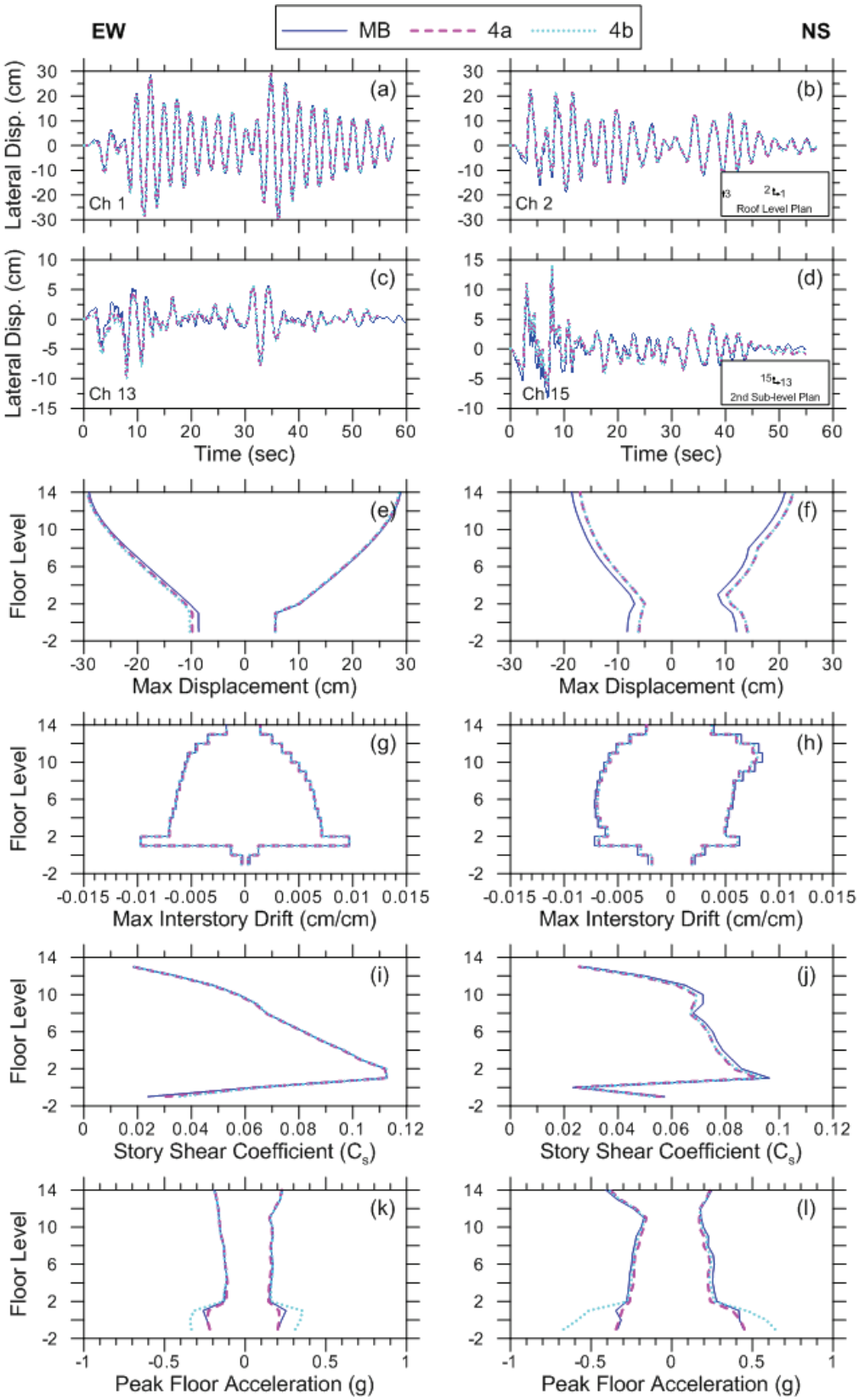

Figure 7-12 Comparison of displacements, drifts, story shears, and accelerations between Model MB and Model 4 for the Sherman Oaks building.

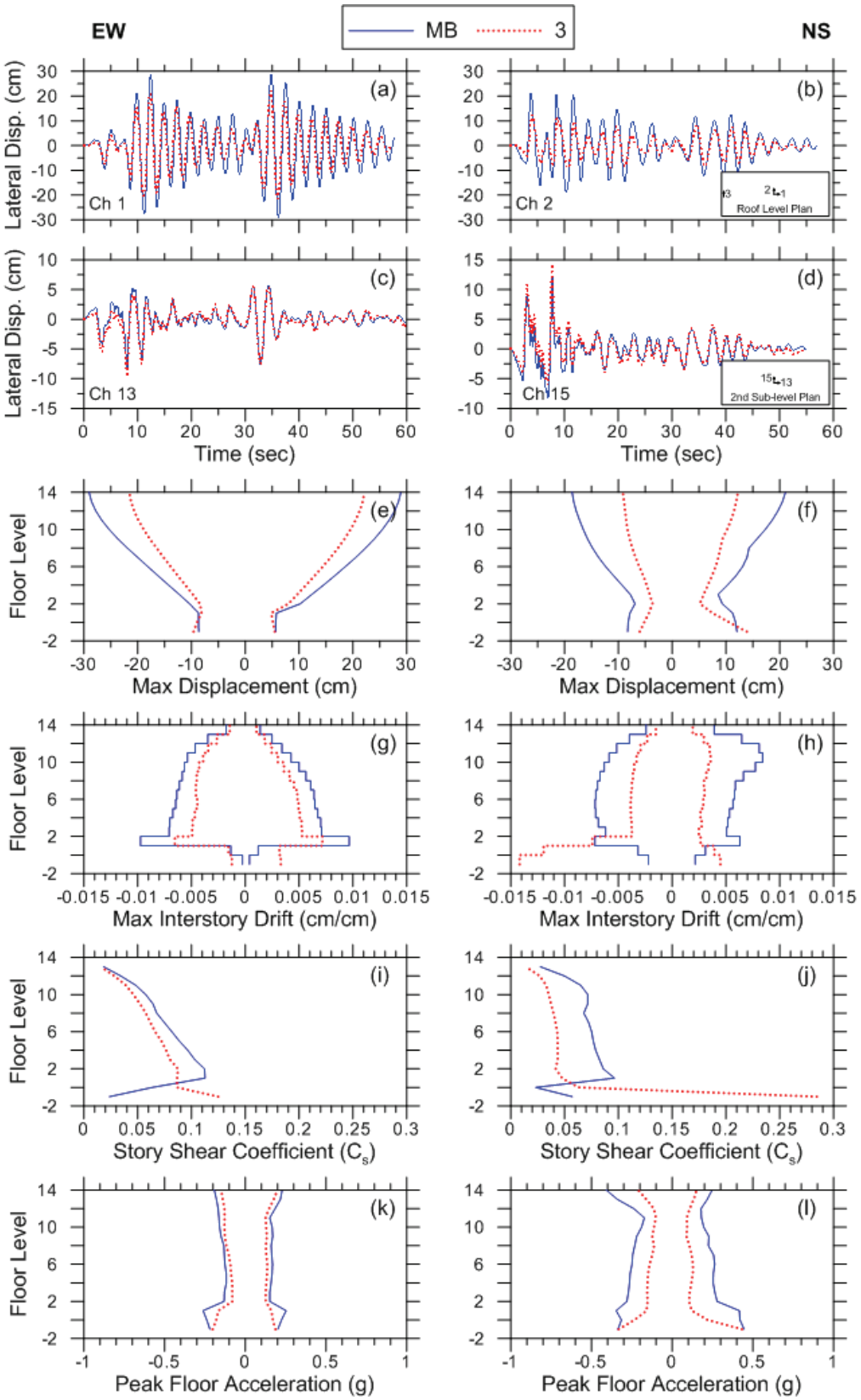

Figure 7-13 Comparison of displacements, drifts, story shears, and accelerations between Model MB and Model 3 for the Sherman Oaks building.

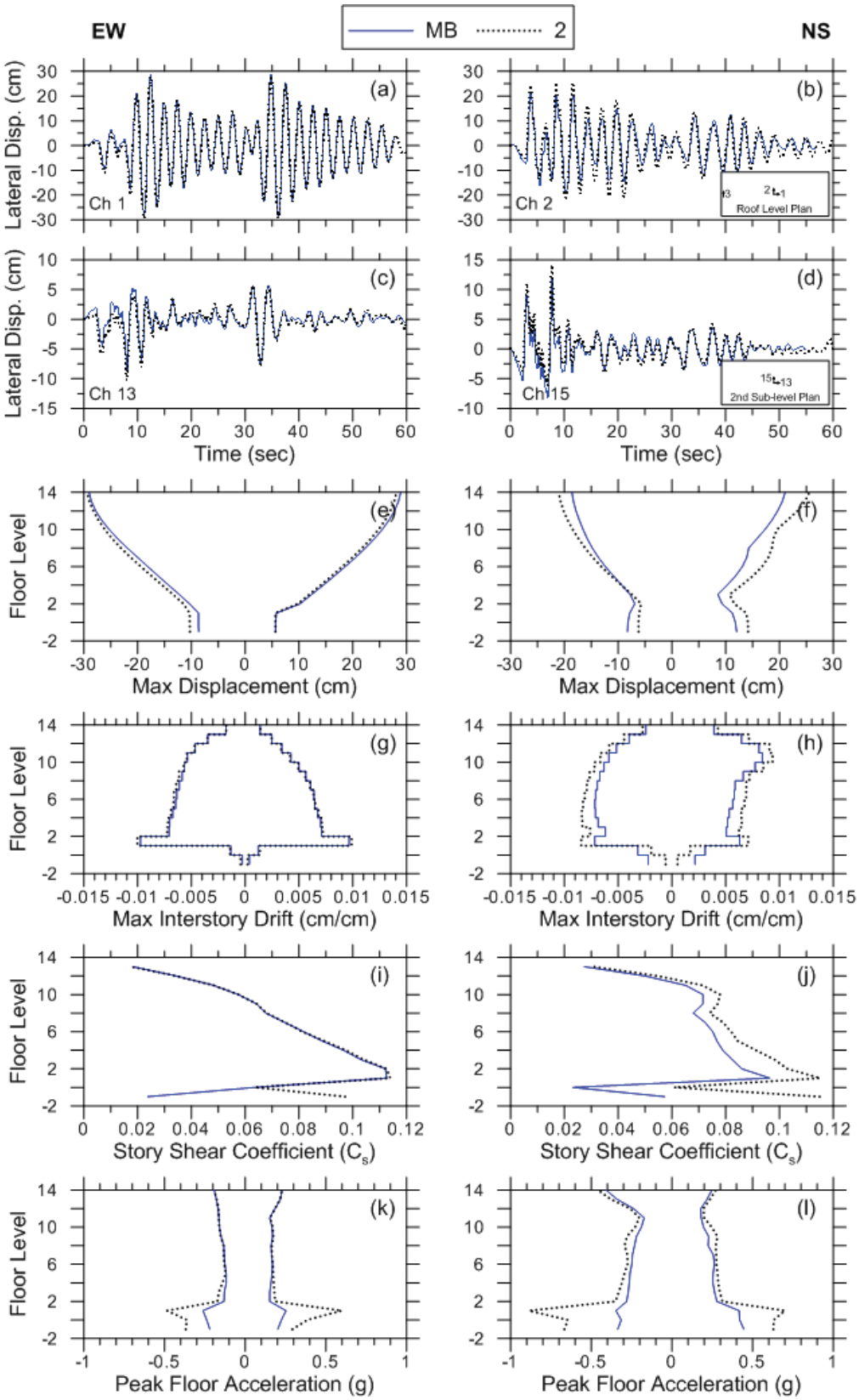

Figure 7-14 Comparison of displacements, drifts, story shears, and accelerations between Model MB and Model 2 for the Sherman Oaks building.

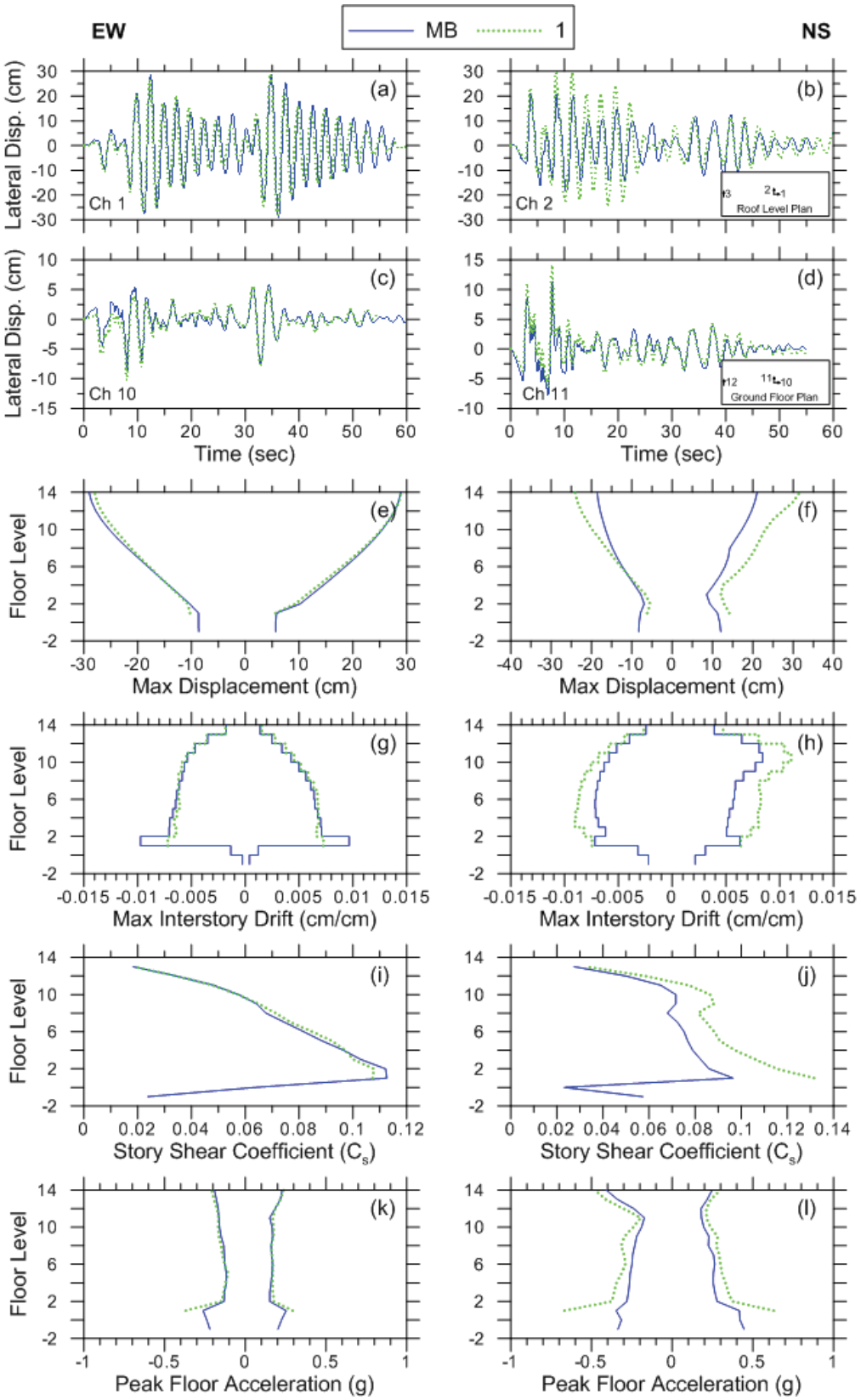

Figure 7-15 Comparison of displacements, drifts, story shears, and accelerations between Model MB and Model 1 for the Sherman Oaks building.

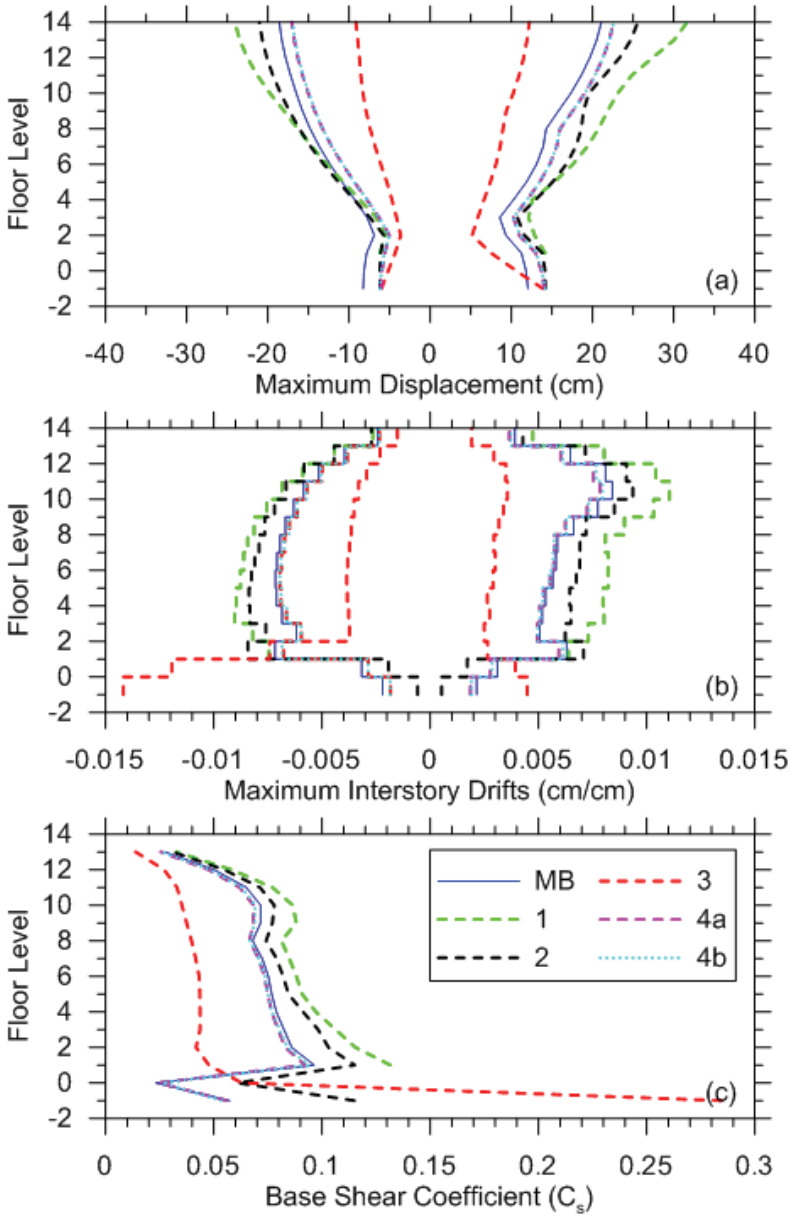

Figure 7-16 Comparison of peak displacements, drift ratios, and story shears from all model configurations, in the transverse direction.

7.3 Sherman Oaks Building Parametric Studies

Analysis of the Sherman Oaks building showed that key building response quantities can be affected by the foundation modeling assumptions, even when the structure-to-soil stiffness ratio, $h/(V_sT)$, does not indicate a strong dependence on SSI effects. Additional parametric studies were performed to investigate how different structural system characteristics might influence the magnitude of SSI effects on modeled response. A series of simplified stick models of the Sherman Oaks building were developed, and the resulting response quantities for each model were compared.

The key parameter varied between the models was structural stiffness. The moment frame system of the Sherman Oaks building was idealized as a stick model, and the stiffness scaled to different factors representing the stiffness of a series of core shear wall and perimeter shear wall variations in the structural system. The parametric stick models of the Sherman Oaks building are summarized in Table 7-7.

Table 7-7 Summary of Sherman Oaks Building Parametric Stick Models

					Y-Direction (N-S) [2]		X-Direction (E-W) [3]	
System	*Stiffness Scale Factor*	*Fdn. Model*	*Model ID*	*Modeled Height (m)* [1]	T_y *(sec)*	*h/(VsT)*	T_x *(sec)*	*h/(VsT)*
Moment Frame	1	1	1-MF	50	2.83	0.05	2.61	0.05
		2	2-MF	56.25	2.86	0.05	2.62	0.05
		4a	4a-MF	56.25	2.87	0.05	2.63	0.05
		MB	MB-MF	56.25	2.87	0.05	2.62	0.05
Shear Wall Core	5	1	1-SW	50	1.32	0.10	1.17	0.10
		2	2-SW	56.25	1.39	0.11	1.20	0.11
		4a	4a-SW	56.25	1.40	0.11	1.20	0.11
		MB	MB-SW	56.25	1.40	0.11	1.20	0.11
Perimeter Shear Wall	25	1	1-SW1	50	0.73	0.19	0.56	0.21
		2	2-SW1	56.25	0.84	0.18	0.63	0.21
		4a	4a-SW1	56.25	0.88	0.18	0.62	0.22
		MB	MB-SW1	56.25	0.87	0.18	0.62	0.22
Perimeter Shear Wall	50	1	1-SW2	50	0.63	0.22	0.42	0.29
		2	2-SW2	56.25	0.75	0.21	0.52	0.26
		4a	4a-SW2	56.25	0.79	0.20	0.51	0.26
		MB	MB-SW2	56.25	0.78	0.20	0.51	0.26
Perimeter Shear Wall	125	1	1-SW3	50	0.55	0.25	0.32	0.38
		2	2-SW3	56.25	0.69	0.22	0.44	0.31
		4a	4a-SW3	56.25	0.73	0.21	0.43	0.31
		MB	MB-SW3	56.25	0.72	0.21	0.43	0.31

Notes: [1] h = 2/3 x Modeled Height

[2] V_s =243.0 m/s in the N-S direction (average effective profile velocity for xx-rotation)

[3] V_s =277.7 m/s in the E-W direction (average effective profile velocity for yy-rotation)

Each system was investigated considering the foundation modeling configurations associated with Model 1, Model 2, Model 4, and Model MB. Based on results from the Sherman Oaks building analyses, Model 3 was not considered further. As shown in Table 7-7, the change in structural stiffness affects the modeled period in each direction, and correspondingly changes the resulting structure-to-soil stiffness ratio, $h/(V_sT)$. As the stiffness increases, the ratio eventually exceeds 0.1, and the expected impact of SSI effects becomes more significant.

An idealized stick model for the Sherman Oaks building is shown in Figure 7-17. Although the superstructure has been simplified into a single equivalent stick, each model includes detailed modeling at the foundation level, essentially maintaining foundation geometry, and spring and dashpot configurations. Details on stick model development and calibration with the full-building model are provided in Appendix B.

Figure 7-17 Elevation an idealized stick model of the Sherman Oaks building.

7.3.1 Parametric Study Results

Detailed analytical results for all parametric stick models are provided in Appendix B. Results are compared between the moment frame stick model and the

full-building model to demonstrate the level of consistency in model predictions using the idealized stick configuration. Results for key response quantities including maximum displacement, story drift, story shear, and peak floor acceleration are compared for each structural system variant across building all foundation modeling configurations to document the change in relative SSI effects observed as the structural system parameters were changed.

Table 7-8 summarizes relative comparisons between the results for each response quantity for the moment frame (MF), core shear wall (SW), and perimeter shear wall (SW3) models. Information is based on plots provided in Appendix B. An explanation for the nomenclature used in the table is provided in the footnotes.

Table 7-8 Comparison of Results for Moment Frame, Core Shear Wall, and Perimeter Shear Wall Stick Models and Alternative Foundation Modeling Configurations

Response Quantity	Location	Moment Frame (MF)		Core Shear Wall (SW)		Perimeter Shear Wall (SW3)	
		X-Direct. (E-W)	*Y-Direct. (N-S)*	*X-Direct. (E-W)*	*Y-Direct. (N-S)*	*X-Direct. (E-W)*	*Y-Direct. (N-S)*
Period	---	1 < 2, 4a, MB	Similar	1 < 2, 4a, MB	1 < 2, 4a, MB	1 < 2 < 4a, MB	1 < 2, 4a, MB
Displacement	Superstructure	4a, MB <1, 2	4a, MB <2<1	1<< 4a, MB <2	1<<2<4a, MB	1< 4a, MB <2	1<<2, 4a < MB
	Basement	4a, MB <1, 2	Similar	4a,MB < 2	4a,MB < 2	4a,MB < 2	4a,MB < 2
Story Drift	Superstructure	2, 4a, MB <1	4a<MB <2<1	Varies	1 < 2, 4a, MB	Similar	1, 2< 4a < MB
	Basement	2,4a < MB	4a<2<< MB	4a<2< MB	4a<2<< MB	4a<2, MB	4a<2<< MB
Story Shear	Superstructure	2, 4a, MB <1	2, 4a, MB <1	4a,MB <2<1	1< 4a, MB <2	4a< MB< 2<<1	2< 4a< MB<<1
	Basement	4a<<2 < MB	4a<<2 < MB	4a<<2<< MB	4a<<2<< MB	4a<2<< MB	4a<<2<< MB
Peak Floor Acceleration	Superstructure	Similar	4a< 1< MB< 2	4a < MB <1, 2	4a < MB <1, 2	4a < MB <1< 2	2, 4a, MB <<1
	Basement	4a, MB<<2	4a, MB<<2	4a, MB < 2	4a, MB < 2	4a, MB<<2	4a, MB<<2

Notes:
(1) 1, 2, 4a, and MB refer to Model 1, Model 2, Model 4a, and Model MB foundation modeling configurations.
(2) "1<<2, 4a < MB" indicates, for example, that the response of Model 1 is less than the response of Models 2 and 4a; the response of Models 2 and 4a are similar; and the response of all models is less than the response of Model MB.
(3) "<<" indicates a comparatively larger difference in response than "<".
(4) "Similar" indicates that the results do not vary significantly across the model types.
(5) "Varies" indicates that the trend in the results is not clear; some models have larger values in some cases and smaller values in other cases.

Figures 7-18 through 7-21 summarize maximum displacement envelopes comparing results across different foundation modeling configurations for all five building types (MF, SW, SW1, SW2, and SW3). Full scale plots are provided in Appendix B. Compared in this way, the trends are clearly discernible in which SSI effects are larger as the building stiffness increases. Response quantities in the basement levels were consistently the most influenced by alternative foundation modeling conditions.

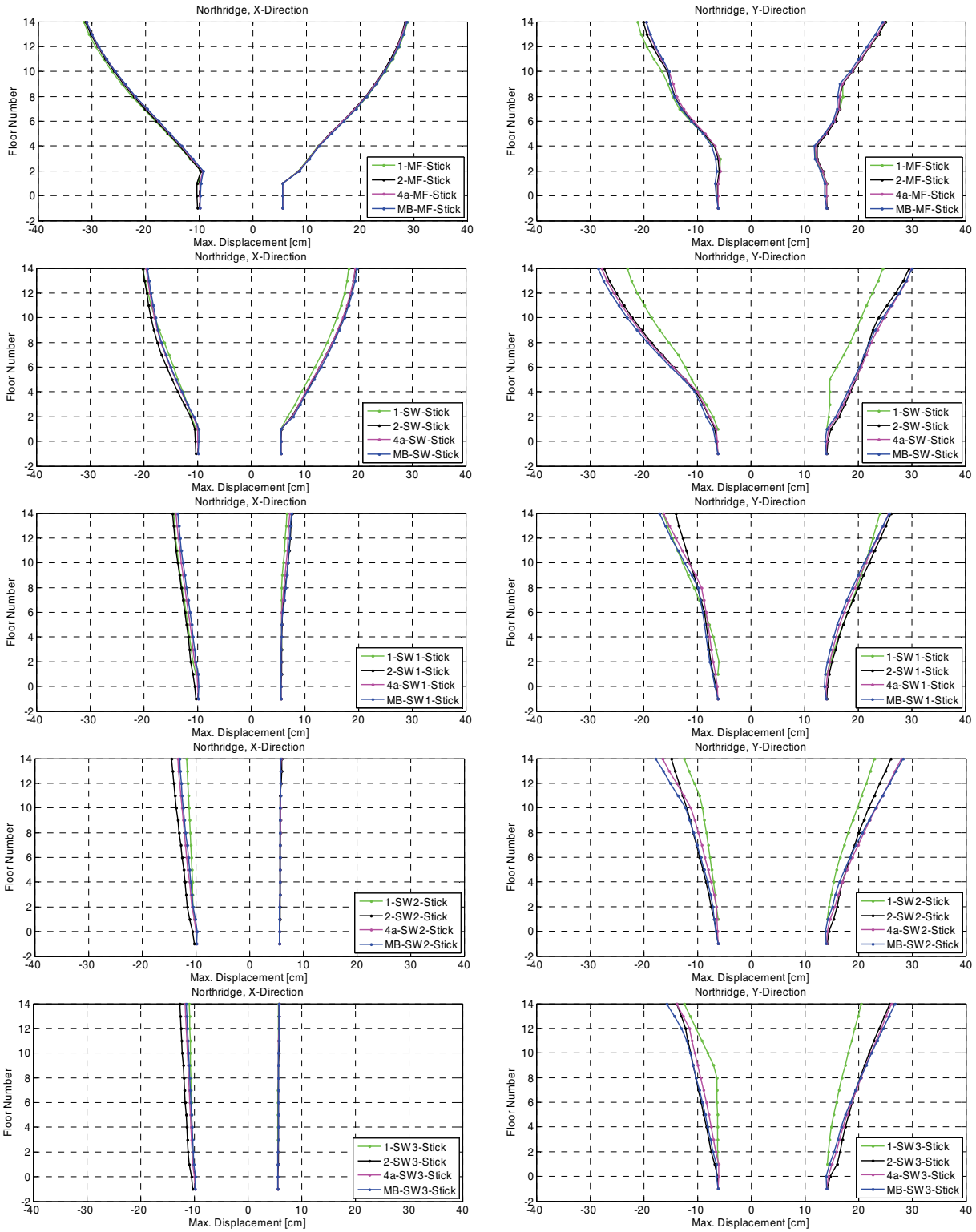

Figure 7-18 Comparison of maximum displacement envelopes in each direction for foundation Models 1, 2, 4a, and MB, for each structural system variant (MF, SW, SW1, SW2, and SW3).

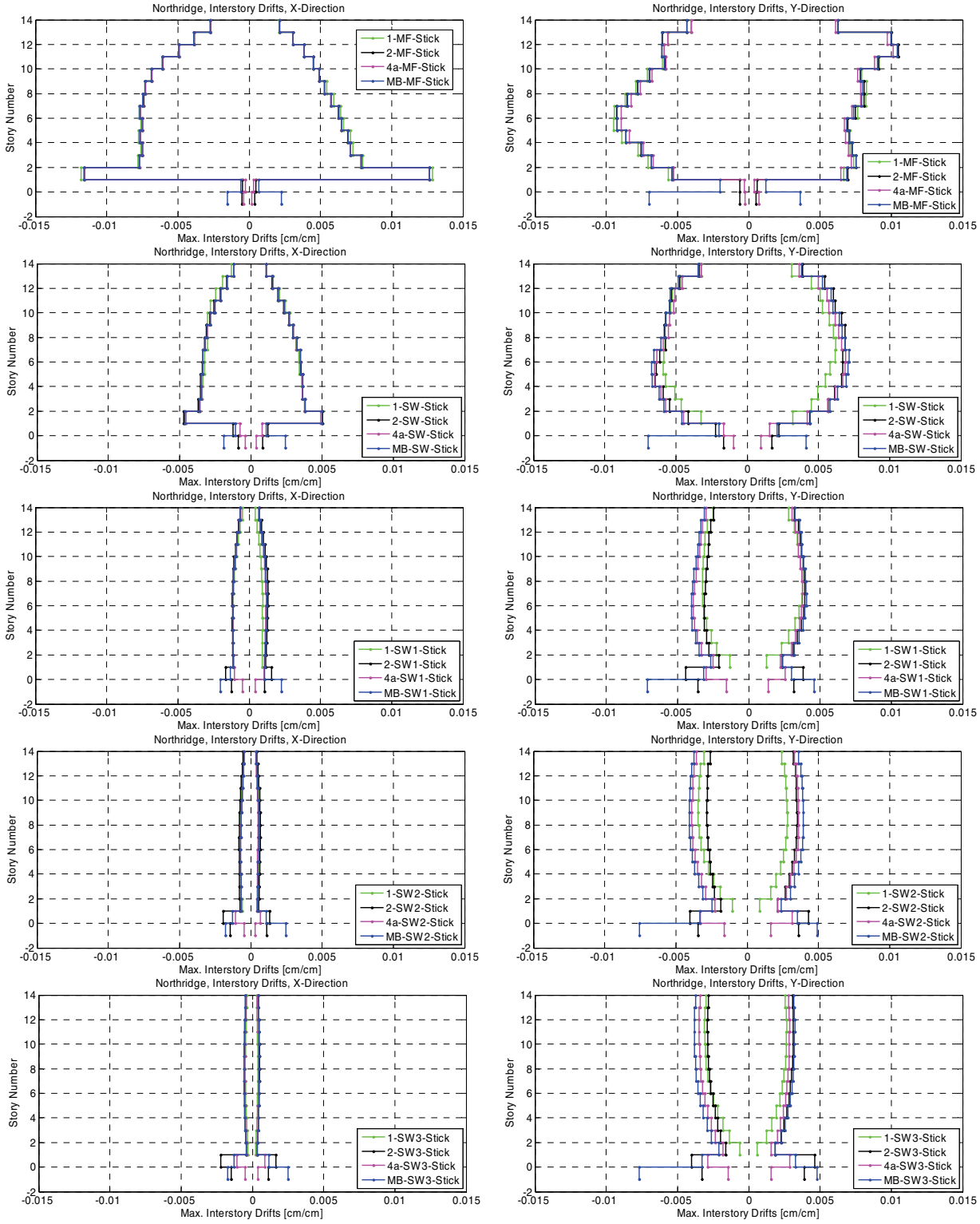

Figure 7-19 Comparison of maximum story drift envelopes in each direction for foundation Models 1, 2, 4a, and MB, for each structural system variant (MF, SW, SW1, SW2, and SW3).

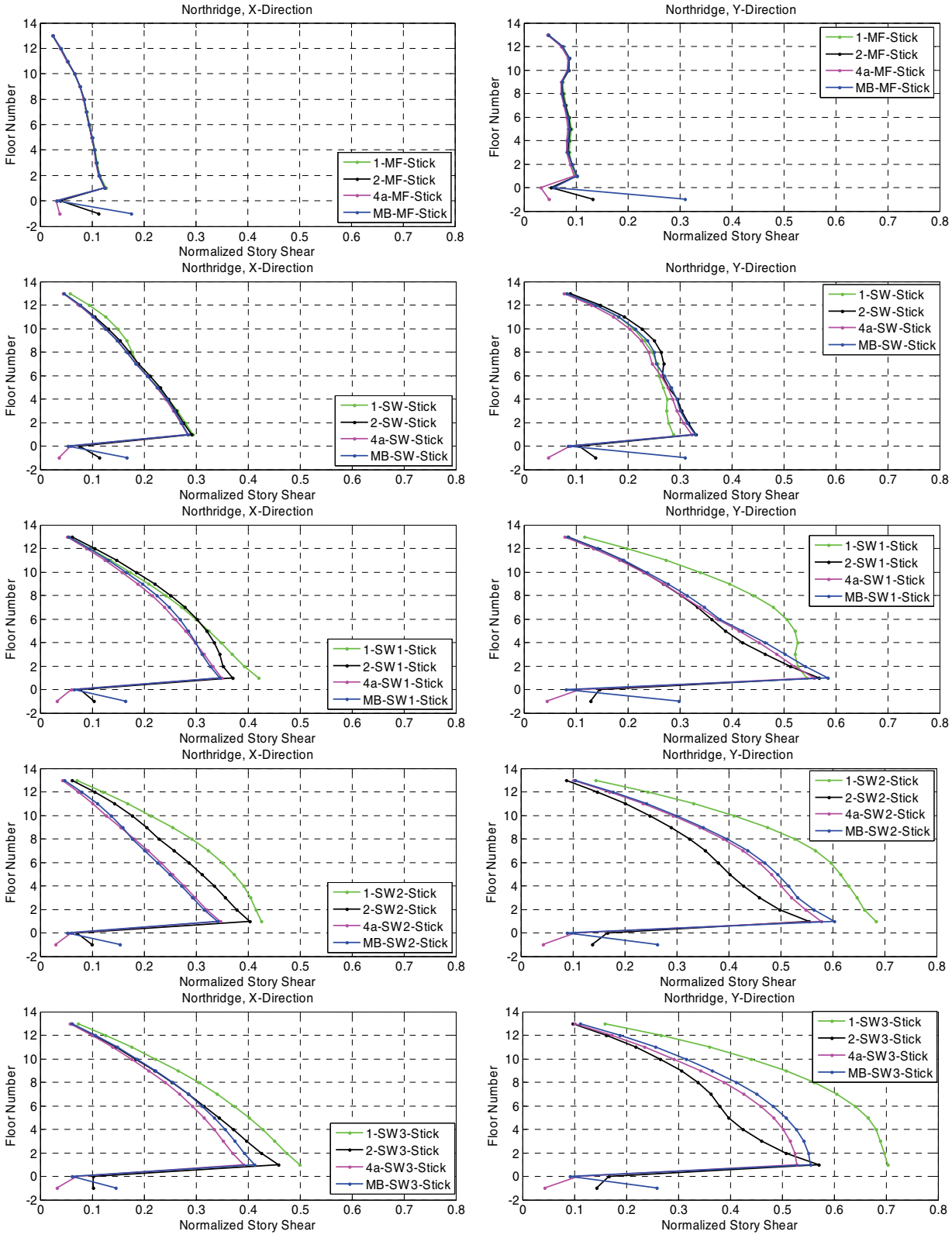

Figure 7-20 Comparison of maximum story shear envelopes in each direction for foundation Models 1, 2, 4a, and MB, for each structural system variant (MF, SW, SW1, SW2, and SW3).

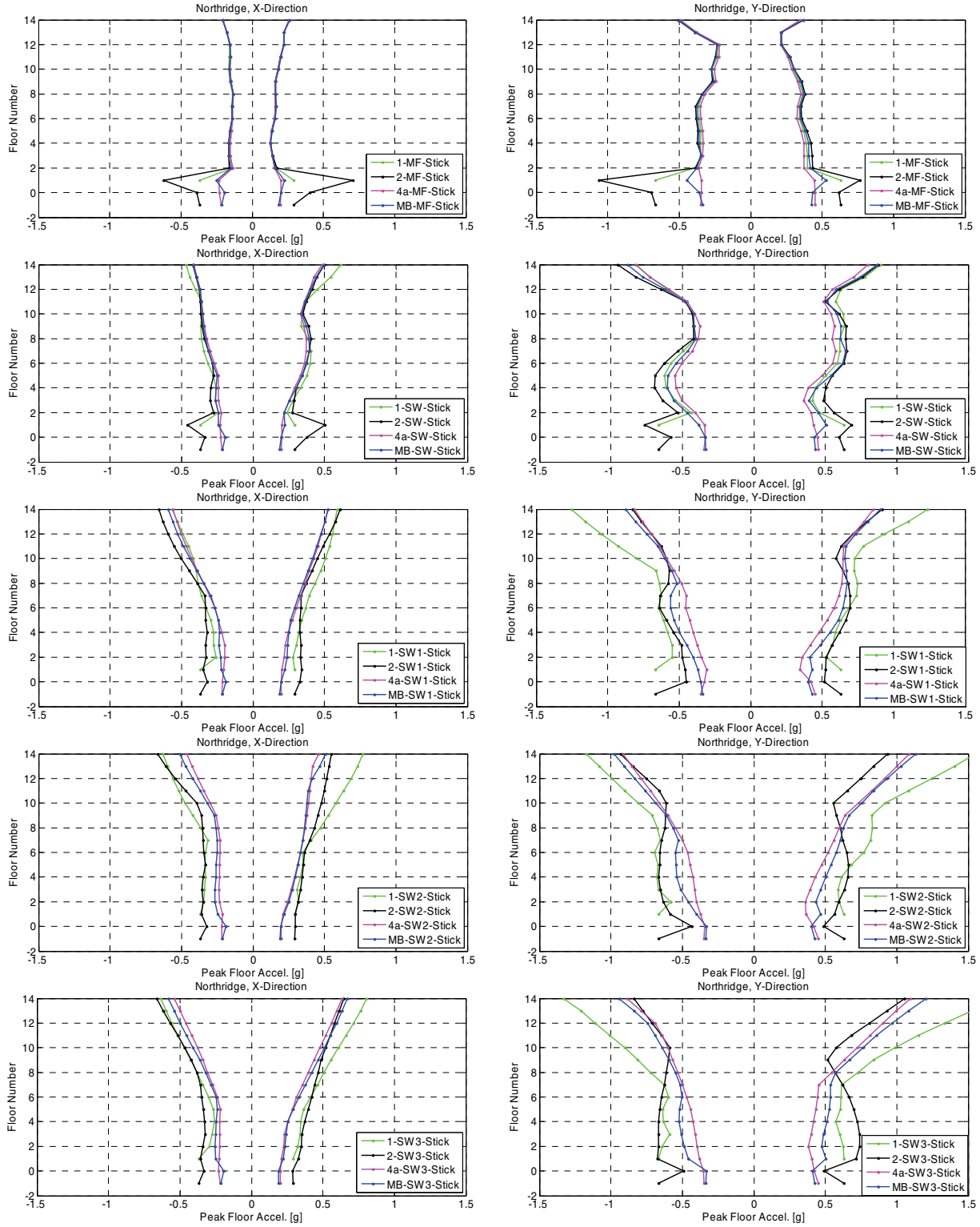

Figure 7-21 Comparison of peak floor acceleration envelopes in each direction for foundation Models 1, 2, 4a, and MB, for each structural system variant (MF, SW, SW1, SW2, and SW3).

7.3.2 Parametric Study Observations

The following general observations from parametric studies of the Sherman Oaks building were made:

- Observed SSI effects became larger as the building stiffness increased. They were relatively minor for the moment frame (MF) building, more discernible for the core shear wall (SW) building, and readily apparent for the stiffest perimeter shear wall building (SW3).
- Observed SSI effects correlated well with the structure-to-soil stiffness ratio, $h/(V_sT)$; the larger the ratio, the greater the observed SSI effect.

The following additional observations were made, relative to the specific case of these building variants and these input motions:

- For all building variants in this study, fundamental periods are past the peak spectral response and located on the descending (i.e., velocity-controlled) branch of the response spectrum for the Northridge earthquake. As such, any stiffening in the structure could be assumed to lead to an increase in response.
- Observed differences in modeled periods between the different foundation models were relatively small for a given structure. A possible exception occurred in the case of shear wall buildings, in which Model 1 periods were noticeably less than the other models.
- Large differences were observed between model results in the basement levels. Different trends were observed in comparisons between superstructure results and comparisons between basement results.
- As the superstructure stiffened, model-to-model variations in superstructure response increased such that they approached the magnitude of observed variations in basement level response. This was particularly noticeable in the case of peak floor acceleration.
- In the superstructure, Model 4a overall results were the most similar to Model MB results for all building types. Model 1 and Model 2 were usually conservative for story shear and peak floor acceleration for all building types. Model 1 was observed to result in conservative displacements and drifts in the moment frame building, but unconservative displacements and drifts in the shear wall buildings.
- In the basement levels, Model 2 results were higher than Models 4a results across all response quantities. In the case of displacements and peak floor accelerations, Model 2 results exceeded Model MB results, but in the case of story drift and story shear, Model MB often had larger values than Model 2.

- In the case of moment frame structures, Model 1 and Model 2 led to comparable or conservative results relative to Model MB. Therefore, Model 1 and Model 2 represent reasonable alternatives for practical foundation modeling of moment frame structures.
- In the case of shear wall structures, Model 4a results were most consistent with Model MB, and Model 2 results conservatively bounded Model MB results. Therefore, Model 2 and Model 4a represent reasonable alternatives for practical foundation modeling of shear wall structures.
- In the case of the SW3 shear wall building, the peak story shear in Model 1 was 1.2 times that of Model MB, and the peak floor acceleration of Model 1 was 1.5 times that of Model MB. Shear wall building designs based on Model 1 would be "overdesigned" for shears and accelerations relative to response characterized by Model MB.

7.4 Walnut Creek Building

The Walnut Creek building is a10-story structure with no subterranean levels. The seismic force-resisting system consists of a reinforced concrete shear wall core with perimeter precast and cast-in-place concrete frames. Construction drawings of the Walnut Creek building were made available for inspection through the auspices of the California Strong Motion Instrumentation Program. The building was designed in 1970. The plan dimensions of the building are 31.8 m (104 ft) wide by 45.2 m (148 ft) long. A typical floor plan is shown in Figure 7-22.

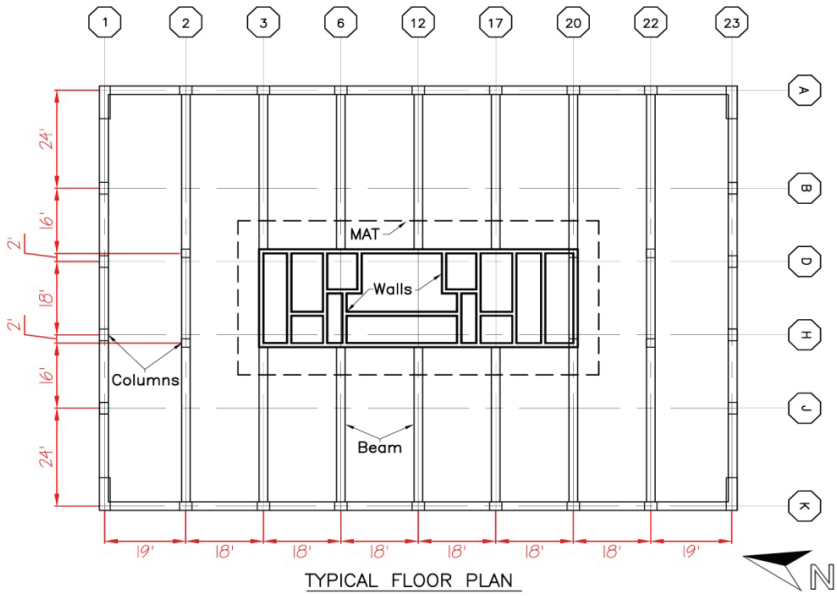

Figure 7-22 Walnut Creek building typical floor plan, based on construction drawings provided by CSMIP.

The gravity system consists of 7 cm (2.75 in) lightweight concrete topping slabs over 7 cm (2.75 in) precast panel slabs supported on precast, prestressed reinforced concrete beams. A longitudinal elevation of the building is shown in Figure 7-23. The building measures 39.2 m (128.5 ft) tall from the ground surface to the roof. The height of the first story is 4.9 m (16 ft), and all other stories are 3.8 m (12.5 ft). Note that the ground surface is not level at the site, although for simplicity, this detail was not considered in the structural model. The characteristics of the foundation are described in Section 7.4.3, below.

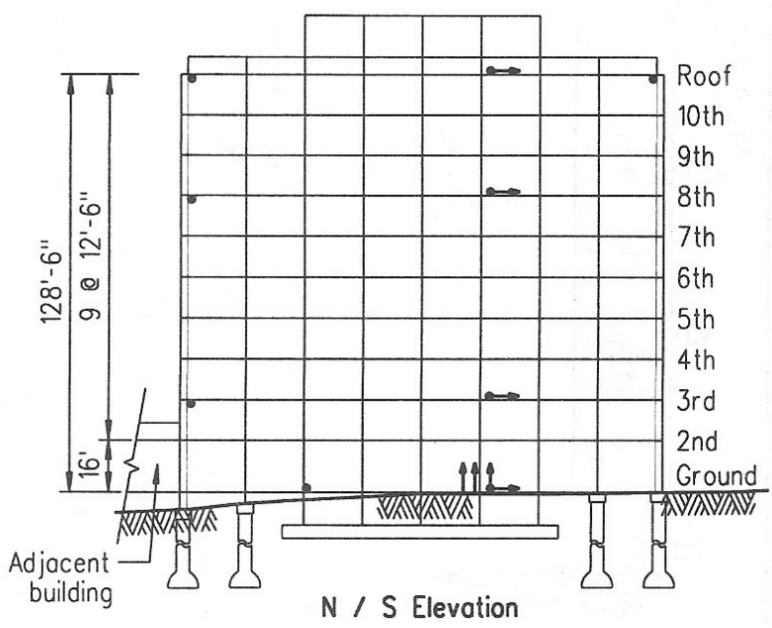

Figure 7-23 Walnut Creek building longitudinal elevation, based on construction drawings provided by CSMIP (Stewart and Stewart, 1997, with permission).

7.4.1 Site Characterization

A plan view of the Walnut Creek site is shown in Figure 7-24. The ground surface elevation is approximately 51.8 m (170 ft) above mean sea level. Soil conditions for the site were obtained from portions of a geotechnical report, prepared by Harding, Miller, Lawson & Associates (1970), and from a geotechnical report with seismic refraction investigation of the subsurface soils, prepared by Raney Geotechnical (1983), in the vicinity of the site. Information from a total of 19 borings ranging in depth from 1.5 m (5 ft) to 17.4 m (57 ft), and four seismic refraction surveys, were obtained from within and around the footprint of the Walnut Creek building.

Borings indicated predominantly west-dipping contacts of sandy clays and silts with variable thicknesses of 0.6 m (2 ft) to 5.5 m (18 ft) overlaying siltstone and sandstone of the Orinda Formation. The depth of the water table was measured between 6.1 m (20 ft) and 12.2 m (40 ft) below the ground surface. The average moist unit weight

was taken to be approximately 18.1 kN/m^3 (115 lb/ft^3). Geophysical data was developed from the seismic refraction surveys. Shear wave velocities in the soil layers were estimated based on correlations by Fumal and Tinsley (1985), while the shear wave velocity in the rock was based on the seismic refraction data presented by Raney Geotechnical.

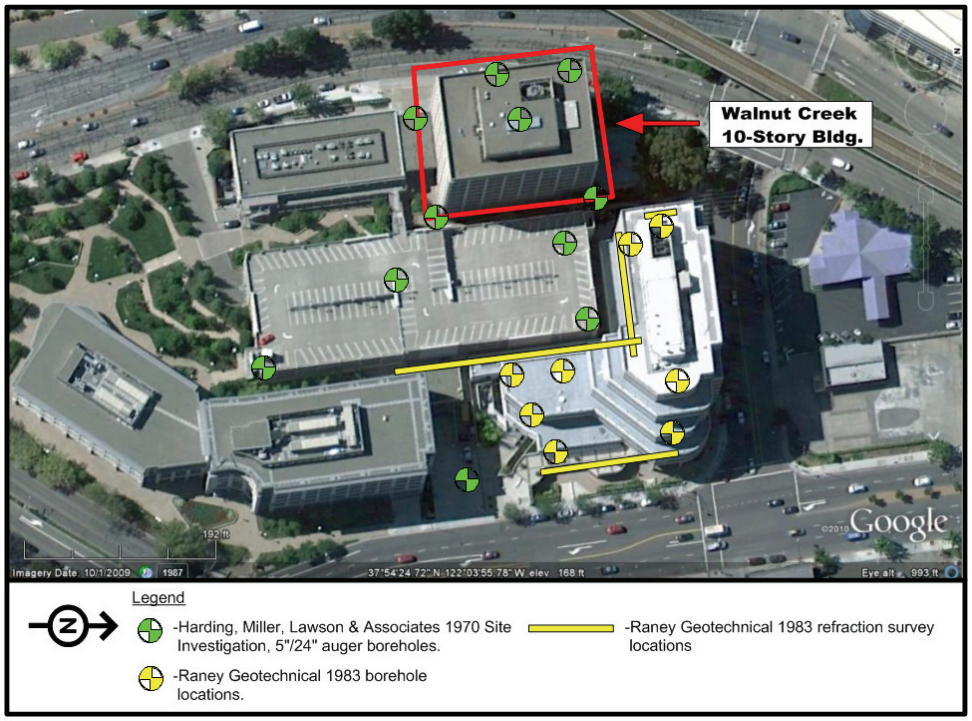

Figure 7-24 Plan view of the Walnut Creek site showing borehole and refraction survey locations used for site characterization (adapted from Harding, Miller, Lawson & Associates, 1970; Raney Geotechnical, 1983).

Based on available geotechnical information, an interpretation of the soil layering at the site, in terms of a shear wave velocity profile and material profile, is shown in Figure 7-25.

7.4.2 Ground Motion Recordings

The Walnut Creek building was instrumented in 1979 by the California Strong Motion Instrumentation Program and designated CSMIP Station No. 58364. Instrumentation includes 16 accelerometers at the locations including the ground floor, third floor, eighth floor, and roof levels. There are two vertical sensors at the ground level, allowing the base rocking effects to be measured. There are no free-field instruments in the vicinity of the site.

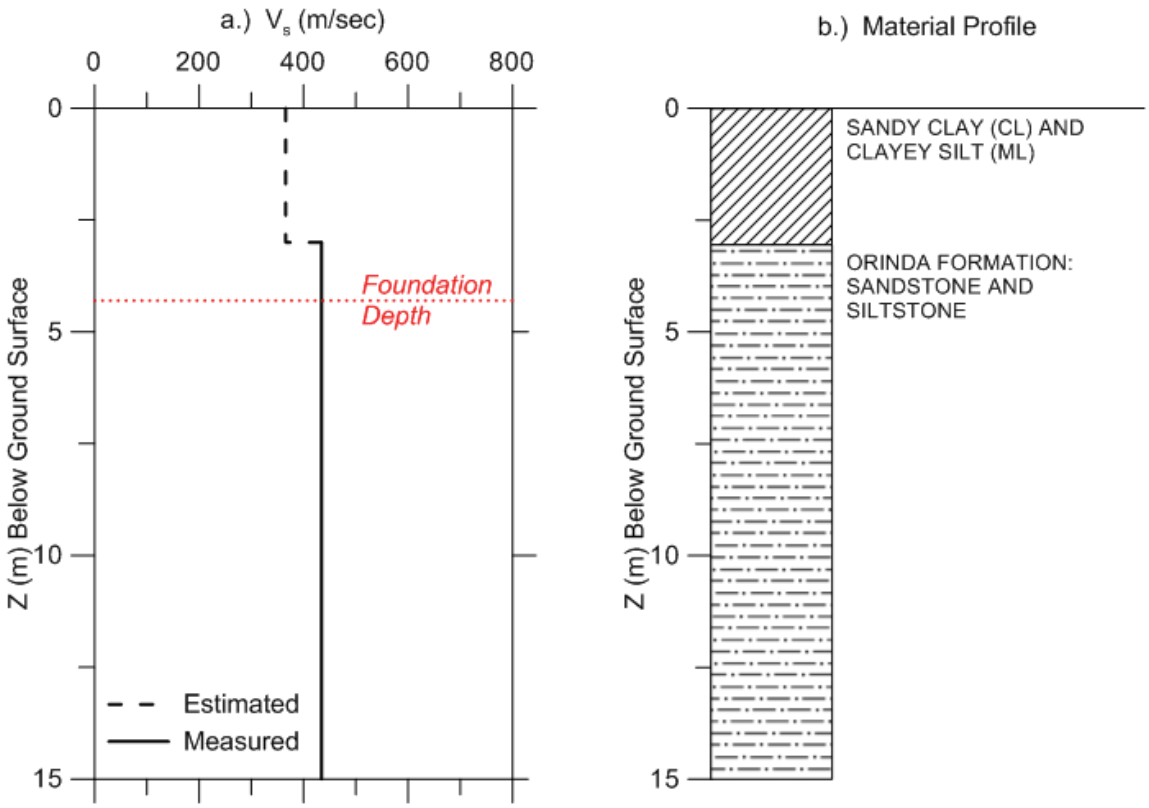

Figure 7-25 Subsurface characteristics of the Walnut Creek site: (a) shear wave velocity profile; and (b) material profile (adapted from Harding, Miller, Lawson & Associates, 1970; Raney Geotechnical, 1983).

Since 1979, five earthquake events have been recorded and processed by CSMIP at this station. The events, along with peak accelerations for the ground floor and roof are presented in Table 7-9.

Table 7-9 Summary of Earthquake Events Recorded at the Walnut Creek Building

Earthquake	Ground Floor (g)				Roof (g)		
	N-S	*E-W*	*V1*	*V2*	*N-S*	*E-W*	*V*
Livermore 80A	0.030	0.033	0.022	0.023	0.116	0.108	----
Livermore 80B	0.061	0.048	0.024	0.018	0.137	0.192	----
1989 Loma Prieta	0.102	0.046	0.053	0.047	0.208	0.164	----
2007 AlumRock	0.005	0.003	NR	NR	0.018	0.015	----
2008 Alamo	0.029	0.018	NR	NR	0.057	0.034	----

Symbols: N-S=north-south; E-W=east-west; V=vertical; V1=Chan.12 (west); V2=Chan.13 (East); and NR=no record available.

Instrumentation locations are shown in Figure 7-26. Horizontal translations recorded at the ground level of the building were assumed to incorporate base-slab averaging effects due to kinematic interaction. Because the bottom of the foundation is 4.2 m

(14 ft) below the ground level, it is reasonable to assume that embedment effects were not captured in the recorded motion. Transfer functions derived using the embedment procedures in Section 3.2 were used to develop foundation input motions, u_{FIM}, from the recorded motions.

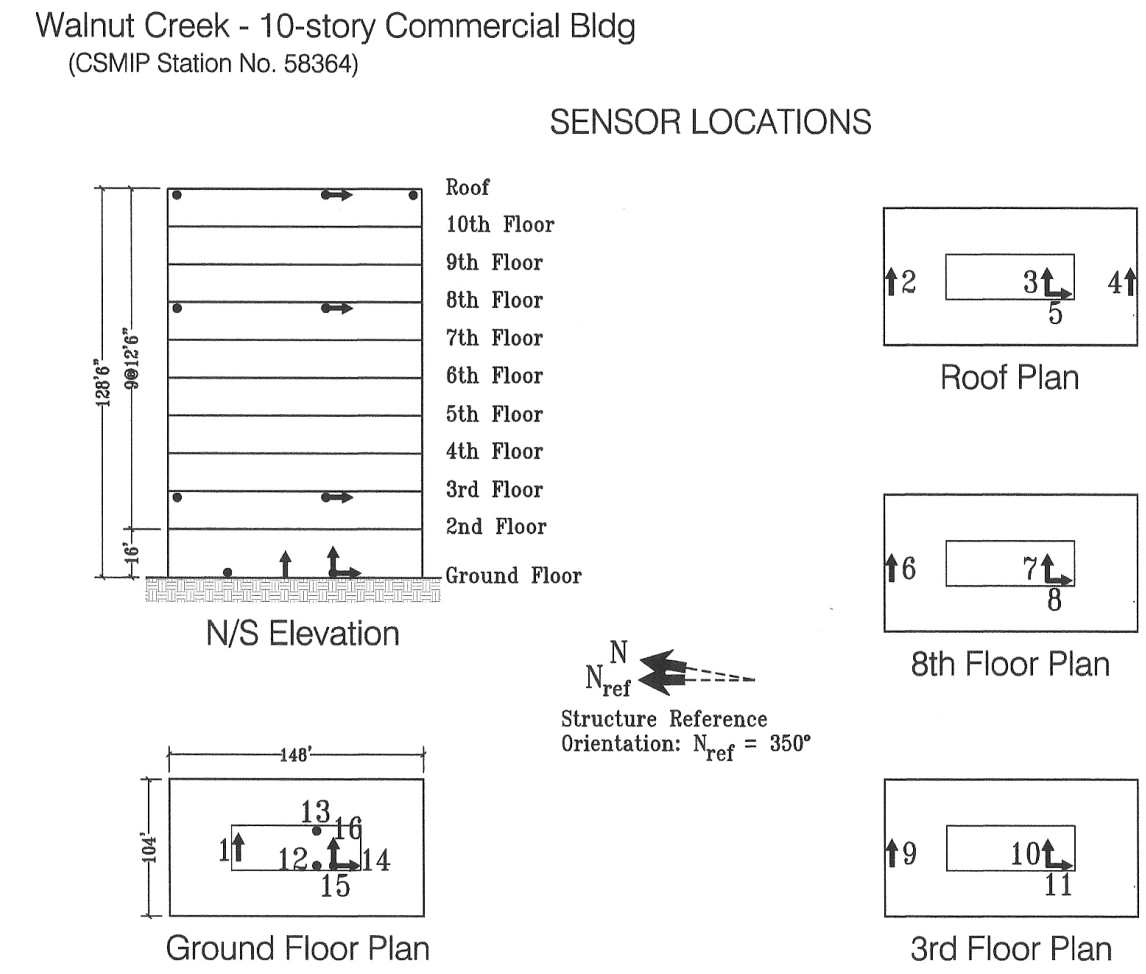

Figure 7-26 CSMIP Station No. 58364: Walnut Creek 10-Story commercial building, sensor location sketch (CESMD, 2011).

Since there were no free-field instruments in the vicinity of the site, free-field ground motions, u_g, were obtained from the recorded motions using transfer functions to remove the base-slab averaging effects. The u_{FIM} and u_g response spectra for the 1989 Loma Prieta earthquake are shown in Figure 7-27.

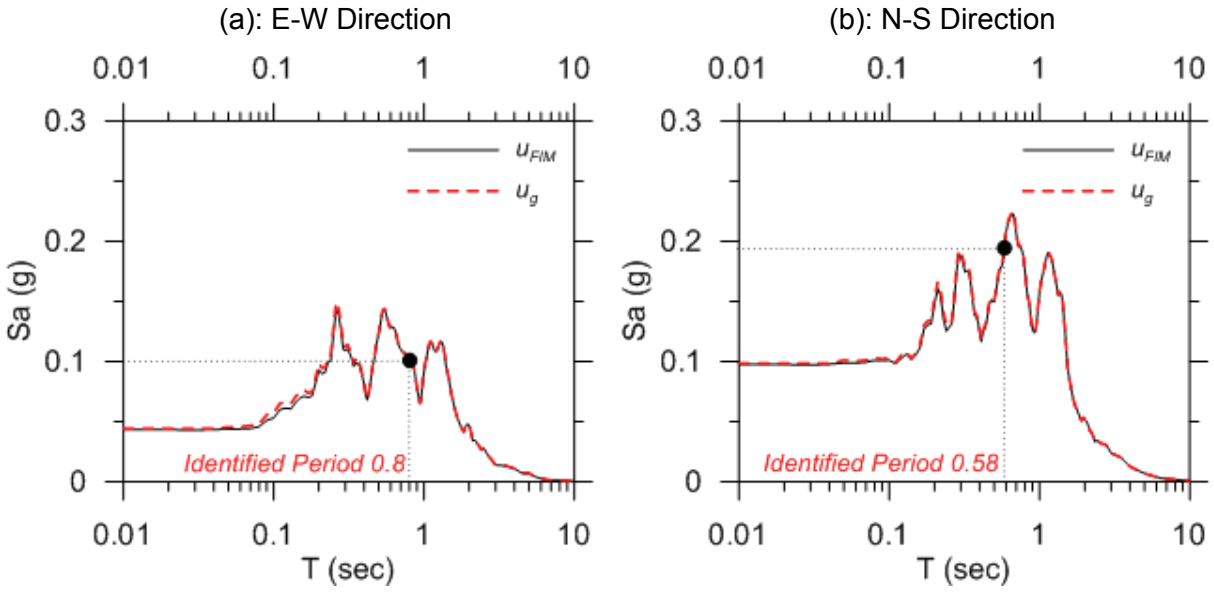

Figure 7-27 Response spectra for foundation input motion, u_{FIM}, and free-field motion, u_g, at the Sherman Oaks building, 1989 Loma Prieta earthquake.

7.4.3 Foundation Conditions

The foundation is rectangular in plan, measuring 31.8 m (104 ft) wide by 45.2 m (148 ft) long. The foundation consists of concrete spread footings, drilled shafts, and mat elements. A foundation plan developed based on information contained in construction drawings provided by CSMIP is shown in Figure 7-28.

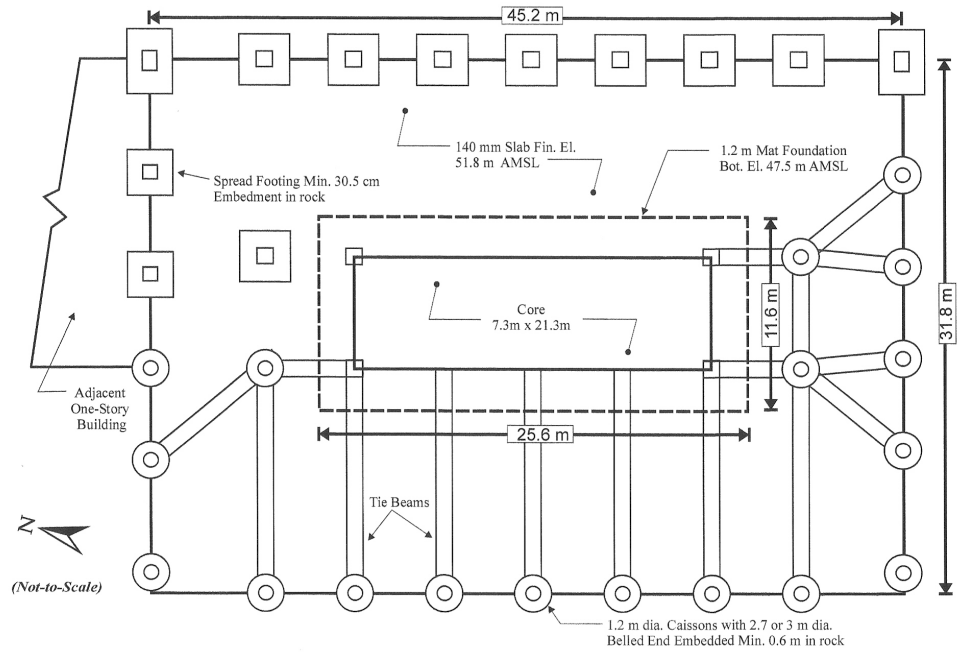

Figure 7-28 Walnut Creek building foundation plan, based on construction drawings provided by CSMIP.

The core walls extend 3 m (10 feet) below the ground level, supported on mat foundation that is 1.2 m (4 feet) thick. The plan dimensions of the mat are 11.6 m (38 ft) by 25.6 m (84 ft), and the bottom of the mat is a total of 4.3 m (14 feet) below the ground level surface. Soil above the mat foundation was backfilled with concrete and sand. Perimeter frame elements terminate at the ground level, where they are supported on spread footings or belled caissons bearing on rock, and interconnected with grade beams.

7.4.4 Development of Foundation Springs and Dashpots

The methodologies described in Chapter 2 were applied to the development of foundation springs and dashpots for the Walnut Creek building. Critical input parameters included the foundation dimensions, fundamental vibration periods of the structure, soil properties, and the amplitude of the input motion. Modeling of the Walnut Creek foundation and site conditions included the following:

- Determination of average effective profile velocity, considering foundation dimensions, overburden pressures from the structure, and nonlinear effects.
- Determination of the structure-to-soil stiffness ratio for estimating the significance of soil-structure interaction effects.
- Evaluation of the effects of mat foundation flexibility on foundation impedance.
- Calculation of mat foundation horizontal stiffness and damping coefficients, considering base slab friction and neglecting passive pressure resistance against the embedded core walls.
- Calculation of vertical stiffness and damping coefficients for springs under the mat foundation, considering adjustment for rotational impedance for shallow foundation elements.
- Calculation of springs and dashpots for the footings and drilled shafts supporting the perimeter frames.

Average Effective Profile Velocity. Foundation stiffness and damping coefficients were based on an average effective profile velocity calculated over an effective profile depth, z_p. Table 7-10 summarizes the effective profile depth, z_p, the depth range, and the average effective profile velocity calculated using Equation 2-18 for each foundation vibration mode over the depth range considered. The maximum depth considered is greater than z_p by the amount of the foundation embedment, D (i.e., the depth range extends to $D + z_p$). For the specific case of the horizontal base spring, the depth interval begins at the base of the foundation.

Values $V_{s,\,avg}$ in Table 7-10 have not been corrected for overburden pressures due to the added weight of the structure. Before averaging, measured free-field velocities, V_s, should be increased to account for the presence of structural overburden.

Table 7-10 Summary of Effective Profile Depths and Average Effective Profile Velocities for the Walnut Creek Building

Vibration Mode	Basis [1]	z_p (m)	Depth Range (m)	$V_{s,avg}$ (m/s)
Horizontal translation (x and y), base spring	$\sqrt{BL}$	8.6	4.3 to 12.9	434.3
Vertical Translation (z)	$\sqrt{BL}$	8.6	0 to 12.9	415.9
Rocking along x-axis (xx)	$\sqrt[4]{B^3 L}$	7.1	0 to 11.3	413.5
Rocking along y-axis (yy)	$\sqrt[4]{BL^3}$	10.5	0 to 14.8	418.2

Notes: [1] Calculated using mat foundation half-width, B=5.8 m; half-length, L=12.8 m; depth D=4.3 m.

For the Walnut Creek building, the increase in vertical stress due to the weight of the structure, $\Delta\sigma_v$, was evaluated at two-foot intervals below the foundation assuming a 2V:1H distribution (Holtz et al., 2010). Overburden-corrected shear wave velocities below the foundation, $V_{s,F}$, were calculated using Equation 2-17, and averaged using Equation 2-18. Values of average effective profile velocity for both the overburden-corrected and non-overburden-corrected cases are compared in Table 7-11.

Table 7-11 Comparison of Average Effective Profile Velocities with and without Correction for Structural Overburden Weight

Z	$V_{s,avg}$ [1] (m/s)	$V_{s,F,avg}$ [2] (m/s)
Horizontal Translation (x and y)	434.3	517.8
Vertical Translation (z)	415.9	463.7
Rocking along x-axis (xx)	413.5	460.8
Rocking along y-axis (yy)	418.2	465.5

Notes: [1] $V_{s,avg}$ is the non-overburden-corrected average effective profile velocity.

[2] $V_{s,F,avg}$ is the overburden-corrected average effective profile velocity.

Structure-to-soil stiffness ratio. Taking the transverse (E-W) direction as critical, the structure-to-soil stiffness ratio, $h/(V_sT)$, for the Walnut Creek building is 0.1, calculated using two-thirds of the modeled building height from foundation to roof, h = 2/3(43.5 m) = 29.0 m, the average effective profile velocity for rocking about the *xx*-axis, corrected for structural overburden, $V_{s,F,avg}$ = 460.8 m/s (from Table 7-11), and the fundamental period for the fixed base condition in the transverse direction, T = 0.66 sec (from system identification, Stewart and Stewart, 1997). Because this ratio is on the order of 0.1, inertial SSI effects (i.e., period lengthening, foundation damping) would be expected to be significant.

Mat Foundation Flexibility. The Walnut Creek building has a central core consisting of shear walls supported by an underlying reinforced concrete mat foundation that is larger in plan and extends beyond the dimensions of the core.

Extension of the mat foundation beyond the core shear walls introduces flexibility into the structural foundation elements. As discussed in Section 2.2.3, flexibility in structural foundation elements can reduce stiffness and radiation damping in the rocking mode (Iguchi and Luco, 1982).

To evaluate the effects of this flexibility on the resulting foundation impedance, plots similar to Figure 2-7 (from Iguchi and Luco, 1982) were utilized with a ratio of core to foundation radius equal to 0.75. Results are shown in Table 7-12, which indicate that the foundation stiffness ratios are close to one, meaning there is little deviation from the rigid foundation case. Therefore, the full mat dimensions of 11.6 m (38 ft) by 25.6 m (84 ft) were used to calculate foundation impedance below the core walls in the Walnut Creek building.

Table 7-12 Evaluation of Soil-to-Foundation Stiffness Ratios for Flexible Mat Foundation below Shear Wall Core in the Walnut Creek Building

Vibration Mode	Basis for Equivalent Radius, r_f	Core Radius r_c (m)	Mat Radius r_f (m)	Ratio $\frac{r_c}{r_f}$	Ψ [1] (Eq. 2-19)	$\frac{k}{k_{\psi=0}}$ [2]
Vertical Translation (z)	$\sqrt{A_f/\pi}$	7.0	9.7	0.72	100	0.9
Rocking along x-axis (xx)	$\sqrt[4]{4I_f/\pi}$	9.3	12.0	0.78	188	0.8
Rocking along y-axis (yy)	$\sqrt[4]{4I_f/\pi}$	5.5	8.1	0.68	59	0.8

Notes: [1] Calculated using E_f=22,894.7 MPa; ν_f=0.2, t_f=1.22 m, a_0=0.13, and G based on $V_{s,F,avg}$ from Table 7-11.
[2] Assessed based on Iguchi and Luco (1982), using r_c/r_f=0.75 and Ψ=100.

Mat Foundation Horizontal Stiffness and Damping. Calculations for horizontal stiffness and damping ratios are shown in Table 7-13. Horizontal stiffness calculations were based on contributions from base friction only, and passive pressure resistance along the embedded portion of the core walls was neglected. Because the base shear reaction mobilizes only soil below the embedment depth D, the effective profile velocity for the horizontal base spring was taken from D to $D+z_p$ (shown in Table 7-10).

In Table 7-13, shear modulus, G, was evaluated from Equation 2-9, using a soil mass density, ρ_s, of 18.1 kN/m^3/g, and values of average effective profile velocity determined using overburden-corrected shear wave velocities below the foundation (shown in Table 7-11). Values of shear modulus should be reduced to account for large strain effects associated with nonlinear behavior. Using Table 2-1, assuming Site Class C, and peak acceleration (at the foundation level) of about 0.1 g from the 1989 Loma Prieta earthquake, the shear modulus reduction factor, G/G_0 = 0.95.

Table 7-13 Calculation of Mat Foundation Stiffness and Damping Parameters for the Walnut Creek Building

Spring/Dashpot	G[1] Eq. 2-9 (MPa)	K_{sur}[2] Table 2-2a (kN/m; kN-m/rad)	η Table 2-2b	a_0[3] Eq. 2-15	α Table 2-3a	β_{sur} Table 2-3a	β_{emb} Table 2-3b	Dynamic Stiffness Eq. 2-14a	Dashpot Coefficient Eq. 2-13a
Horizontal, base spring x-direction $\left(k_{x,base}, c_{x,base}\right)$	469.4	2.24e7	---	0.11	1	0.057	---	$k_{x,base} = \alpha_x K_{x,sur}$	$c_{x,base} = 2k_{x,base}\left(\frac{\beta_{sur}+\beta_s}{\omega}\right)$
Horizontal, base spring y-direction $\left(k_{y,base}, c_{y,base}\right)$	469.4	2.40e7	---	0.11	1	0.053	---	$k_{y,base} = \alpha_y K_{y,sur}$	$c_{y,base} = 2k_{y,base}\left(\frac{\beta_{sur}+\beta_s}{\omega}\right)$
Vertical, z $\left(k_z, c_z\right)$	376.4	2.35e7	1.22	0.12	1	---	0.111	$k_z = \alpha_z K_{z,sur}\eta_z$	$c_z = 2k_z\left(\frac{\beta_{emb}+\beta_s}{\omega}\right)$
Rocking about x-axis $\left(k_{xx}, c_{xx}\right)$	371.6	8.49e8	1.70	0.12	1	---	0.005	$k_{xx} = \alpha_{xx} K_{xx,sur}\eta_{xx}$	$c_{xx} = 2k_{xx}\left(\frac{\beta_{emb}+\beta_s}{\omega}\right)$
Rocking about y-axis $\left(k_{yy}, c_{yy}\right)$	379.3	2.78e9	1.54	0.12	0.99	---	0.002	$k_{yy} = \alpha_{yy} K_{yy,sur}\eta_{yy}$	$c_{yy} = 2k_{yy}\left(\frac{\beta_{emb}+\beta_s}{\omega}\right)$

Notes: [1] Calculated using a shear modulus reduction factor, G/G_0=0.95 for the Loma Prieta earthquake; for other events G/G_0=1.0.

[2] Calculated using overall foundation half-width, B=5.8 m; half-length, L=12.8 m; and ν=0.33.

[3] Calculated at a frequency corresponding to the first-mode period of the flexible-base structure (from system identification, Stewart and Stewart, 1997).

.

A modulus reduction factor of 1.0 was used for the other smaller events. Other parameters were determined using the equations referenced in the table.

Dashpot coefficients were determined using Equation 2-13a and the total foundation damping ratio. The total foundation damping ratio is equal to the sum of the radiation damping ratio (determined using equations in Chapter 2) and the soil hysteretic damping ratio, β_s. For the Walnut Creek site, the soil hysteretic damping ratio was evaluated using Menq (2003), and determined to be 0.01.

Mat Foundation Vertical Stiffness and Damping. Calculation of overall vertical and rotational stiffness and damping ratios is shown in Table 7-13, using values of average effective profile velocity based on overburden-corrected shear wave velocities (shown in Table 7-11). Vertical springs were distributed over the footprint of the foundation, as shown in Figure 7-29, using a vertical stiffness intensity that is normalized by area (Equation 2-20). Stiffness intensities were adjusted near the edges of the foundation to match the overall rocking stiffness values given in Table 7-13 (using Equation 2-21 and an end length ratio of $R_e = 0.4$). The stiffness of any individual spring in the model was then computed as the product of stiffness intensity and the tributary area for the spring.

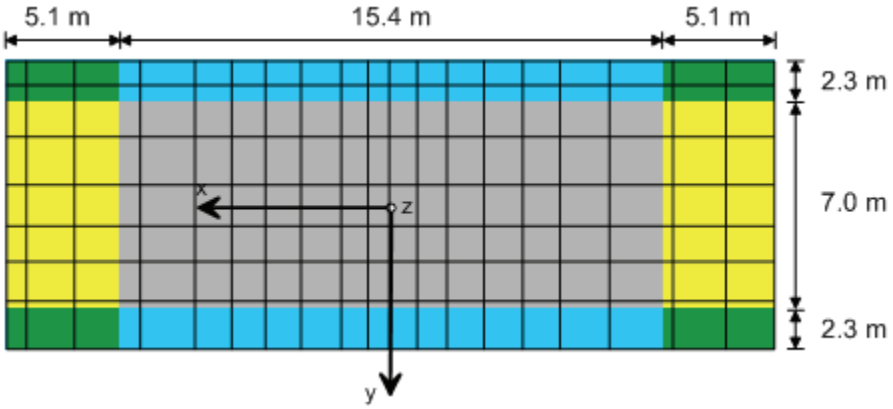

	$k_z^i\left(\text{kN/m}^3\right)$	$c_z^i\left(\text{kN-sec/m}^3\right)$
	96	275
	308	778
	418	1,235
	526	1,697

Figure 7-29 Vertical spring and dashpot intensities distributed over the mat foundation of the Walnut Creek building. Solid lines represent tributary area boundaries.

Vertical stiffness intensities in the central zone of the mat foundation were computed using Equation 2-20a. Edge intensities were increased by factors of $R_k = 5.48$ for the *xx*-direction and $R_k = 3.21$ for the *yy*-direction to correct for underestimation of rotational stiffness (Equations 2-21a, 2-21b). Corner intensities were evaluated as the

average of the intensities in the *xx*- and *yy*-directions. Dashpot intensities were calculated based on stiffness intensities using Equation 2-20b, and reduced by R_c (Equations 2-21c, 2-21d), to correct for overestimation of rotational damping.

Footing and Drilled Shaft Stiffness and Damping. Individual springs and dashpots were calculated for horizontal and vertical translation modes for the spread footings and drilled shafts supporting the columns of the perimeter frames. For simplicity, spread footings and drilled shafts were treated as individual shallow square foundations with dimensions of 3.05 m (10 ft) by 3.05 m (10 ft). Calculations were similar to those presented for the mat foundation, using the same soil parameters. For reference, calculated values were 3.91 x 10^6 kN/m for horizontal springs (k_x and k_y); 4.97 x 10^6 kN/m for vertical springs (k_z); 1.68 x 10^3 kN-s/m for horizontal dashpots (c_x and c_y); and 2.75 x 10^4 kN-s/m for vertical dashpots (c_z).

7.4.5 Analysis Results

The Walnut Creek building was analyzed in OpenSees (McKenna, 1997), incorporating foundation springs and dashpots described above. Details for the development and validation of the model are described in Appendix C. To expedite analyses and post-processing of results, the three-dimensional model was collapsed into a simplified two-dimensional model. Adjustments to the shear and flexural stiffness for cracked concrete were used to produce a reasonably close match to the periods and displacement histories in recordings from the 1989 Loma Prieta earthquake. Based on validation studies, the model was considered a reasonable engineering approximation for the Walnut Creek building.

Because the Walnut Creek core wall foundation has limited embedment, and there are no basement levels, multi-support excitation along embedded portion of the building was not considered. As a result, Model MB converges to Model 4 (bathtub model). Using this model as a basis, alternative modeling configurations were developed and studied, and the resulting response quantities were compared for the following variants:

- Model 2, which included explicit modeling of the subterranean foundation elements, assuming a fixed base at the foundation level and omitting the surrounding soil; and
- Model 1, which ignored the response of the subterranean foundation elements by assuming a rigid base at the ground level.

Implementation of Model 4 (bathtub model), Model 2, and Model 1 for the Walnut Creek building is illustrated in Figure 7-30. Because of the minimal embedment of the Walnut Creek building structure, Model 1 and Model 2 are nearly identical.

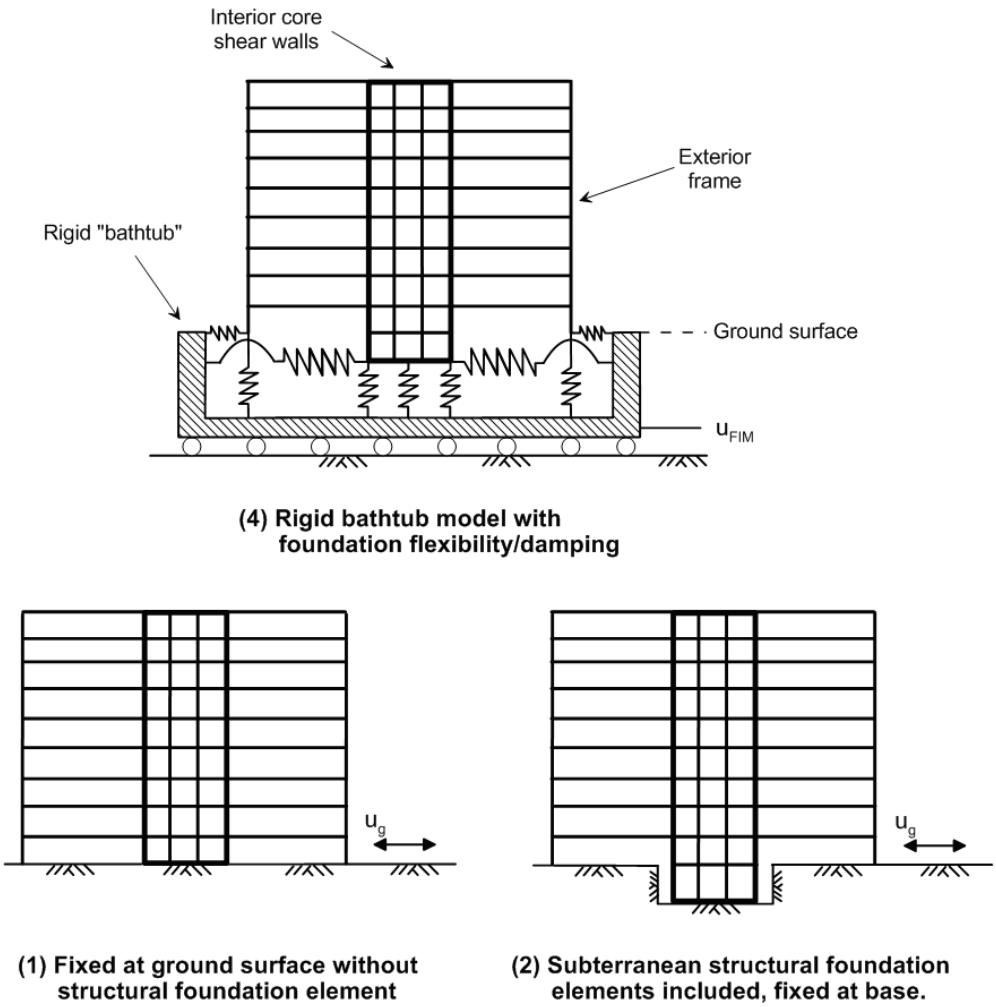

Figure 7-30 Schematic illustration of Model 4 (bathtub); Model 2 (fixed at foundation level); and Model 1 (fixed at ground surface) for the Walnut Creek building.

Fundamental periods of vibration for each of the model variants are shown in Table 7-14. The resulting modeled periods were only modestly affected by different idealizations of the soil-foundation interface (i.e., Model 1 and Model 2 have the same fundamental period; Model 4 is slightly more flexible with a longer fundamental period).

Table 7-14 Comparison of Fundamental Periods for Alternative Foundation Modeling Configurations for the Walnut Creek Building

	Fundamental Period (sec)
Model	*E-W Direction*
Model 4 (bathtub)	0.83
Model 2 (fixed at foundation)	0.78
Model 1 (fixed at grade)	0.78

Comparisons of computed acceleration and displacement histories, maximum displacement, drift ratios, story shear coefficients, and peak floor accelerations between Model 4 (taken as Baseline Model MB), Model 2, and Model 1 are shown in Figure 7-31 and Figure 7-32.

In Figure 7-31, the fixed-base models (Model 1 and Model 2) capture roof acceleration and displacement histories reasonably well, but the phasing was quite different. Observed differences in phasing are likely due to differences in higher mode response.

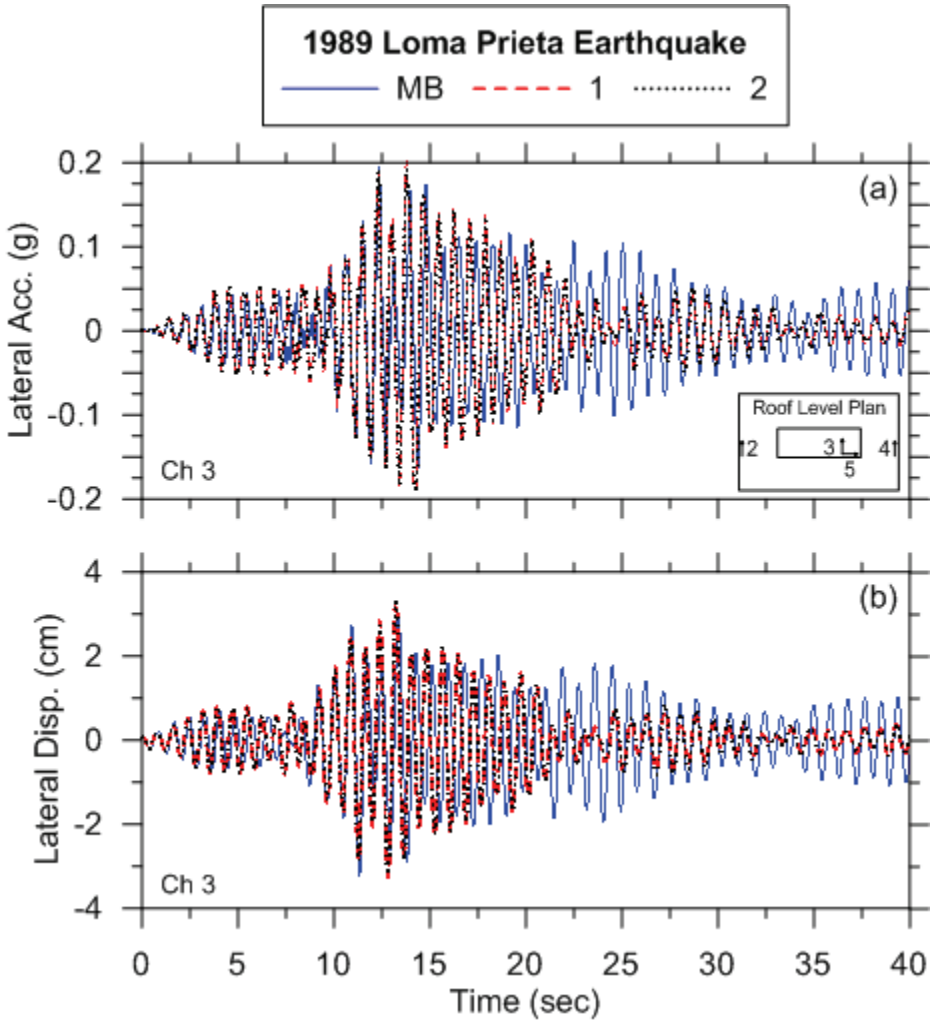

Figure 7-31 Comparison of roof acceleration and displacement histories for Model 4 (taken as Baseline Model MB), Model 1, and Model 2 for the Walnut Creek building.

In Figure 7-32, there is a general trend towards over-prediction of response by the fixed-base models (Model 1 and Model 2) relative to Model 4 (taken as Baseline Model MB). Observed differences were largest in peak floor acceleration response, and are likely the result of differences in higher-mode effects.

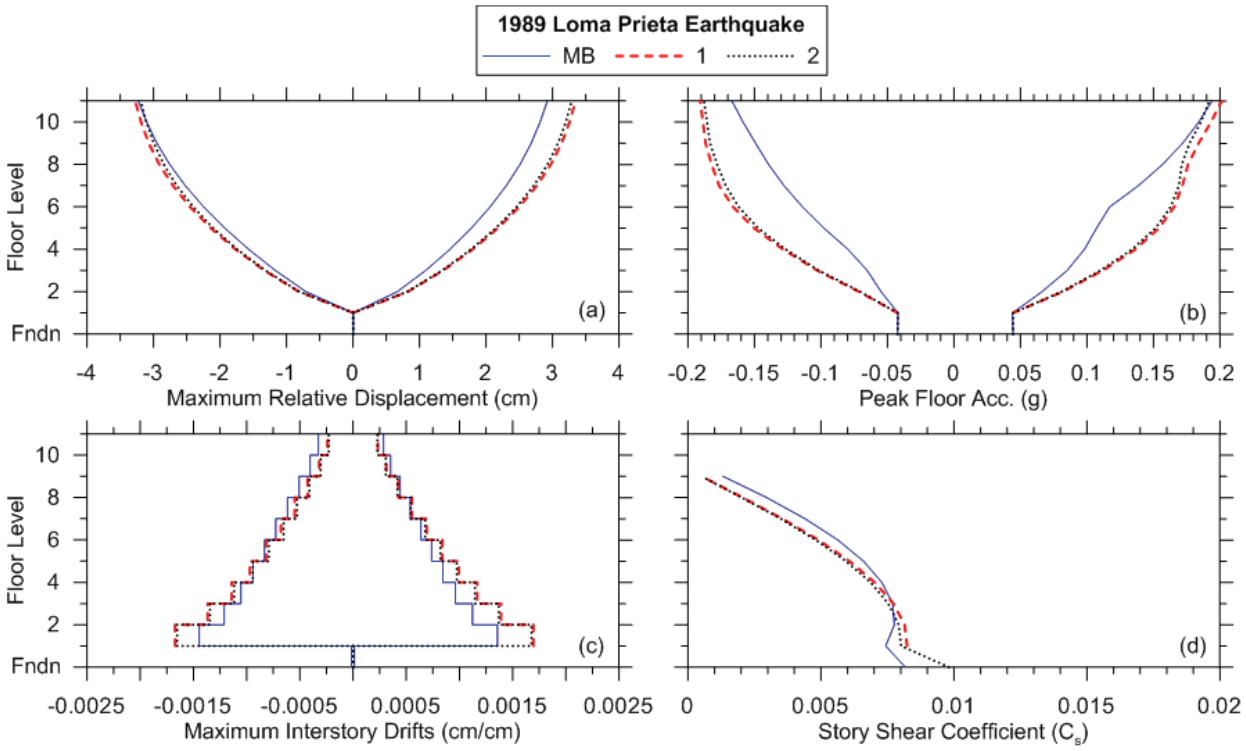

Figure 7-32 Comparison of maximum relative displacement, peak floor acceleration, maximum story drift, and story shear coefficients for Model 4 (taken as Baseline Model MB), Model 1, and Model 2 for the Walnut Creek building.

The presence of two vertical instruments at the ground level allowed for the evaluation of base rotation, and computation of lateral roof displacement due to base rocking. High-pass filtering of the base rocking data, which was needed to produce a physically meaningful result, is described in Appendix C. Comparison of modeled versus recorded roof displacement histories due to base rotation are shown in Figure 7-33.

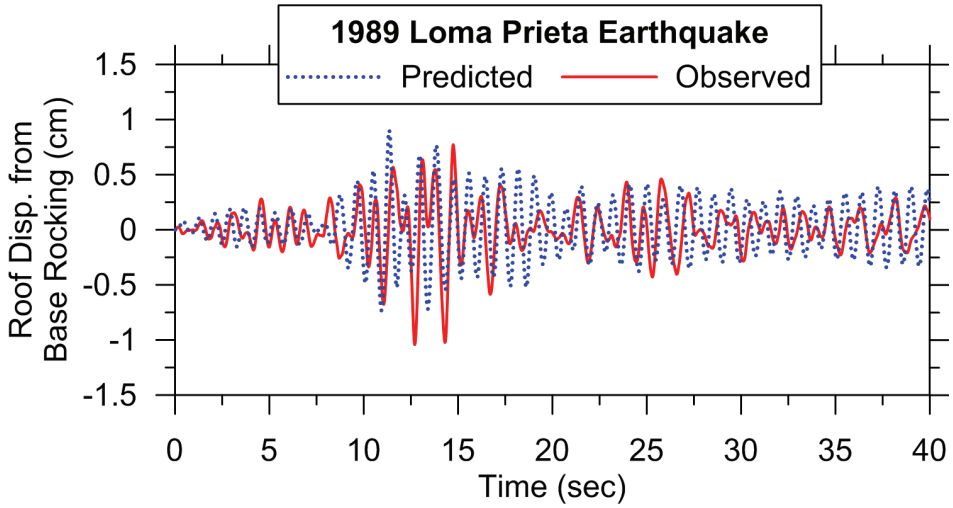

Figure 7-33 Comparison of modeled versus recorded roof displacement histories due to base rotation of the Walnut Creek building.

In the figure, the numerical model captured the maximum amplitude and approximate frequency content of the observed rocking data. The phasing was reasonably well predicted, although there were observed differences in amplitude over the length of the record that can be attributed to discrepancies between predicted and observed structural responses in upper levels due to standard modeling uncertainty. These results showed that, in general, the foundation impedance functions for the Walnut Creek building had about the correct level of flexibility.

7.5 Example Applications Summary and Conclusions

Based upon previous findings from Naeim et al. (2008), Tileylioglu et al. (2010), and observations from example applications and parametric studies herein, the following conclusions can be made:

- MB-type models have an encouraging ability to match observed building responses from recorded motions with modest tuning of structural parameters (e.g., damping ratios, building masses, or element stiffnesses). These results suggest that the relatively simple equivalent-linear spring and dashpot approach for SSI modeling presented in Chapter 2 can provide a satisfactory representation of foundation impedance.
- Of the model types studied, Model 4, including foundation springs and dashpots within a rigid bathtub element, provided the best match to MB-type models, and is a reasonable and practical simplification to variable support excitation. Model 2, which omits foundation springs, but explicitly includes modeling of the subterranean structure, was the next best alternative. Model 1 results were observed to vary significantly from MB-type model results, but generally provided a conservative estimate of force-based demands for design use. Model 3 results were highly variable, and use of Model 3 approaches to foundation modeling is not recommended.
- Above-ground building responses, as measured by envelopes of peak response parameters such as displacement, drift, story shear, and floor acceleration, were only modestly affected by soil-structure interaction effects in the buildings studied. The effects became more significant as the stiffness of the superstructure increased. In contrast, below-ground responses were very sensitive to soil-structure interaction effects and foundation modeling assumptions (i.e., kinematic ground motion descriptions and spring/dashpot configurations). Sensitivity of below-ground response was observed for all structures, across the full parametric range of stiffnesses studied.

Chapter 8
Conclusions and Recommendations

In this chapter, conclusions and recommendations from prior chapters are distilled into specific, step-by-step procedures to guide the implementation of soil-structure interaction modeling in a design setting. Section 8.1 answers the three questions posed in Chapter 1, which are intended to help guide decisions regarding when SSI is likely to be important and what geotechnical information is needed to model SSI effects. Section 8.2 provides guidance on implementation of inertial and kinematic interaction effects. Section 8.3 describes further study and future research needed to improve the state of knowledge for soil-structure interaction.

8.1 When is Consideration of Soil-Structure Interaction Important?

In Chapter 1, three questions were posed regarding implementation of SSI. In this section, those questions are answered, along with references to more detailed information.

Question 1: When is the use of foundation springs and dashpots important, and which structural response parameters are affected?

The structure-to-soil stiffness ratio, $h/(V_sT)$, can be used as a relative measure for determining when SSI effects will become significant. In this expression, h is the structure height, V_s is the soil shear wave velocity; and T is the fixed-base building period. In applying the structure-to-soil stiffness ratio, values of h, V_s, and T for a given soil-foundation-structure system are not unique. The following values should be used:

- **Height.** Height, h, is the effective height to the center of mass for the first mode shape, taken as approximately two-thirds of the modeled building height.
- **Shear wave velocity.** Shear wave velocity should be taken as the average effective profile velocity, $V_{s,\,avg}$, calculated based on overburden-corrected shear wave velocities below the foundation, $V_{s,\,F}(z)$. Guidance on calculating average effective profile velocities is provided in Section 2.2.2 and illustrated in Chapter 7.
- **Period.** Period should be taken as the best estimate value of the fixed-based building period in the direction under consideration. The structure-to-soil stiffness ratio should be evaluated separately in each direction.

When $h/(V_sT) > 0.1$, SSI can significantly lengthen the building period and modify (i.e., generally increase) damping in the system. This will modify the design base shear (up or down, depending on spectral shape) and the distribution of force and deformation demands within the structure, relative to a fixed-base analysis. The use of springs and dashpots to represent the flexibility and damping at the soil-foundation interface will be most significant for stiff structural systems such as shear walls and braced frames.

When using the structure-to-soil stiffness ratio, it is important to recognize that the ratio is an approximate relative measure, and not an absolute criterion. Even when $h/(V_sT) < 0.1$, relative distributions of moments and shear forces in a building can be modified relative to the fixed-base condition, particularly in dual systems, structures with significant higher-mode responses, and subterranean levels of structures. Additional information is provided in Chapter 2, and SSI effects on other building response quantities are investigated in Chapter 7.

Question 2: Under what conditions is consideration of the differences between foundation input motions and free-field ground motions important?

Foundation motions differ from free-field ground motions because of kinematic interaction effects resulting from the presence of stiff foundation elements on or in the soil. Kinematic interaction includes base-slab averaging and embedment effects in which the stiffness and strength of the foundation elements cause averaging or reductions in localized maxima of spatially variable motions that would have otherwise occurred within the footprint of the foundation.

Base-slab averaging effects become important within the period range of engineering interest for foundation sizes (measured as an equivalent foundation half width) of about 20 m (66 ft) or larger for typical soil or weathered rock sites in California. Embedment effects are sensitive to the depth of embedment, and typically become important when a structure has two or more subterranean levels. Both base-slab averaging and embedment effects principally impact short period spectral ordinates (at periods less than approximately 1.0 sec). Base-slab averaging and embedment effects are introduced in Chapter 3. Implementation in standards and guidelines is described in Chapter 4.

Inertial interaction effects are not a significant contributor to differences between foundation motions and free-field motions, except in a narrow frequency range centered on the fundamental frequency of the SSI system.

Question 3: What field and laboratory investigations are necessary to develop foundation springs and dashpots for SSI analysis?

When foundation springs and dashpots are to be implemented in an analysis, it is necessary to have an engineering characterization of the soil stratigraphy (i.e., soil types, layer thicknesses, depth to groundwater, depth to rock), seismic shear wave velocities, and appropriate shear strength parameters for soil materials in the vicinity of the foundation. In general, this type of information is routinely developed in geotechnical investigations, so the scope of site investigations to support SSI analysis is not significantly different than most typical investigations. The interpretation of soil profile data for the development of foundation springs and dashpots is described in Chapter 2. Checklists guiding the collection of geotechnical information for SSI analyses are provided in Chapter 6, and examples of the use of this data are provided in Chapter 7.

8.2 Summary of Soil-Structure Interaction Analysis Procedures

In this section, procedures for developing springs and dashpots, modifying ground motions due kinematic interaction, and including soil-structure interaction in response history analyses are summarized, along with references to more detailed information.

8.2.1 Developing Springs and Dashpots

The steps for developing springs and dashpots in SSI analyses are summarized as follows:

1. Develop the required input parameters for analysis:
    a. *Geotechnical and shear wave velocity profiles*. Examples of the type of information that is required are given in Figure 7-4 and Figure 7-25. Uncertainty in the shear wave velocity profile should be considered on the basis of scatter in data from measurements at the site.
    b. *Shear strength parameters and their variation with depth*. Below the ground water table, undrained strength parameters are required. Drained strength parameters are generally acceptable above the ground water table. Variability in shear strengths should be considered based on the range observed in material-specific testing.
    c. *Poisson's ratio, (ν).* Can generally be taken as 0.3 for sands and 0.45 for clays.
    d. *Soil hysteretic damping ratio, (β_s)*. Strain-dependent soil damping can be measured using site-specific dynamic material testing, but for most projects can be taken from existing empirical relationships. Several such

relationships are summarized in Kramer (1996). More recent relationships are presented by Darendeli (2001) and Menq (2003). These relations are for damping as a function of shear strain. For most design applications in the Western United States, strain levels between about 0.1% to 0.5% would be a reasonable, first-order estimate.

e. *Foundation information*. Required information includes gross dimensions (e.g., length, width, depth), the foundation types envisioned for the project (e.g., mats, inter-connected footings, piles), and the degree of connectivity between foundation elements (e.g., tie beams, floor slabs). This information should be developed in cooperation with the structural engineer.

f. *Building period and mass*. Fundamental mode periods are needed for the two primary axes of the building. The building mass should include dead load and the live load expected to be present during earthquake shaking. Approximate estimates of period and mass are generally sufficient and should be obtained from the structural engineer.

g. *NEHRP site class and ground motion level*. Site class can be developed from the velocity profile using the average shear wave velocity in the upper 30 m (V_{s30}). The primary ground motion parameter for the development of soil springs is peak ground acceleration (PGA) in the free-field.

2. Evaluate the average effective profile velocity for calculation of foundation stiffness values. For shallow foundations, proceed as follows:

   a. For heavily loaded foundations, the overburden pressure due to the weight of the structure will modify shear wave velocities relative to values measured in the free-field. A correction for overburden effects can be made using Equation 2-17.

   b. Calculate the effective foundation sizes B_e^A and B_e^I using Equations 2-18.

   c. Calculate the average effective profile velocity, $V_{s,\,avg}$, over profile depths $z_p = B_e^A$ for horizontal springs and $z_p = B_e^I$ for rotational springs. Details are provided in Section 2.2.2. Example applications are provided in Section 7.2.4 and Section 7.4.4.

   d. Apply an appropriate shear wave velocity (or shear modulus) reduction to account for large strain effects using Table 2-1.

   e. Repeat as needed to develop alternative values of effective velocity that account for uncertainty in the soil profile.

3. Calculate the static stiffness of the foundation for each vibration mode, j. Vibration modes are designated as: horizontal (x and y), vertical (z), and rotational (xx and yy).

a. Calculate the stiffness of a shallow foundation for a surface condition (i.e., not including embedment effects), $K_{j,sur}$, using the equations in Table 2-2a.

b. If applicable, calculate the stiffness modifier for embedment effects, η_j, using equations in Table 2-2b.

c. The modified stiffness for embedment is taken as the product of $K_{j,sur}$ and η_j.

d. Repeat the calculations as needed using the range of effective velocities that account for uncertainty in the soil profile.

4. Apply dynamic stiffness modifiers, α_j, and calculate damping ratios, β_j:

   a. Calculate the angular frequency corresponding to the first mode period of the structure (T) as $\omega = 2\pi/T$. For three-dimensional analyses, the period can be taken as the average of the first mode periods in each orthogonal direction.

   b. Calculate the dimensionless frequency, a_0, using Equation 2-15.

   c. Calculate the dynamic stiffness modifier, α_j, using equations in Table 2-3a.

   d. Calculate radiation damping ratios, β_j, using equations in Table 2-3a for surface foundations, or Table 2-3b for embedded foundations.

5. Evaluate frequency-dependent spring and dashpot (impedance) coefficients:

   a. Stiffness, k_j, can be taken as the product of the static stiffness, $K_{j,sur}$, the modifier for embedment, η_j, and the dynamic stiffness modifier, α_j, using Equation 2-14a.

   b. Dashpot coefficient, c_j, can be evaluated from radiation damping ratios, β_j, using Equation 2-13a.

   c. Repeat as needed for the range of static stiffnesses that account for uncertainty in the soil profile.

6. Evaluate limiting spring forces (i.e., capacities), which depend on the strength of the foundation soils, as described in Section 2.2.4:

   a. For vertical springs, the capacity is the unfactored foundation bearing capacity.

   b. For horizontal springs at the base-slab level, the capacity is derived from shear-sliding resistance at the soil-foundation interface.

   c. For basement walls, the capacity is derived using passive earth pressure theory.

   d. Repeat as needed to account for uncertainty in shear strength parameters.

7. Distribute vertical springs and dashpots around the foundation:

a. Calculate stiffness and damping intensities k_z^i and c_z^i using Equations 2-20a and 2-20b.

b. Select a value for the end length ratio, R_e, (typically 0.3 to 0.5).

c. Calculate the spring and dashpot amplifier, R_k, and dashpot reduction factor, R_c, using Equations 2-21a through 2-21d.

d. Apply stiffness intensity $R_k \times k_z^i$ and dashpot intensity $R_k \times R_c \times c_z^i$ within the end regions.

e. Evaluate individual springs and dashpots based on the appropriate intensity multiplied by the tributary area (at each location within the foundation footprint).

f. Repeat as needed for the range of stiffness and dashpot values that account for uncertainty in the soil profile.

8. Distribute horizontal springs and dashpots around the footprint of the foundation:

   a. The horizontal spring at the base-slab level is evaluated as $k_{j,sur} = k_j/\eta_j$ and is applied at the base-slab level. A similar procedure is applied for damping.

   b. For embedded foundations, the remaining lateral stiffness is distributed over the depth of the embedment (e.g., height of basement walls). The remaining stiffness is taken as $k_j(1-1/\eta_j)$, as specified in Section 2.2.3 (similar for damping).

Procedures for deep (e.g., pile) foundations, described in Section 2.3, are similar to those presented above for shallow foundations. Differences include the depth range over which dynamic properties are evaluated; the equations used to calculate static stiffness, dynamic modifiers, and damping ratios; and the need for group modifiers in the case of pile groups. Computer programs (e.g., DYNA6, Western Engineering, 2011; SASSI, Lysmer et al., 1999) can perform Step 2 through Step 5 for finite element analyses, utilizing procedures similar to those discussed in this report. The DYNA6 program can also be used for analysis of pile impedance as well.

An important consideration when deep foundation elements (e.g., piles) are combined with shallow foundation elements (e.g., spread footings or mats) is whether or not resistance from both shallow and deep foundation elements can be combined. If the soil is expected to settle away from the shallow foundation elements (e.g., the case of consolidating soils and end-bearing piles), then lateral load resistance should be derived on the basis of the piles, pile caps, and basement walls only, and the resistance provided by shallow foundation elements should be ignored.

8.2.2 Modifying Ground Motions due to Kinematic Interaction

The steps for modifying ground motions due to kinematic interaction are summarized as follows:

1. Collect the required input for the analysis:
   a. *Specification of seismic demand*. Determine if seismic demands for design are to be specified in the form of an acceleration response spectrum a set of ground motion acceleration time histories.
   b. *Foundation Dimensions*. Determine the area of foundation, as represented by B_e^A, and the embedment depth, D.
   c. *Shear wave velocity profile*. Determine shear wave velocities to depth, D.
2. Calculate the transfer function for base-slab averaging:
   a. Transfer function, $H_u(\omega)$, is calculated using Equation 3-3 and Equation 3-4. Input parameters include B_e^A and κ_a.
   b. Parameter, κ_a, is evaluated using Equation 3-5. This base-slab averaging model is calibrated for B_e^A in the range of 15 m to 40 m.
3. Calculate the transfer function for embedment (if $D > 0$). The transfer function, $H_u(\omega)$, for embedment is calculated using Equations 3-6a through 3-6d. Input parameters include depth, D, and the average effective profile velocity, $V_{s,\,avg}$, over that depth.
4. For each frequency, ω, the combined transfer function ordinate for base-slab averaging and embedment is taken as the product of the results from (2) and (3).
5. Modify free-field ground motions to foundation input motions:
   a. Calculate response spectrum modifiers using Equation 3-7a or Equation 3-7b, which relate the ratio of foundation to free-field response spectral ordinates to the transfer function at the corresponding frequency.
   b. Modify acceleration time histories, as needed, using the procedures in Section 3.4. Note the limitations described in Section 3.4 are for ground motions dominated by long-period energy (e.g., soft soils and near-fault effects).

8.2.3 Incorporating Soil-Structure Interaction in Response History Analyses

Summary guidance for implementing soil-structure interaction in response history analyses includes the following:

1. As a minimum, the subterranean levels of a structural system (if present) should be included in the structural model that is fixed at the base. Seismic excitation

can be specified using the free-field motion or a foundation input motion derived considering kinematic interaction effects. This corresponds to Model 2 illustrated in Figure 6-2. This approach neglects inertial SSI effects.

2. Based on current software capabilities, inertial SSI effects can be incorporated into the structural model in a practical manner using a "bathtub" configuration. In this approach, springs and dashpots are developed for the foundation system, each of which is connected to a rigid bathtub surrounding the foundation. Seismic excitation is applied to the bathtub using the free-field motion or a foundation input motion derived considering kinematic interaction effects. This corresponds to Model 4 illustrated in Figure 6-2.
3. The most complete modeling that can be implemented, within the context of substructure methods of analysis, extends the bathtub model to include the effects of multi-support excitation along the basement walls. This corresponds to the Baseline Model (Model MB) illustrated in Figure 6-2. Multi-support excitation requires an analysis of wave propagation in the free-field over the depth of embedment. Depth-dependent motions from wave propagation analyses are applied as displacements at the ends of the horizontal foundation springs. Depth-dependent motions inherently include the effects of embedment described in Section 3.2, and should be further adjusted for base-slab averaging.

8.3 Future Research Needs

Future research needs in soil-structure interaction have been organized into two general thematic areas. The first theme involves relatively short-term recommendations expanding on current studies to: (1) provide tangible insights into the benefits of SSI analysis for owners and practicing engineers; and (2) further explore the benefits and limitations of SSI response history analysis procedures, possibly leading to improved procedures. The second theme involves relatively long-term recommendations intended to address fundamental limitations in the state of SSI knowledge, which limit the accuracy and reliability of SSI models available for use in engineering practice.

8.3.1 Theme 1: Expansion of Current Studies

Example applications presented in Chapter 7 presented case studies on buildings with available earthquake recordings. This effectively limited range of possible structural configurations that could be investigated to the types of structural systems for which data were available. In particular, case-study buildings had modest SSI effects and lacked strongly nonlinear responses. Additional studies should be performed on a common building configuration that is specifically selected to produce large SSI effects.

One such example might include a low-rise dual system building (i.e., shear wall plus moment frame system) with a basement. The building could be designed using a fixed base model (i.e., Model 2 from Figure 6-2) using a typical design spectrum and then redesigned using a bathtub model (i.e., Model 4 from Figure 6-2) for the same design spectrum.

Both large-amplitude and modest-amplitude ground motions could be applied to the model to evaluate the effects of nonlinearity in the structural response on the impact of SSI effects. Alternative SSI element configurations that better account for uplift and nonlinear soil behavior, as described in Section 2.4, could also be applied to assess their relative impact on elastic-plastic procedures. Analysis using a direct approach (as opposed to a substructure approach) could be performed, especially in the case of strongly nonlinear response.

Expanded studies on such a building could be used to provide quantitative comparisons of the effects of different foundation modeling approaches on structural member sizes and, ultimately, construction costs.

8.3.2 Theme 2: Research to Address Knowledge Gaps

Research needs for expanding the state of knowledge for soil-structure interaction are as follows:

- The foundation damping model of Veletsos et al. (various) produces different results than similar models by others. A critical examination of the derivation of that model is needed, followed by the development of equations for foundation damping that properly consider hysteretic damping from soil response, radiation damping from rotational and translational vibration modes, and the sensitivity of radiation damping to different soil stiffness profiles. This problem is discussed in Section 2.1.
- The rotational stiffness of shallow foundation systems with non-rigid structural foundation elements is poorly understood. In particular, the effects of coupled versus uncoupled rotations at the base of lateral-load bearing elements on radiation damping and overall system impedance need to be investigated. This problem is discussed in Section 2.2.3.
- The impedance of pile-supported foundations is poorly understood for realistic pile and soil conditions, especially for pile groups. Elasto-dynamic solutions for piles in idealized soil profiles exist in the literature, but are not used in practice, in part because they only apply at low displacement levels. The discrete element models that are used (e.g., LPILE, APILE) are poorly constrained for stiffness, and are intended for non-seismic problems. Next-generation element models for dynamic loading of piles are needed that accurately capture the stiffness from

elasto-dynamic analyses and the capacity from discrete element models. This problem is discussed in Section 2.3.

- The kinematic interaction problem for pile-supported mat foundations subjected to incoherent wave fields has not been explored to a sufficient degree. Data from Japan suggest that existing models (for base-slab averaging and kinematic response of pile foundations) are unable to capture observed foundation/free-field transfer functions, which decay rapidly with frequency. This problem is discussed in Section 3.3.
- The conversion of transfer functions, derived from kinematic interaction analyses, to ratios of response spectra currently relies on guidelines provided in FEMA 440, *Improvement of Nonlinear Static Seismic Analysis Procedures* (FEMA, 2005). A relatively robust statistical model is needed for the relationships between these ordinates as a function of frequency and ground motion characteristics. This problem is discussed in Section 3.4.
- Values of the *R*-factor used in force-based methods for seismic design are based on engineering judgment, considering observations of building performance in past earthquakes and anticipated performance of similarly designed buildings in future earthquakes. Nonlinear response (without collapse) of good performing systems is used to justify high *R*-values. However, for some buildings, good performance may result, in part, from soil-structure interaction effects that also serve to reduce seismic demands. SSI effects may be partially reflected in current values of the *R*-factor, resulting in a potential for double-counting. There is a need to revisit the definition of *R* factors with respect to SSI effects, to make sure that the specified values represent the effects of structural ductility alone. This issue should be considered in the implementation of NIST GCR 12-917-20, *Tentative Framework for Development of Advanced Seismic Design Criteria for New Buildings* (NIST, 2012). This problem is discussed in Section 4.1.
- Available experimental data described in Chapter 5 should be distilled into a common format of impedance ordinates, and compared to a consistent set of predictions utilizing the procedures and parameter selection protocols given in this report.
- Case studies of buildings with recordings from seismic instrumentation are extremely valuable. Unfortunately, current protocols for structural instrumentation seldom provide the information needed for SSI studies, so additional data are needed. At a minimum, sensors are needed to record structural translations at the foundation and roof, at least two vertical sensors on the foundation to record rocking, and a ground instrument near the building.

Appendix A
Sherman Oaks Building Model Development

This appendix provides detailed information on the structural modeling and calibration for the Sherman Oaks building example application presented in Chapter 7.

A.1 Baseline Model Development

Response history analysis of a three-dimensional model of the soil-foundation-structure system of the Sherman Oaks building was performed using OpenSees, *Open System for Earthquake Engineering Simulation* (McKenna, 1997; OpenSees, 2011). This model was based on a previous OpenSees structural model of the building provided by the California Strong Motion Instrumentation Program (CSMIP), and United States Geological Survey (USGS). Construction drawings of the Sherman Oaks building were made available for inspection through the auspices of CSMIP. The structural system and foundation configuration of the Sherman Oaks building are described in Chapter 7.

Renderings of the Sherman Oaks building configuration are provided in Figure A-1. The renderings include cut-away views showing details in the first story, basement, and foundation regions. The structural configuration in the first story and basement levels were modeled in a simplified manner to keep the structural modeling aspects tractable, and to focus on comparisons between variations in the idealization of the soil-foundation interface.

In the first story of the building, the one-story extension of the structure along the south longitudinal face of the building (shown in Figure A-1) was not included in the structural model (i.e., both the mass and the stiffness of the one-story extension were excluded). In the basement region, the geometry was simplified such that the shear walls were placed in-line with the perimeter frames of the superstructure. This kept the footprint of the model at 21.9 m wide by 57.6 m long (72 ft by 189 ft) from foundation to roof. Although this geometric simplification was made, the flexibility inherent in the real configuration was captured through elastic connecting springs modeled with the stiffness properties of the horizontal slab components that interconnect the frame lines of the superstructure with the basement wall lines. This is shown schematically in Figure A-2.

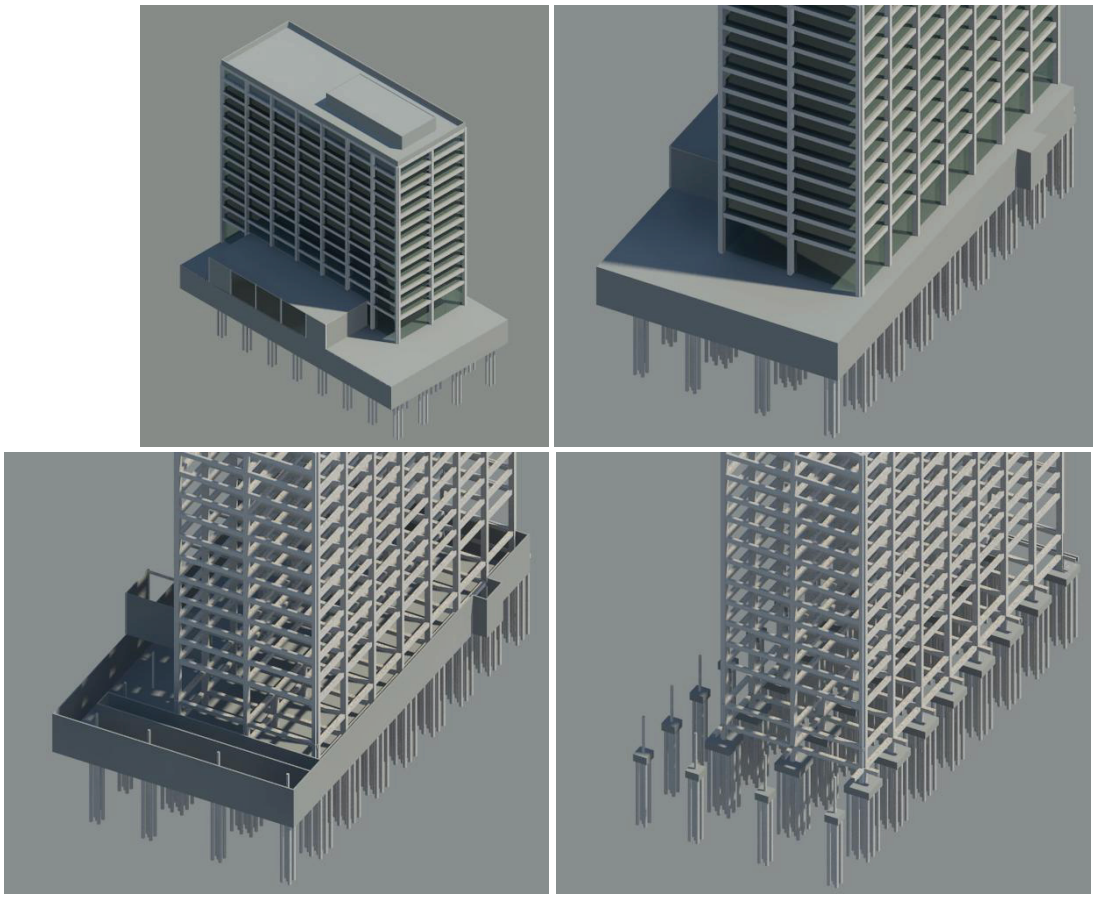

Figure A-1 Renderings of the Sherman Oaks building, including cut-away views showing structural details in the first story, basement, and foundation regions.

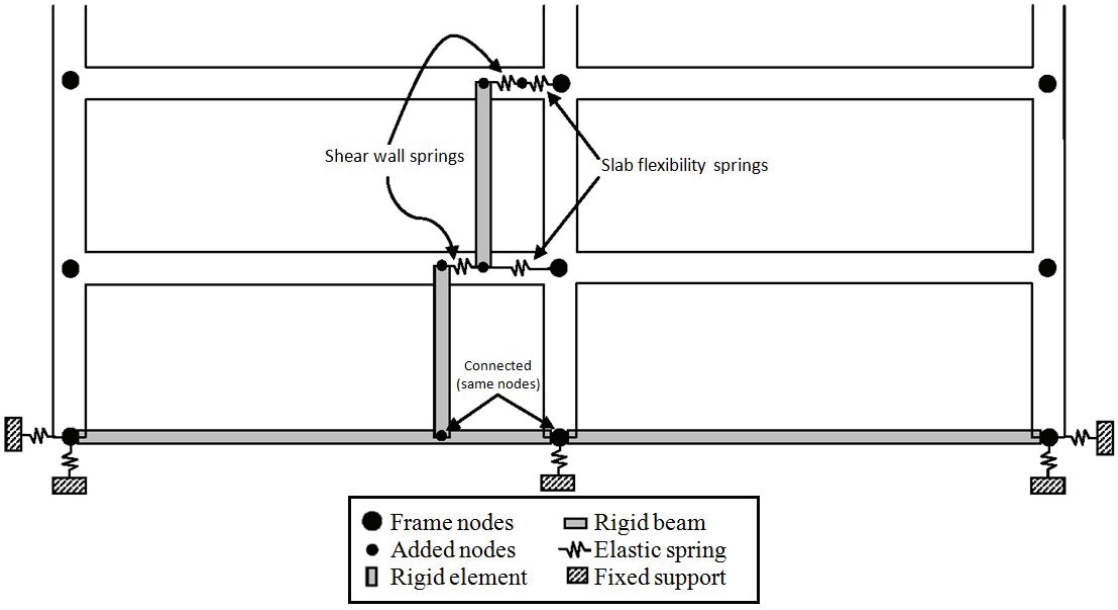

Figure A-2 Schematic illustration of elastic springs connecting the framing lines of the superstructure with the wall lines in the basement levels.

The superstructure of the Sherman Oaks building model is a three-dimensional frame of fiber elements (nonlinearBeamColumn in OpenSees). The model is a centerline model that does not include finite joint elements. The two basement levels include fiber element beams and columns, basement slabs, shear walls, and basement grade beams. A rigid diaphragm constraint is used at each floor level.

Fiber elements are composed of both core and cover concrete materials (Concrete04 in OpenSees) and reinforcing steel materials (Steel02 in OpenSees). Fiber elements model flexural behavior using nonlinear concrete and steel material models. Shear and torsional flexibilities are modeled to be linear-elastic, and are combined together into a single component model using the SectionAggregator approach in OpenSees. An expected yield strength of 462 MPa (67 ksi) was used for the grade 60 steel (Melchers, 1999). This value is slightly lower than, but still comparable to, an expected yield strength of 517 MPa (75 ksi), which is suggested in ASCE/SEI 41-06 (ASCE, 2007). An expected initial stiffness of 20,000 GPa (29,000 ksi) was used, along with a post-yield hardening stiffness of 2% of the initial stiffness. A nominal concrete strength of 35 MPa (5.0 ksi) was included in the model, without provision for expected strength. Use of nominal concrete strength in lieu of expected strength was judged to have minimal impact on the structural response predictions because of the mild nonlinearity experienced in the Northridge earthquake.

The calculated building mass included the mass of all structural elements (beams, columns, and slabs); 0.5 kPa (10 psf) for partitions; 0.6 kPa (12 psf) for mechanical, electrical, and plumbing components; and 25% of the design live load taken as 0.6 kPa (12 psf) for a design live load of 2.5 kPa (50 psf). These masses are accounted for both above and below grade.

Damping was modeled as 4.5% Rayleigh damping, anchored to the first and second mode periods of the building (2.9 sec and 1.0 sec, respectively). This level of damping is a calibrated value, which is discussed below. In developing the Rayleigh damping matrix, degrees-of-freedom associated with foundation springs were excluded. This was necessary to avoid double counting of foundation damping because the soil-foundation model included dashpots at these degrees-of-freedom.

Basement shear walls are 30 cm (1 ft) thick, modeled in the simplified manner described above (and shown in Figure A-2). Figure A-2 shows how the moment resisting frame, simplified shear wall, and slab elements connect to the framing nodes in the two basement levels of the building. At each connection location, the nodes are placed at the same coordinates in the model (but are shown offset in Figure A-2 to illustrate the connectivity). Vertical and rotational degrees of freedom are constrained together for all nodes at each connection location. Figure A-2 also depicts the rigid beams needed to support the simplified shear wall models and the soil springs at the base of the building (soil dashpots are not shown). Stiffness in the

plane of the shear walls was computed based on shear behavior using G=0.4E_c, as recommended in PEER/ATC-72-1, *Modeling and Acceptance Criteria for Seismic Design and Analysis of Tall Buildings* (ATC, 2010), E_c=23,200 MPa (3,370 ksi), and a factor to account for the cracked properties of the wall (another calibrated value discussed below). The out-of-plane stiffness of the walls was not included in the model.

The stiffness and damping properties of the soil are modeled using vertical and horizontal springs and dashpots, as described in Chapter 7. Soil springs are linear-elastic (with model variant MB.2 considering the no-tension gap springs). Dashpots are linear in all model variations.

The depth-variable nature of input ground motions over the height of the basement walls were specified using the MultipleSupportExcitation approach in OpenSees. In this approach, the acceleration, velocity, and displacement acceleration-histories are all specified at each subterranean level. Specifying each ground motion history removes the need to integrate motions within OpenSees.

A.2 Baseline Model Calibration

The Sherman Oaks Baseline Model (MB) was calibrated against recordings from the 1994 Northridge earthquake. The calibrated model was then used to predict the response of the building for the 1992 Landers and 1987 Whittier earthquakes to assess the stability of the calibration.

The first stage of calibration targeted the shear stiffness of the reinforced concrete walls and slabs in the subterranean levels. A multiplier on the theoretical shear modulus of the uncracked concrete, G_c, was used as the calibration parameter to match near-ground response. A definitive ratio of cracked to uncracked stiffness in shear walls is not available in the literature. For example, ASCE/SEI 41-06 suggests that the full (unreduced) value of G_c be used for both cracked and uncracked walls. PEER/ATC-72-1 states that the cracked shear stiffness should be "substantially lower" than the uncracked shear stiffness, but there are limited test data available for use in quantifying this ratio. It was found that, over the range of 0.25 to 0.40 considered, near-ground response was not highly sensitive to this parameter, and acceptable results were achieved with a stiffness multiplier of 0.25.

The second stage of calibration targeted the building period. Adjustments to the structural mass and stiffness were used as the calibration parameters for the modeled building period. The structure mass was modified through the application of a scale factor. In fiber element models, stiffness is not an input parameter, but is computed from component dimensions and material properties. Component stiffness was adjusted through modification of the stiffness of reinforcing steel within the fiber element model. This approach is not meant to suggest that the rebar stiffness is

highly variable; rather it is an indirect approach to modifying the stiffness of reinforced concrete elements, which is known to be highly variable (Haselton et al., 2011)

The initial modeled building period was found to be too low. To increase the period, final calibration factors included multipliers of 0.7 on rebar stiffness and 1.0 on mass. Table A-1 compares the first mode periods of the building in each direction with the periods predicted by the Baseline Model (MB). Measured building periods were computed using non-parametric system identification through the calculation of transfer functions between the base-level and roof acceleration histories. Although not an exact match in all cases, Table A-1 shows that modeled periods agree reasonably well with the measured periods in the three events studied.

Table A-1 Comparison of Measured and Modeled Periods for the Sherman Oaks Building

Earthquake	Identified Period Mode 1 (sec)		Identified Period Mode 2 (sec)		MB Period Mode 1 (sec)		MB Period Mode 2 (sec)	
	Long	Trans	Long	Trans	Long	Trans	Long	Trans
1994 Northridge	2.92	3.28	0.84	0.94	2.67	2.72	0.84	0.94
1992 Landers	2.56	2.72	0.73	0.80	2.14	2.68	0.74	0.80
1987 Whittier	2.33	2.29	0.82	0.83	2.33	2.29	0.82	0.83

The third stage of calibration targeted Rayleigh damping. Adjustments to the level of damping were used to match the amplitude of displacements in the superstructure. The OpenSees model used full Rayleigh damping with two matching frequencies, taken as the first- and second-mode vibration frequencies. A target level of 4.5% of critical damping was found to provide reasonable results.

Soil spring capacities were compared to demands computed for the 1994 Northridge using the calibrated Model MB to investigate the potential for failure of the foundation during earthquake shaking. Limiting spring capacities for the Sherman Oaks building (presented in Chapter 7) exceeded spring force demands by a factor of three or more. This margin of safety indicates that foundation failure is unlikely, and limiting spring capacities were not needed in the present simulations.

Displacement histories obtained from the calibrated Model MB are compared to recordings from the 1994 Northridge earthquake in Figure A-3. The match in both horizontal directions at the foundation and ground floor levels is excellent. Over the height of the building, the quality of the match is generally better in the longitudinal (EW) direction than in the transverse (NS) direction. Base rocking results in the bottom frames show that rocking does not significantly contribute to expected roof displacements. Because there was only one recording instrument at the ground level, there are no base rocking data available for comparison to modeled results.

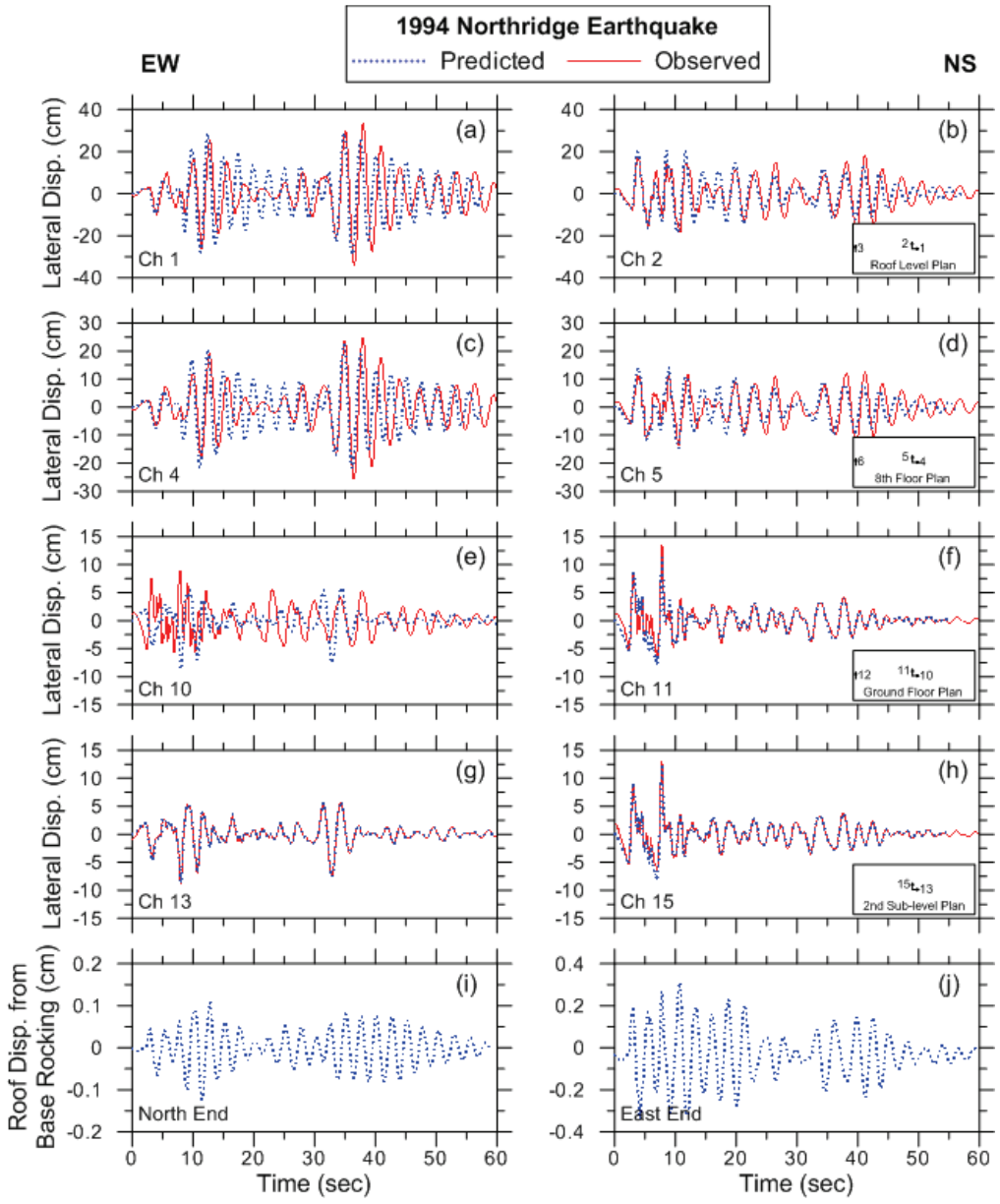

Figure A-3 Comparison of modeled versus recorded displacement histories for Model MB in the 1994 Northridge earthquake: roof level (a) and (b); 8th floor (c) and (d); ground level (e) and (f); foundation level (g) and (h); and roof displacement due to base rocking (i) and (j).

Profiles of peak floor displacements and peak floor accelerations obtained from the calibrated Model MB are compared to recordings from the 1994 Northridge earthquake in Figure A-4. The fit for displacements is better than for accelerations. Peak accelerations are surprisingly high at ground level and are slightly larger than expected over the height of the structure. In general, the quality of the fit is acceptable, and meets the intent of the calibration criteria.

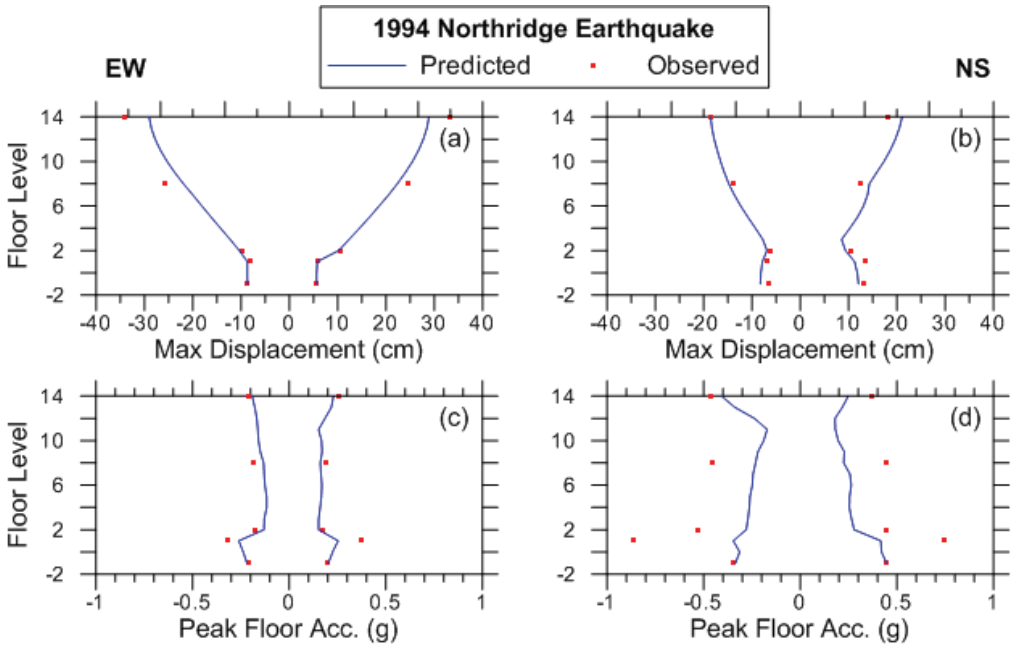

Figure A-4 Comparison of modeled versus recorded peak displacements and accelerations for Model MB in the 1994 Northridge earthquake.

The calibrated Model MB was then used to predict the response of the building for the 1992 Landers and 1987 Whittier earthquakes to assess the stability of the calibration. Results for displacement histories and peak displacements are shown in Figure A-5 through Figure A-8. The quality of the match for Whittier is better than for Northridge, likely due to a lack of nonlinearity in the response. In the case of Landers, the predicted response is consistently weaker than the recorded response.

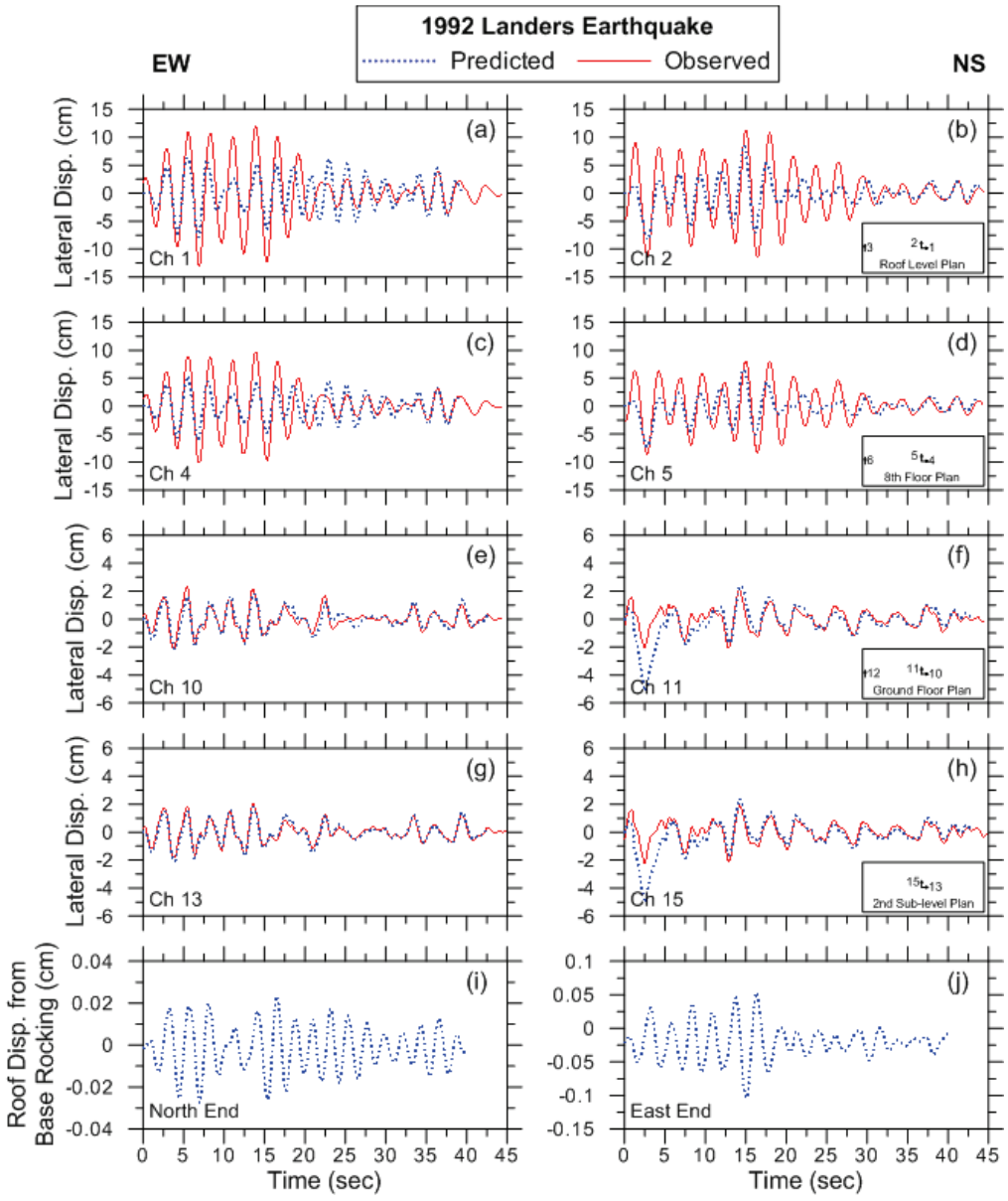

Figure A-5 Comparison of modeled versus recorded displacement histories for Model MB in the 1992 Landers earthquake: roof level (a) and (b); 8th floor (c) and (d); ground level (e) and (f); foundation level (g) and (h); and roof displacement due to base rocking (i) and (j).

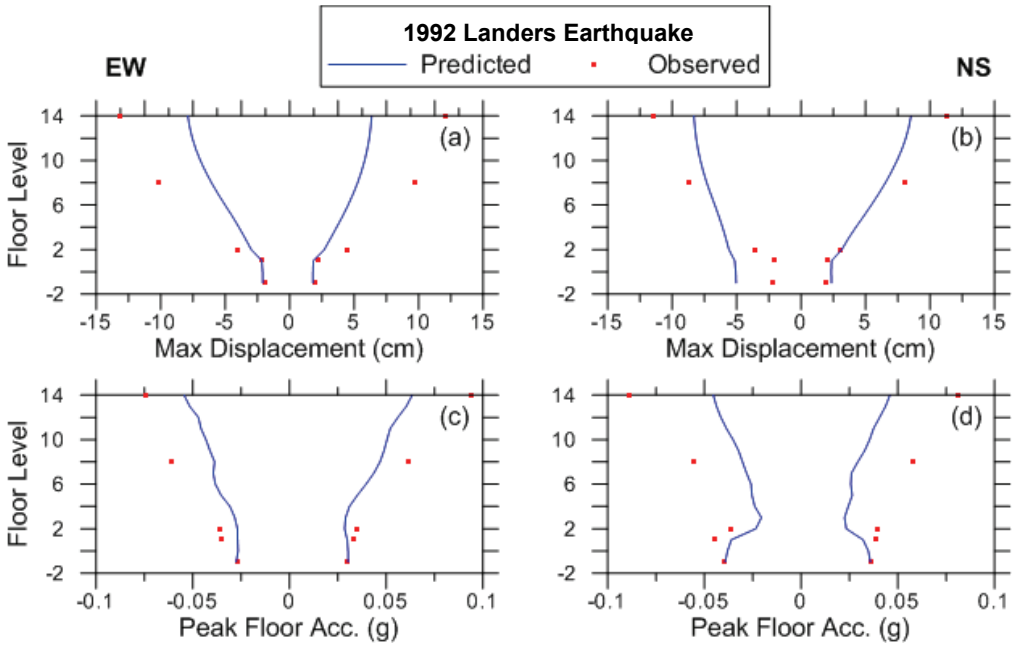

Figure A-6 Comparison of modeled versus recorded peak displacements and accelerations for Model MB in the 1992 Landers earthquake.

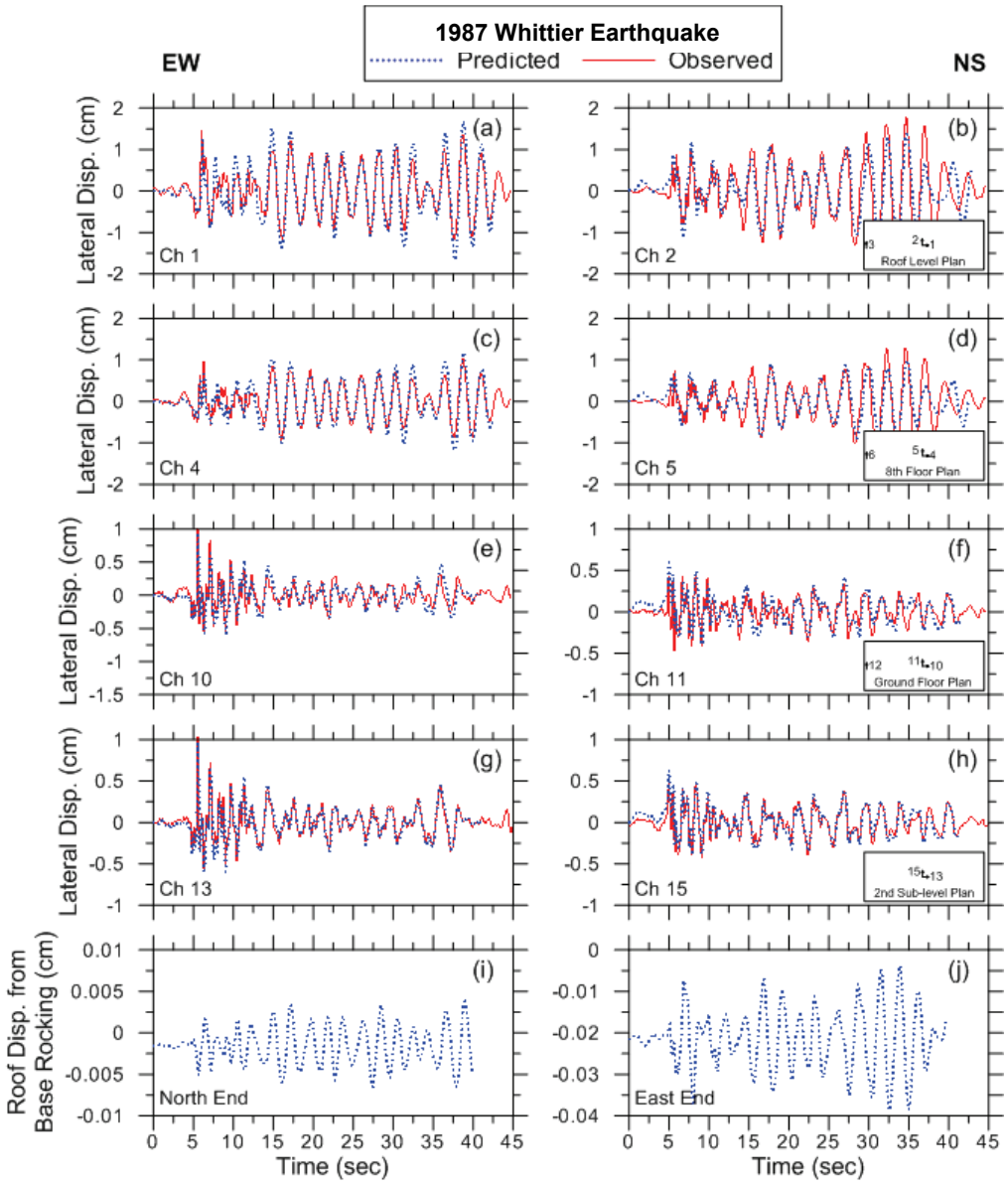

Figure A-7 Comparison of modeled versus recorded displacement histories for Model MB in the 1987 Whittier earthquake: roof level (a) and (b); 8th floor (c) and (d); ground level (e) and (f); foundation level (g) and (h); and roof displacement due to base rocking (i) and (j).

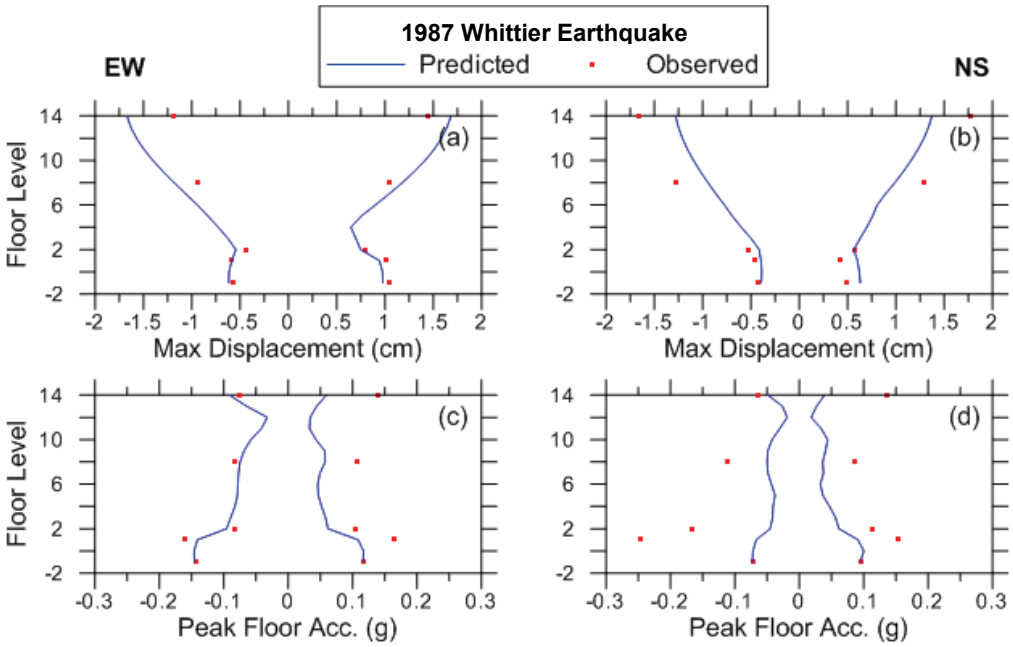

Figure A-8 Comparison of modeled versus recorded peak displacements and accelerations for Model MB in the 1987 Whittier earthquake.

Appendix B
Sherman Oaks Building Stick Model Development

This appendix provides detailed information on the structural modeling and calibration for the Sherman Oaks building stick model variations used in parametric studies presented in Chapter 7. This appendix also includes detailed results comparing key response quantities from each model variant.

B.1 Stick Model Development

Stick models were used to condense, or simplify, the seismic-force-resisting system in the superstructure for parametric studies on structural system properties. The key parameter varied between the models was structural stiffness. The moment frame system of the Sherman Oaks building was first idealized as a stick model and calibrated to the results of the full-building Baseline Model (MB). Once comparable results were achieved for the moment frame stick model, the stiffness was scaled to different factors representing the stiffness of a series of core shear wall and perimeter shear wall variations.

B.1.1 Moment Frame Stick Model Development

The Sherman Oaks building moment frame is a 13-story structure above grade, with a total of seven bays in the east-west (E-W) direction (X-direction) and a total of two bays in the north-south (N-S) direction (Y-direction). The overall configuration of the full-building Baseline Model (MB) is shown in Figures B-1 through B-3. These figures also show the location of the master nodes used in the stick model. The stick model configuration is shown in Figure B-4.

In the stick model, the mass of each floor, the effective lateral, axial, and rotational stiffness, and the effective yield strength, are all lumped at the master node for each level. Geometric and material definitions from the full-building OpenSees model code were extracted and the rotational and axial stiffness at each floor level were calculated. A static pushover analysis of the full-building Model MB was used to determine the lateral stiffness and yield strength at each level.

First, a series of static pushover analyses were performed involving the application of a single point load at the master node of the floor under consideration, while constraining all other master nodes of the structure. The pushover analysis was displacement-controlled, and the recorded force-displacement data at the master node

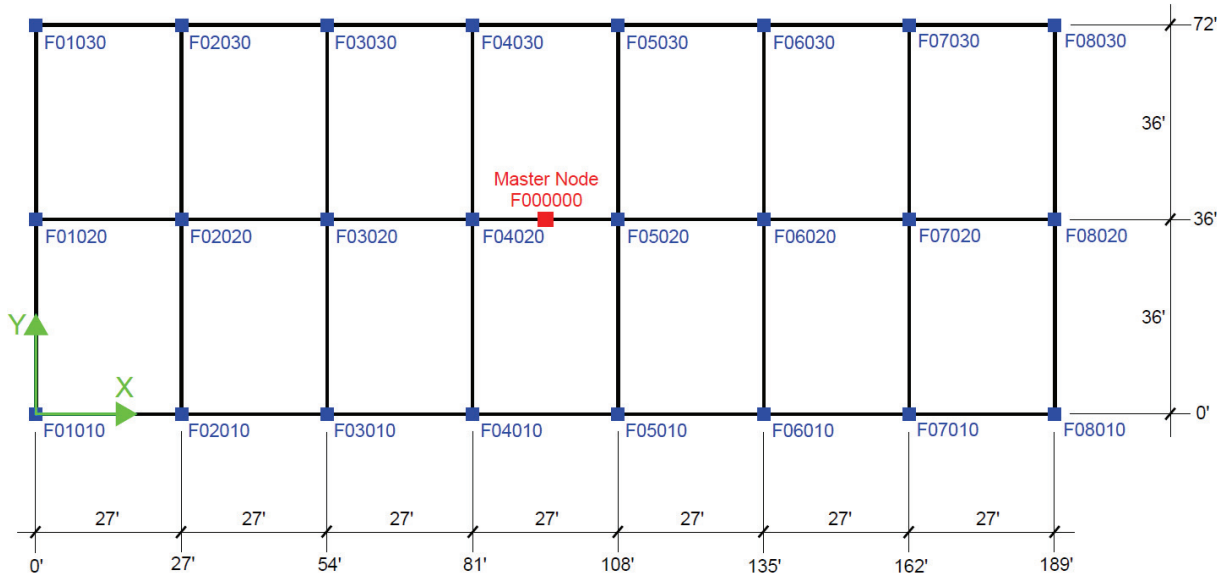

Figure B-1 Plan view of the full-building model of the Sherman Oaks building.

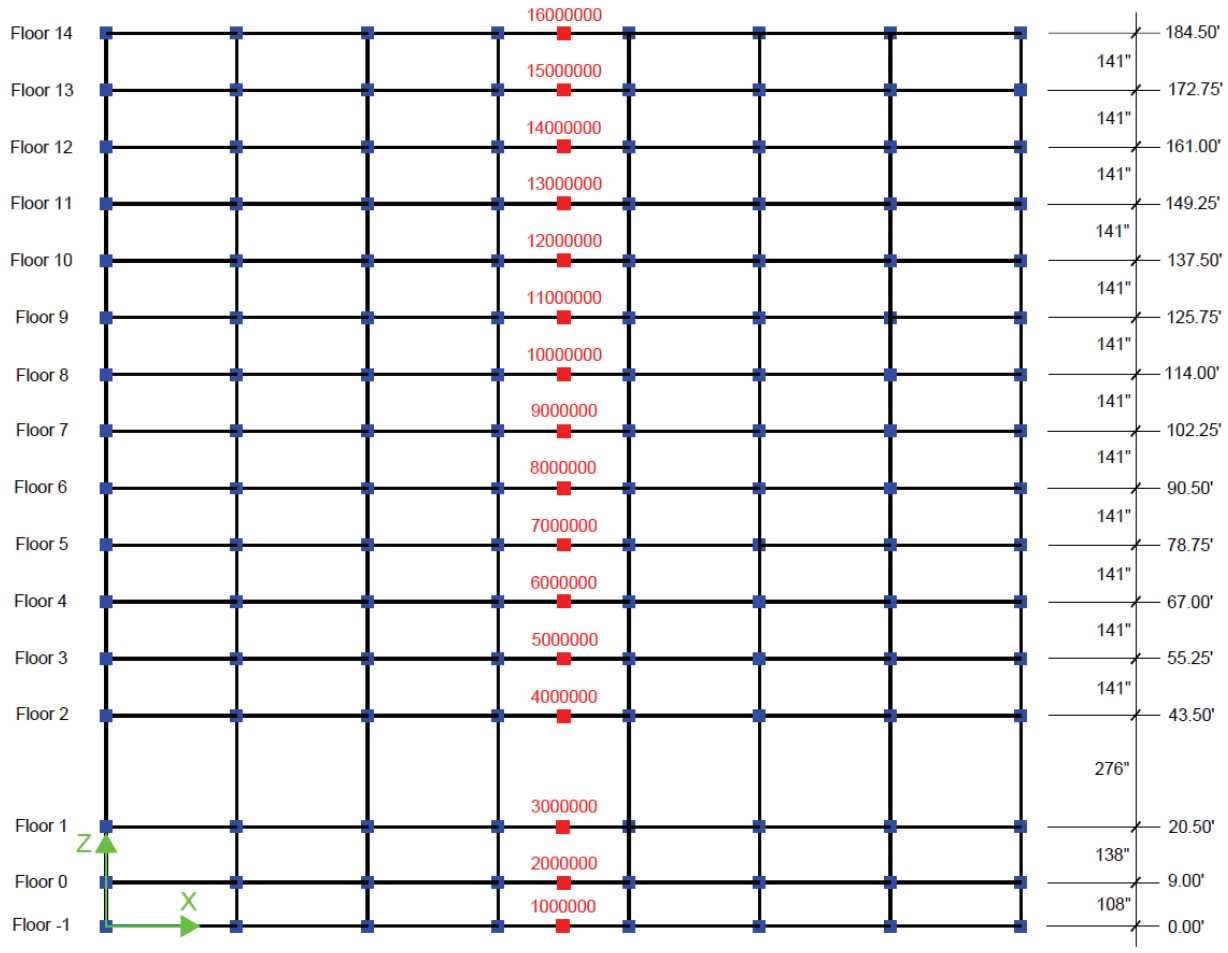

Figure B-2 Longitudinal elevation (X-direction) of the full-building model of the Sherman Oaks building.

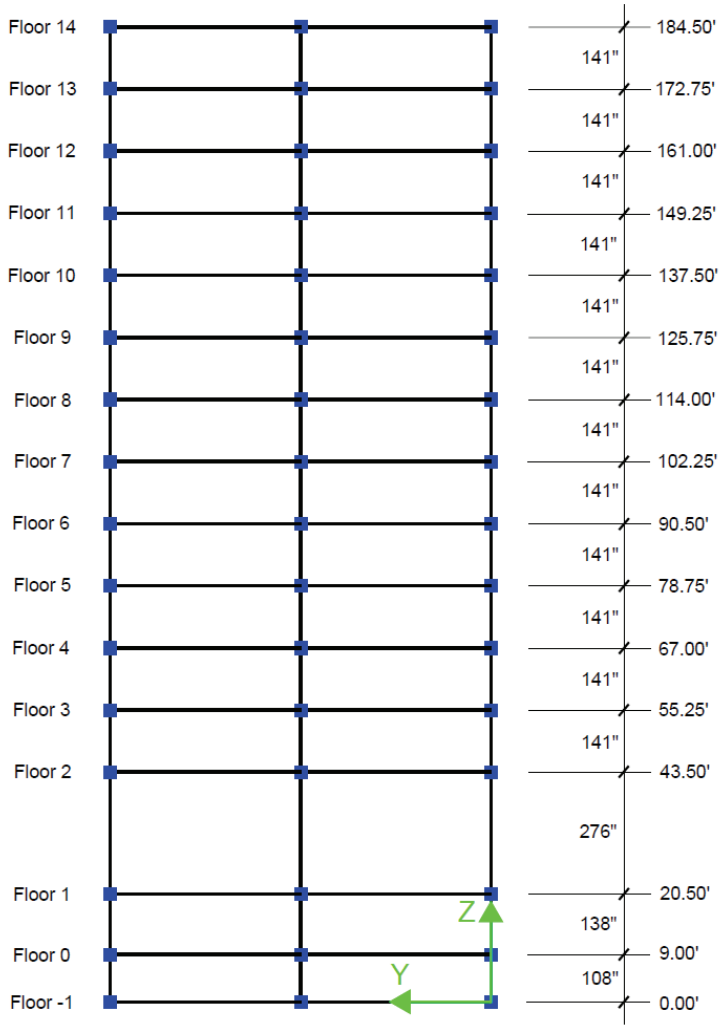

Figure B-3 Transverse elevation (Y-direction) of the full-building model of the Sherman Oaks building.

under consideration was used to determine the effective lateral stiffness at each floor level. Adjustments to the effective lateral stiffness were made as needed to account for the stiffness contribution of adjacent floors. Once all contributions to stiffness had been accounted for, force-displacement curves were created. These force-displacement curves were then used to create idealized force-displacement curves per ASCE/SEI 41-06 (ASCE, 2007). An example force-displacement curve is shown in Figure B-5.

This methodology, however, resulted in overall stiffness and yield strength values for the stick model that exceeded the full-building Model MB values. Another pushover analyses was performed involving the application of a single point load at the master node of the roof, pushed to a defined displacement of 20 cm (8 in). This

Figure B-4 Elevation the idealized stick model of the Sherman Oaks building.

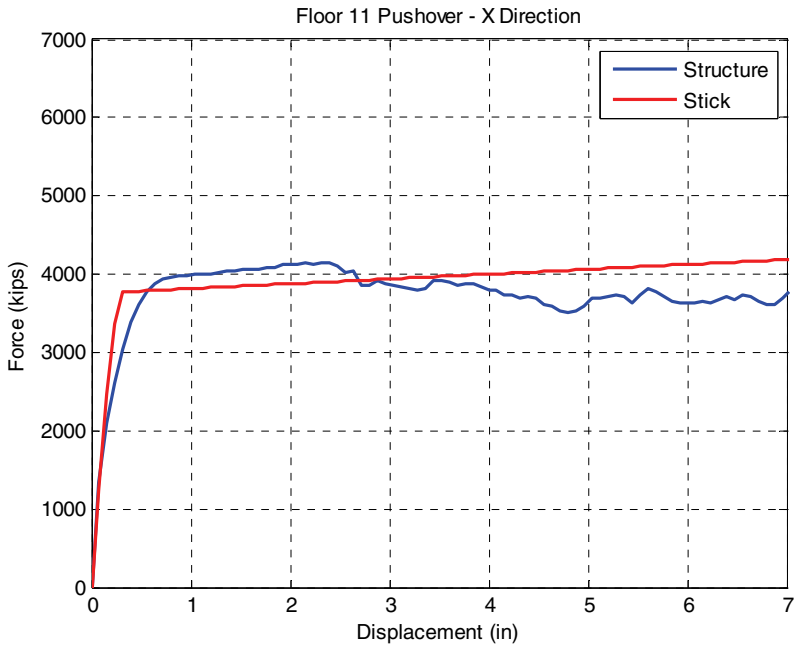

Figure B-5 Idealized force-displacement curve for the Sherman Oaks building.

displacement level provided adequate story drift over the height of the structure, without yielding of the structural elements. The force-displacement data recorded at the master nodes of all levels was then used to calculate the story drifts at each floor level for a given force. This method produced elastic stiffness values consistent with the full-building Model MB. Because nonlinear behavior was not observed in the full-building model for pushover displacements in the range of 20 cm to 50 cm (8 in to 20 in), the stick model was idealized as an elastic element.

A basement structure node connectivity scheme was developed to properly associate the idealized stick element with the ground level diaphragm. Node definitions and connectivity at Floor 1 and below are shown in Figure B-6. All of the nodes in a given floor level exist at the same location. The nodes labeled 301010, 201010, and 101010 are nodes that define the diaphragms of the substructure. The actual basement walls occur outside of the lateral frame lines. Fixed support nodes provide connectivity of the soil-to-wall spring that define interaction between the soil and the basement wall. Multi-support constraint nodes provide nodal definitions that simulate the stiffness of the basement walls, both in-plane and out-of-plane, and account for the offset of the basement wall to the frame line. Rigid body constraints simulate the vertical stiffness of the basement wall.

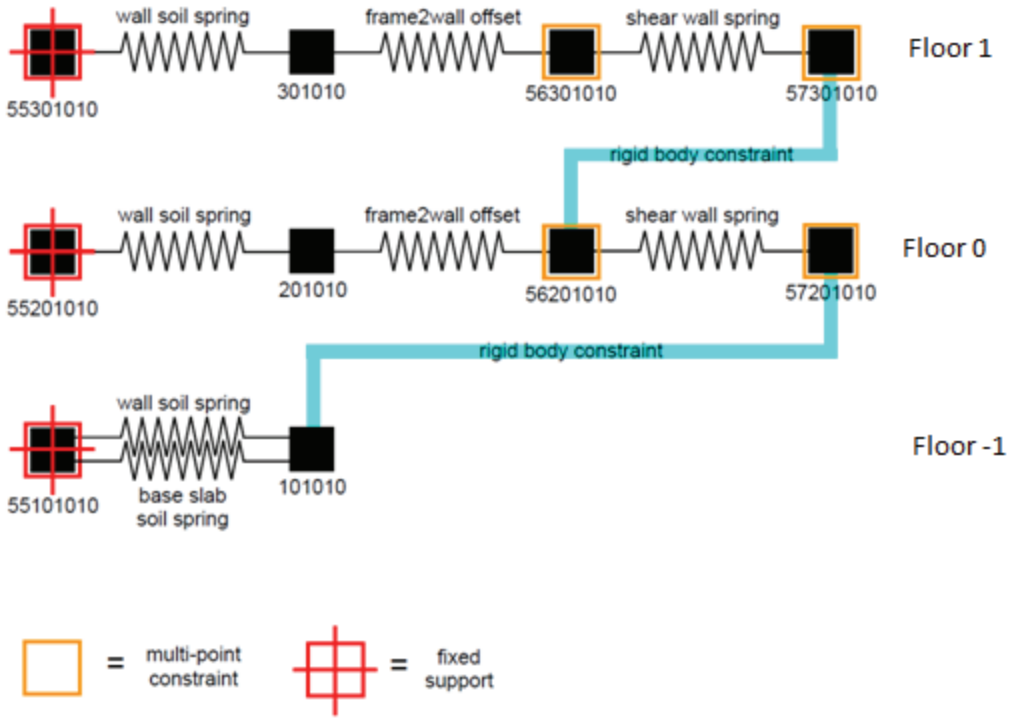

Figure B-6 Shear wall and basement level node definitions, constraints, and connectivity for the Sherman Oaks stick model.

Using these nodal definitions, the base connectivity of the stick element at Floor 1 was defined using rigid elements linking the base of the stick to each of the unconstrained nodes defining the diaphragm at Floor 1. This produced rigid body constraints at the ground level that distributed the stick element demands to the walls of the subterranean structure.

B.1.2 Moment Frame Stick Model Calibration

A limited calibration process was undertaken, with a focus on achieving closer convergence between floor displacements and peak floor accelerations in the stick model and full-building model. It was recognized, however, that the process of idealizing a complex superstructure into a simplified stick representation is an approximation.

The first stage of calibration targeted the hysteretic behavior observed at each floor during the response histories. Hysteresis curves were used to compare the predefined lateral stiffness of the stick model to the full-building Model MB. Softening of the lateral stiffness of the stick model was needed in both lateral directions at all floor levels. Plots of absolute displacement and peak acceleration response showed greater convergence after this calibration.

The second stage of calibration targeted the mild bilinear behavior observed in story levels above the first story. This stage consisted of defining the yield force at each level where bilinear behavior occurred in an attempt to match maximum floor displacements and peak floor accelerations. Each iteration caused divergence of results with no clear trend toward better calibration, so further adjustment of this parameter was abandoned.

Final Stick Model Properties. The final stick model was created using twoNodeLink element objects. This allowed the stick elements spanning from floor to floor to be modeled as axial, shear, and rotational springs. Final element properties for the moment frame stick model are given in Tables B-1 through B-3.

The axial and rotational spring stiffness values in Table B-1 are based on length (story height), area (total column area per story level), and elastic modulus information taken directly from the full-building Model MB. Rotational stiffness about global X- and Y-directions were determined by solving a system of linear equations for a unit rotation. The lateral force-deformation properties in Table B-2 are based on lateral pushover analyses described above. Masses (weights) used in the stick model are provided in Table B-3.

Each element property was defined using uniaxial stress-strain (force-deformation) relationships. Axial and rotational element properties were constructed with an elastic material object. Properties in both lateral directions were constructed with uniaxial bilinear material objects with kinematic hardening.

Table B-1 Axial and Rotational Properties of the Moment Frame Stick Model

Property	Story 1	Story 2 to Story 13
Length	276 in	141 in
Area	25056 in^2	24480 in^2
Elastic Modulus	4287 ksi	3713 ksi
Rotational Stiffness about Global x-axis (E-W)	4508×10^7 kip-in / rad	7359×10^7 kip-in / rad
Rotational Stiffness about Global y-axis (N-S)	2243×10^8 kip-in / rad	3608×10^8 kip-in / rad
Torsional Stiffness about Global z-axis	Fixed	Fixed

Table B-2 Lateral Force-Deformation Properties of the Moment Frame Stick Model

Story	Yield Strength (kips)		Initial Stiffness (kips/in)		Strain-Hardening Ratio	
	E-W	*N-S*	*E-W*	*N-S*	*E-W*	*N-S*
1	5500	6500	2566.8	2521.9	0.0371	0.0142
2	12000	13050	5342.1	4415.0	-0.0541	-0.0176
3	10171	11605	4893.8	3755.8	-0.0348	-0.0478
4	9600	10200	4724.2	3521.5	-0.0318	0.0000
5	8000	8214	4584.9	3429.5	-0.0643	-0.0234
6	6700	7300	4452.4	3389.5	-0.0460	-0.0255
7	5286	6000	4375.8	3351.1	-0.0345	-0.0312
8	5000	5733	4261.2	3293.0	-0.0210	-0.0370
9	4343	5086	4169.9	3242.0	0.0183	-0.0225
10	3771	4571	4141.1	3205.5	0.0040	-0.0090
11	3000	3743	4142.6	3215.3	0.0245	0.0339
12	3000	3600	4235.6	3346.7	0.0263	0.0115
13	5500	5000	4920.4	3864.7	0.0820	0.2642

Table B-4 compares the first-, second-, and third-mode periods of the moment frame (MF) stick model and the full-building Model MB. Development and calibration of the stick model was performed using a relatively early version of the Sherman Oaks OpenSees Model MB, which changed over time as model components and ground motion inputs were refined. For this reason, Model MB results presented in this appendix are not an exact match to those presented in Section 7.2.

Table B-3 Masses in the Moment Frame Stick Model

Level	Node	Weight (kips)
Floor -1	Distributed	3824
Floor 0	Distributed	3824
Floor 1	Distributed	3010
Floor 2	4000000	2522
Floor 3	5000000	2522
Floor 4	6000000	2522
Floor 5	7000000	2522
Floor 6	8000000	2522
Floor 7	9000000	2522
Floor 8	10000000	2522
Floor 9	11000000	2522
Floor 10	12000000	2522
Floor 11	13000000	2522
Floor 12	14000000	2522
Floor 13	15000000	2522
Roof	16000000	3314

Table B-4 Comparison of Modeled Periods for the Moment Frame Stick Model and the Full-Building Model MB

	Identified Period Mode 1 (sec)	Identified Period Mode 2 (sec)	Identified Period Mode 3 (sec)
Model	Translational (Global Y-axis)	Torsional (about Global Z-axis)	Translational (Global X-axis)
MB-MF-Full	2.45	2.31	2.21
MB-MF-Stick	2.87	N.A.	2.62

Figure B-7 compares the roof displacement response history for the moment frame stick model to the center of the full-building Model MB in the X-direction and the Y-direction. Responses in the Y-direction are more in phase than in the X-direction. Displacement amplitudes match fairly well. In some cases, larger amplitudes are observed in the stick model, but in other cases, larger amplitudes are observed in the full-building model. Similar results were obtained for nodes located at the mid-height of the building.

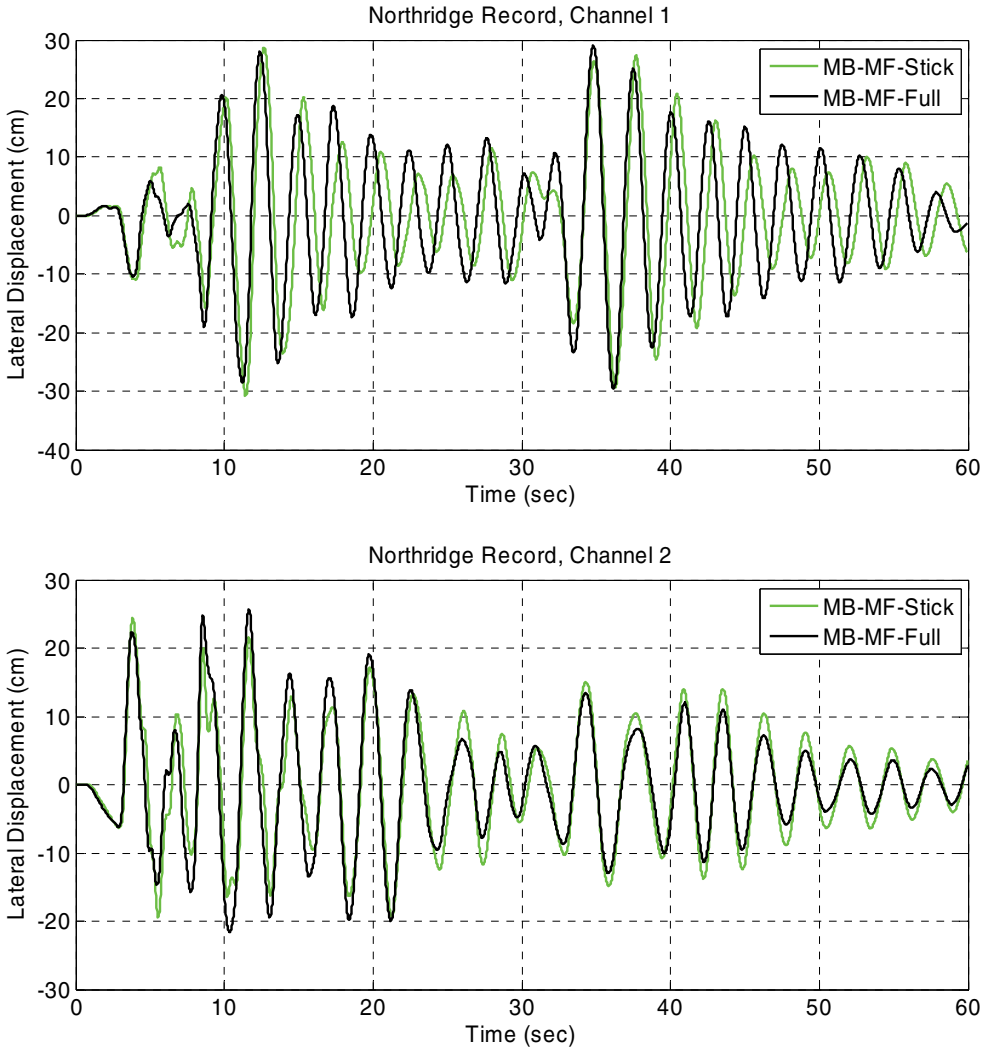

Figure B-7 Comparison of roof displacement histories for the moment frame stick model and the full-building Model MB.

Figures B-8 through B-11 compare response envelopes for maximum displacement, story drift, story shear, and peak floor acceleration for each direction. Results for the moment frame stick model are typically within about 10% of those for the full-building Model MB. Maxima in the positive and negative directions are reported. In some cases, results for the moment frame stick model are larger in one direction, but smaller in the perpendicular direction. It was found that calibration attempts often improved results in one direction at the expense of the other direction.

Based on the following comparisons, the calibration process for the moment frame stick model was judged to be sufficient for the purposes of the parametric study.

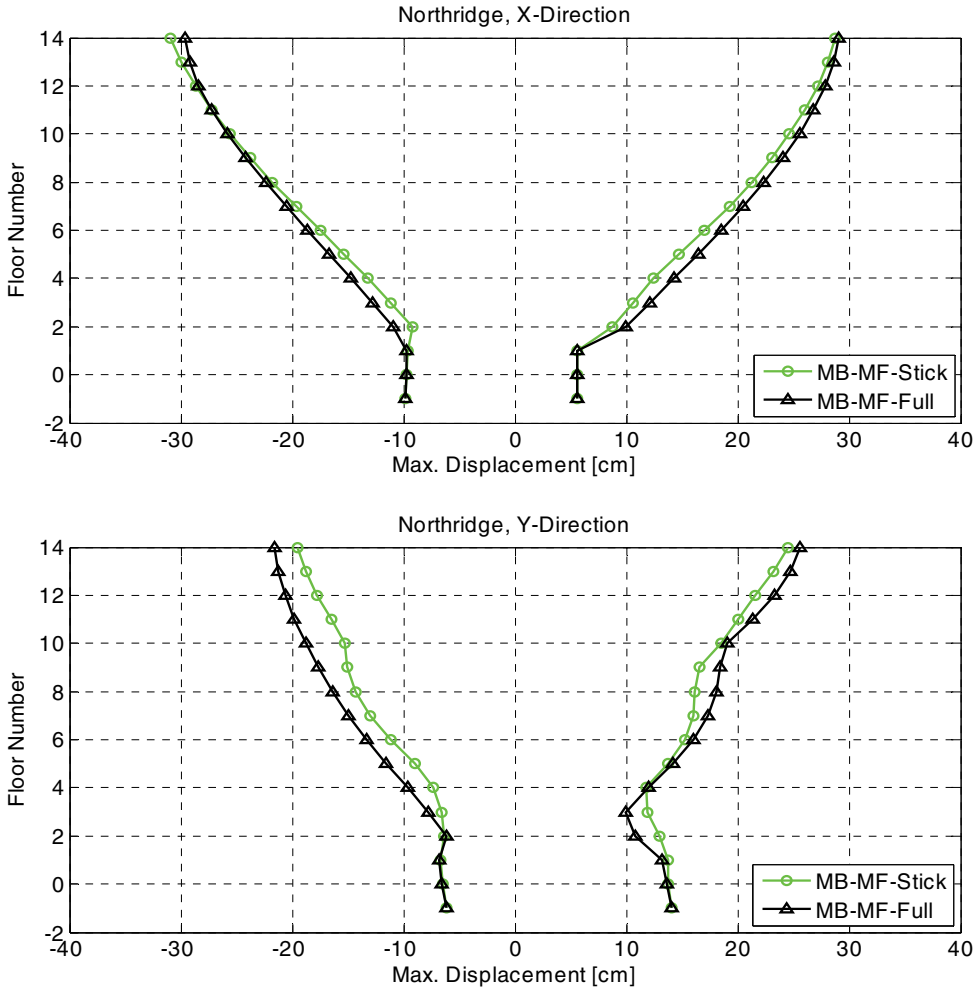

Figure B-8 Comparison of maximum displacement envelopes for the moment frame stick Model MB and the full-building Model MB.

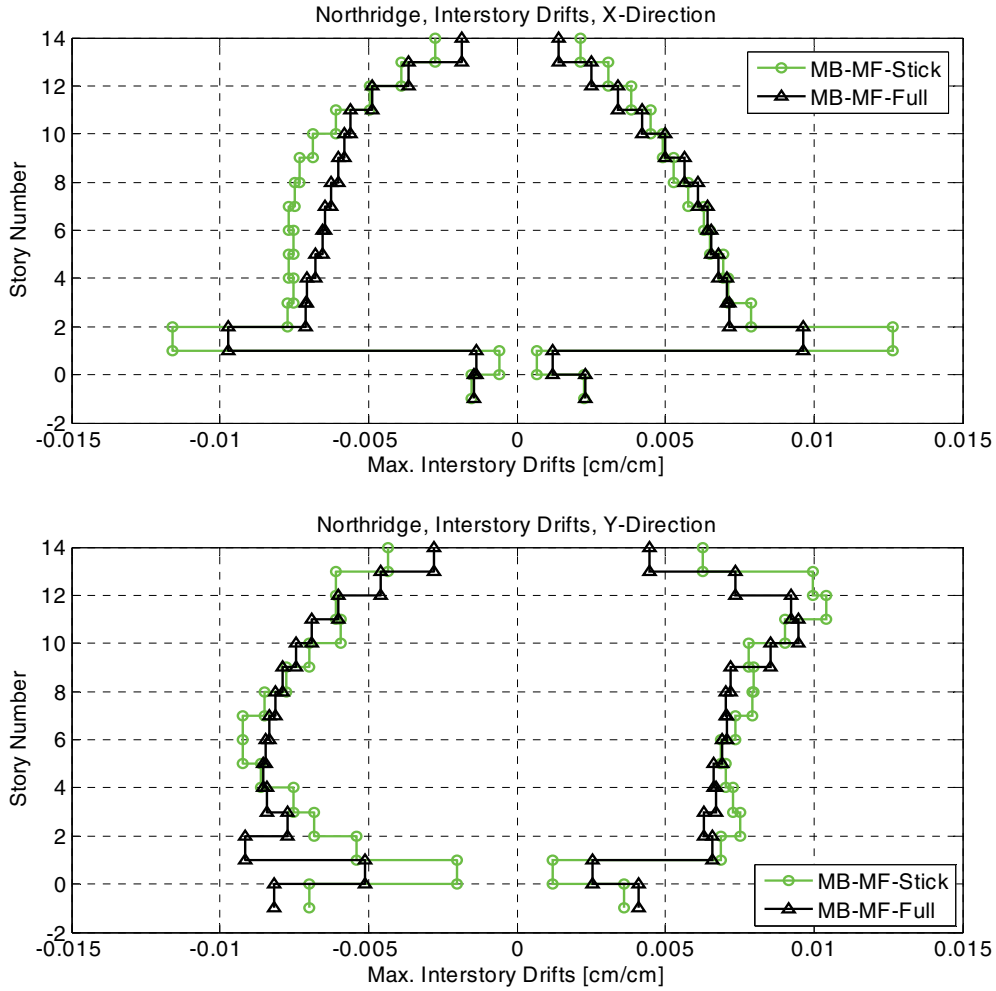

Figure B-9 Comparison of maximum story drift envelopes for the moment frame stick Model MB and the full-building Model MB.

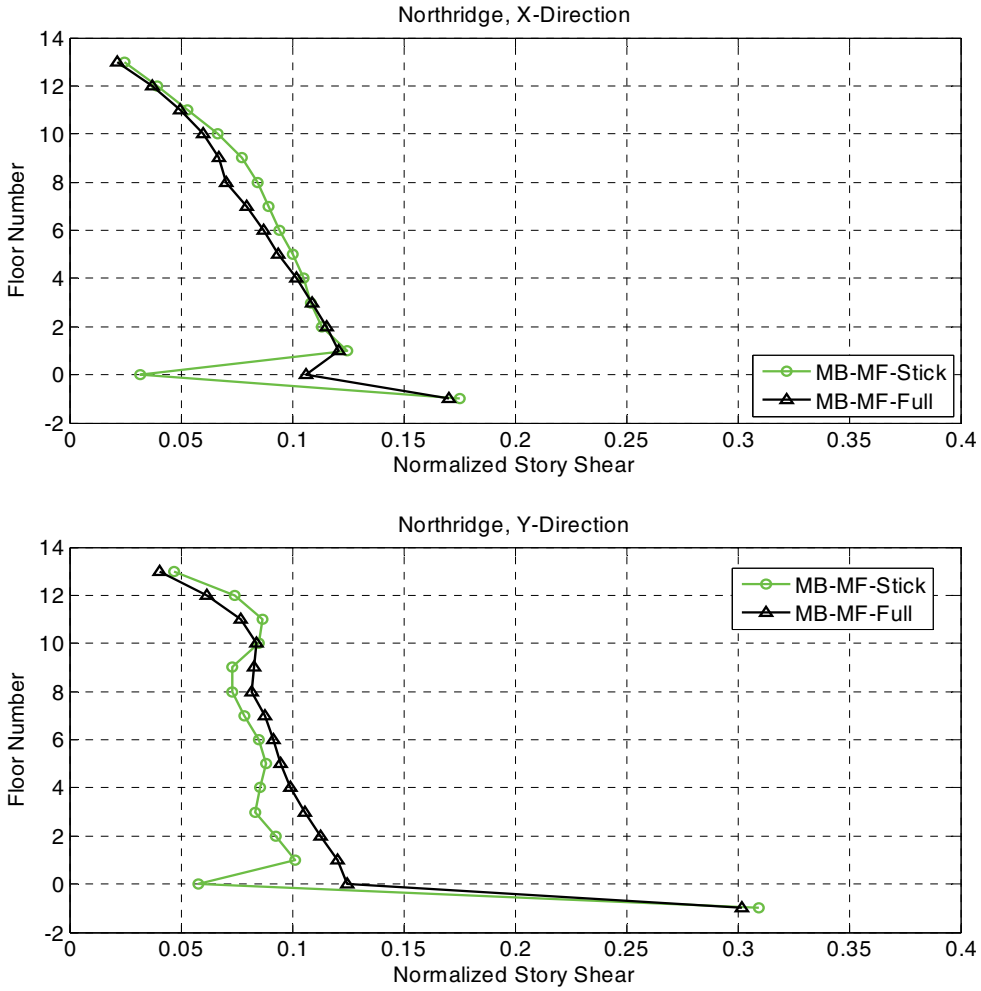

Figure B-10 Comparison of maximum story shear envelopes for the moment frame stick Model MB and the full-building Model MB.

As mentioned earlier, development and calibration of the stick model was performed using a relatively early version of the Sherman Oaks OpenSees Model MB, which changed over time. In Figure B-10, a spike in story shear force can be observed in the basement level for the stick model. This is because early versions of the full-building Model MB included an artificial phase shift in the ground motions used for multi-support excitation, which caused a similar spike in shear demand. This phase shift was removed in subsequent versions of the full-building Model MB, and the spike no longer appears in the results for the final full-building model depicted in the figure.

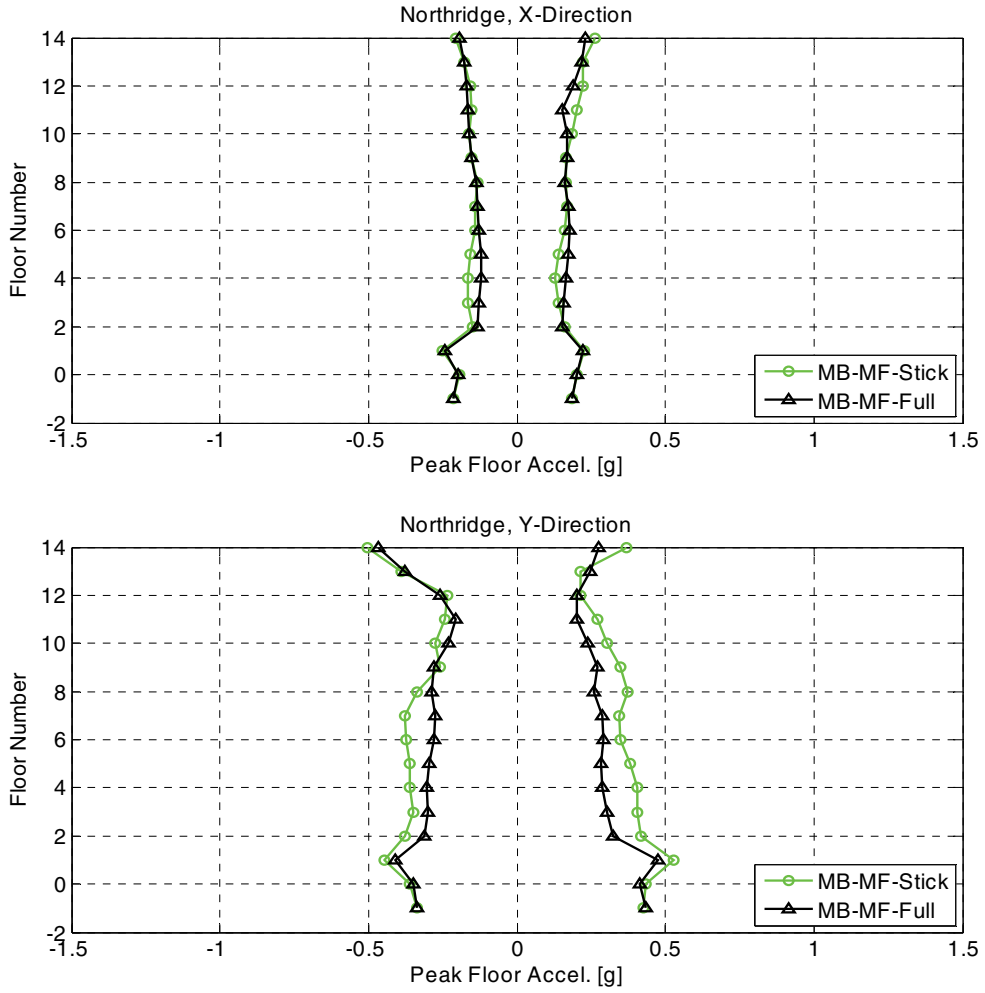

Figure B-11 Comparison of peak floor acceleration envelopes for the moment frame stick Model MB and the full-building Model MB.

B.2 Additional Moment Frame Stick Model Comparisons to Full-Building Model Results

Calibrations were applied to Baseline Model (MB) results only. The calibrated moment frame stick model was imported into models capturing the foundation modeling configurations associated with Model 1, Model 2, and Model 4a. Table B-5 compares the first-, second-, and third-mode periods of the moment frame stick model and the full-building model for each foundation configuration.

Table B-5 Comparison of Modeled Periods for the Moment Frame Stick Model and the Full-Building Model for each Alternative Foundation Configuration

	Identified Period Mode 1 (sec)	Identified Period Mode 2 (sec)	Identified Period Mode 3 (sec)
Model	Translational (Global Y-axis)	Torsional (about Global Z-axis)	Translational (Global X-axis)
1-MF-Full	2.26	2.19	2.09
1-MF-Stick	2.83	N.A.	2.61
2-MF-Full	2.46	2.31	2.22
2-MF-Stick	2.86	N.A.	2.62
4a-MF-Full	2.47	2.32	2.21
4a-MF-Stick	2.87	N.A.	2.63

Periods in each simplified stick model are longer than the periods observed in the corresponding full-building model. This was attributed to the stick elements being modeled as linear elements and calibrated with an elastic stiffness that was softer than the full-building model.

Figures B-12 through B-23 compare response envelopes for maximum displacement, story drift, story shear, and peak floor acceleration for each alternative foundation model in each direction. In general, comparisons are similar to trends observed for Model MB.

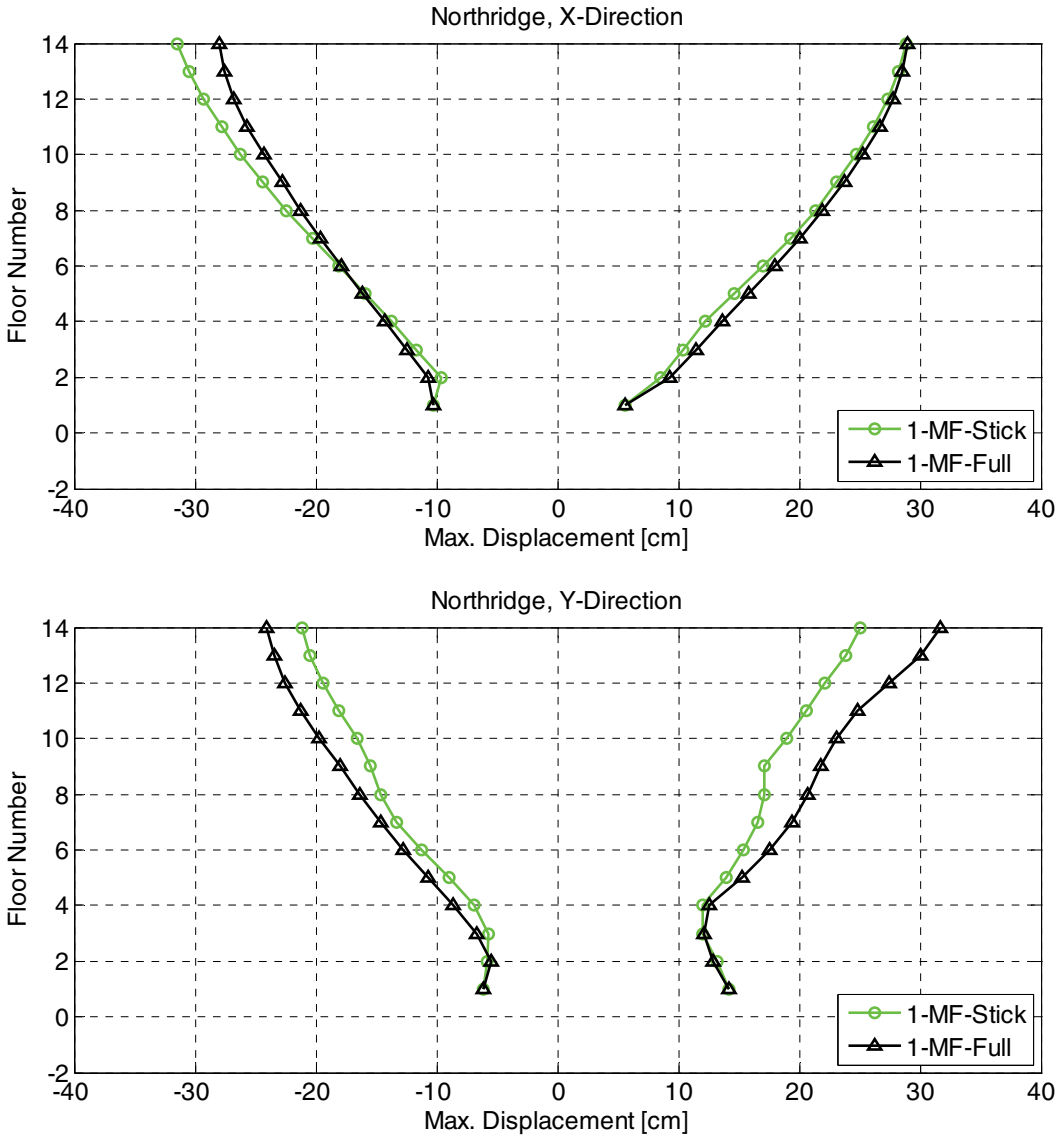

Figure B-12 Comparison of maximum displacement envelopes for the moment frame stick Model 1 and the full-building Model 1.

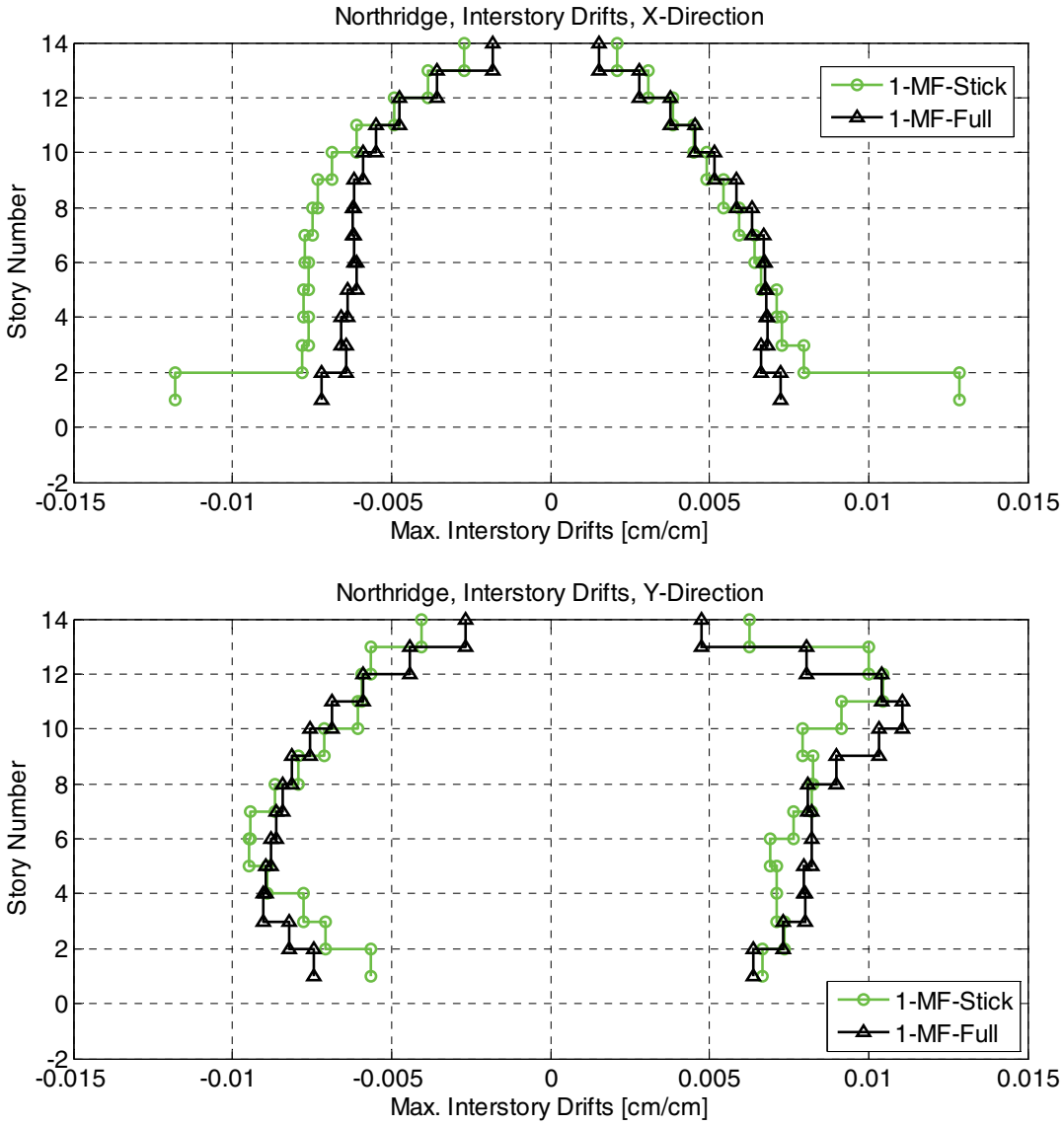

Figure B-13 Comparison of maximum story drift envelopes for the moment frame stick Model 1 and the full-building Model 1.

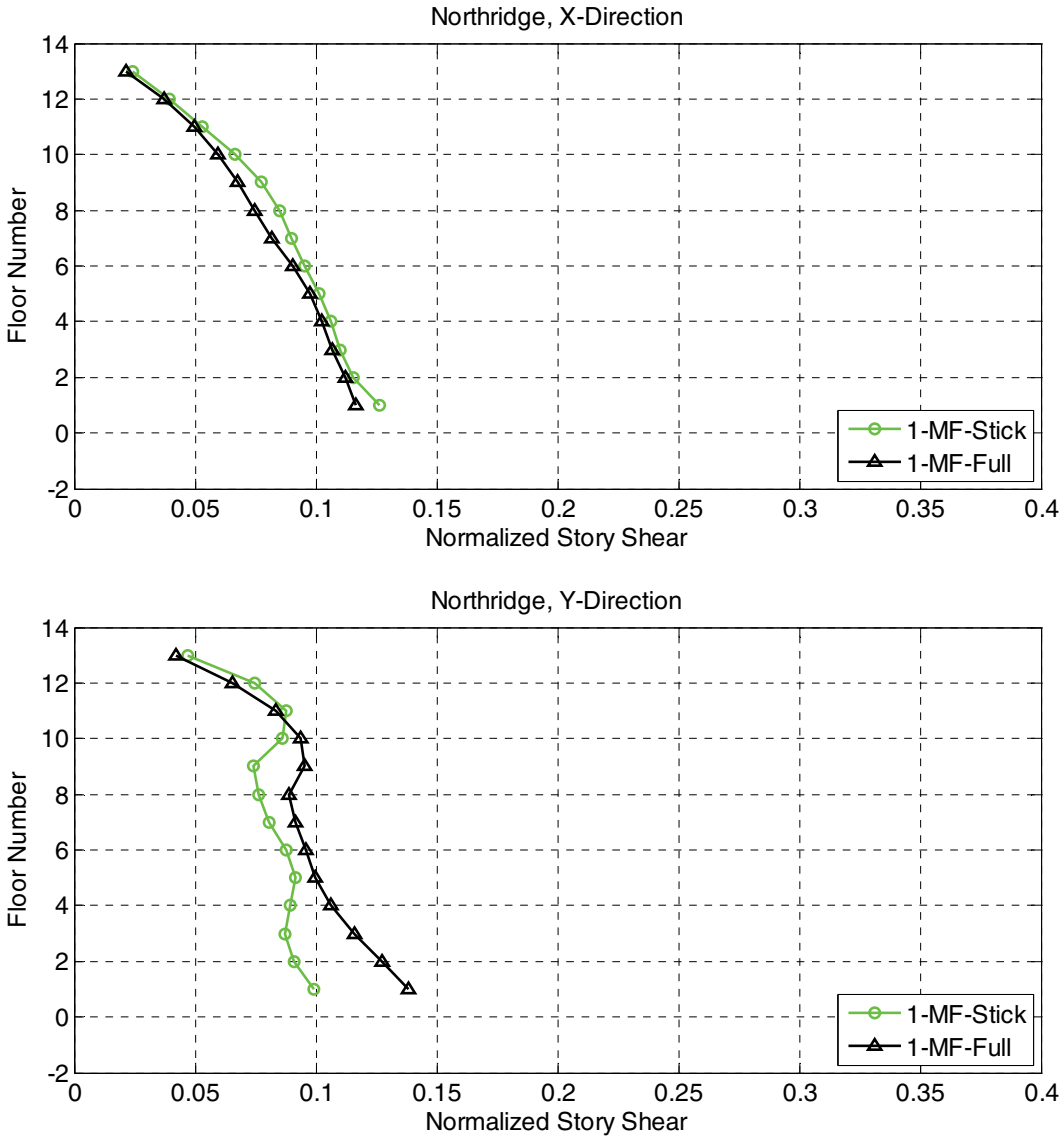

Figure B-14 Comparison of normalized story shear envelopes for the moment frame stick Model 1 and the full-building Model 1.

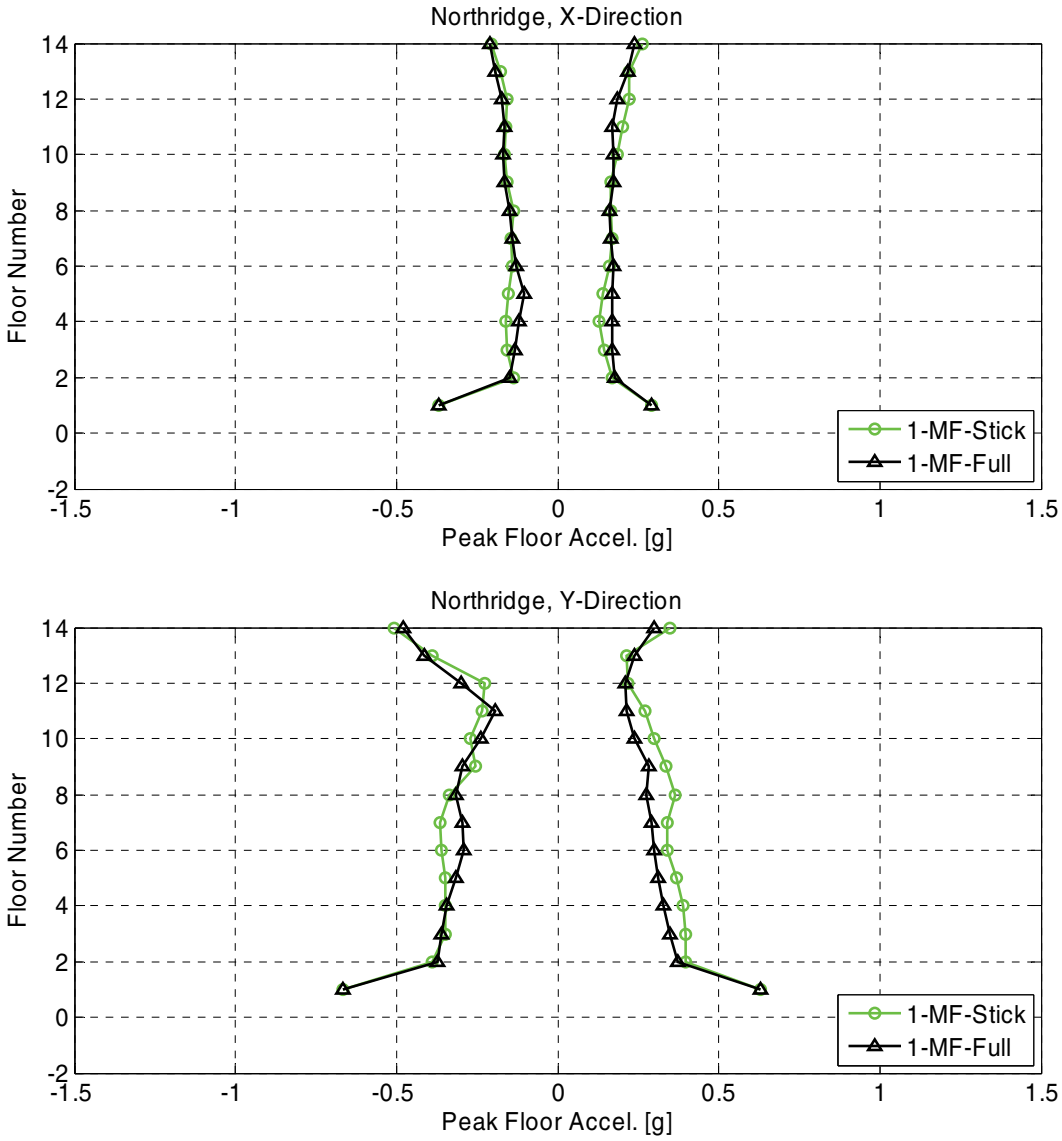

Figure B-15 Comparison of peak floor acceleration envelopes for the moment frame stick Model 1 and the full-building Model 1.

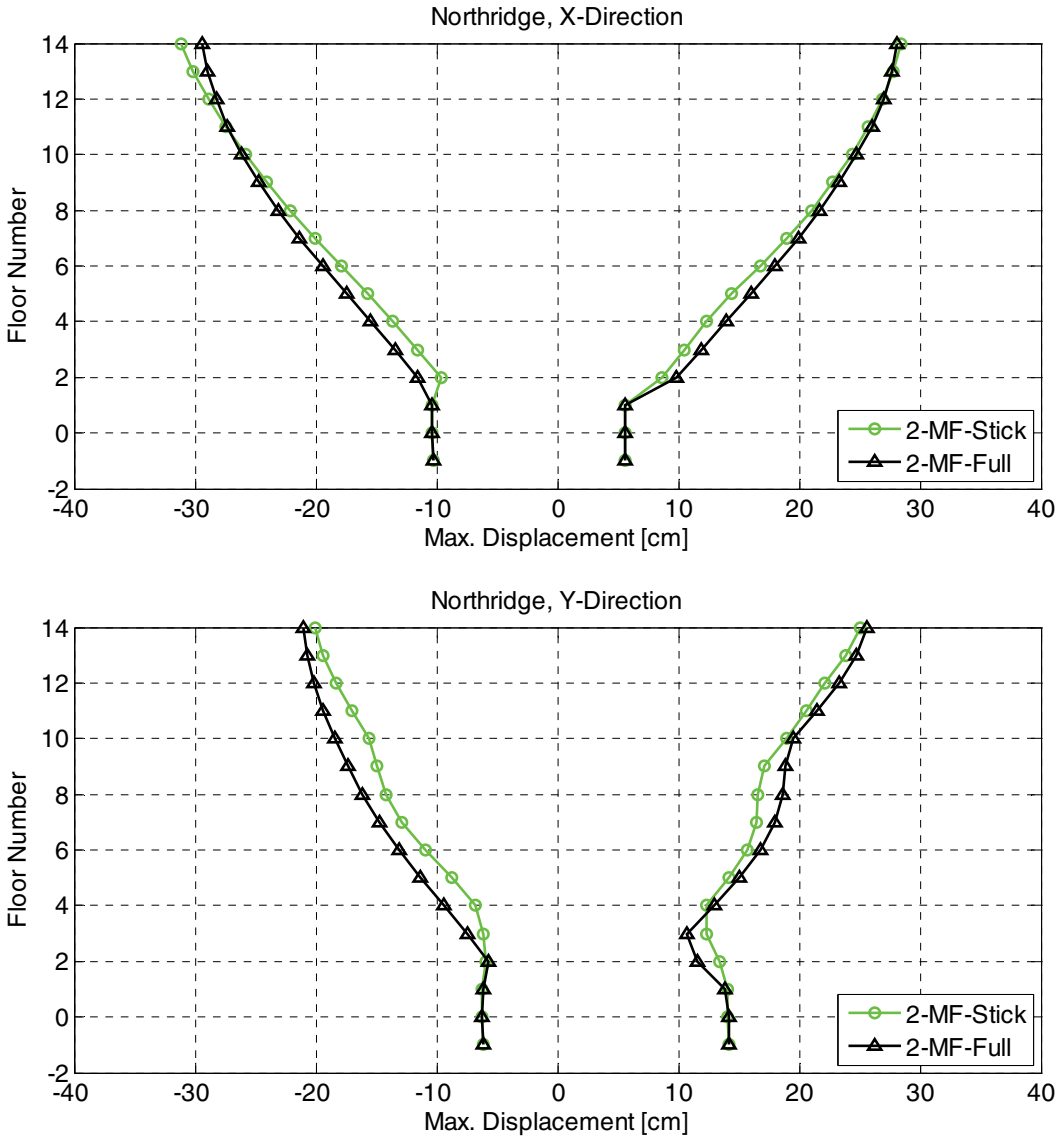

Figure B-16 Comparison of maximum displacement envelopes for the moment frame stick Model 2 and the full-building Model 2.

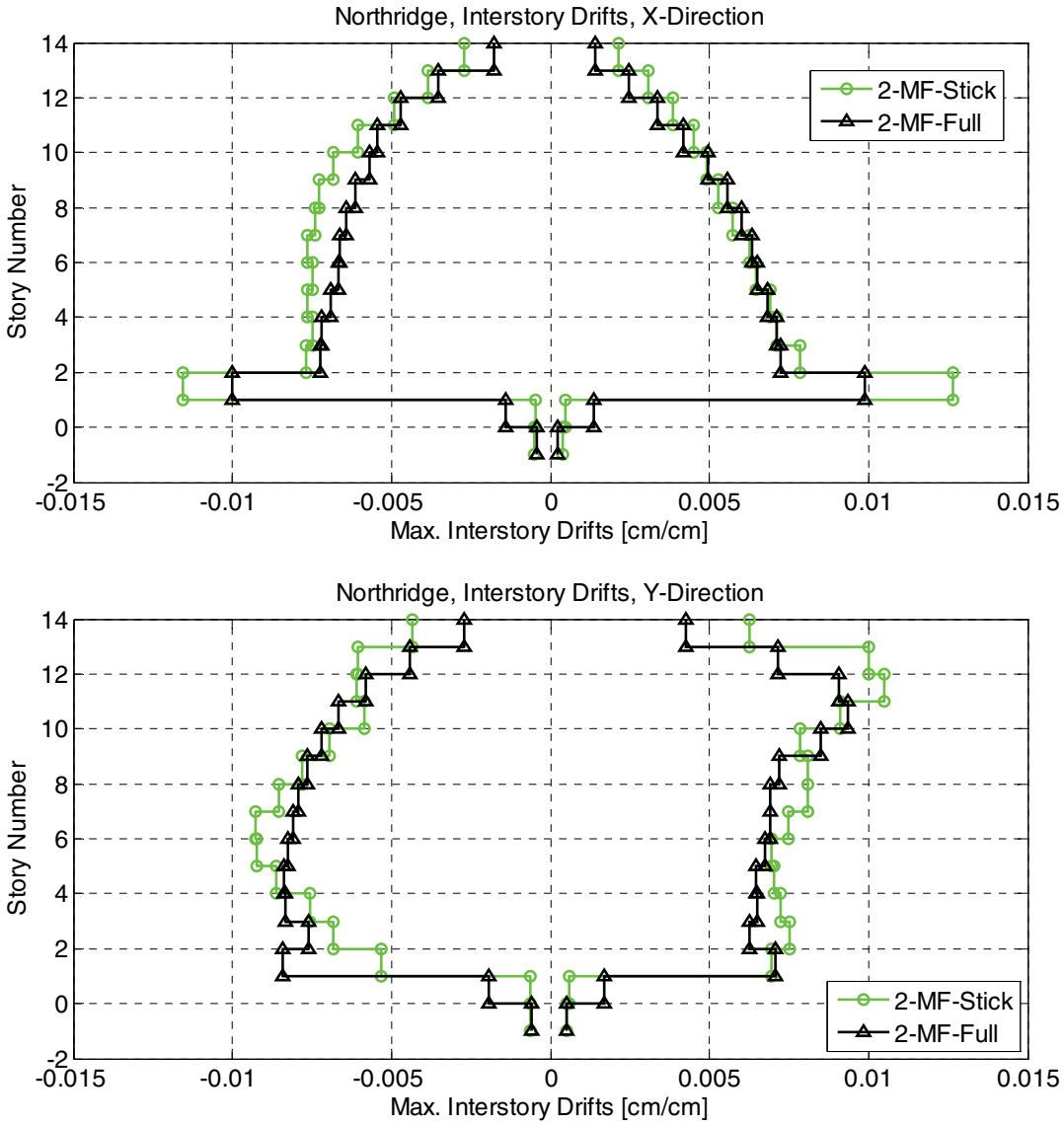

Figure B-17 Comparison of maximum story drift envelopes for the moment frame stick Model 2 and the full-building Model 2.

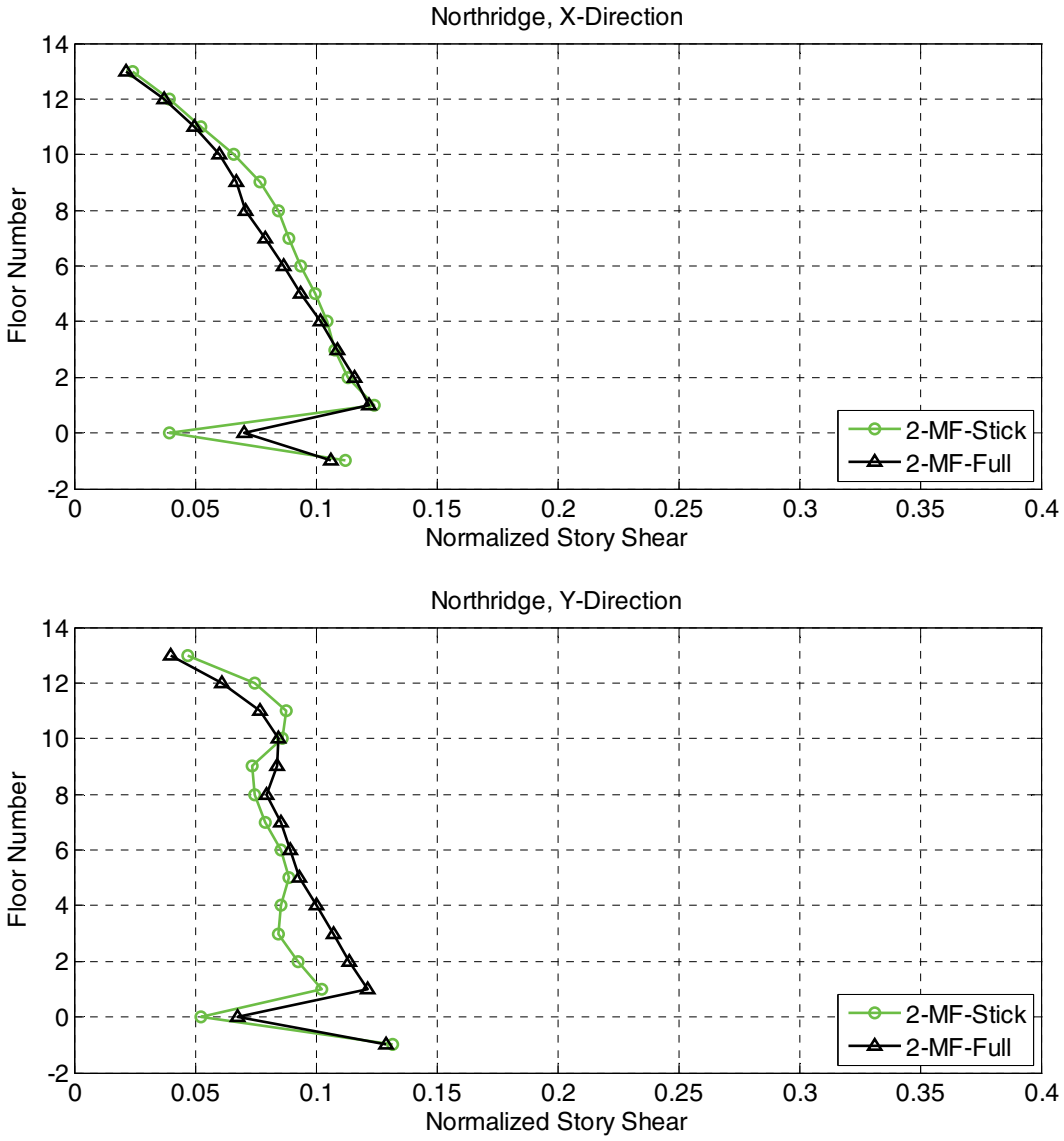

Figure B-18 Comparison of normalized story shear envelopes for the moment frame stick Model 2 and the full-building Model 2.

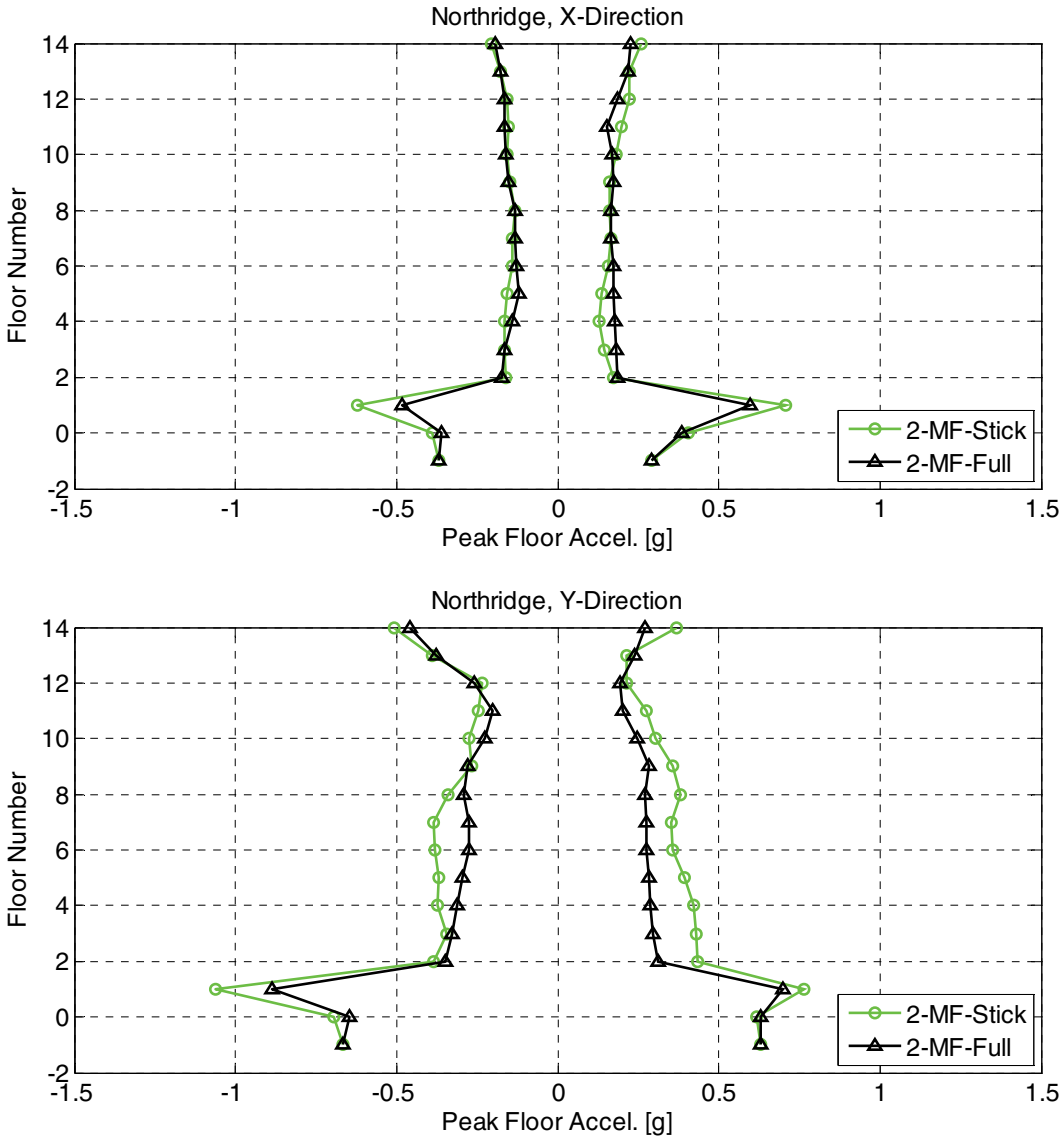

Figure B-19 Comparison of peak floor acceleration envelopes for the moment frame stick Model 2 and the full-building Model 2.

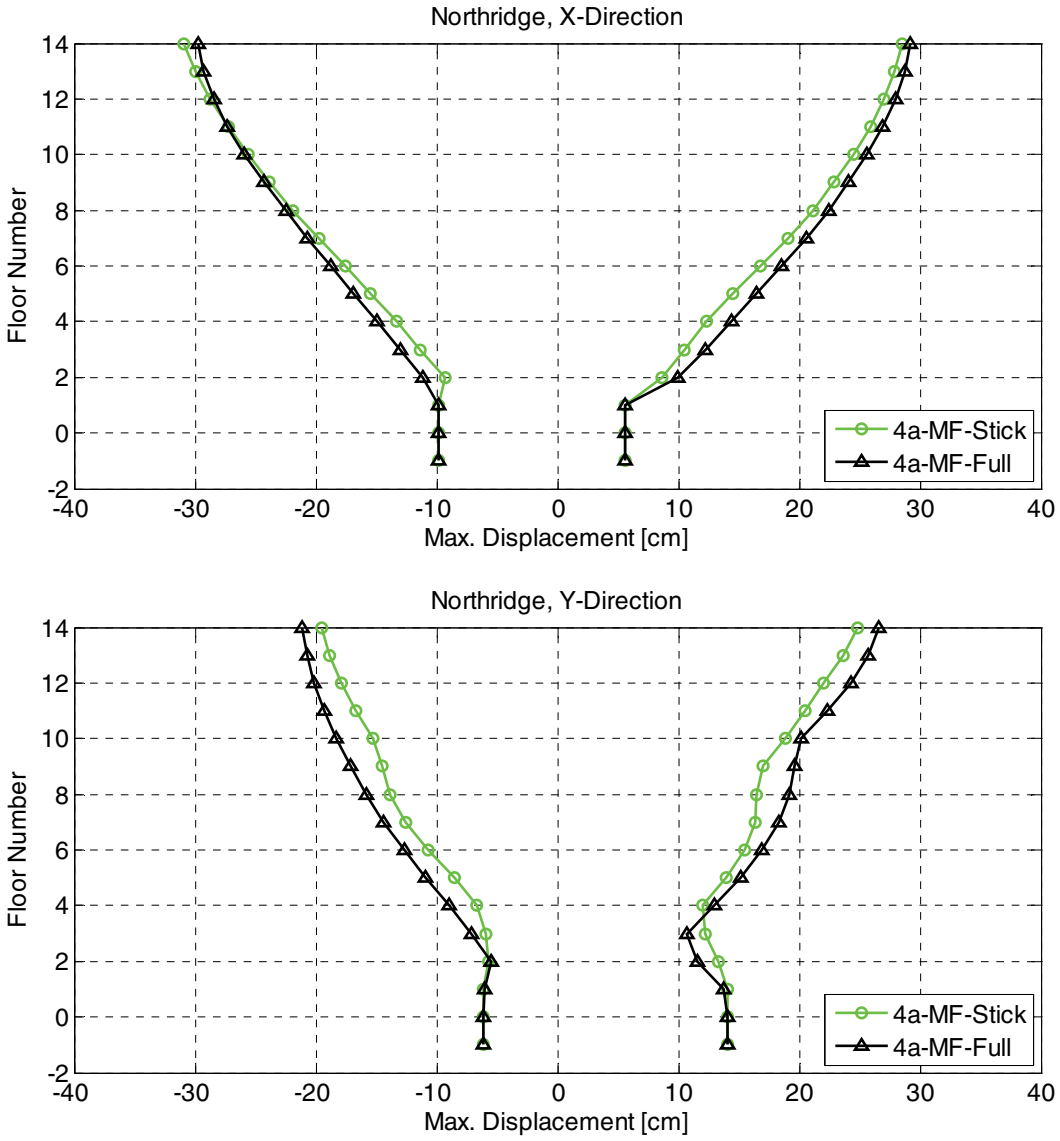

Figure B-20 Comparison of maximum displacement envelopes for the moment frame stick Model 4a and the full-building Model 4a.

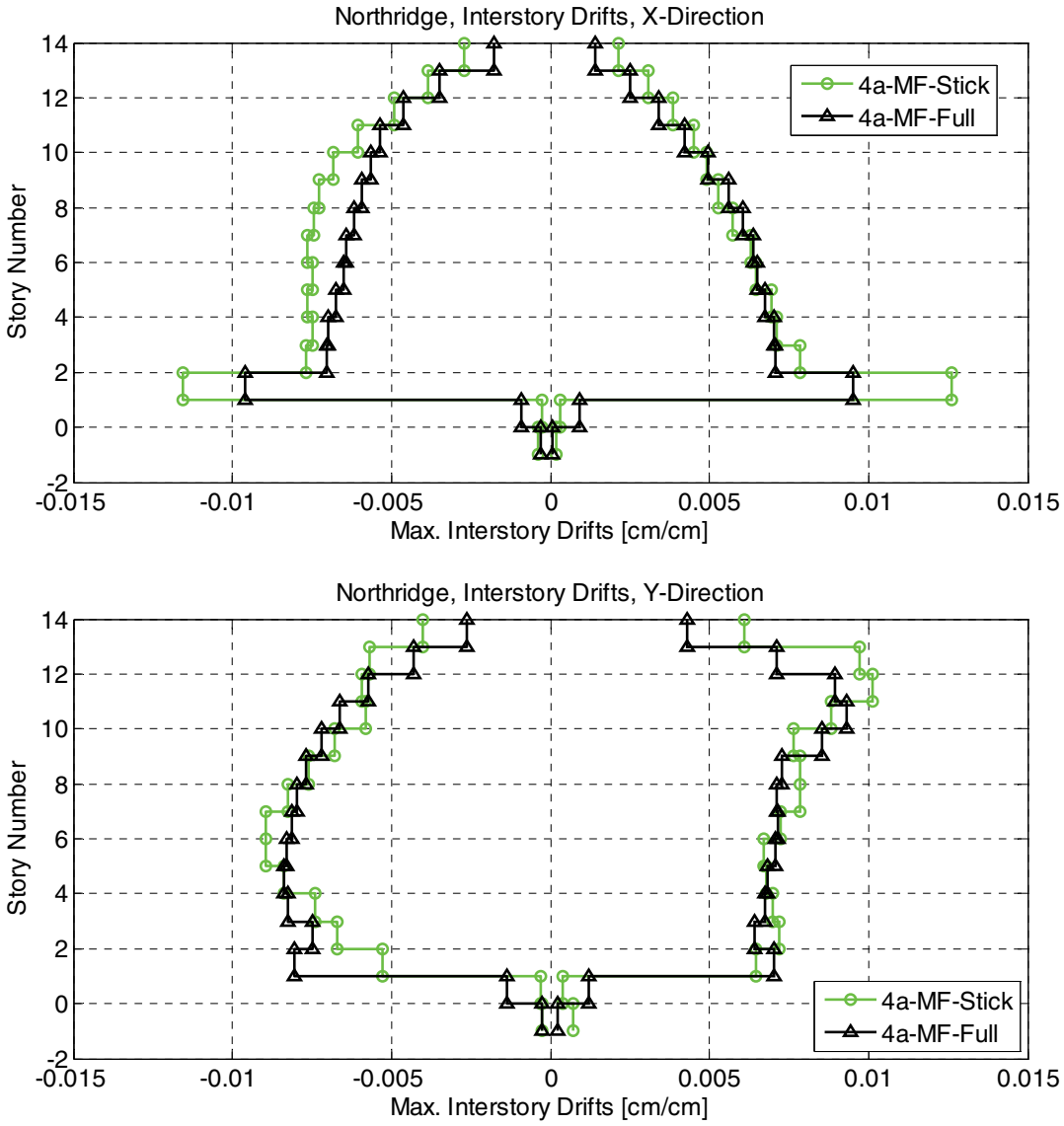

Figure B-21 Comparison of maximum story drift envelopes for the moment frame stick Model 4a and the full-building Model 4a.

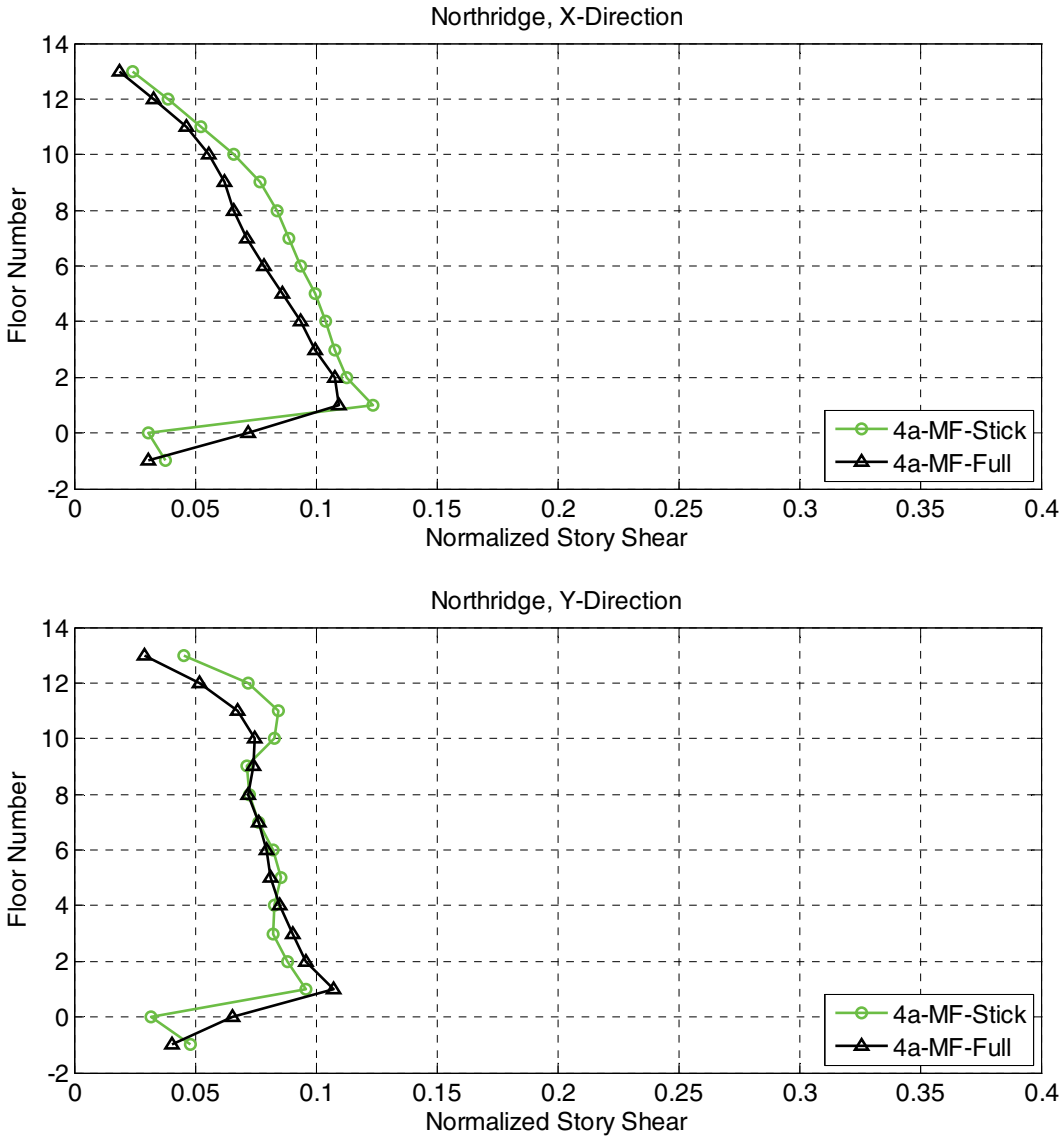

Figure B-22 Comparison of normalized story shear envelopes for the moment frame stick Model 4a and the full-building Model 4a.

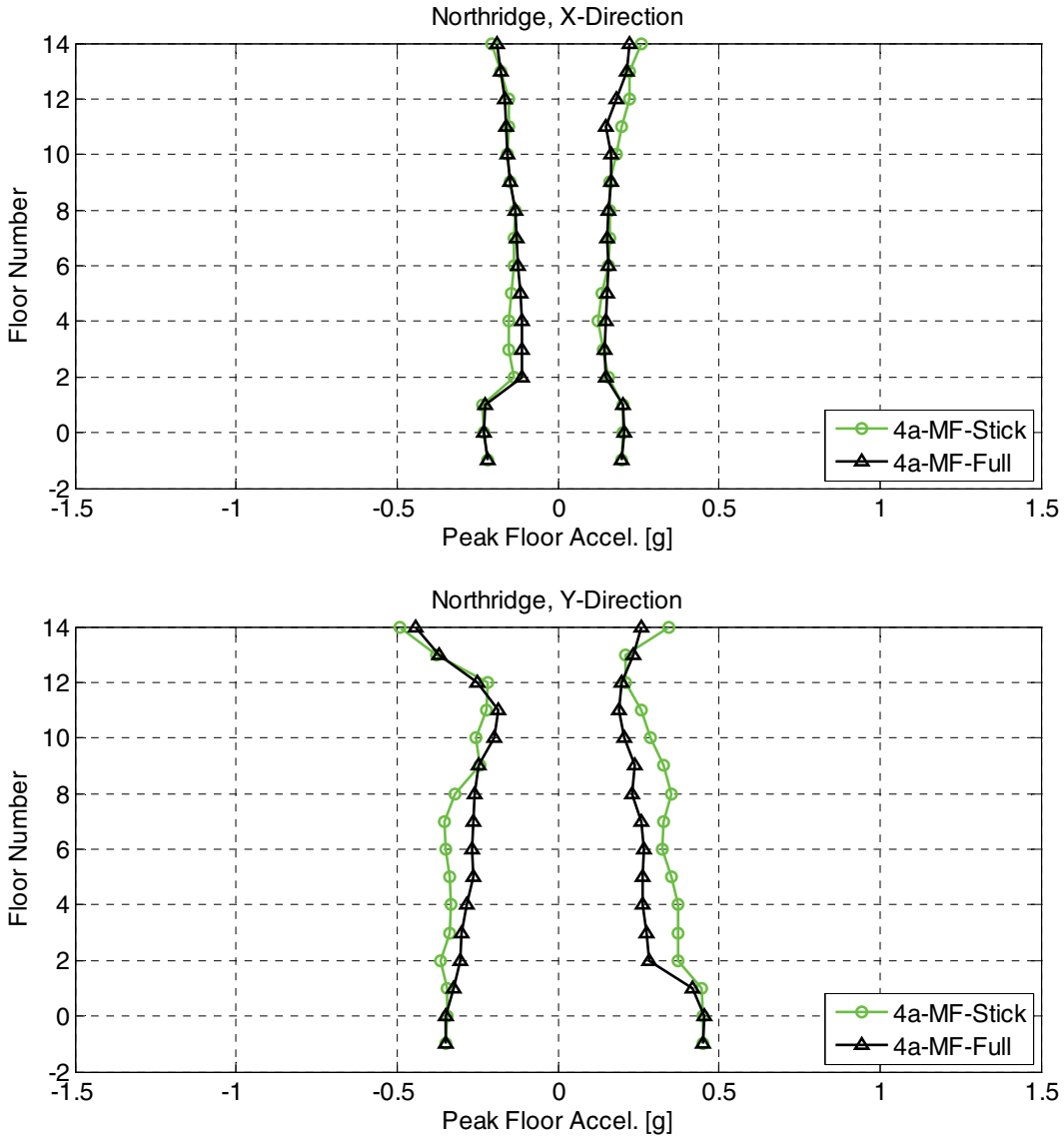

Figure B-23 Comparison of peak floor acceleration envelopes for the moment frame stick Model 4a and the full-building Model 4a.

B.3 Moment Frame Stick Model Comparisons for Different Foundation Configurations

Figures B-24 through B-27 overlay response envelopes for maximum displacement, story drift, story shear, and peak floor acceleration for each alternative foundation configuration of the moment frame models in each direction. The following trends were observed:

- Displacements for Model 1 are typically the largest, followed by Model 2. Displacements for Model 4a are very similar to Model MB.
- Drifts trends are similar to displacement trends, except that Model MB has larger drifts than the others models in the basement levels.
- Story shear results for Model 1 are the largest. Story shears for Model 2, Model 4a and Model MB are similar.
- Peak floor acceleration results for all models are similar in the upper floors. Model 2 produces significantly larger results in the ground story and basement levels.

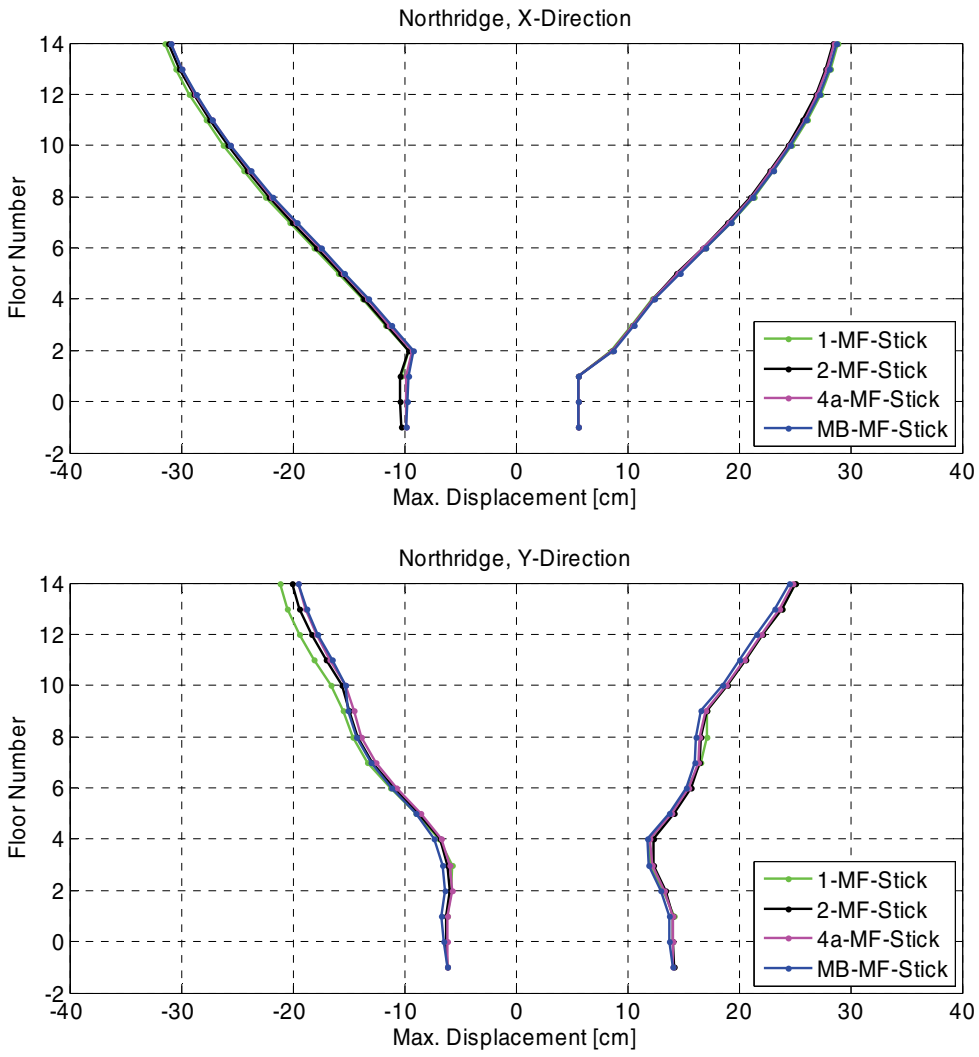

Figure B-24 Comparison of maximum displacement envelopes for the moment frame stick Models 1, 2, 4a, and MB.

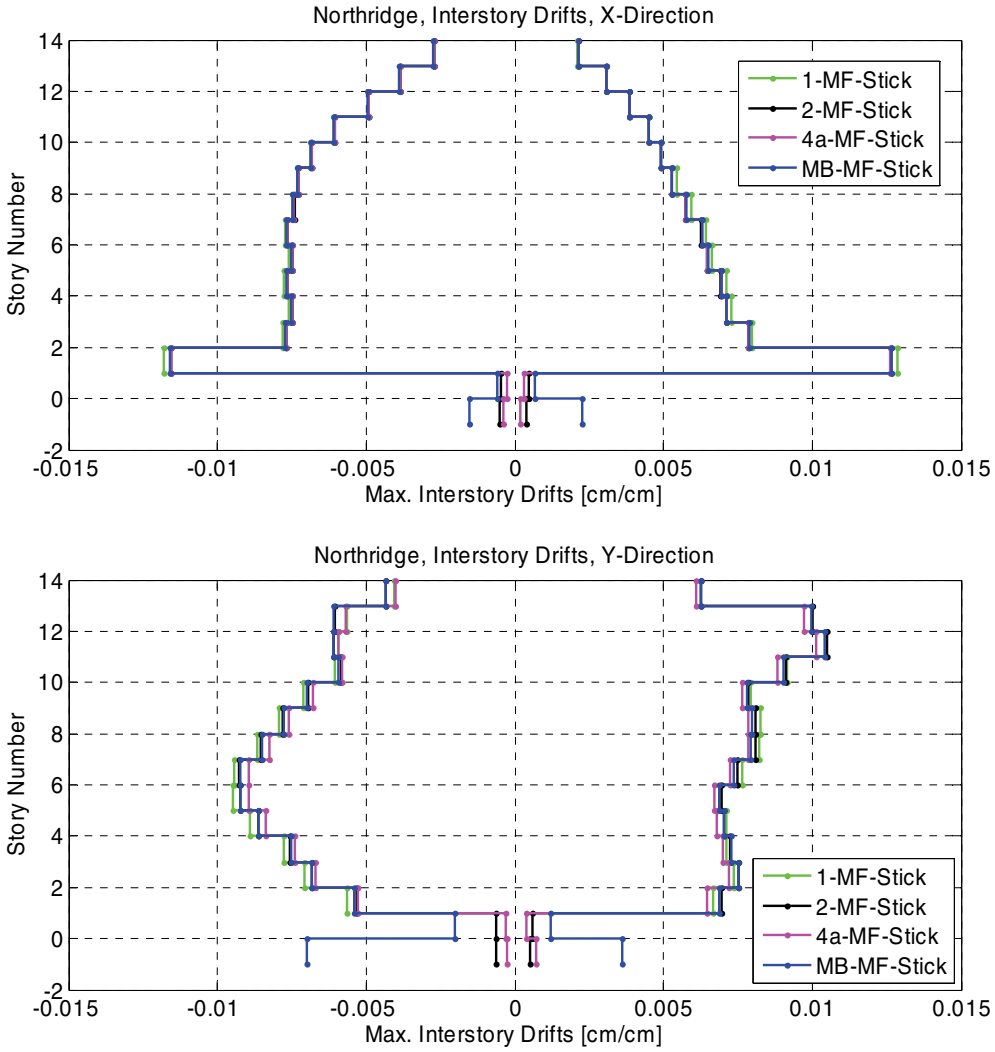

Figure B-25 Comparison of maximum story drift envelopes for the moment frame stick Models 1, 2, 4a, and MB.

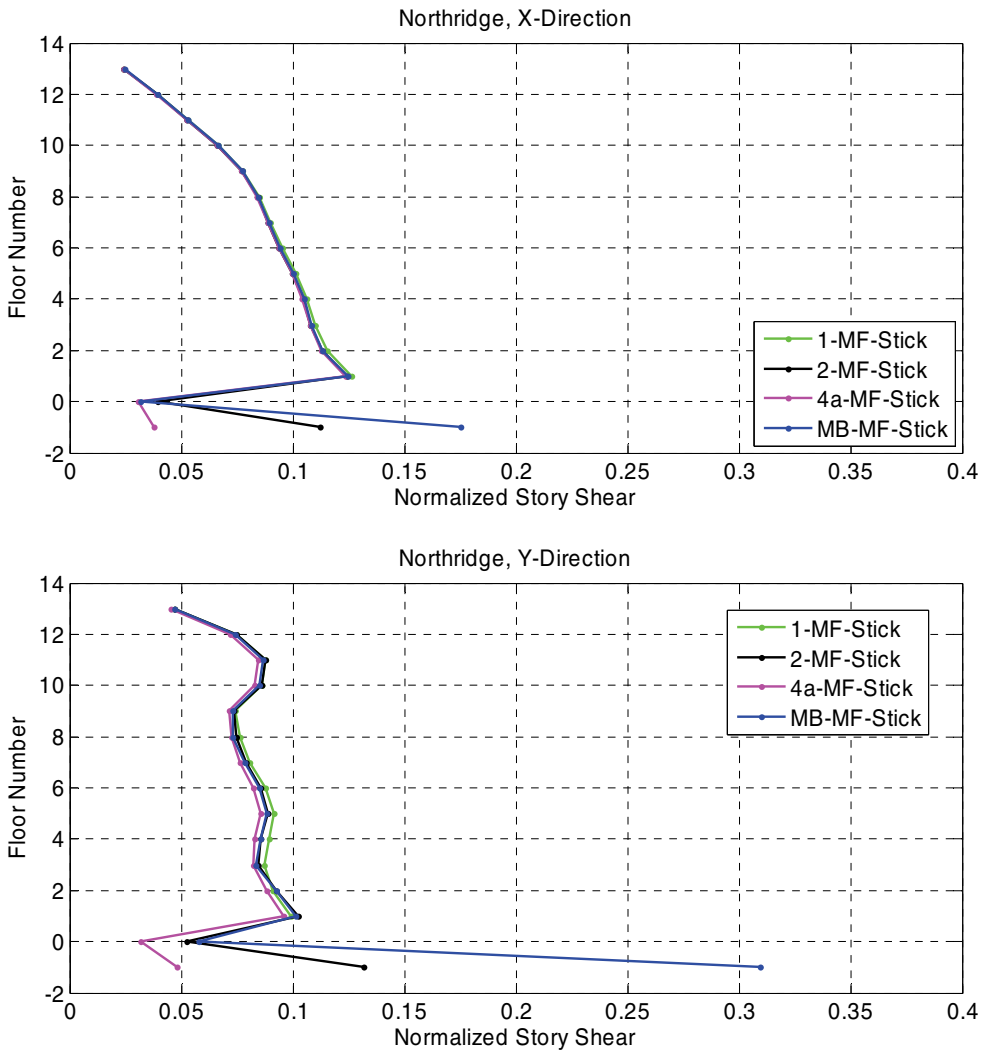

Figure B-26 Comparison of normalized story shear envelopes for the moment frame stick Models 1, 2, 4a, and MB.

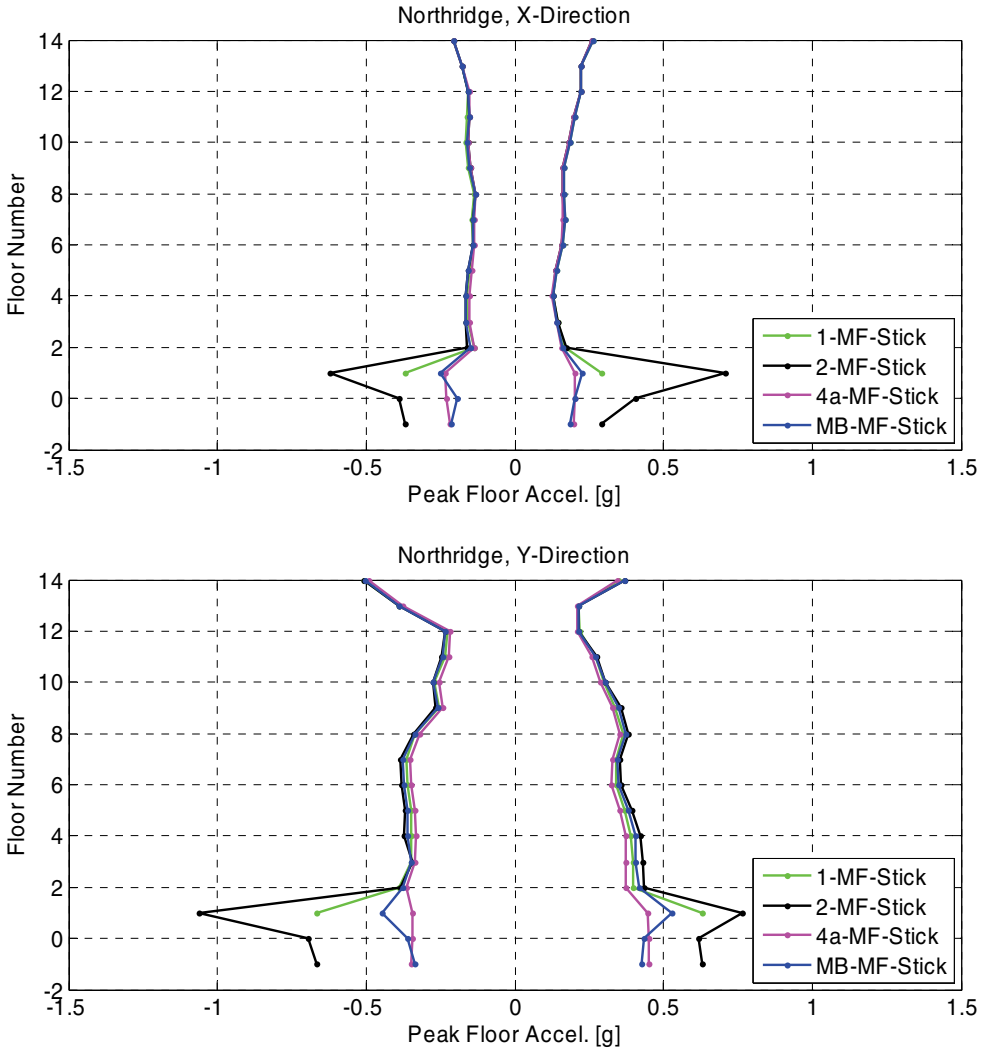

Figure B-27 Comparison of peak floor acceleration envelopes for the moment frame stick Models 1, 2, 4a, and MB.

B.4 Shear Wall Stick Model Development

To investigate the effects of structural stiffness on SSI, moment frame stick model parameters were scaled to represent the stiffness associated with shear wall systems. ASCE/SEI 7-10 (ASCE, 2010) and ACI 318-08 (ACI, 2008) were used as references for determining appropriate scale factors for stiffness. A shear wall stick model was created by converting the base shear of the full-building Model MB into a design base shear for an equivalent shear wall using the ratio of response modification coefficients (*R* factors) for the special reinforced concrete moment frame and special reinforced concrete shear wall systems, respectively. Assuming a bearing wall system, this ratio is 1.6. Based on an amplified base shear, and material properties predefined in the full-building Model MB, a required shear wall area was determined.

In the case of the core wall configuration, a geometry using two separate interior core walls, 16 inches thick, was assumed. The cores were configured to match the size and dimensions of typical elevator, stair, and restroom core areas in typical buildings. The stiffness was then determined by summing the flexural and shear deflections of a slender cantilever wall using the following equation:

$$\Delta = \Delta_b + \Delta_b = \frac{Vh^3}{12EI} + \frac{1.2Vh}{G_c A} \tag{B-1}$$

Where the shear modulus of concrete, G_c, was assumed to be 40% of the elastic modulus of concrete. Total deflection was primarily controlled by the flexural term, and the stiffness of the shear wall system was approximately three times the stiffness of the moment frame system. The stiffness contribution from the gravity system was also considered. When combined with the stiffness of the shear wall system, a total stiffness scale factor of 5 was obtained. The core shear wall building model, with a scale factor of 5, was designated SW. Table B-6 compares the first-, second-, and third-mode periods of the shear wall stick models for each foundation configuration.

Table B-6 Comparison of Modeled Periods for the Shear Wall Stick Models for each Alternative Foundation Configuration

	Identified Period Mode 1 (sec)	Identified Period Mode 2 (sec)	Identified Period Mode 3 (sec)
Model	Translational (Global Y-axis)	Torsional (about Global Z-axis)	Translational (Global X-axis)
1 Stick (SW)	1.32	N.A.	1.17
2 Stick (SW)	1.38	N.A.	1.19
4a Stick (SW)	1.40	N.A.	1.20
MB Stick (SW)	1.40	N.A.	1.20

Additional shear wall systems with scale factors of 25, 50, and 125, representing perimeter shear wall configurations, were also considered. These models were designated SW1, SW2, and SW3, respectively.

B.5 Shear Wall Stick Model Comparisons

Figures B-28 through B-43 overlay response envelopes for maximum displacement, story drift, story shear, and peak floor acceleration for each alternative foundation configuration, for each shear wall model, in each direction. The following trends were observed:

- Differences between the models are much more significant in the stiffer shear wall systems than the moment frame system, demonstrating that SSI effects have a larger influence on response in stiffer structural systems.
- Displacements in Model 1 are typically the smallest. Displacements in Model 4a are very similar to Model MB.
- Drift results are similar to displacement results, except that the Model MB has larger drifts in the basement levels.
- Story shear results vary between the X-direction and Y-direction for all models.
- Peak floor accelerations in the superstructure are larger in Model 1 and Model 2. Model 2 produces significantly larger floor accelerations in the ground story and basement levels.

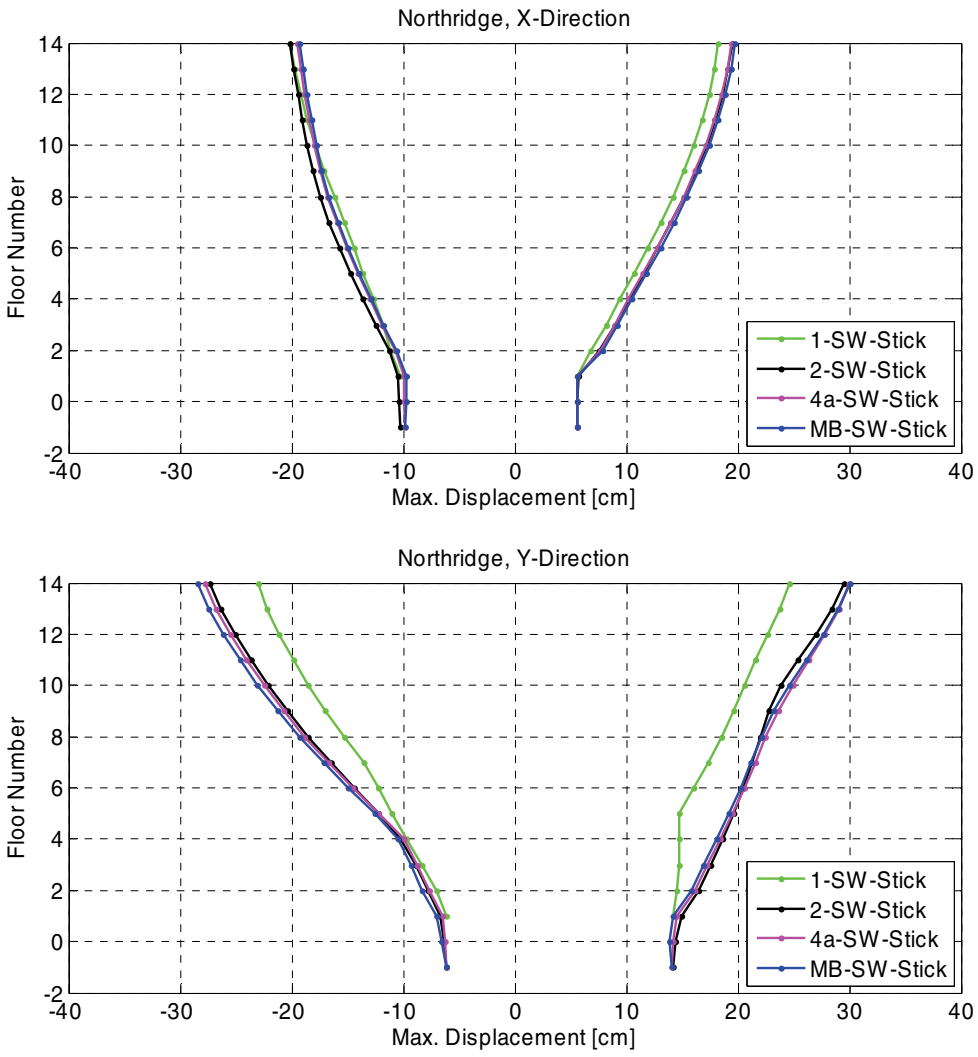

Figure B-28 Comparison of maximum displacement envelopes for the SW stick Models 1, 2, 4a, and MB.

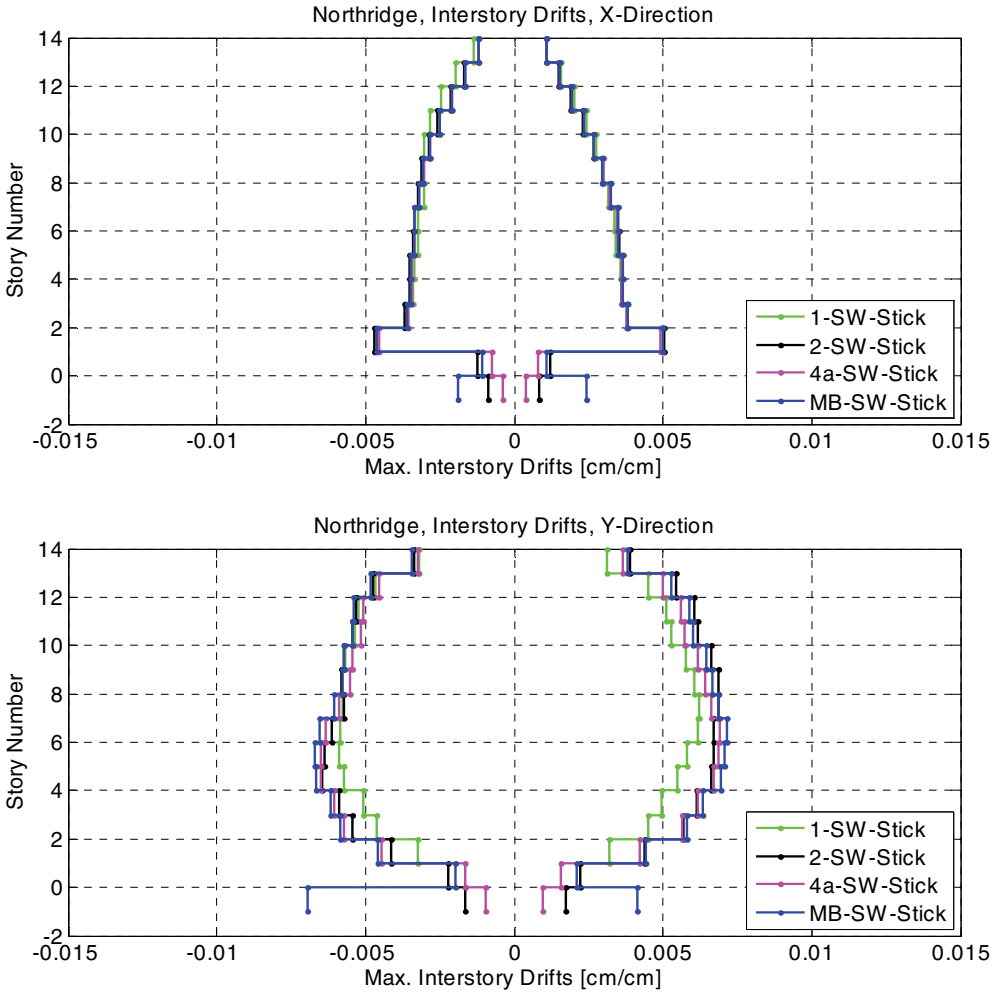

Figure B-29 Comparison of maximum story drift envelopes for the SW stick Models 1, 2, 4a, and MB.

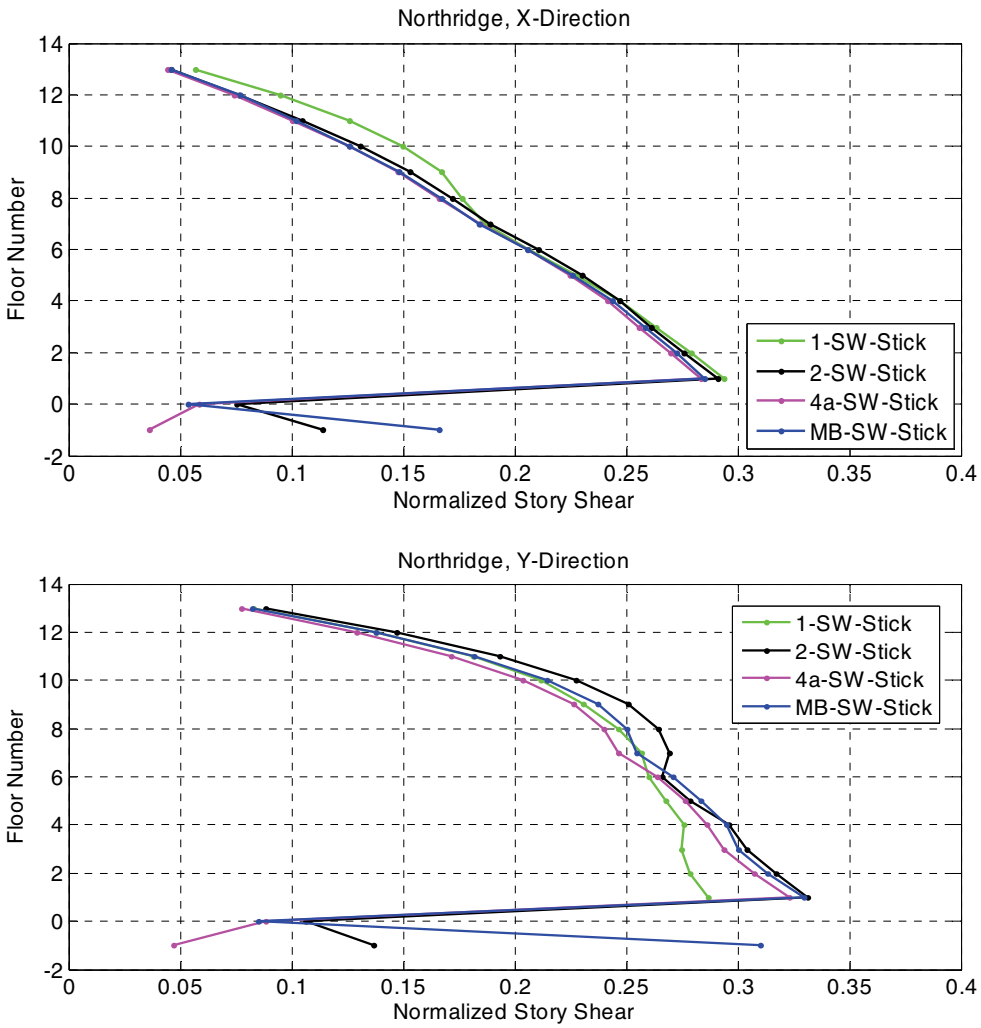

Figure B-30 Comparison of normalized story shear envelopes for the SW stick Models 1, 2, 4a, and MB.

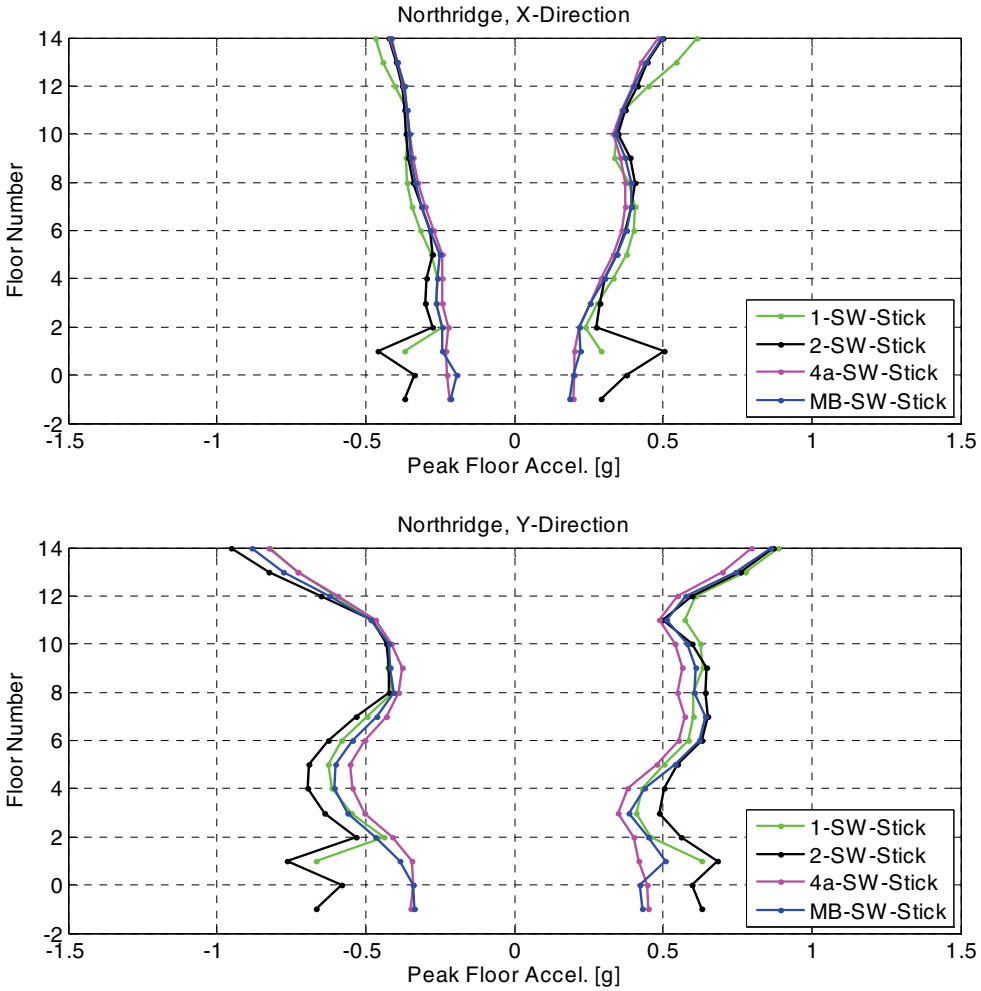

Figure B-31 Comparison of peak floor acceleration envelopes for the SW stick Models 1, 2, 4a, and MB.

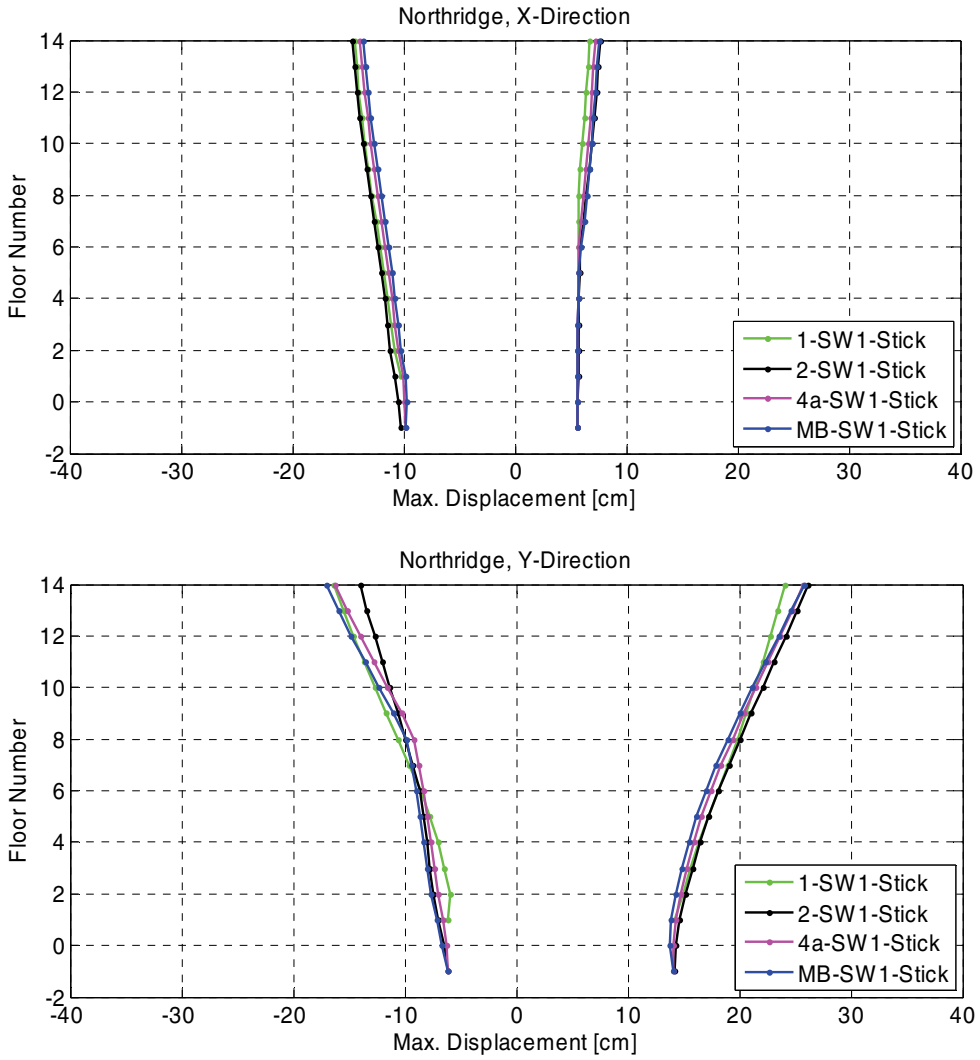

Figure B-32 Comparison of maximum displacement envelopes for the SW1 stick Models 1, 2, 4a, and MB.

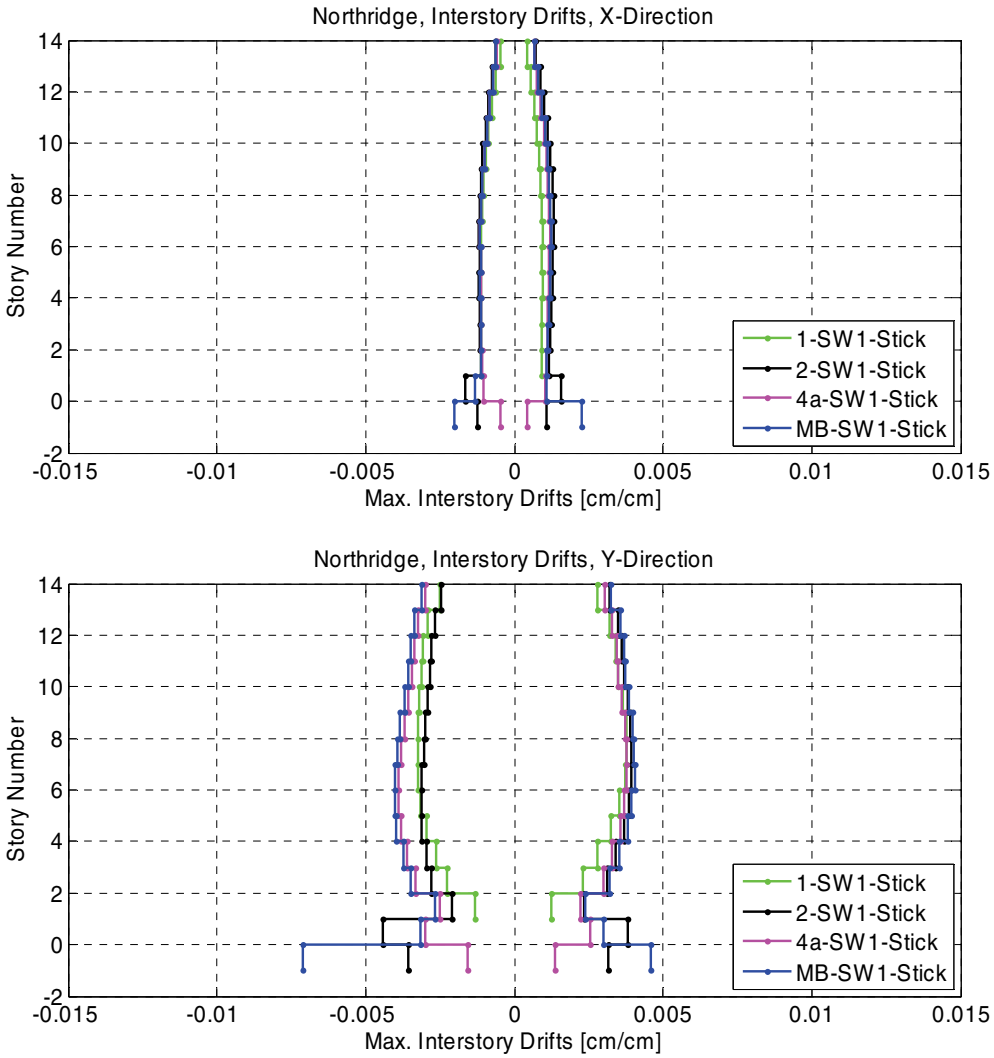

Figure B-33 Comparison of maximum story drift envelopes for the SW1 stick Models 1, 2, 4a, and MB.

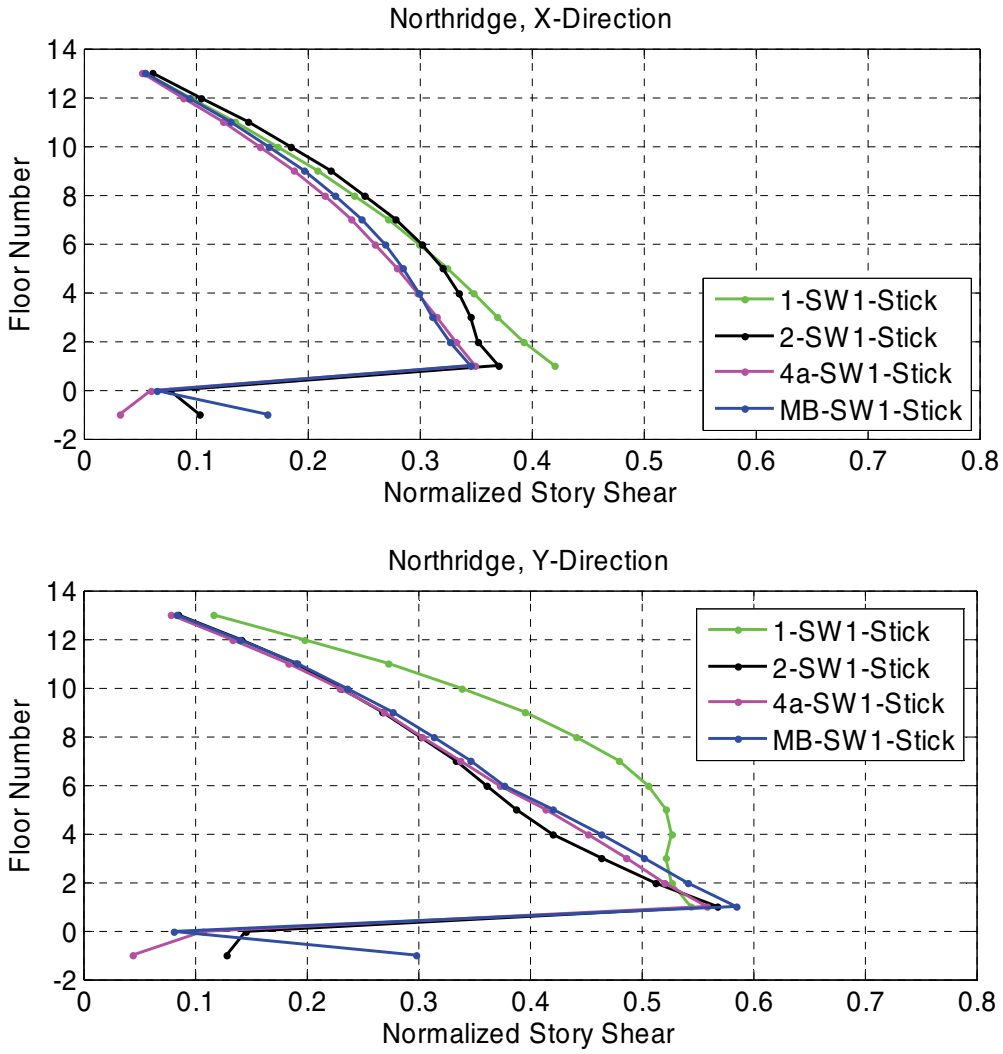

Figure B-34 Comparison of normalized story shear envelopes for the SW1 stick Models 1, 2, 4a, and MB.

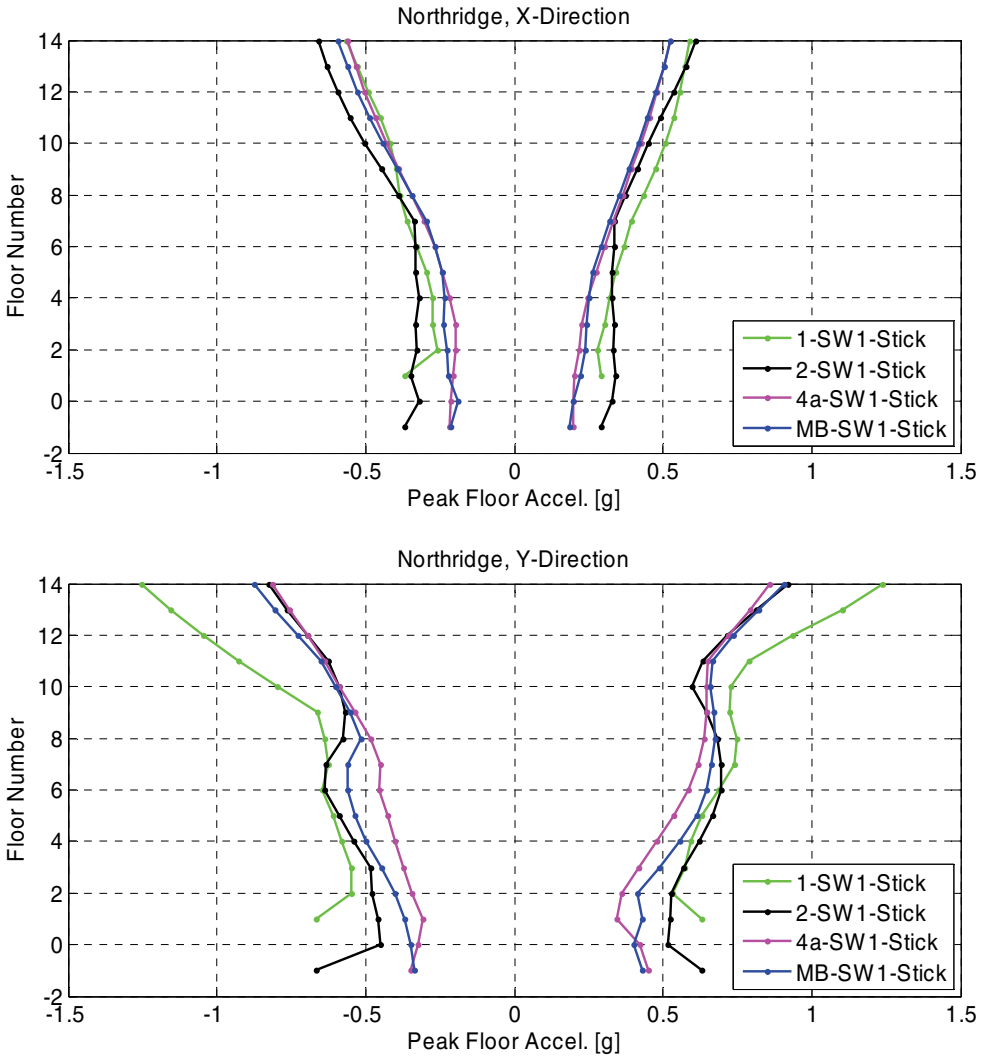

Figure B-35 Comparison of peak floor acceleration envelopes for the SW1 stick Models 1, 2, 4a, and MB.

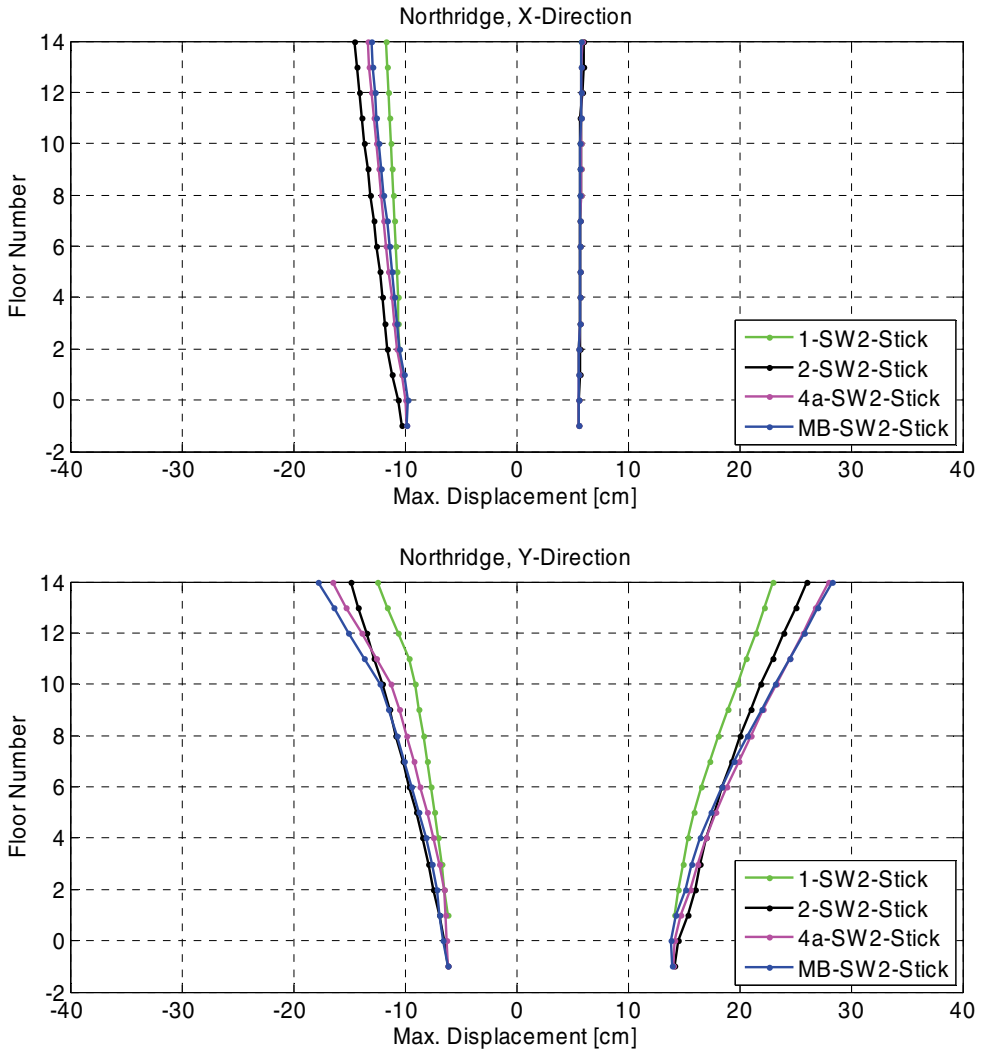

Figure B-36 Comparison of maximum displacement envelopes for the SW2 stick Models 1, 2, 4a, and MB.

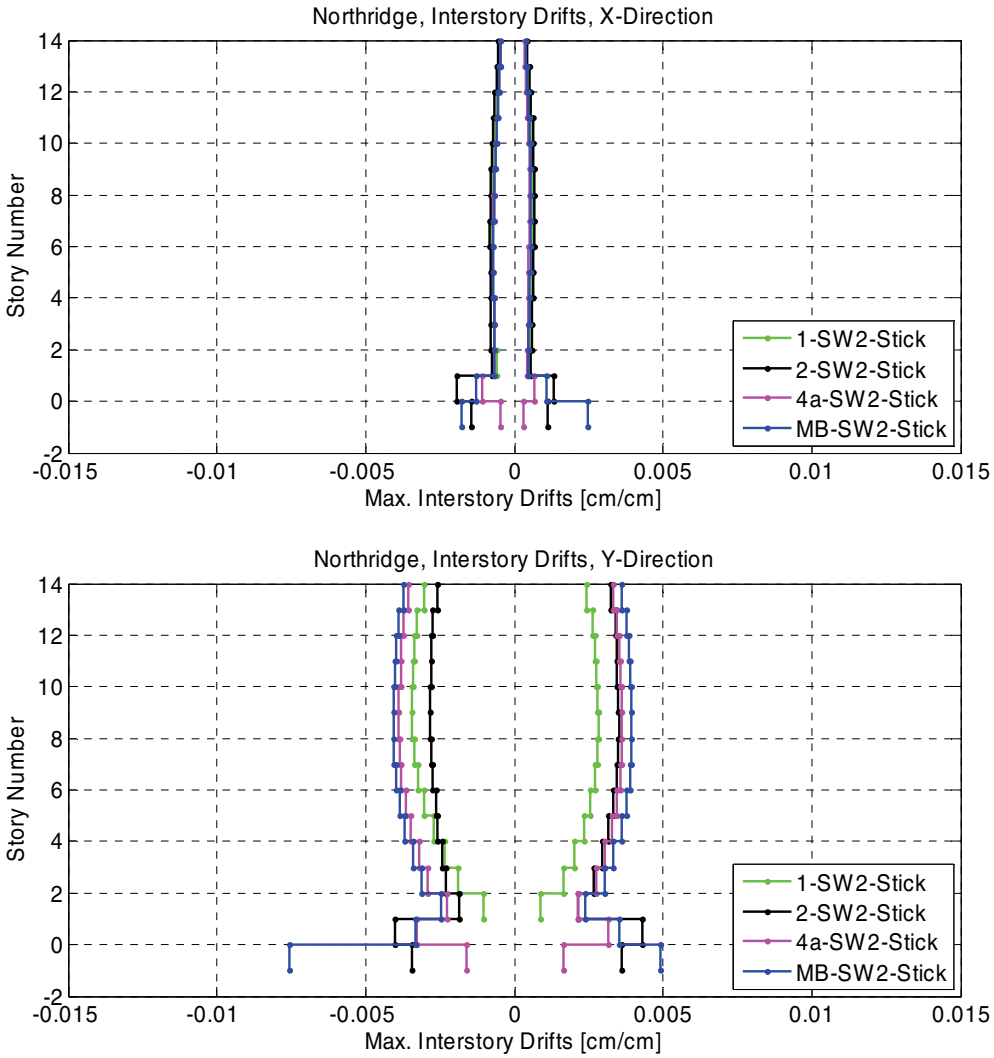

Figure B-37 Comparison of maximum story drift envelopes for the SW2 stick Models 1, 2, 4a, and MB.

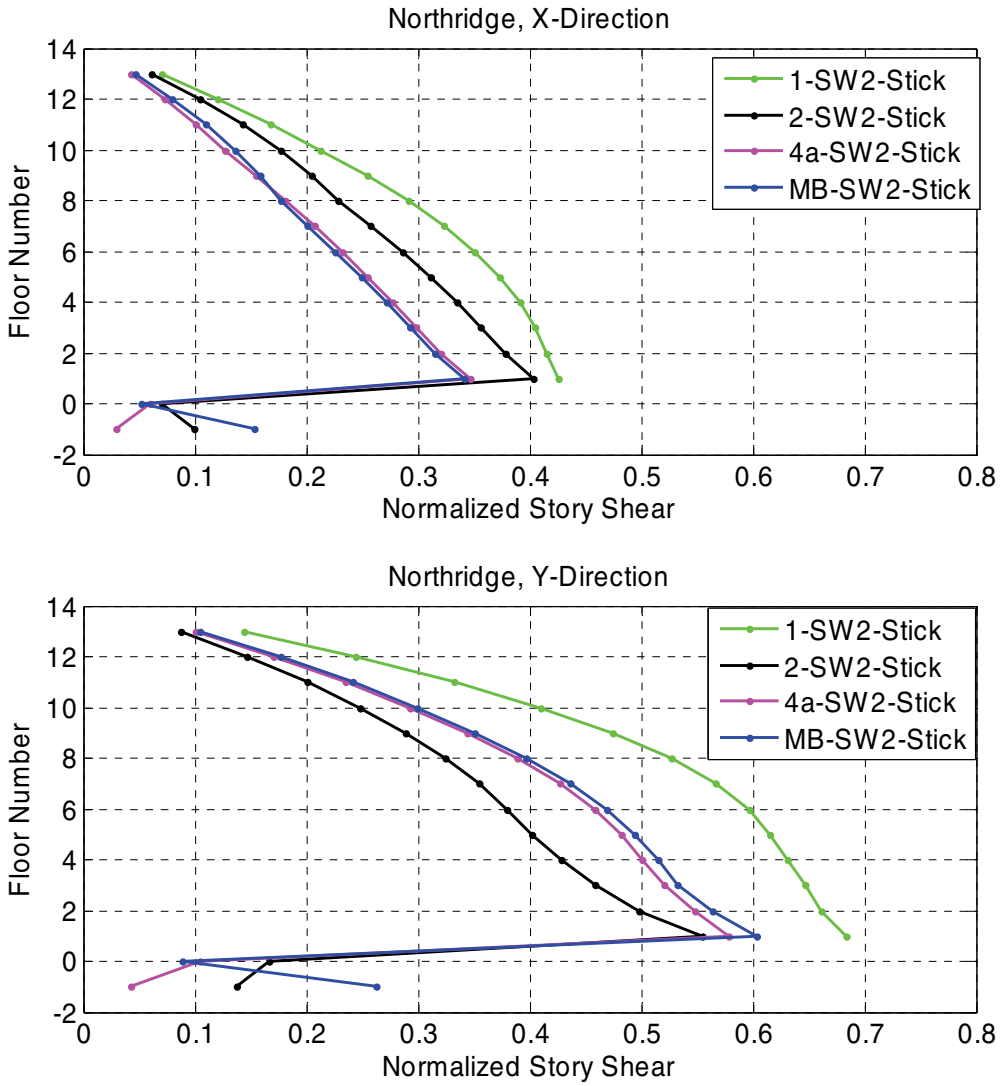

Figure B-38 Comparison of normalized story shear envelopes for the SW2 stick Models 1, 2, 4a, and MB.

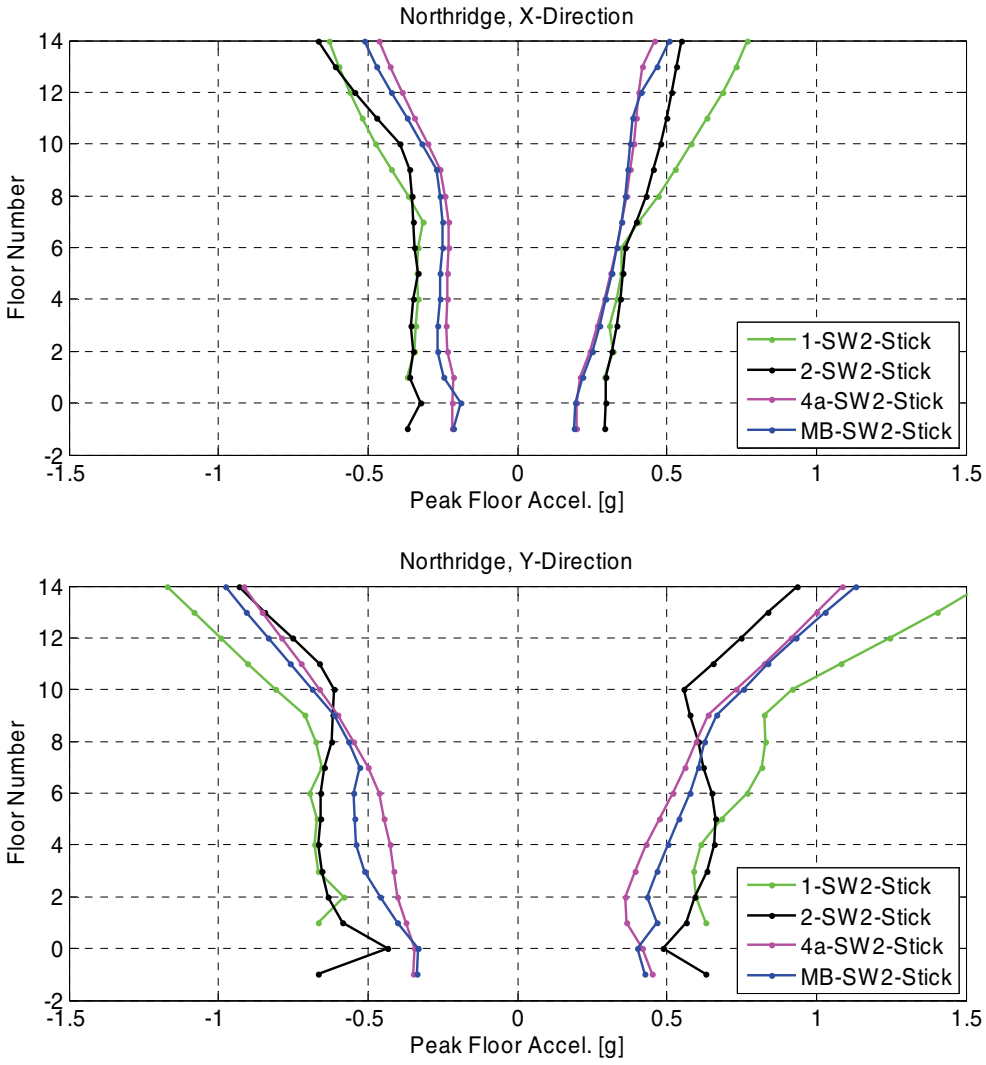

Figure B-39 Comparison of peak floor acceleration envelopes for the SW2 stick Models 1, 2, 4a, and MB.

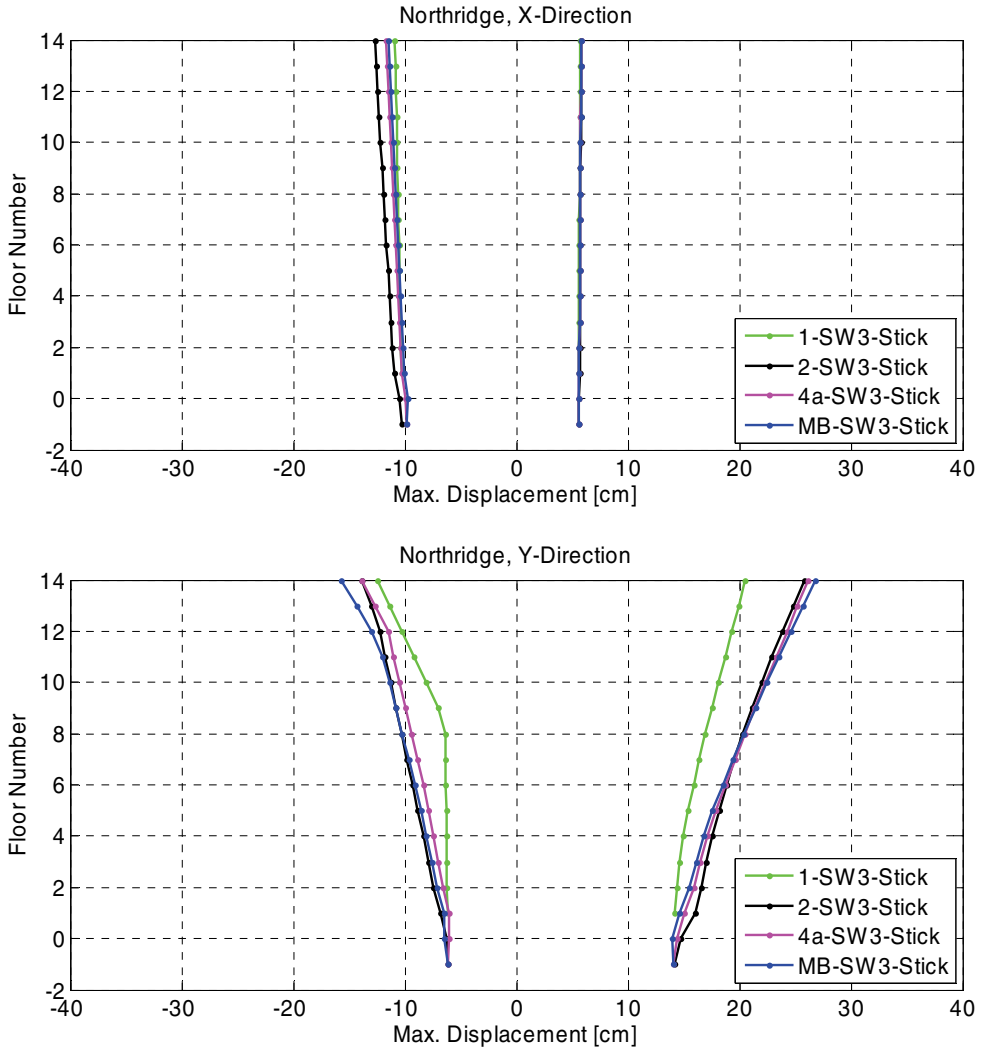

Figure B-40 Comparison of maximum displacement envelopes for the SW3 stick Models 1, 2, 4a, and MB.

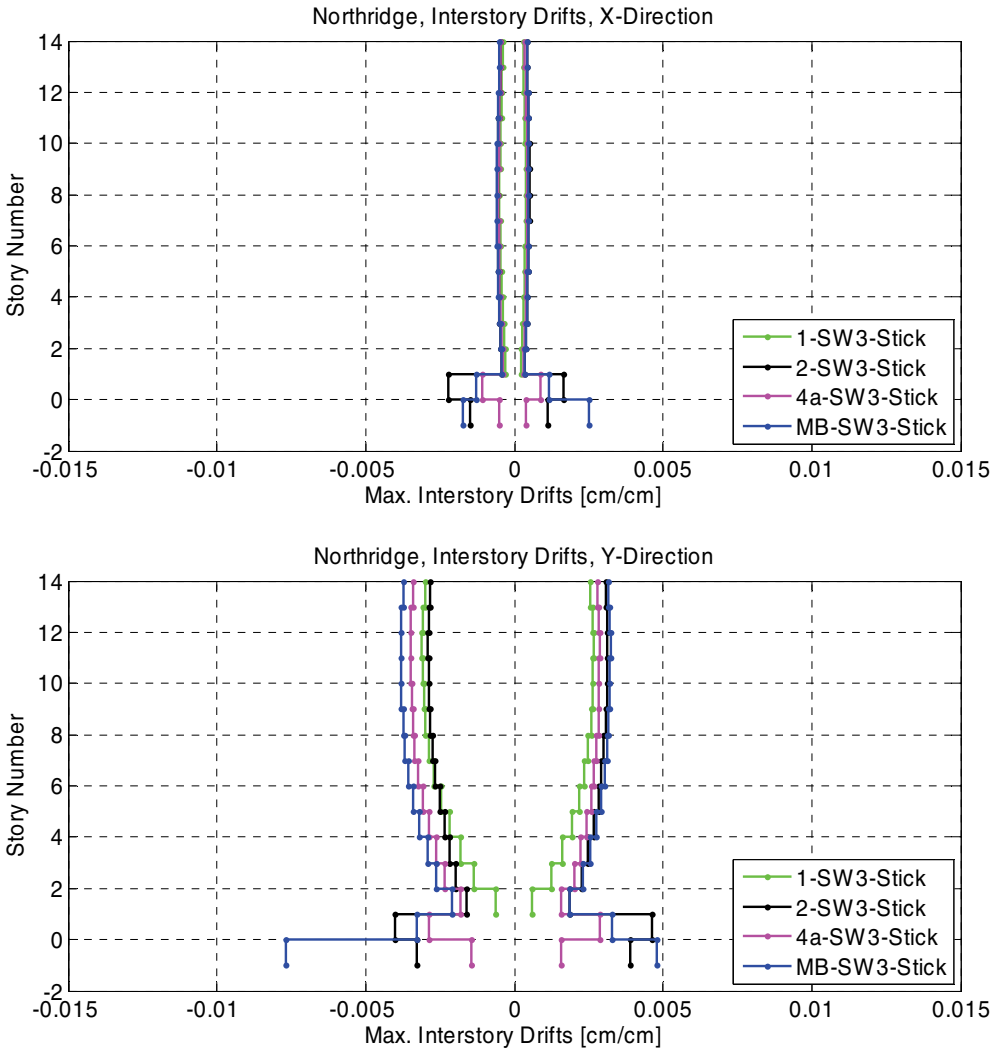

Figure B-41 Comparison of maximum story drift envelopes for the SW3 stick Models 1, 2, 4a, and MB.

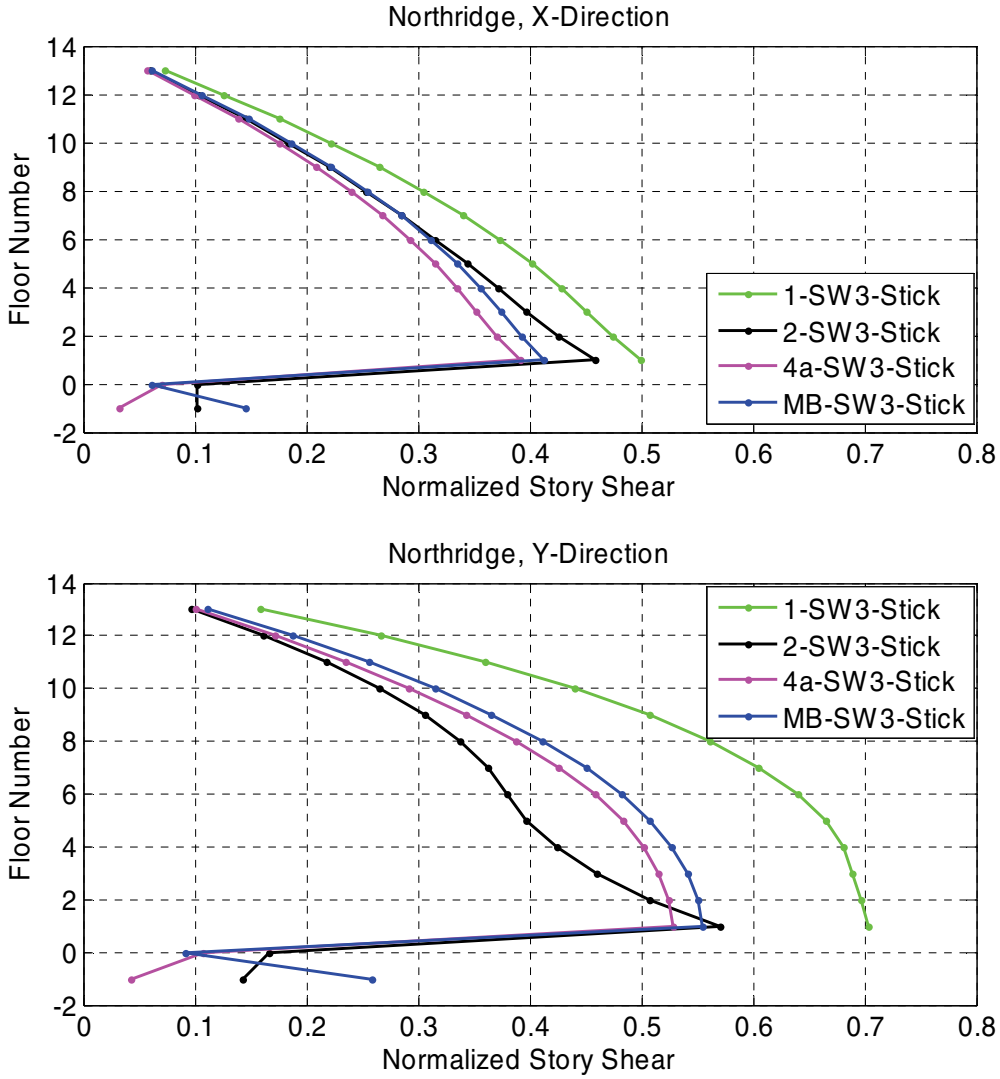

Figure B-42 Comparison of normalized story shear envelopes for the SW3 stick Models 1, 2, 4a, and MB.

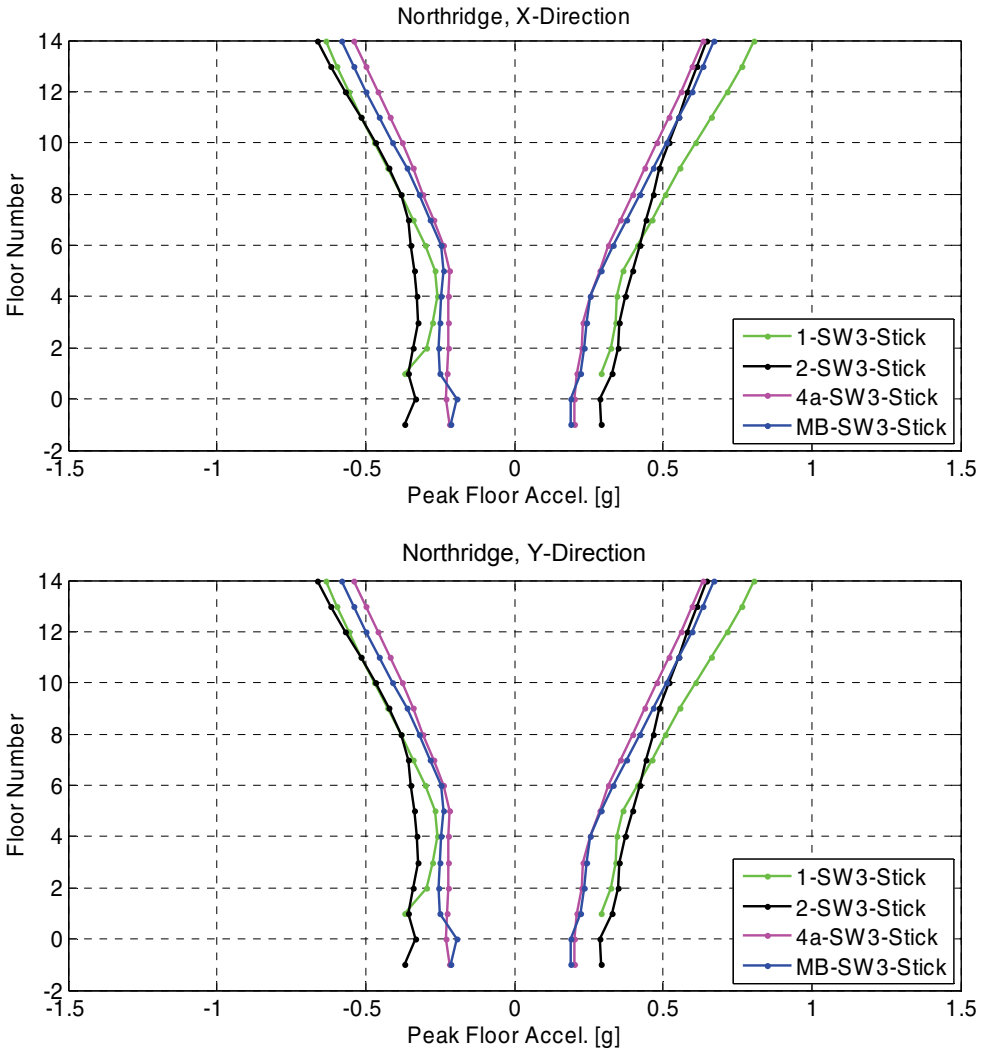

Figure B-43 Comparison of peak floor acceleration envelopes for the SW3 stick Models 1, 2, 4a, and MB.

B.6 Moment Frame Stick Model and Shear Wall Stick Model Comparisons

Figures B-44 through B-47 show comparisons between moment frame stick Model MB and shear wall stick Model MB results for maximum displacement, story drift, story shear, and peak floor acceleration in each direction. Results clearly indicate a significant difference in building response between stiffer and more flexible structural systems.

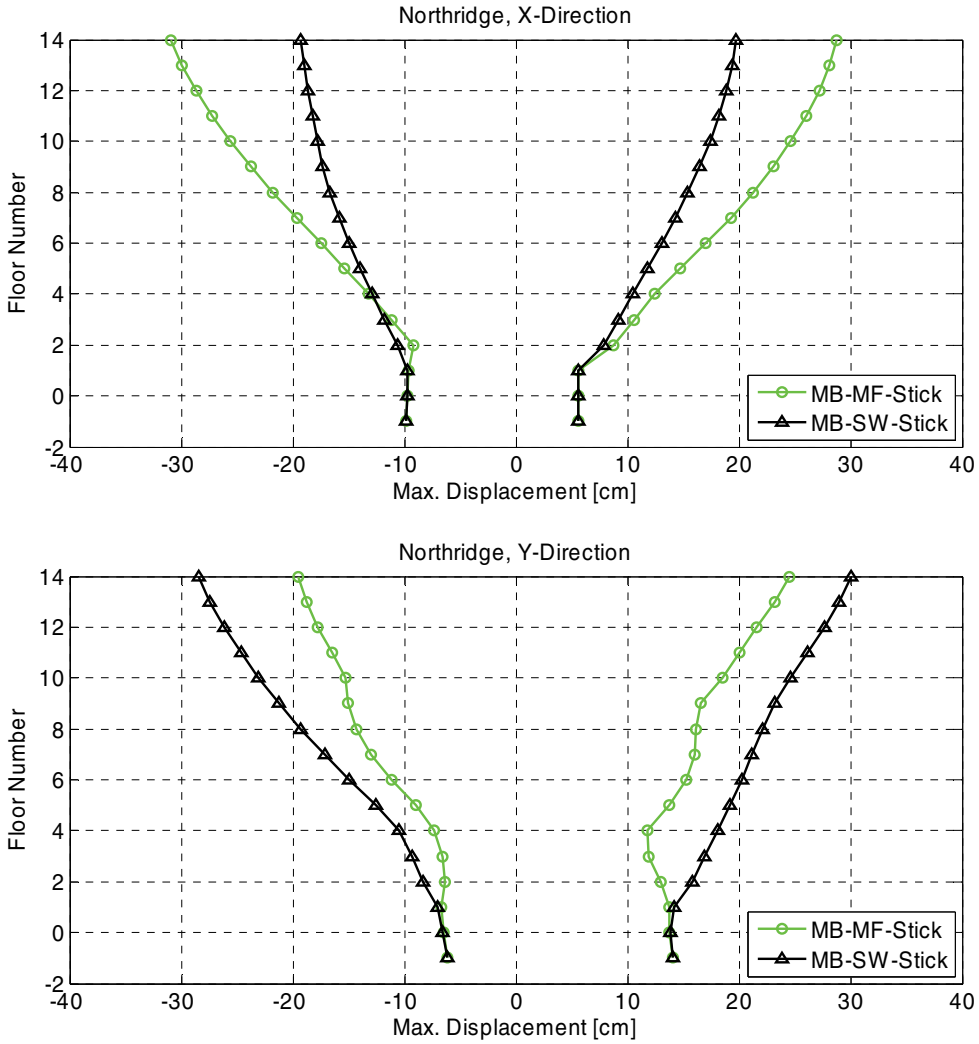

Figure B-44 Comparison of maximum displacement envelopes for the moment frame stick Model MB and the shear wall stick Model MB.

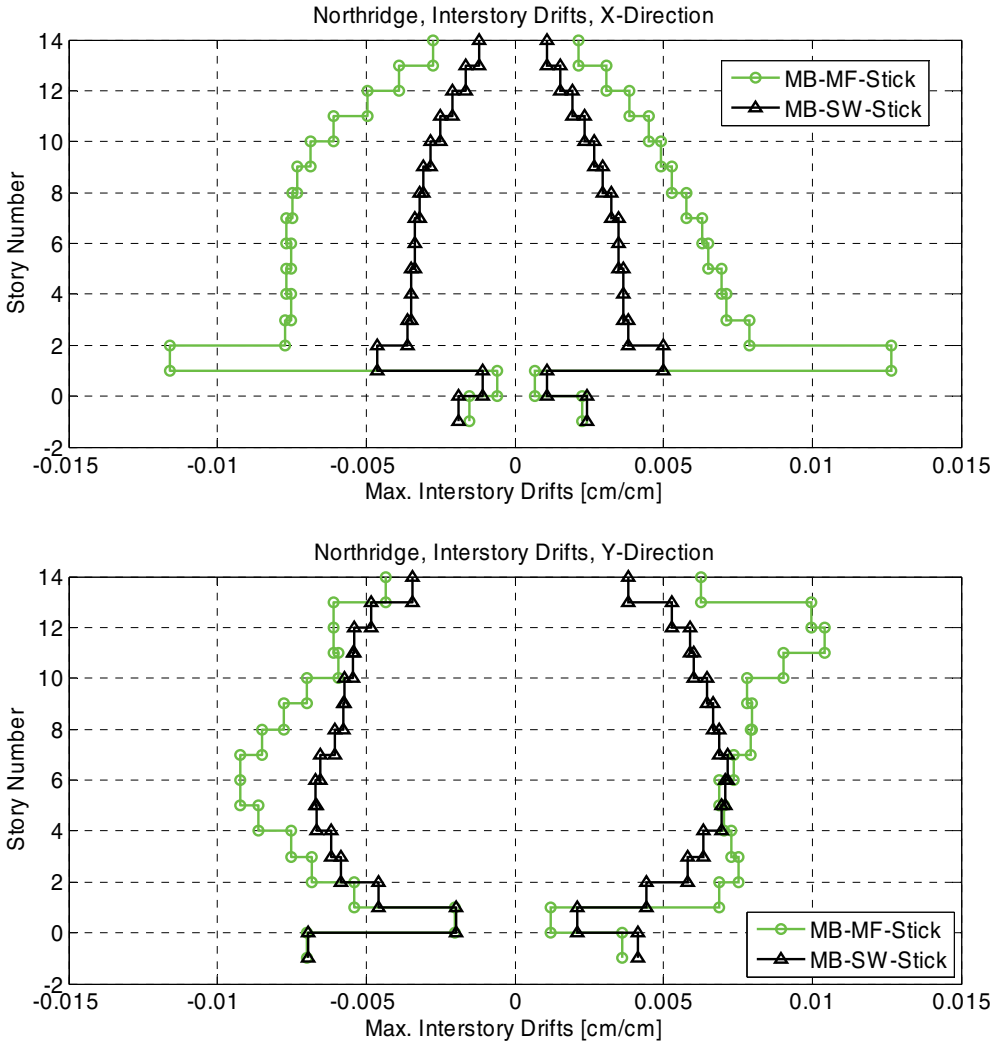

Figure B-45 Comparison of maximum story drift envelopes for the moment frame stick Model MB and the shear wall stick Model MB.

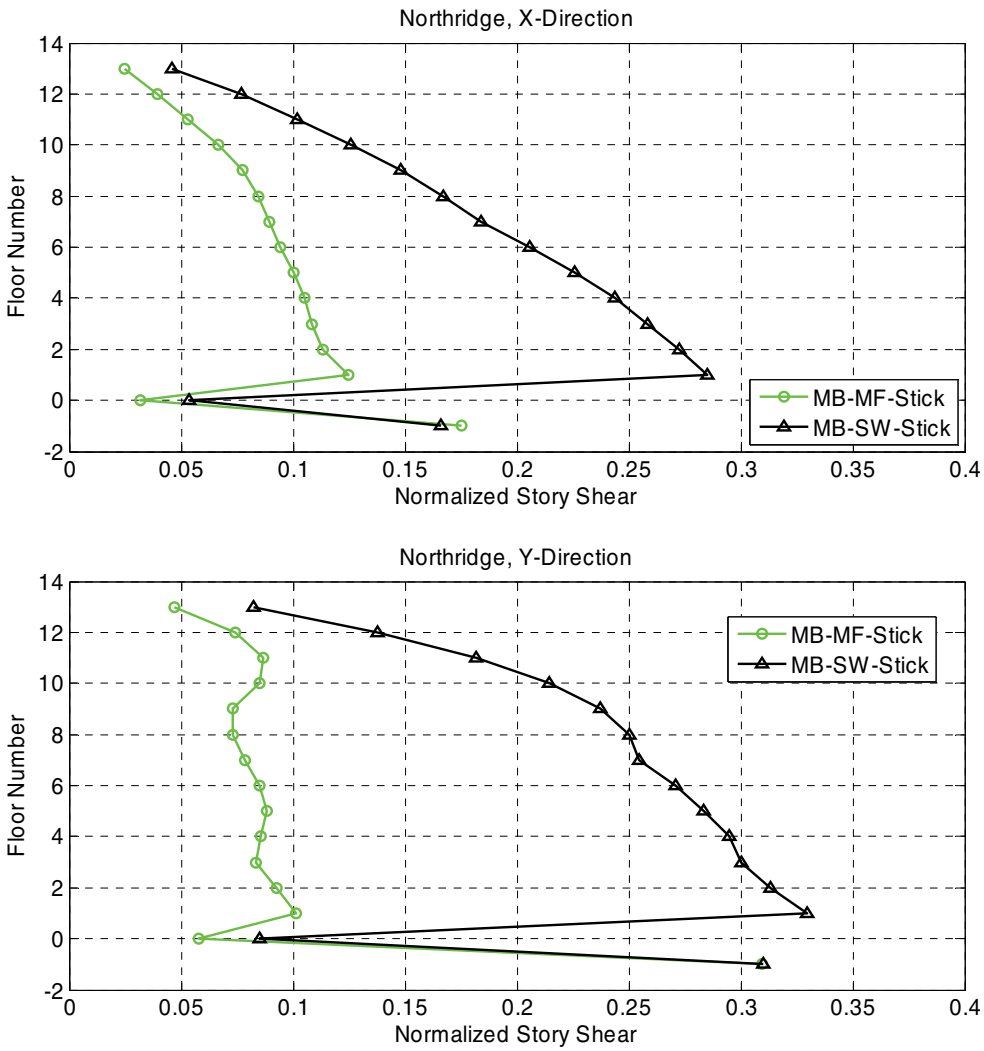

Figure B-46 Comparison of normalized story shear envelopes for the moment frame stick Model MB and the shear wall stick Model MB.

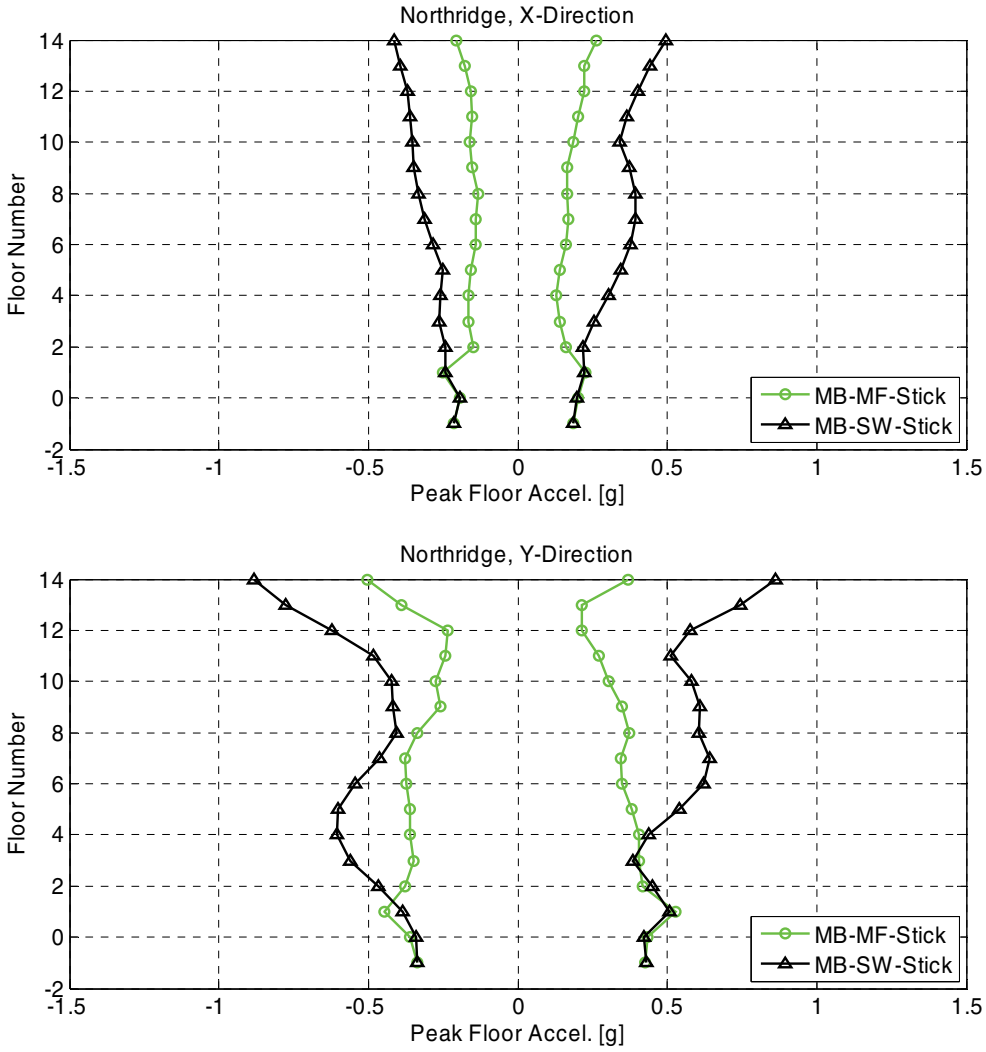

Figure B-47 Comparison of peak floor acceleration envelopes for the moment frame stick Model MB and the shear wall stick Model MB.

Appendix C
Walnut Creek Building Model Development

This appendix provides detailed information on the structural modeling and validation for the Walnut Creek building example application presented in Chapter 7.

C.1 Walnut Creek Building Model Development

Response history analysis of a three-dimensional model of the soil-foundation-structure system of the Walnut Creek building was performed using OpenSees, *Open System for Earthquake Engineering Simulation* (McKenna, 1997; OpenSees, 2011). Construction drawings of the building were made available for inspection through the auspices of CSMIP. The structural system and foundation configuration are described in Chapter 7.

Renderings of the Walnut Creek building configuration are provided in Figure C-1. The renderings include cut-away views showing details of the core wall and perimeter frame configurations, as well as the interior layout of a typical floor level. Figure C-2 provides plan views of the Walnut Creek building shear wall core at the foundation, first floor, and typical floor levels.

The building model is composed of the core walls and the perimeter frame. The framing elements were modeled with force-based beam-column elements using fiber sections (nonlinearBeamColumn elements in OpenSees). Two methods of modeling the core wall were considered: (1) use of four-node quadrilateral elements (Quad or Shell elements in OpenSees); and (2) use of horizontal and vertical boundary frame elements in combination with diagonal strut elements.

The core walls are 30.5 cm (12 in) thick. To account for the cracked section properties of the concrete walls, a multiplier on the theoretical uncracked stiffness must be applied. This multiplier should be dependent on the level of in-situ cracking of the shear wall and on the intensity of ground shaking, which would dictate the level of cracking that the wall will experience during an earthquake. A definitive ratio of cracked to uncracked stiffness in shear walls is not available in the literature. In the case of flexural stiffness, ASCE/SEI 41-06 (ASCE, 2007) suggests a multiplier of 0.8 for nominally uncracked walls, and a multiplier of 0.5 for cracked walls.

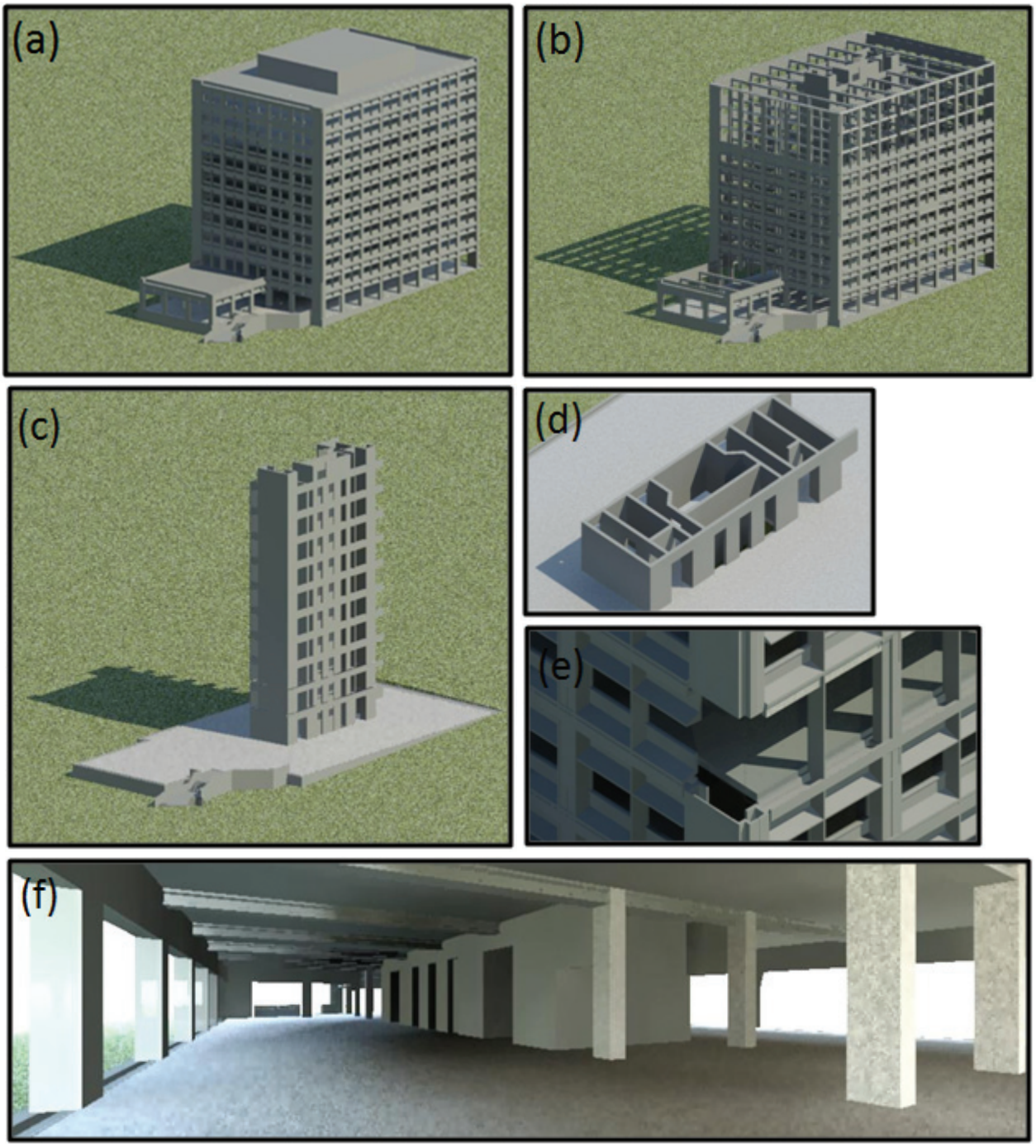

Figure C-1 Renderings of the Walnut Creek building, including cut-away views showing: (a) the exterior facade; (b) structural framing; (c) core wall elevations; (d) core wall layout; (e) details of the precast cladding system; and (f) interior layout of a typical floor level.

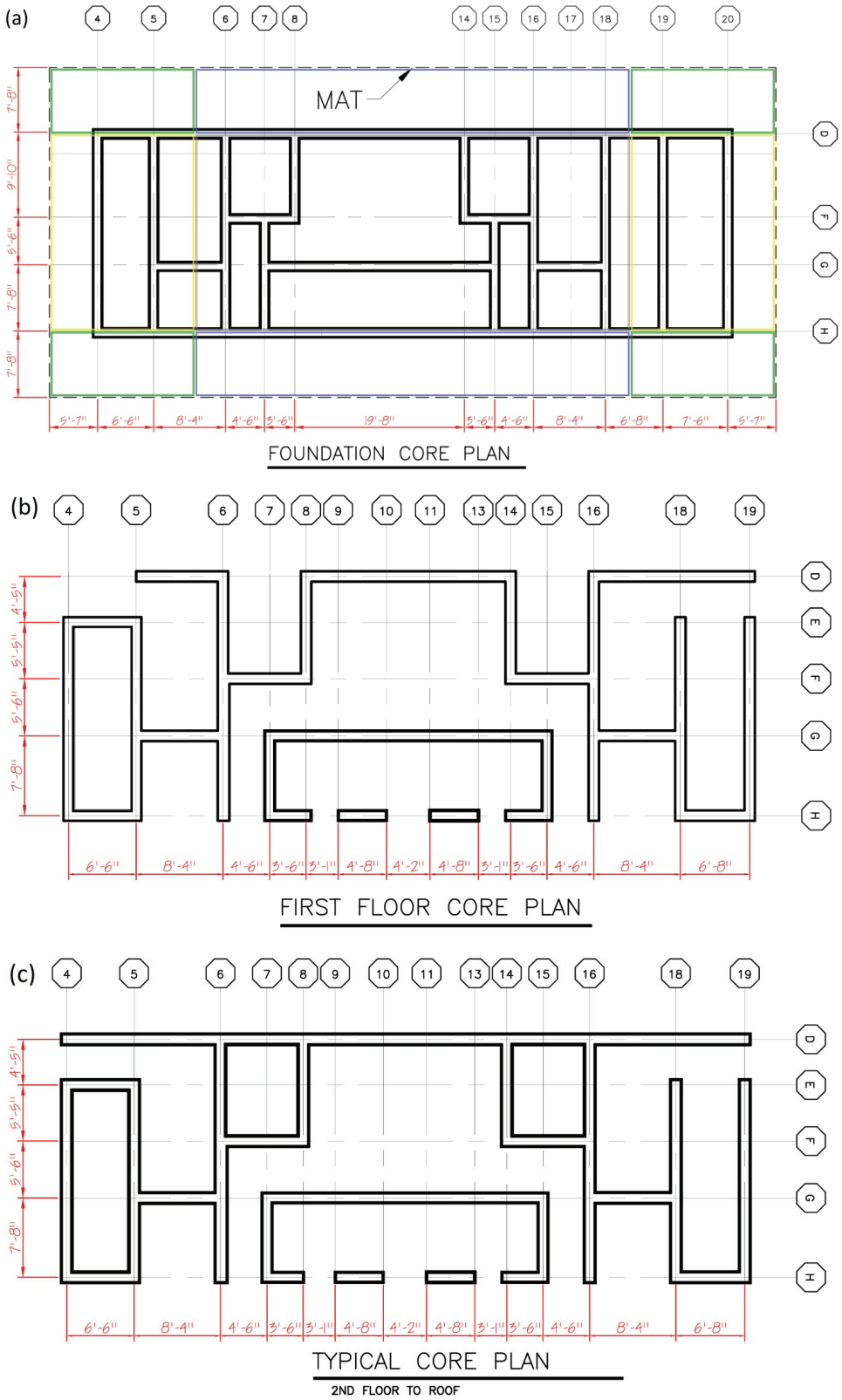

Figure C-2 Plan views of the Walnut Creek building shear wall core: (a) foundation level; (b) first floor; and (c) typical floor level.

In the case of shear stiffness, ASCE/SEI 41-06 suggests that the full (unreduced) value of G_c be used for both cracked and uncracked walls. The PEER/ATC-72-1 report (ATC, 2010) states that the cracked shear stiffness should be "substantially lower" than the uncracked shear stiffness, but there are limited test data available for use in quantifying this ratio. Considering that the level of shaking during the Loma Prieta earthquake was modest at the Walnut Creek site, a factor of 0.3 was used for the approximate ratio between cracked and uncracked concrete shear stiffness.

When using plane-stress Quad elements, the stiffness in the plane of each wall element is based on the input values of wall dimensions, material behavior, and Poisson's ratio, ν (taken as 0.25). The material chosen to represent the concrete was an elastic isotropic material (nDMaterial type called ElasticIsotropic in OpenSees). The out-of-plane stiffness of each wall element is not represented in this type of model. In the current version of OpenSees, Quad elements with an elastic isotropic material can only capture the elastic behavior of the wall elements. Also, the implementation of quadrilateral elements into a three-dimensional model can be complicated because of the difference in the number of degrees of freedom at the nodes.

Because of the above limitations, a combination of boundary frame elements and diagonal struts was also considered for modeling the core walls. This type of model permits modeling of inelastic behavior and out-of-plane behavior. In this type of model, the boundary elements are intended to represent the flexural characteristics of the wall, and diagonal compression-only truss elements are used to represent diagonal compression struts in the concrete, which carry a significant portion of the shear in the concrete walls. The beam and column elements were assigned high elastic axial stiffness. The beams were also given high flexural stiffness, but the columns were assigned finite stiffness based on a square section with dimensions equal to the wall thickness and an elastic modulus reduced to 30% of the gross value. The dimensions of the diagonal truss elements were also set equal to the wall thickness, and the elastic modulus was reduced to 30% of the gross value. Reductions in section stiffness were estimated to account for cracking as well as the reduced efficiency of the diagonal compression strut. Stiffness reductions were validated through comparisons between the modeled response and the measured response of the building to the 1989 Loma Prieta earthquake input motions.

Frame elements were composed of nonlinear beam-column elements with fiber sections representing inelastic behavior of both core and cover concrete materials (Concrete02 in OpenSees) and reinforcing steel materials (Steel02 in OpenSees). Shear and torsional flexibilities can be modeled as linear-elastic, and combined together into a single component model using the SectionAggregator approach in OpenSees. For expediency, however, the current model did not consider these modes of deformation. An expected yield strength of 462 MPa (67 ksi) was used for the

grade 60 steel (Melchers, 1999), with an initial stiffness of 20,000 GPa (29,000 ksi), and a post-yield hardening stiffness of 2% of the initial stiffness. A nominal concrete strength of 35 MPa (5.0 ksi) was modeled, and the expected strength was taken as 1.5 times the nominal strength (52 MPa, 7.5 ksi), in accordance with ASCE/SEI 41-06.

The three-dimensional OpenSees model is depicted in Figure C-3. To expedite the analyses and post-processing of results, the model was simplified to a two-dimensional model, also shown in Figure C-3. The two-dimensional model includes the framing elevations spanning the E-W direction, which was generated by collapsing the coordinates of the three-dimensional model into two dimensions, and constraining overlapping nodes to have the same horizontal displacement. The stiffness and damping properties of the soil are modeled using vertical and horizontal springs and dashpots, as described in Chapter 7. The soil springs are linear-elastic, and the dashpots are linear in all model versions. Foundation spring and dashpot locations are shown in Figure C-4. At the base of the mat, a grid of rigid beams was created to model the larger footprint of the mat foundation (since it is larger than the core wall in plan).

The calculated building mass included the mass of all structural elements (beams, columns, and slabs); 0.5 kPa (10 psf) for partitions; 0.6 kPa (12 psf) for mechanical, electrical, and plumbing components; and 25% of the design live load taken as 0.6 kPa (12 psf) for a design live load of 2.5 kPa (50 psf). The base of the core wall extends 4.3 m (14 feet) below the ground level, which includes a 3 m (10 feet) extension of the core wall, 1.2 m (4 feet) of mat foundation, and sand backfill. The mass of the core wall (including the sand) is also included in the calculated building mass. In the model, the mass of the slab and framing elements is assigned to the nodes, and the mass of each shear wall is distributed to the lower boundary beam.

Damping was modeled as 5% of critical Rayleigh damping, anchored to the first and third mode periods of the building. The damping was uniformly distributed to all structural elements, but degrees-of-freedom associated with foundation springs were excluded. This was necessary to avoid double counting of foundation damping because the soil-foundation model included dashpots at these degrees-of-freedom.

A preliminary evaluation of the relative accuracy of two-dimensional and three-dimensional models was performed. A comparison between modeled and recorded roof displacement histories is shown in Figure C-5. The data indicate that a significant improvement in accuracy is obtained using the three-dimensional representation of the numerical model. Although the three-dimensional model was more accurate in representing the amplitude of the recorded displacements, the two-dimensional model was a good match to the phasing, and was judged to be a reasonable approximation of the physical structure for the purposes of this study.

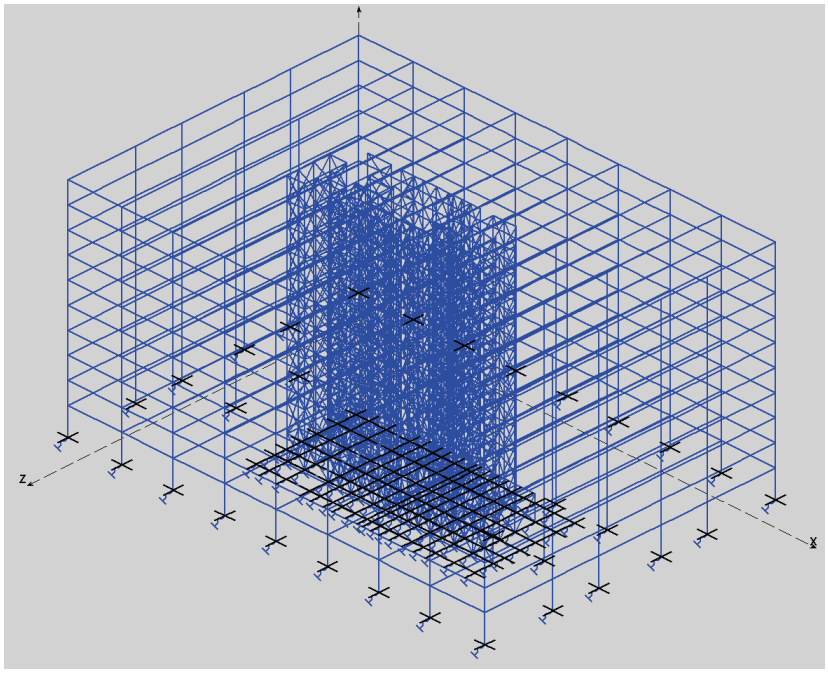

(a) Three-dimensional model

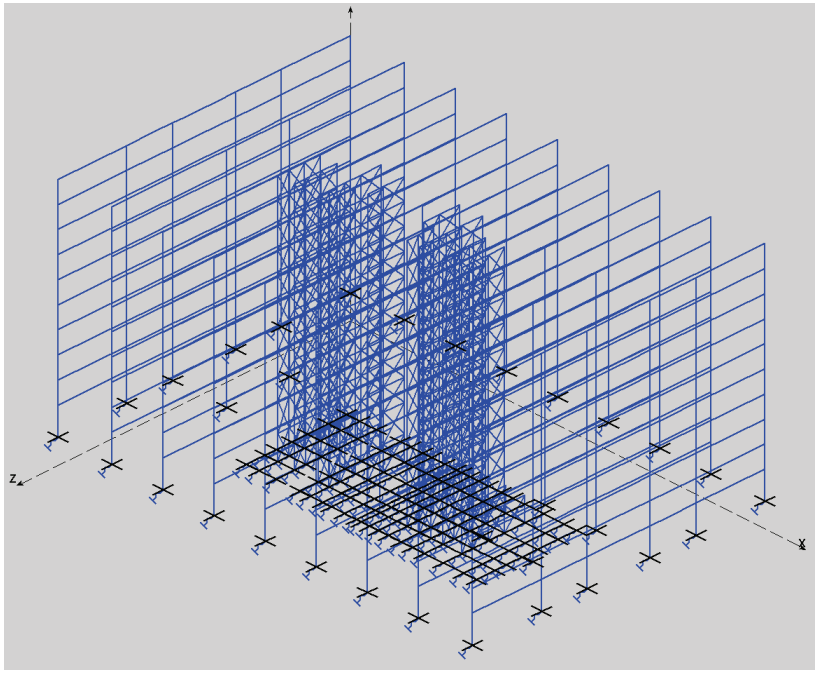

(b) Simplified two-dimensional model

Figure C-3 Illustrations of the Walnut Creek building OpenSees model: (a) three-dimensional model; and (b) simplified two-dimensional model.

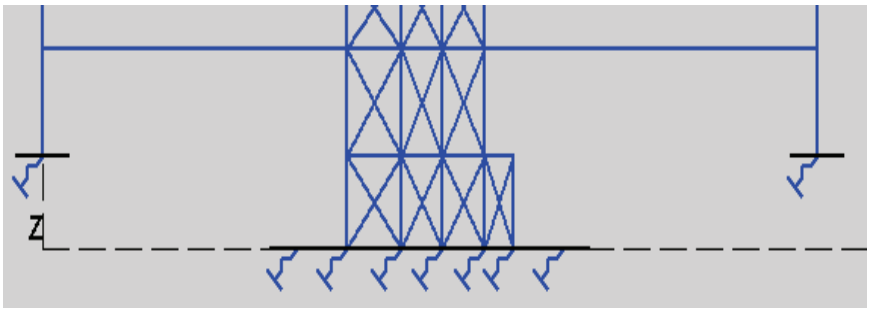

Figure C-4 Horizontal and vertical spring and dashpot locations for the Walnut Creek building model.

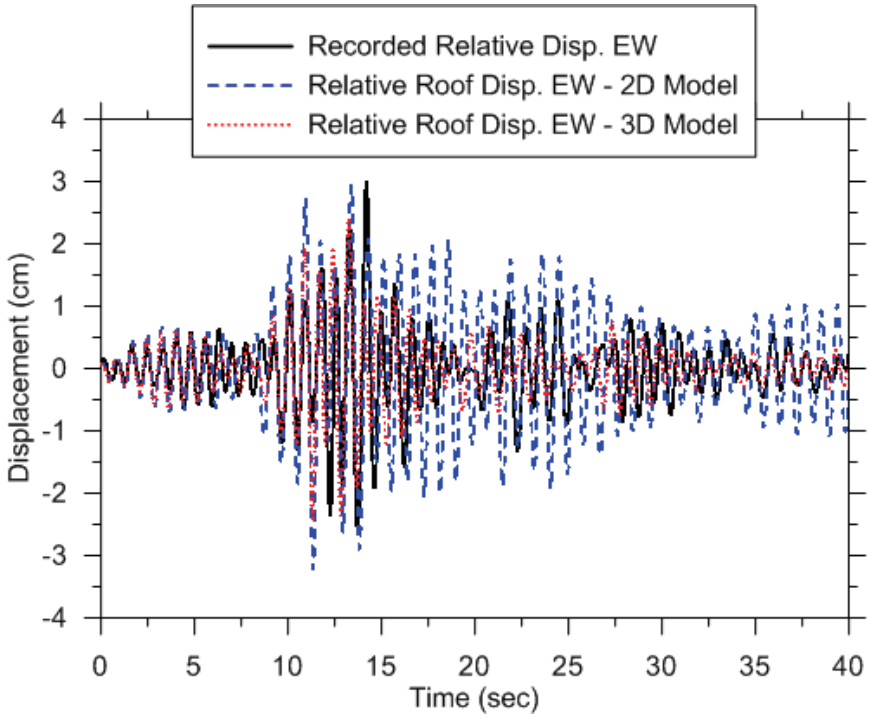

Figure C-5 Comparison of relative roof displacement histories from recorded data, two-dimensional (2D) model results, and three-dimensional (3D) model results for the Walnut Creek building.

C.2 Model Validation

Because of limitations in available site-characterization data, it was decided to pursue model validation, with a focus on matching overall stiffness and deformation characteristics, rather than full model calibration. As a result, only the effective stiffness of the wall elements (columns and struts) was adjusted. In addition, only the response in the E-W direction was evaluated.

Recorded motions from the 1989 Loma Prieta earthquake were used to validate the numerical model. The first step in the validation was a system identification to

compare the fundamental period of the system. The 5%-damped elastic response spectra were calculated for the ground-floor and roof level recorded accelerations, as shown in Figure C-6.

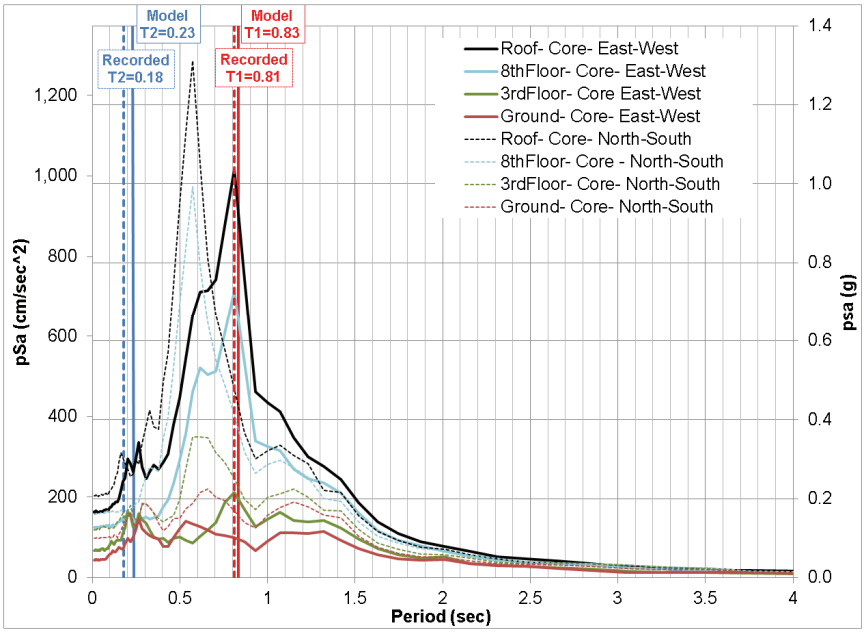

Figure C-6 5%-damped elastic response spectra of recorded motions for the Walnut Creek building in the 1989 Loma Prieta earthquake.

The first two periods identified for the E-W direction were 0.81sec and 0.18sec, respectively. The effective stiffness of the wall columns and diagonal struts were then modified so that the numerical model gave an accurate representation of the first two periods as well as the relative displacement history between the ground floor and the roof. An effective stiffness equal to 30% of the gross section properties resulted in the first two modeled periods equal to 0.83sec and 0.23sec, respectively.

Comparisons of modeled versus recorded acceleration and relative displacement histories for the Walnut Creek building in the 1989 Loma Prieta earthquake are shown in Figure C-7. The plots indicate that the numerical model is a reasonable representation of the dynamic response of the physical structure.

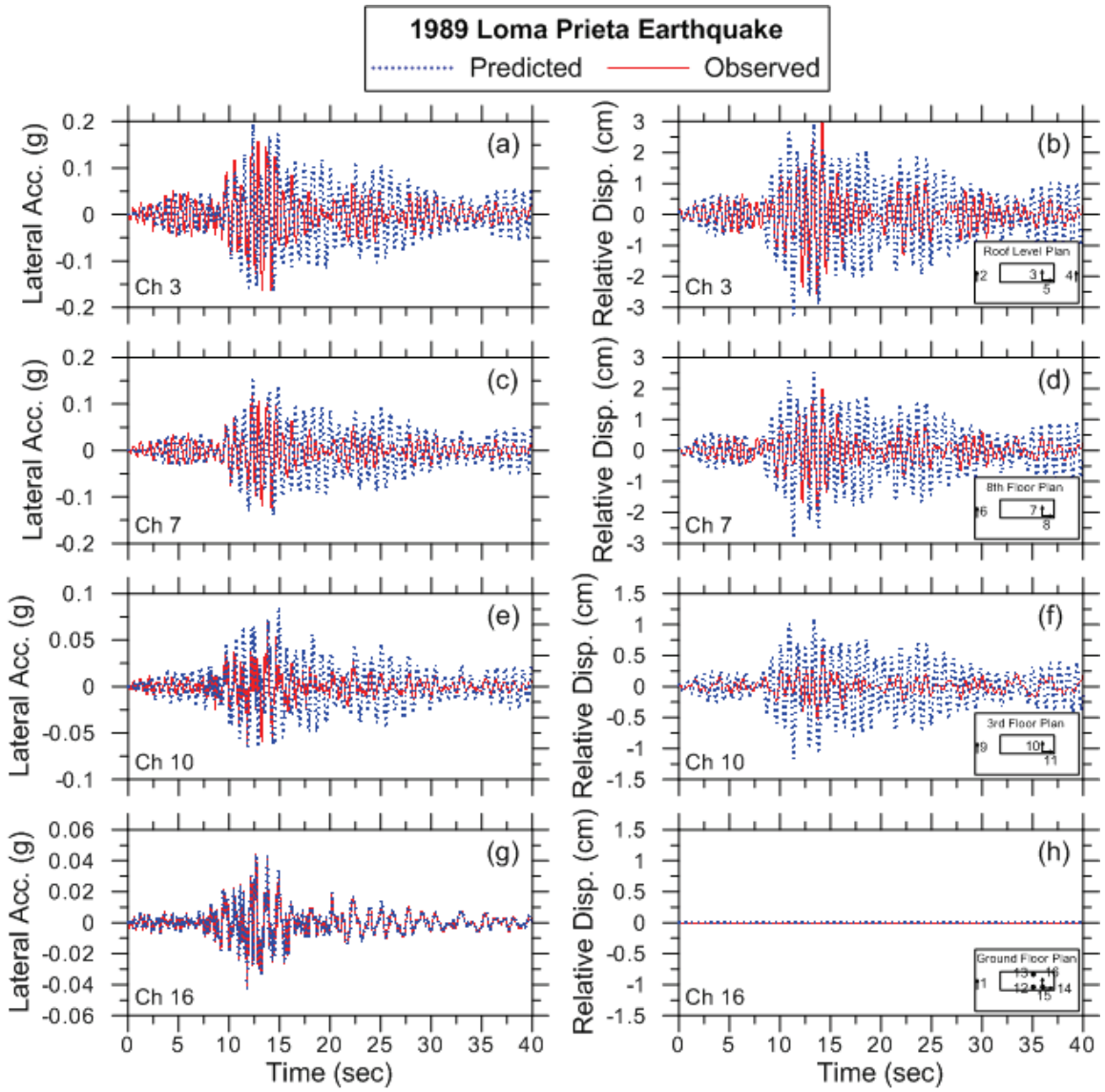

Figure C-7 Comparison of modeled versus recorded acceleration and relative displacement histories for the Walnut Creek building in the 1989 Loma Prieta earthquake: roof level (a) and (b); 8th floor (c) and (d); 3rd floor (e) and (f); and ground floor (g) and (h).

Comparisons of the modeled versus recorded maximum relative displacements and peak accelerations are shown in Figure C-8. Maximum relative displacements are somewhat over-predicted relative to observed maxima. The maximum story drift profile of the model is shown in Figure C-9.

Because two vertical instruments were present at the ground floor level, it is possible to compute base rocking (i.e., the difference between the two vertical recordings divided by the horizontal distance between them). As shown in Figure C-10, however, low frequency noise causes base rocking contributions evaluated in this manner to have unrealistic features. Accordingly, the vertical records were filtered using high-pass Butterworth filters with a corner frequency of 0.4 Hz.

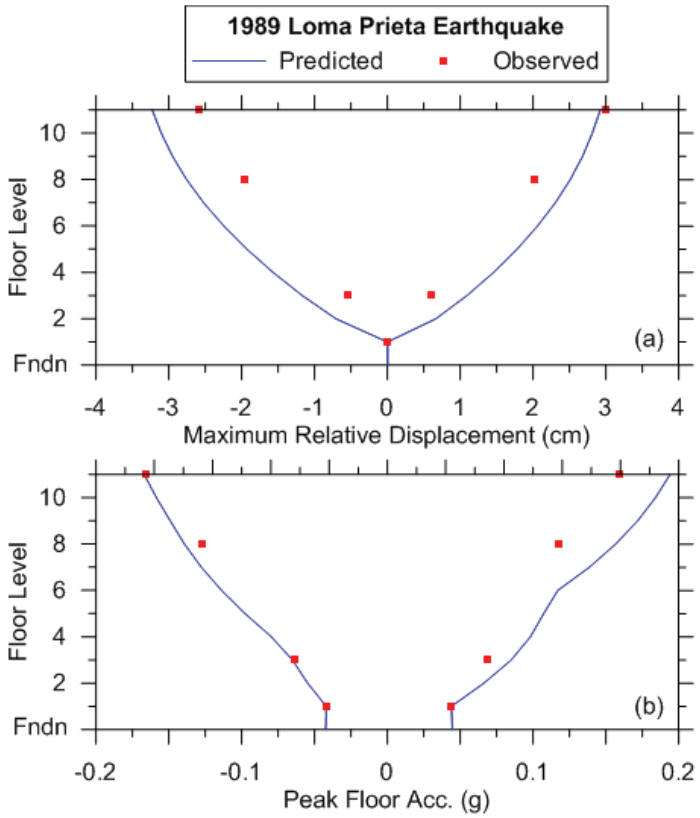

Figure C-8 Comparison of modeled versus recorded maximum relative displacements and peak accelerations for the Walnut Creek building in the 1989 Loma Prieta earthquake.

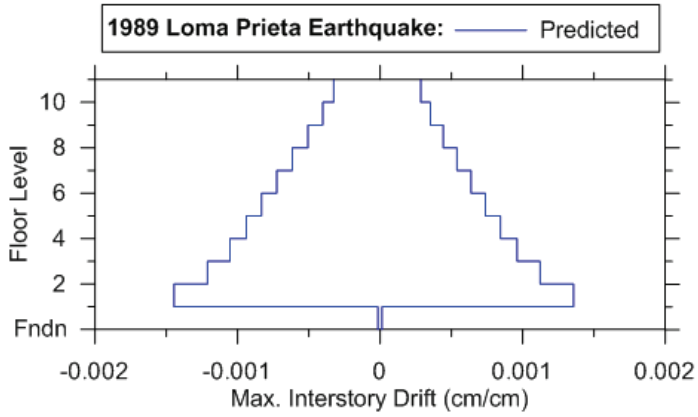

Figure C-9 Maximum story drift profile for the Walnut Creek building model subjected to the 1989 Loma Prieta earthquake.

A corner frequency of 0.4 Hz was selected through examination of displacement histories with different corner frequencies shown in Figure C-10, following the recommendations of Bommer and Boore (2005), which results in the minimum filter corner that removes the low frequency noise features in the rocking displacement history. The resulting comparison between modeled and recorded roof displacement due to base rotation of the Walnut Creek building is presented in Chapter 7.

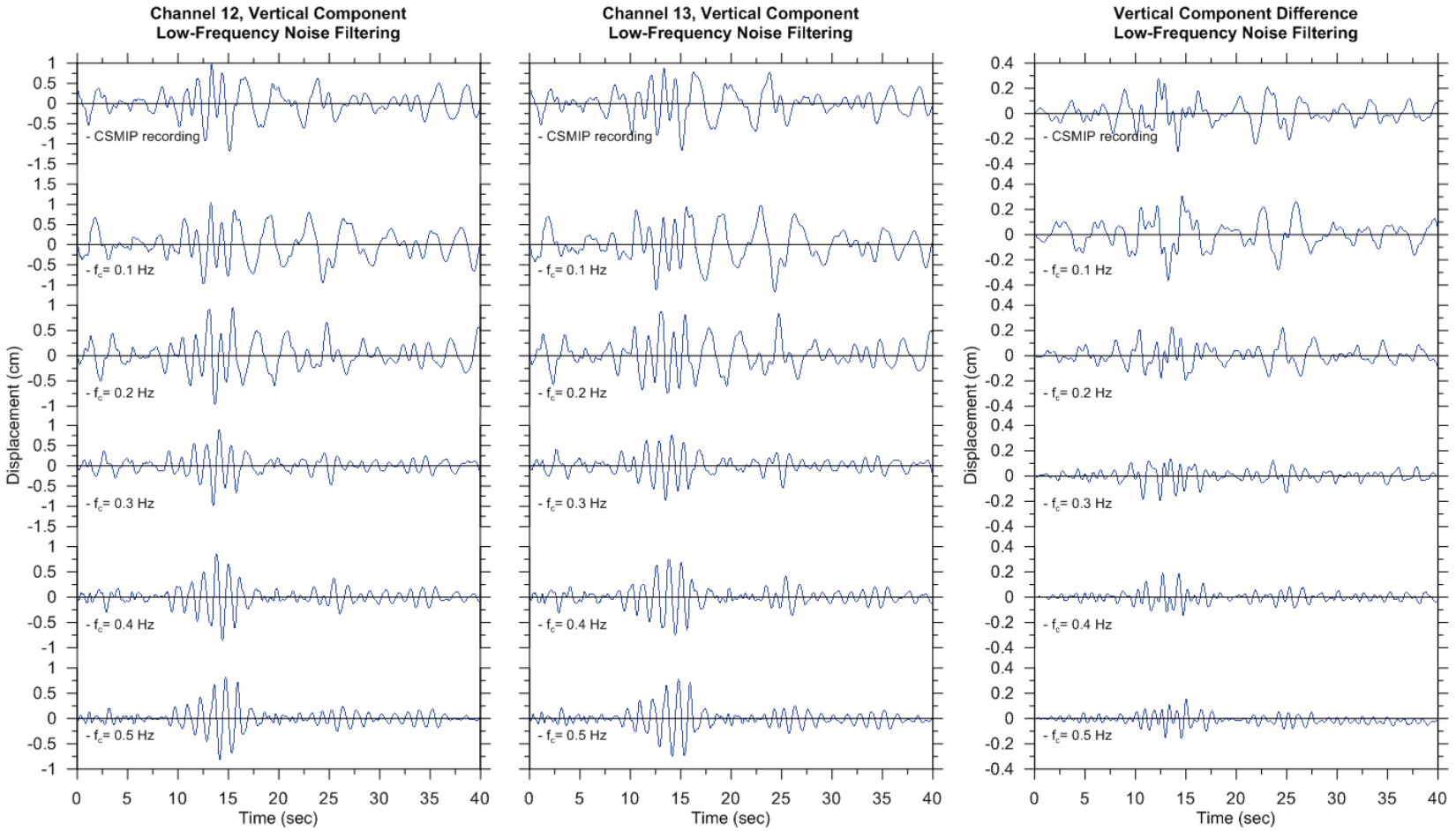

Figure C-10 High-pass filtering of vertical motions at base level showing the effects of corner frequency on displacement and rocking histories.

Symbols

A	footing area, m^2 (ft^2)
A_c	footing-soil contact area required to support vertical and shear loads, m^2 (ft^2)
a_0	dimensionless frequency for footings
a_0^k	dimensionless frequency related to base contact area
a_0^p	dimensionless frequency for piles
B	foundation half-width (small plan dimension), m (ft)
B_e^A	half-dimension of an equivalent square footing matching the area of the actual footing, m (ft)
B_e^I	half-dimension of an equivalent square footing matching the moment of inertia of the actual footing, m (ft)
c'	soil shear strength, kN/m^2 ($kips/ft^2$)
c_j	dashpot coefficient for translation along the j-axis, kN-sec/m (kipf-sec/ft)
c_{jj}	dashpot coefficient for rotation about the j-axis, kN-m/rad (kipf-ft/rad)
c_j^p	dashpot coefficient for single pile, kN-m/rad (kipf-ft/rad)
c_z^i	dashpot intensity, $kN\text{-}sec/m^3$ ($kipf\text{-}sec/ft^3$)
C_r	OpenSees parameter for BNWF models
C_s	seismic coefficient
$\tilde{C}_s$	seismic coefficient at an elongated period $\tilde{T}$
d	pile diameter, m (ft)
D	embedment depth, m (ft)
D_L	internal node spacing, m (ft)
D_r	relative density
d_w	height of effective side wall contact of embedded foundation, m (ft)
E_f	foundation Young's modulus, MPa (ksi)
E_s	Young's modulus of the soil, MPa (ksi)
E_p	Young's modulus of a pile, MPa (ksi)
F	force, kN (kips)

f_E fundamental frequency (Hz)

f_L limiting frequency (Hz)

FS_v vertical factor of safety

G soil shear modulus, kPa (ksi)

G_0 maximum soil shear modulus (at small strains), kPa (ksi)

G_a soil shear modulus at atmospheric pressure, kPa (ksi)

h height of the center of mass for the first-mode shape, m (ft)

H_u kinematic transfer function

I_i area moment of inertia of soil-foundation contact, m^4 (ft^4); i denotes the axis about which the surface is taken

j index denoting modes of translation displacement or rotation

J_t polar moment of inertia of soil-foundation contact surface, m^4 (ft^4)

k spring stiffness, translation, kN/m (kips/ft), and rotation, kN-m/rad (kip-ft/rad)

k_j spring stiffness, translation, along the j-axis, kN/m (kips/ft)

K_j foundation static stiffness for mode j, translation, kN/m (kips/ft), and rotation, kN-m/rad (kip-ft/rad)

$\bar{k}_j$ complex-valued impedance function for mode j, translation, N/m (lbf/ft), and rotation, N-m/rad (lbf-ft/rad)

k_{jj} spring stiffness, rotation, about the j-axis, kN-m/rad (kip-ft/rad)

k_j^G efficiency factor for a group of piles

k_j^p spring stiffness for a single pile, kN/m (kips/ft)

K_j^p pile static stiffness for mode j, kN/m (kips/ft)

k_z^i stiffness intensity (coefficient of subgrade reaction), kN/m^3 ($kips/ft^3$)

L foundation half-length (large plan dimension), m (ft)

L_a active pile length (typically in lateral mode, $< L_p$), m (ft)

l_e spring spacing, m (ft)

L_{end} end region length of foundation with increase stiffness, m (ft)

L_p pile length, m (ft)

m mass, Mg (lbm, kipm)

$\bar{M}$ first mode participating mass, Mg (lbm, kipm)

n, n_s, n_x, n_{yy} exponents related with foundation damping

p-x horizontal passive load-displacement behavior against side of footing

q spring force, kN (kips)

q_0 upper limit of the linear elastic region, kPa (ksi)

q_{ult} ultimate load, kPa (ksi)

q-z vertical load-displacement curve

Q vertical load on footing, kN (kips)

Q_{ULT} ultimate vertical load, kN (kips)

R_c dashpot intensities scalar

R_e end length ratio

R_k spring stiffness intensities scalar

R_v rebound ratio

r, r_f foundation radius, m (ft)

s spring deflection, m (ft)

s_0 displacement at load q_0, m (ft)

s_{50} displacement at which 50% of the ultimate load is mobilized, m (ft)

S spring spacing, m (ft)

S_a fixed-base spectral acceleration, m/s^2, (ft/s^2), g

$\tilde{S}_a$ spectral acceleration for a flexible-base structure, m/sec^2, (ft/sec^2), g

S_a^e equivalent spectral acceleration, m/sec^2 (ft/sec^2), g

$S_{a\text{-}FIM}$ fixed-base spectral acceleration with FIM effects, m/s^2, (ft/s^2), g

S_d spectral displacement, m (ft)

S_d^e equivalent spectral displacement, m (ft)

T undamped natural vibration period, sec

$\tilde{T}$ flexible-base period, sec

t_f foundation thickness, m (ft)

T_p predominant period of ground motion, sec

T_x, T_{yy} fictitious vibration periods, calculated as if the only source of the vibration was translation or rotation, sec

$\tilde{T}/T$ period lengthening ratio due to soil-structure interaction

t-x horizontal shear-sliding curve at the base of a footing

u_f horizontal deflection amount in a SDOF structure due to base shear force F, cm (in)

u_{FIM} foundation input motion, acceleration, m/sec^2; velocity, m/sec; or displacement, m

u_g free-field ground motion, acceleration, m/sec^2; velocity, m/sec; or displacement, m

V base shear force, kN (kips)

V_{app} apparent wave propagation velocity, m/sec (ft/sec)

V_s shear wave velocity in a homogeneous isotropic half-space; measured free-field shear wave velocity, m/sec (ft/sec)

$V_s(z)$ measured free-field shear wave velocity at depth z, m/sec (ft/sec)

$V_{s,\,avg}$ average effective profile velocity over depth z_p, m/sec (ft/sec)

$V_{s,\,F}$ overburden-corrected shear wave velocity below foundation, m/sec (ft/sec)

V_{ULT} ultimate vertical load, kN (kips)

$\bar{W}$ effective weight of structure, kN (kips)

w_{pj}, w_{sj}, w_{bj} weight factors, for the pile, soil, and pile tip stiffness contributions for mode j

z depth, m (ft)

z_p effective profile depth, m (ft)

z_w depth to centroid of effective sidewall contact, m (ft)

α_j dynamic (frequency-dependent) stiffness modifier for surface foundation for mode j

α_j^p dynamic (frequency-dependent) stiffness modifier for single pile for mode j

α_v vertical angle of incident waves

β_0 flexible-base system damping ratio

β_f foundation damping ratio

β_i fixed-base structural damping ratio

β_j dynamic damping ratio for mode j

β_j^p pile dynamic damping ratio for mode j

β_p pile damping ratio

β_{rj} radiation damping ratio for mode j

β_s soil hysteretic damping ratio

Δ deflection, m (ft)

$\tilde{\Delta}$ total deflection with respect to free-field at the top of a SDOF structure, cm (in)

Δ_{max} maximum earthquake-induced displacement in a structural member, cm (in)

$\tilde{\Delta}_{max}$ maximum earthquake-induced displacement at the top of a structure, cm (in)

Δ_y yield displacement of a structural member, cm (in)

$\tilde{\Delta}_y$ yield displacement at the top of a structure, cm (in)

$\Delta\sigma_v$ increment of vertical stress at depth z from the structural weight, kPa (ksi)

δ_j dimensionless modulus of subgrade reaction

η_j, η_{jj} embedment correction factor for rigid footing spring constants for mode j

θ rotation deflection amount in a SDOF structure due to base moment (rad)

$\theta_{elastic}$ elastic rotation limit (rad)

κ_a dimensionless parameter accounting for effects of incoherence from wave passage and stochastic processes, as well as Fourier amplitude variability

Λ dimensionless parameter for active pile length

λL dimensionless pile length parameter

μ dimensionless constant exponent for active pile length

μ_s, μ global structural system ductility demand, individual structural member ductility demand, respectively

ν soil Poisson's ratio

ν_f foundation Poisson's ratio

ρ_p pile mass density, Mg/m^3 (lbm/ft^3)

ρ_s soil mass density, Mg/m^3 (lbm/ft^3)

σ_m' effective confining stress, kPa (ksi)

σ'_{v0} effective stress from the self-weight of the soil, kPa (ksi)

ϕ' angle of internal friction, rad (deg)

ϕ_j loss angle due to damping, rad (deg)

χ_j dimensionless constant for vibration for mode j

Ψ soil-to-foundation stiffness ratio, representing the flexibility of the foundation

Ω	dimensionless pile tip stiffness
ω	undamped natural vibration frequency (rad/sec)

References

Abrahamson, N.A., 1985, *Estimation of Seismic Wave Coherency and Rupture Velocity Using the SMART 1 Strong-Motion Array Recordings*, Report No. UCB/EERC-85/02, Earthquake Engineering Research Center, University of California, Berkeley, California.

Abrahamson, N.A., 1992, *Spatial Variation of Earthquake Ground Motion for Application to Soil-Structure Interaction*, Report. No. EPRI TR-100463, Electrical Power Research Institute, Palo Alto, California.

Abrahamson, N.A., Schneider, J.F., and Stepp, J.C., 1991, "Empirical spatial coherency functions for application to soil-structure interaction analyses," *Earthquake Spectra*, Vol. 7, No. 1, pp. 1-27.

ACI, 2008, *Building Code Requirements for Structural Concrete*, ACI 318-08, American Concrete Institute, Farmington Hills, Michigan.

Allotey, N., and Naggar, M.H.E., 2003, "Analytical moment–rotation curves for rigid foundations based on a Winkler model," *Soil Dynamics and Earthquake Engineering*, Vol. 23, pp. 367-381.

Allotey, N., and Naggar, M.H.E., 2007, "An investigation into the Winkler modeling of the cyclic response of rigid footings," *Soil Dynamics and Earthquake Engineering*, Vol. 28, pp. 44-57.

Anoyatis, G., and Mylonakis, G., 2012, "Dynamic winkler modulus for axially loaded piles," *Geotechnique*, Vol. 62, pp. 521-536.

Ancheta, T.D., 2010, *Engineering Characterization of Spatially Variable Ground Motions*, Ph.D. Dissertation, University of California, Los Angeles, California.

Ancheta, T.D., Stewart, J.P., and Abrahamson, N.A., 2011, "Engineering characterization of earthquake ground motion coherency and amplitude variability," *Proceedings*, 4th International Symposium on Effects of Surface Geology on Seismic Motion, IASPEI / IAEE, University of California Santa Barbara, California.

Andrus, R.D., Stokoe, K.H. II, and Juang, C.H., 2004. "Guide for shear-wave-based liquefaction potential evaluation," *Earthquake Spectra*, Vol. 20, No. 2, pp. 285-308.

Apsel, R.J., and Luco, J.E., 1987, "Impedance functions for foundations embedded in a layered medium: an integral equation approach," *Earthquake Engineering and Structural Dynamics*, Vol. 15, No. 2, pp. 213-231.

Aviles, J., and Perez-Rocha, L.E., 1996, "Evaluation of interaction effects on system period and the system damping due to foundation embedment and layer depth," *Soil Dynamics and Earthquake Engineering*, Vol. 15, pp. 11-27.

ASCE, 2000, *Seismic Analysis of Safety-Related Nuclear Structures and Commentary*, ASCE 4-98, American Society of Civil Engineers, Reston, Virginia.

ASCE, 2005, *Seismic Design Criteria for Structures, Systems, and Components in Nuclear Facilities,* ASCE/SEI 43-05, American Society of Civil Engineers, Reston, Virginia.

ASCE, 2007, *Seismic Rehabilitation of Existing Buildings*, ASCE/SEI 41-06, American Society of Civil Engineers, Reston, Virginia.

ASCE, 2010, *Minimum Design Loads for Buildings and Other Structures,* ASCE/SEI 7-10, American Society of Civil Engineers, Reston, Virginia.

ASCE, 2013, *Seismic Evaluation and Retrofit of Existing Buildings*, ASCE/SEI 41-13, American Society of Civil Engineers, Reston, Virginia.

ASCE, (in preparation), *Seismic Analysis of Safety-Related Nuclear Structures and Commentary*, ASCE 4, Reston, Virginia.

ATC, 1996, *Seismic Evaluation and Retrofit of Concrete Buildings*, ATC-40 Report, Applied Technology Council, Redwood City, California.

ATC, 2010, *Modeling and Acceptance Criteria for Seismic Design and Analysis of Tall Buildings*, PEER/ATC-72-1 Report, prepared by Applied Technology Council in cooperation with Pacific Earthquake Engineering Research Center, Redwood City, California.

Barghouthi, A.F., 1984, *Pile Response to Seismic Waves*, Ph.D. Dissertation, University of Wisconsin, Madison, Wisconsin.

Barkan, D.D., 1962, *Dynamics of bases and foundations*, McGraw-Hill, New York, New York.

Bielak, J., 1975, "Dynamic behavior of structures with embedded foundations," *Earthquake Engineering and Structural Dynamics*, Vol. 3, pp. 259-274.

Bielak, J., 1976, "Modal analysis for building-soil interaction," *Journal of Engineering Mechanics*, Vol. 102, pp. 771-786.

Blaney, G.W., Kausel, E., and Roesset, J.M., 1975, "Dynamic stiffness of piles," *Proceedings*, 2nd International Conference on Numerical Methods in Geomechanics, Virginia Polytechnical Institute and State University, Blacksburg, Virginia, pp. 1010-1012.

Boore, D.M., and Boomer, J.J., 2005, "Processing of strong-motion accelerograms: needs, options and consequences," *Soil Dynamics and Earthquake Engineering*, Vol. 25, pp. 93-115.

Borja, W.I., and Wu, W.H., 1994, "Vibration of foundations on incompressible soils with no elastic region," *Journal of Geotechnical Engineering*, Vol. 120, No. 9, pp. 1570-1592.

Boulanger, R.W., Curras, C.J., Kutter, B.L., Wilson, D.W., and Abghari, A., 1999, "Seismic soil-pile-structure interaction experiments and analyses," *Journal Geotechnical and Geoenvironmental Engineering*, Vol. 125, pp. 750-759.

CESMD, 2011, "CESMD – A Cooperative Effort," Center for Engineering Strong Motion Data (CESMD), accessed in 2011, http://www.strongmotioncenter .org.

Chang, B.J., Thomas, J.M., Raychowdhury, P., Gajan, S., Kutter, B.L., and Hutchinson, T.C., 2007, *Soil-Foundation-Structure Interaction: Shallow Foundations*, SSRP 07/24, University of California, San Diego, California.

Chatzigogos, C.T., Pecker, A., and Salencon, J., 2009, "Macroelement modeling of shallow foundations," *Soil Dynamics and Earthquake Engineering*, Vol. 29, pp. 765-781.

Chopra, A.K., and Goel, R.K., 1999, "Capacity-demand-diagram methods based on inelastic design spectrum," *Earthquake Spectra*, Vol. 15, No. 4, pp. 637-656.

Chopra, A., and Yim S.C., 1985, "Simplified earthquake analysis of structures with foundation uplift," *Journal of Structural Engineering*, Vol. 111, No. 4, pp. 906-930.

Ciampoli, M., and Pinto, P.E., 1995, "Effects of soil-structure interaction on inelastic seismic response of bridge piers," *Journal of Structural Engineering*, Vol. 121, No. 5, pp. 806-814.

Clough, R.W., and Penzien, J., 1993, *Dynamics of Structures*, McGraw Hill, New York.

Coduto, D.P., 1994, *Geotechnical Engineering: Principles and Practices*, 2nd Edition, Prentice-Hall, Upper Saddle River, New Jersey.

Cox, W., Reese, L., and Grubbs, B., 1974, "Field testing of laterally loaded piles in sand," *Proceedings*, Offshore Technology Conference, Houston, Texas, Paper 2079.

Cremer, C., Pecker, A., and Davenne, L., 2001, "Cyclic macro-element of soil structure interaction: Material and geometrical nonlinearities," *International Journal of Numerical and Analytical Methods in Geomechanics*, Vol. 25, pp. 1257-1284.

Crouse, C.B., 2001, "Commentary on soil-structure interaction in U.S. seismic provisions," *Proceedings*, 2nd UJNR Workshop on Soil-Structure Interaction, Tsukuba, Japan.

Crouse, C.B., Hushmand, B., Luco, J.E., and Wong, H.L., 1990, "Foundation impedance functions: Theory versus experiment," *Journal of Geotechnical Engineering*, Vol. 116, No. 3, pp. 432-449.

Darendeli, 2001, *Development of a New Family of Normalized Modulus Reduction and Material Damping Curves*, Ph.D. Dissertation, University of Texas at Austin, Texas.

Day, S.M., 1978, "Seismic response of embedded foundations," *Preprints of Conference Proceedings of ASCE Convention and Exposition, Chicago, IL*, Preprint No. 3450, American Society of Civil Engineers, New York, New York.

De Barros, F.C.P., and Luco, J.E., 1995, "Identification of foundation impedance functions and soil properties from vibration tests of the Hualien containment model," *Soil Dynamics and Earthquake Engineering*, Vol. 14, pp. 229-248.

Dobry, R., and Gazetas, G., 1988, "Simple method for dynamic stiffness and damping of floating pile groups," *Geotechnique*, Vol. 38, No. 4, pp. 557-574.

Dobry, R., Gazetas, G., and Stokoe, K.H. II, 1986, "Dynamic response of arbitrarily shaped foundations: Experimental verification," *Journal of Geotechnical Engineering*, Vol. 112, No. 2, pp. 136-154.

Dobry, R., Vicente, E., O'Rourke, M.J., and Roesset, J.M., 1982, "Horizontal stiffness and damping of single piles," *Journal of the Geotechnical Engineering Division*, Vol. 108, No. 3, pp. 439-459.

El-Naggar, M.H., and Novak, M., 1994, "Non-linear model for dynamic axial pile response," *Journal of Geotechnical Engineering*, Vol. 120, No. 2, pp. 308-329.

El-Naggar, M.H., and Novak M., 1995, "Nonlinear analysis for dynamic lateral pile response," *Soil Dynamics and Earthquake Engineering*, Vol. 15, No. 4, pp. 233-244.

EPRI, 2007, *Hard-Rock Coherency Functions Based on the Pinyon Flat Array Data*, ADAMS Accession No. ML071980104, Electric Power Research Institute, Palo Alto, California.

Erden, S.M., 1974, *Influence of Shape and Embedment on Dynamic Foundation Response*, Ph.D. Dissertation, University of Massachusetts, Amherst, Massachusetts.

Fadum, R.E., 1948, "Influence values for estimating stresses in elastic foundations," *Proceedings*, 2nd International Conference on Soil Mechanics and Foundation Engineering, Rotterdam, Netherlands, Vol. 3, pp. 77-84.

Fan, K., Gazetas, G., Kaynia, A., and Kausal, E., 1991, "Kinematic seismic response of single piles and pile groups," *Journal of Geotechnical Engineering*, Vol. 117, No. 12, pp. 1860-1879.

FEMA, 1997, *NEHRP Guidelines for the Seismic Rehabilitation of Buildings*, FEMA 273, prepared by the Applied Technology Council and the Building Seismic Safety Council for the Federal Emergency Management Agency, Washington, D.C.

FEMA, 2000, *Prestandard and Commentary for the Seismic Rehabilitation of Buildings*, FEMA 356, prepared by the American Society of Civil Engineers for Federal Emergency Management Agency, Washington, D.C.

FEMA, 2004a, *NEHRP Recommended Provisions for Seismic Regulations for New Buildings and Other Structures*, *Part 1: Provisions*, FEMA 450-1/2003 Edition, prepared by the Building Seismic Safety Council for the Federal Emergency Management Agency, Washington, D.C.

FEMA, 2004b, *NEHRP Recommended Provisions for Seismic Regulations for New Buildings and Other Structures*, *Part 2: Commentary*, FEMA 450-2/2003 Edition, prepared by the Building Seismic Safety Council for the Federal Emergency Management Agency, Washington, D.C.

FEMA, 2005, *Improvement of Nonlinear Static Seismic Analysis Procedures*, FEMA 440, prepared by the Applied Technology Council for Federal Emergency Management Agency, Washington, D.C.

FEMA, 2009, *NEHRP Recommended Seismic Provisions for New Buildings and Other Structures*, FEMA P-750/2009 Edition, prepared by the Building Seismic Safety Council of the National Institute of Building Sciences for the Federal Emergency Management Agency, Washington, D.C.

Fleming, W.G.K., Weltman, A.J., Randolph, M.F., and Elson, W.K., 1992, *Piling Engineering*, 2nd Edition, John Wiley & Sons, New York, New York.

Flores-Berrones, R., and Whitman, R.V., 1982, "Seismic response of end-bearing piles," *Journal of the Geotechnical Engineering Division*, Vol. 108, No. 4, pp. 554-569.

Fumal, T.E., and Tinsley, J.C., 1985, "Mapping shear wave velocities of near surface geologic materials, in evaluating earthquake hazards in the Los Angeles region-an earth-science perspective," *USGS Survey Professional Paper 1360*, pp. 101-126.

Gadre, A., and Dobry, R., 1998, "Lateral cyclic loading centrifuge tests on square embedded footings," *Journal Geotechnical and Geoenvironmental Engineering*, Vol. 124, No. 11, pp. 1128-1138.

Gajan S., 2006, *Physical and Numerical Modeling of Nonlinear Cyclic Load-Deformation Behavior of Shallow Foundations Supporting Rocking Shear Walls*, Ph.D. Dissertation, University of California, Davis, California.

Gajan, S., Hutchinson, T.C., Kutter, B.L., Raychowdhury, P., Ugalde, J.A., and Stewart, J.P., 2008, *Numerical models for analysis and performance-based design of shallow foundations subject to seismic loading*, Report No. PEER-2007/04, Pacific Earthquake Engineering Research Center, University of California, Berkeley, California.

Gajan, S., and Kutter, B.L., 2008, "Capacity, settlement, and energy dissipation of shallow footings subjected to rocking," *Journal Geotechnical and Geoenvironmental Engineering*, Vol. 134, No. 8, pp. 1129-1141.

Gajan, S., and Kutter, B.L., 2009, "A contact interface model for shallow foundations subjected to combined cyclic loading," *Journal Geotechnical and Geoenvironmental Engineering*, Vol. 135, pp. 407-419.

Gajan, S., Phalen, J.D., and Kutter, B.L., 2003, *Soil-Foundation-Structure Interaction: Shallow Foundations*, Report No. UCD/CGMDR-03/01, Center for Geotechnical Modeling, University of California, Davis, California.

Gajan, S., Raychowdhury, P., Hutchinson, T.C., Kutter, B.L., and Stewart, J.P., 2010, "Application and validation of practical tools for nonlinear soil-foundation interaction analysis," *Earthquake Spectra*, Vol. 26, No. 1, pp. 111-129.

Gazetas, G., 1991, "Foundation vibrations," *Foundation Engineering Handbook*, 2nd Edition, Chapter 15, H.-Y. Fang, ed., Chapman and Hall, New York, New York.

Gazetas, G., 2006, "Seismic design of foundations and soil-structure interaction,"*Proceedings*, First European Conference on Earthquake Engineering and Seismology, Geneva, Switzerland.

Gazetas, G., and Dobry, R., 1984a, "Horizontal response of piles in layered soil," *Journal of the Geotechnical Engineering Division*, Vol. 110, No. 1, pp. 20-40.

Gazetas, G., and Dobry, R., 1984b, "Simple radiation damping model for piles and footings," *Journal of the Geotechnical Engineering Division*, Vol. 110, No. 6, pp. 937-956.

Gazetas, G., and Stokoe, K.H. II, 1991, "Free vibration of embedded foundations: Theory versus experiment," *Journal of Geotechnical Engineering*, Vol. 117, No. 9, pp. 1382-1401.

Ghosh, B., and Madabhushi, S.P.G., 2007. "Centrifuge modelling of seismic soil structure interaction effects." *Nuclear Engineering and Design*, Vol. 237, No. 8, pp. 887-896.

Givens, M.J., 2013, *Dynamic Soil-Structure Interaction of Instrumented Buildings and Test Structures*, Ph.D. Dissertation, Department of Civil and Environmental Engineering, University of California, Los Angeles, California.

Guzina, B.B., and Pak, R.Y.S., 1998, "Vertical vibration of a circular footing on a linear-wave-velocity half space," *Geotechnique*, Vol. 48, No. 2, pp. 159-168.

Harden, C.W., and Hutchinson, T.C., 2009, "Beam-on-nonlinear-Winkler-foundation modeling of shallow, rocking-dominated footings," *Earthquake Spectra*, Vol. 25, pp. 277-300.

Hardin, B.O., and Black, W.L., 1968, "Vibration modulus of normally consolidated clay," *Journal of the Soil Mechanics and Foundation Division*, Vol. 94, No. 2, pp. 353-369.

Harding, Miller, Lawson, and Associates, 1970, *Foundation Investigation Walnut Creek Office Building for Dillingham Corporation*, *Walnut Creek*, *California*, Report 3008,002.04, San Francisco, California.

Haselton, C.B., Leil, A.B., Deierlein, G.G., and Chou, J.H., 2011, "Seismic Collapse Safety of Reinforced Concrete Buildings: I, Assessment of Ductile Moment Frames," *Journal of Structural Engineering*, Vol. 137, pp. 481-491.

Holtz, R.D., Kovacs, W.D., and Sheahan, T.C., 2010, *An Introduction to Geotechnical Engineering*, 2nd Edition, Prentice Hall, Englewood Cliffs, New Jersey.

Houlsby, G.T., and Cassidy, M.J., 2002, "A plasticity model for the behavior of footings on sand under combined loading," *Geotechnique*, Vol. 52, No. 2, pp. 117-129.

Iguchi, M., and Luco, J.E., 1982, "Vibration of flexible plate on viscoelastic medium," *Journal of Engineering Mechanics*, Vol. 108, No. 6, pp. 1103-1120.

Jeremic, B., Jie, G.Z., Preisig, M., Tafazzoli, N., 2009, "Time domain simulation of soil-foundation-structure interaction in non-uniform soils," *Journal of Earthquake Engineering and Structural Dynamics*, Vol. 38, No. 5, pp. 699-718.

Kagawa, T., and Kraft, L.M., 1981, "Lateral pile response during earthquakes," *Journal of Geotechnical Engineering*, Vol. 107, pp. 1713-1731.

Karatzia X., and Mylonakis, G., 2012, "Horizontal response of piles in layered soil: Simple analysis," *2nd International Conference on Performance-Based Design in Geotechnical Engineering*, Taormina, Italy.

Kausel, E., 2010, "Early history of soil-structure interaction," *Soil Dynamics and Earthquake Engineering*, Vol. 30, No. 9, pp. 822-832.

Kausel E., Whitman A., Murray J., Elsabee F., 1978, "The spring method for embedded foundations," *Nuclear Engineering and Design*, Vol. 48, pp. 377-392.

Kaynia, A.M., and Kausel, E., 1982, *Dynamic Stiffness and Seismic Response of Pile Groups*, Research Report R82-03, Massachusetts Institute of Technology, Cambridge, Massachusetts.

Kaynia, A.M., and Novak, M., 1992, "Response of pile foundations to Rayleigh waves and to obliquely incident body waves," *Earthquake Engineering and Structural Dynamics*, Vol. 21, No. 4, pp. 303-318.

Kim, S., and Stewart, J.P., 2003, "Kinematic soil-structure interaction from strong motion recordings," *Journal Geotechnical and Geoenvironmental Engineering*, Vol. 129, No. 4, pp. 323-335.

Kramer, S.L., 1996, *Geotechnical Earthquake Engineering*, Prentice Hall, Upper Saddle River, New Jersey.

Kwok, A.O., Stewart, J.P., Hashash, Y.M.A., Matasovic, N., Pyke, R., Wang, Z., and Yang, Z., 2007, "Use of exact solutions of wave propagation problems to guide implementation of nonlinear seismic ground response analysis procedures," *Journal Geotechnical and Geoenvironmental Engineering*, Vol. 133, No. 11, pp. 1385-1398.

LeRoy, Crandall and Associates, 1978, *Report of Supplementary Studies Proposed Retaining Walls Proposed Sherman Oaks Galleria*, *Ventura and Sepulveda Boulevards*, *Los Angeles*, *California*, Report No. ADE-78044, prepared for Kendall International, provided by MACTEC, Los Angeles, California.

LeRoy, Crandall and Associates, 1982, *Completion of Exploration Program Proposed Office Building and Parking Structure*, *Ventura and Sepulveda Boulevards*, *Los Angeles*, *California*, Report No. ADE-81384, prepared for McNeill Enterprises, provided by MACTEC, Los Angeles, California.

Lin, A.N., and Jennings, P.C., 1984, "Effect of embedment on foundation-soil impedances," *Journal of Engineering Mechanics*, Vol. 110, No. 7, pp. 1060-1075.

Liou, G.S., and Huang, P.H., 1994, "Effect of flexibility on impedance functions for circular foundations," *Journal of Engineering Mechanics*, Vol. 120, No. 7, pp. 1429-1446.

Luco, J.E., Trifunac, M.D., and Wong, H.L., 1988, "Isolation of soil-structure interaction effects by fullscale forced vibration tests," *Earthquake Engineering and Structural Dynamics*, Vol. 16, No. 1, pp. 1-21.

Luco, J.E., and Westmann, R.A., 1971, "Dynamic response of circular footings," *Journal of Engineering Mechanics*, Vol. 97, No. 5, pp. 1381-1395.

Lysmer, J., Ostadan, F., and Chen, C., 1999, *Computer Program SASSI2000*, Geotechnical Division, University of California, Berkeley, California.

Mamoon, S.M., and Banerjee, P.K., 1990, "Response of piles and pile groups to traveling SH waves," *Earthquake Engineering and Structural Dynamics*, Vol. 19, No. 4, pp. 597-610.

Maravas, A., Mylonakis, G., and Karabalis, D.L., 2007, "Dynamic characteristics of simple structures on piles and footings," *Proceedings*, 4th International Conference on Earthquake Geotechnical Engineering, Thessaloniki, Greece, Paper No. 1672.

Marcuson, W.F., and Wahls, H.E., 1972, "Time effects on dynamics shear modulus of clays," *Journal of Soil Mechanics and Foundations Division*, Vol. 98, No. SM 12, pp. 1359-1373.

Matlock, H., 1970, "Correlations for design of laterally loaded piles in soft clay," *Proceedings*, 2nd Offshore Technology Conference, Houston, Texas, Vol. 1, pp. 577-594, Paper No. 1204.

McClelland, B., and Focht, J.A., Jr., 1958, "Soil modulus for laterally loaded piles," *Transactions*, Vol. 123, pp. 1049-1063.

McKenna, F., 1997, *Object Oriented Finite Element Programming Frameworks for Analysis, Algorithms and Parallel Computing,* Ph.D. Dissertation, University of California, Berkeley, California.

Melchers, R.E., 1999, *Structural Reliability Analysis and Prediction*, 2nd Edition, John Wiley & Sons Inc., New York, New York.

Menq, F.-Y., 2003, *Dynamic Properties of Sandy and Gravelly Soils*, Ph.D. Dissertation, University of Texas at Austin, Texas.

Michaelides O., Gazetas, G., Bouckovalas, G., and Chrysikou, E., 1998, "Approximate nonlinear analysis of piles," *Geotechnique*, Vol. 48, No. 1, pp. 33-54.

Mikami, A., Stewart, J.P., Ostadan, F., and Crouse, C.B., 2006, "Representation of ground motion incoherence for the analysis of kinematic soil-structure interaction," *Proceedings*, 8th U.S. National Conference on Earthquake Engineering, April 18-22, San Francisco, California, Paper No. 1071.

Mikami, A., Stewart, J.P., and Kamiyama, M., 2008, "Effects of time series analysis protocols on transfer functions calculated from earthquake accelerograms," *Soil Dynamics and Earthquake Engineering*, Vol. 28, No. 9, pp. 695-706.

Mylonakis, G., 1995, *Contribution to Static and Seismic Analysis of Piles and Pile-Supported Bridge Piers*, Ph.D. Dissertation, Department of Civil Engineering, University at Buffalo, State University of New York, Buffalo, New York.

Mylonakis, G., 2011, Personal Communication (unpublished study), University of Patras, Greece.

Mylonakis, G., and Gazetas, G., 1998, "Settlement and additional internal forces of grouped piles in layered soil," *Geotechnique*, Vol. 48, No. 1, pp. 55-72.

Mylonakis, G., and Gazetas, G., 1999, "Lateral vibration and internal forces of grouped piles in layered soil," *Journal Geotechnical and Geoenvironmental Engineering*, Vol. 125, No. 1, pp. 16-25.

Mylonakis, G., and Gazetas, G., 2000, "Seismic soil-structure interaction: Beneficial or detrimental," *Journal of Earthquake Engineering*, Vol. 4, pp. 377-401.

Mylonakis, G., Nikolaou, S., and Gazetas, G., 2006, "Footings under seismic loading: Analysis and design issues with emphasis on bridge foundations," *Soil Dynamics and Earthquake Engineering*, Vol. 26, pp. 824-853.

Mylonakis, G., and Roumbas, D., 2001, "Dynamic stiffness and damping of piles in inhomogeneous soil media," *Proceedings*, 4th International Conference on Recent Advances in Geotechnical Earthquake Engineering and Soil Dynamics, San Diego, California, Paper No. 6.27.

Naeim, F., Tileylioglu, S., Alimoradi, A., and Stewart, J.P., 2008, "Impact of foundation modeling on the accuracy of response history analysis of a tall building," *Proceedings*, SMIP2008 Seminar on Utilization of Strong Motion Data, California Strong Motion Instrumentation Program, Sacramento, California, pp. 19-55.

Newmark, N.M., 1969, "Torsion of symmetrical buildings," *Proceedings*, 4th World Conference on Earthquake Engineering, Santiago, Chile.

Nie, J., Xu, J., Hofmayer, C., and Ali, S., 2008, "An approach for assessing structural uplifting using blast motions," *Proceedings*, ASME Pressure Vessel and Piping Division Conference, Chicago, Illinois, Paper No. PVP2008-61278.

Nii, Y., 1987, "Experimental half-space dynamic stiffness," *Journal of Geotechnical Engineering*, Vol. 113, No. 11, pp. 1359-1373.

Nikolaou, A., Mylonakis, G., Gazetas, G., and Tazoh, T. 2001, "Kinematic pile bending during earthquakes: analysis and field measurements," *Geotechnique*, Vol. 51, No. 5, pp. 425-440.

NIST, 2012, *Tentative Framework for Development of Advanced Seismic Design Criteria for New Buildings*, GCR 12-917-20, prepared by the NEHRP Consultants Joint Venture, a partnership of the Applied Technology Council and the Consortium of Universities for Research in Earthquake Engineering, for the National Institute of Standards and Technology, Gaithersburg, Maryland.

Nogami, T., 1983, "Dynamic group effect in axial response of grouped piles," *Journal of Geotechnical Engineering*, Vol. 109, No. 2, pp. 228-243.

Nogami, T., Otani, J., Konagai, K., and Chen, H.-L., 1992, "Nonlinear soil-pile interaction model for dynamic lateral motion," *Journal of Geotechnical Engineering*, Vol. 118, No. 1, pp. 89-106.

Nova, R., and Montrasio, L., 1991, "Settlements of shallow foundations on sand," *Geotechnique*, Vol. 41, No. 2, pp. 243-256.

Novak, M., 1987, "Discussion of dynamic response of arbitrarily shaped foundations: experimental verification," *Journal of Geotechnical Engineering*, Vol. 113, No. 11, pp. 1410-1412.

Novak, M., 1991, "Piles under dynamic loads: state of the art," *Proceedings*, 2nd International Conference on Recent Advances in Geotechnical Earthquake Engineering and Soil Dynamics, St. Louis, Missouri, pp. 233-245.

OpenSees, 2011, *Open System for Earthquake Engineering Simulation: OpenSees*, University of California, Berkeley, http://opensees.berkeley.edu.

Ostadan F., 2005, "Seismic soil pressure for building walls – an updated approach," *Soil Dynamics and Earthquake Engineering*, Vol. 25, pp. 785-793.

Ostadan, F., Deng, N., and Kennedy, R., 2005, "Soil-structure interaction analysis including ground motion incoherency effects," *Proceedings,* 18th International Conference on Structural Mechanics in Reactor Technology (SMiRT 18), Beijing, China.

Ostadan, F., Hadjian, A.H., Tseng, W.S., Tang, Y.K., Tang, H.T., 1991, "Parametric evaluation of intermediate SSI solutions on final response," *Proceedings*, 11th International Conference on Structural Mechanics in Reactor Technology (SMiRT 11), Tokyo, Japan, Paper K04/1, pp. 63-68.

Ostadan F., and White, W., 1998, "Lateral seismic soil pressure – an updated approach," *Proceedings*, U.S.-Japan SSI Workshop, U.S. Geological Survey, Menlo Park, California.

Pais, A., and Kausel, E., 1988, "Approximate formulas for dynamic stiffnesses of rigid foundations," *Soil Dynamics and Earthquake Engineering*, Vol. 7, No. 4, pp. 213-227.

Paulay, T., and Priestley, M.J.N., 1992, *Seismic Design of Reinforced Concrete and Masonry Buildings*, John Wiley & Sons, New York, New York.

Pecker, A., and Chatzigogos, C.T., 2010, "Non-linear soil-structure interaction: Impact on the seismic response of structures," *Earthquake Engineering in Europe*, M. Garevski and A. Ansal (editors), Springer, New York, pp. 79-103.

PEER, 2010, *Guidelines for Performance-Based Seismic Design of Tall Buildings*, Report No. 2010/05, developed by the Pacific Earthquake Engineering Research Center as part of the Tall Buildings Initiative, University of California, Berkeley, California.

Pender, M., 1993, "Aseismic pile foundation design analysis," *Bulletin of New Zealand National Society of Earthquake Engineering*, Vol. 26, No. 1, pp. 49-160.

Penzien, J., 1970, "Soil-pile-foundation interaction," *Earthquake Engineering*, R.L. Wiegel (editor), Prentice Hall, New York, New York.

Perez-Rocha, L.E., and Aviles, J., 2003, "The evaluation of interaction effects in inflexible resistances," *Revista de Ingenieria Sismica*, No. 69 (in Spanish).

Powell, G.H., 2006, "Static pushover methods – explanation, comparison and implementation," *Proceedings*, 8th U.S. National Conference on Earthquake Engineering, San Francisco, California.

Priestley, M.J.N., and Park, R., 1987, "Strength and ductility of concrete bridge columns under seismic loading," *ACI Structural Journal*, Vol. 84, No. 1, pp. 61-76.

Randolph, M.F., 1981, "The response of flexible piles to lateral loading," *Geotechnique*, Vol. 31, No. 2, pp. 247-259.

Randolph, M.F., and Wroth, C.P., 1978, "Analysis of deformation of vertically loaded piles," *Journal of Geotechnical Engineering*, Vol. 104, No. 12, pp. 1465-1488.

Raney Geotechnical, 1983, *Foundation Investigation North Main Centre*, *North Main St., and Principle Ave.*, *Walnut Creek*, *CA*, Report 029-005, West Sacramento, California.

Rathje, E.M., Faraj, F., Russell, S., and Bray, J.D., 2004, "Empirical relationships for frequency content parameters of earthquake ground motions," *Earthquake Spectra*, Vol. 20, No. 1, pp. 119-144.

Raychowdhury, P., 2008, *Nonlinear Winkler-Based Shallow Foundation Model for Performance Assessment of Seismically Loaded Structures*, PhD Dissertation, University of California, San Diego, California.

Raychowdhury, P., and Hutchinson, T.C., 2008, "Nonlinear material models for Winkler-based shallow foundation response evaluation," *GeoCongress 2008: Characterization*, *Monitoring*, *and Modeling of GeoSystems*, American Society of Civil Engineers, Reston, Virginia.

Raychowdhury, P., and Hutchinson, T.C., 2009, "Performance evaluation of a nonlinear Winkler-based shallow foundation model using centrifuge test results," *Earthquake Engineering and Structural Dynamics*, Vol. 38, No. 5, pp. 679-698.

Richart, F.E., Jr., and Whitman, E.V., 1967, "Comparison of footing vibration tests with theory," *Journal of Soil Mechanics and Foundations Division*, Vol. 93, No. 6, pp. 143-168.

Riggs, H.R., and Waas, G., 1985, "Influence of foundation flexibility on soil-structure interaction," *Earthquake Engineering and Structural Dynamics*, Vol. 13, No. 5, pp. 597-615.

Roesset, J.M., 1980, "Stiffness and damping coefficients of foundations," *Proceedings*, ASCE Geotechnical Engineering Division National Convention, pp. 1-30.

Rosebrook, K.R., and Kutter, B.L., 2001a, *Soil-Foundation Structure Interaction: Shallow Foundations*, UCD/CGMDR-01, Center for Geotechnical Modeling, University of California, Davis, California.

Rosebrook, K.R., and Kutter, B.L., 2001b, *Soil-Foundation structure interaction: Shallow Foundations*, UCD/CGMDR-02, Center for Geotechnical Modeling, University of California, Davis, California.

Rosebrook, K.R., and Kutter, B.L., 2001c, Soil-Foundation Structure Interaction: Shallow Foundations, UCD/CGMDR-03, Center for Geotechnical Modeling, University of California, Davis, California.

Salgado, R., 2008, *The Engineering of Foundations*, McGraw-Hill, New York, New York.

SCEC, 2002, *Recommended Procedures for Implementation of DMG Special Publication 117 Guidelines for Analyzing and Mitigating Landslide Hazards in California*, Southern California Earthquake Center, June 2002, http://www.scec.org/resources/catalog/hazardmitigation.html.

Scott, R., 1981, *Foundation Analysis*, Prentice Hall, Upper Saddle River, New Jersey.

Soubra, A.-H., 1999, "Upper-bound solutions for bearing capacity of foundations," *Journal Geotechnical and Geoenvironmental Engineering*, Vol. 125, No. 1, pp. 59-68.

Sozen, M.A., and Moehle, J.P., 1993, *Stiffness of Reinforced Concrete Walls Resisting In-Plane Shear*, Electric Power Research Institute, Research Project 3094-01, Palo Alto, California.

Stewart, J.P., and Fenves, G.L., 1998, "System identification for evaluating soil-structure interaction effects in buildings from strong motion recordings," *Earthquake Engineering and Structural Dynamics*, Vol. 27, pp. 869-885.

Stewart, J.P., Fenves, G.L., and Seed, R.B., 1999b, "Seismic soil-structure interaction in buildings II: Empirical findings," *Journal Geotechnical and Geoenvironmental Engineering*, Vol. 125, pp. 38-48.

Stewart, J.P., Kim, S., Bielak, J., Dobry, R., and Power, M., 2003, "Revisions to soil structure interaction procedures in NEHRP design provisions," *Earthquake Spectra*, Vol. 19, No. 3, pp. 677-696.

Stewart, J.P., Seed, R.B., and Fenves, G.L., 1999a, "Seismic soil-structure interaction in buildings I: Analytical aspects," *Journal Geotechnical and Geoenvironmental Engineering*, Vol. 125, pp. 26-37.

Stewart, J.P., and Stewart, A.F., 1997, *Analysis Of Soil-Structure Interaction Effects On Building Response From Earthquake Strong Motion Recordings At 58 Sites*, Report UCB/EERC-97/01, University of California, Berkeley, California.

Stewart, J.P., and Tileylioglu, S., 2007, "Input ground motions for tall buildings with subterranean levels," *Structural Design of Tall and Special Buildings*, Vol. 16, pp. 543-557.

Stokoe, K.H., and Erden, S.M., 1985, *Influence of Base Shape on Dynamic Response of Surface Foundations*, Geotechnical Engineering Report GP85-1, University of Texas at Austin, Texas.

Syngros, K., 2004, *Contributions to the Static and Seismic Analysis of Piles and Pile Supported Bridge Piers Evaluated through Case Histories*, Ph.D. Dissertation, City University of New York, New York.

Thomas, J.M., Gajan S., and Kutter B.L., 2005, *Soil-Foundation-Structure Interaction: Shallow Foundations*, UCD/CGMDR-05/02, Center for Geotechnical Modeling, University of California, Davis, California.

Tileylioglu, S., 2008, *Evaluation of Soil-Structure Interaction Effects from Field Performance Data*, Ph.D. Dissertation, University of California, Los Angeles, California.

Tileylioglu, S., Naeim, F., Alimoradi, A., and Stewart, J.P., 2010, "Impact of foundation modeling on the accuracy of response analysis for a tall building," *Proceedings*, 9th U.S. National & 10th Canadian Conference on Earthquake Engineering, EERI and Canadian Association for Earthquake Engineering, Paper No. 1666.

Tileylioglu, S., Stewart, J.P., and Nigbor, R.L., 2011, "Dynamic stiffness and damping of a shallow foundation from forced vibration of a field test structure," *Journal Geotechnical and Geoenvironmental Engineering*, Vol. 137, No. 4, pp. 344-353.

Ugalde, J., 2007, *Centrifuge Tests on Bridge Columns on Shallow Square Footings*, Master's Thesis, University of California, Davis, California.

University of Illinois, 2011, *DEEPSOIL V4.0*, University of Illinois at Urbana-Champaign, accessed in 2011, http://deepsoil.cee.illinois.edu/.

Veletsos, A.S., and Meek, J.W., 1974, "Dynamic behavior of building-foundation systems," *Earthquake Engineering and Structural Dynamics*, Vol. 3, pp. 121-138.

Veletsos, A.S., and Nair, V.V., 1975, "Seismic interaction of structures on hysteretic foundations," *Journal of Structural Engineering*, Vol. 101, pp. 109-129.

Veletsos, A.S., and Prasad, A. M., 1989. "Seismic interaction of structures and soils: Stochastic approach," *Journal of Structural Engineering*, Vol. 115, No. 4, pp. 935-956.

Veletsos, A.S., Prasad, A.M., and Wu, W.H., 1997, "Transfer functions for rigid rectangular foundations," *Earthquake Engineering and Structural Dynamics*, Vol. 26, No. 1, pp. 5-17.

Veletsos, A.S., and Wei, Y.T., 1971, "Lateral and rocking vibrations of footings," *Journal of Soil Mechanics and Foundations Division*, Vol. 97, No. 9, pp. 1227-1248.

Vrettos, C., 1999, "Vertical and rocking impedances for rigid rectangular foundations on soils with bounded non-homogeneity," *Earthquake Engineering and Structural Dynamics*, Vol. 28, pp. 1525-1540.

Vucetic, M., and Dobry, R., 1991, "Effect of soil plasticity on cyclic response," *Journal of Geotechnical Engineering*, Vol. 117, pp. 89-107.

Watson, G.N., 1995, *A Treatise on the Theory of Bessel Functions*, Cambridge University Press, United Kingdom.

Western Engineering, 2011, "DYNA6 Software," *Western Geotechnical Research Centre*, Western University, accessed December 2011, http://www.eng.uwo.ca/research/grc/dyna6.htm.

Wolf, J.P., 1985, *Dynamic Soil-Structure Interaction*, Prentice-Hall, Upper Saddle River, New Jersey.

Wolf, J.P., and Von Arx, G.A., 1978, "Impedance function of a group of vertical piles," *Proceedings*, Specialty Conference on Earthquake Engineering and Structural Dynamics, Pasadena, California, Vol. 2, pp. 1024-1041.

Wong, H.L., 1979, *Soil-Structure Interaction: A Linear Continuum Mechanics Approach (CLASSI Users Manual)*, Report No. 79-04, Department of Civil Engineering, University of Southern California, Los Angeles, California.

Wong, H.L., and Luco, J.E., 1985, "Dynamic interaction between rigid foundations in a layered half space," *Earthquake Engineering and Structural Dynamics*, Vol. 5, No. 3, pp. 149-158.

Wong, H.L., Trifunac, M.D., and Luco, J.E., 1988, "A comparison of soil-structure interaction calculations with results of full-scale forced vibration test," *Soil Dynamics and Earthquake Engineering*, Vol. 7, pp. 22-31.

Xu, J., Costantino, C., and Hofmayer, C., 2003, *Collaborative Study of NUPEC Seismic Field Test Data for NPP Structures*, Report BNL-NUREG-71355-2003, Brookhaven National Laboratory, Upton, New York.

Yamada, S., Hyodo, M., Orense, R.P., Dinesh, S.V., and Hyodo, T., 2008, "Strain-dependent dynamic properties of remolded sand-clay mixtures," *Journal Geotechnical and Geoenvironmental Engineering*, Vol. 134, No. 7, pp. 972-981.

Yu, E., Whang, D.H., Conte, J.P., Stewart, J.P., and Wallace, J.W., 2005, "Forced-vibration testing of buildings using the linear shaker seismic simulation (LSSS) testing method," *Earthquake Engineering and Structural Dynamics*, Vol. 34, pp. 737-761.

Project Participants

National Institute of Standards and Technology

John (Jack) R. Hayes, Jr.
Engineering Laboratory (MS8604)
National Institute of Standards and Technology
100 Bureau Drive
Gaithersburg, Maryland 20899
www.NEHRP.gov

Steven L. McCabe
Engineering Laboratory (MS8604)
National Institute of Standards and Technology
100 Bureau Drive
Gaithersburg, Maryland 20899
www.NEHRP.gov

John (Jay) L. Harris III
Engineering Laboratory (MS8604)
National Institute of Standards and Technology
100 Bureau Drive
Gaithersburg, Maryland 20899
www.NEHRP.gov

NEHRP Consultants Joint Venture

APPLIED TECHNOLOGY COUNCIL
201 Redwood Shores Parkway, Suite 240
Redwood City, California 94065
www.ATCouncil.org

CONSORTIUM OF UNIVERSITIES FOR
RESEARCH IN EARTHQUAKE ENGINEERING
1301 S. 46th Street, Building 420
Richmond, California 94804
www.CUREE.org

Joint Venture Management Committee

James R. Harris
J.R. Harris & Company
1775 Sherman Street, Suite 1525
Denver, Colorado 80203

Christopher Rojahn
Applied Technology Council
201 Redwood Shores Parkway, Suite 240
Redwood City, California 94065

Robert Reitherman
Consortium of Universities for Research in
Earthquake Engineering
1301 S. 46th Street, Building 420
Richmond, California 94804

Andrew Whittaker
Dept. of Civil, Structural, and Environ. Engin.
230 Ketter Hall
University at Buffalo
Buffalo, New York 14260

Joint Venture Program Committee

Jon A. Heintz (Program Manager)
Applied Technology Council
201 Redwood Shores Parkway, Suite 240
Redwood City, California 94065

Michael Constantinou
Dept. of Civil, Structural, and Environ. Engin.
University at Buffalo
132 Ketter Hall
Buffalo, New York 14260

C.B. Crouse
URS Corporation
1501 4th Avenue, Suite 1400
Seattle, Washington 98101

William T. Holmes
Rutherford & Chekene
55 Second Street, Suite 600
San Francisco, California 94105

Jack P. Moehle
University of California Berkeley
325 Davis Hall – MC 1792
Berkeley, California 94720

James R. Harris (ex-officio)
Andrew Whittaker (ex-officio)

Project Manager

David A. Hutchinson
Buehler & Buehler, Structural Engineers
600 Q Street, Suite 200
Sacramento, California 95811

Project Technical Committee

Jonathan P. Stewart (Project Director)
University of California, Los Angeles
Dept. of Civil and Environmental Engineering
5731 Boelter Hall
Los Angeles, California 90095

C.B. Crouse
URS Corporation
1501 4th Avenue, Suite 1400
Seattle, Washington 98101

Tara C. Hutchinson
University of California, San Diego
Department of Structural Engineering
9500 Gilman Drive
La Jolla, California 92093

Bret Lizundia
Rutherford & Chekene
55 Second Street, Suite 600
San Francisco, California 94105

Farzad Naeim
John A. Martin & Associates, Inc.
950 S. Grand Avenue, 4th Floor
Los Angeles, California 90015

Farhang Ostadan
Bechtel Corporation
50 Beale Street
San Francisco, California 94105

Working Group Members

Fortunato Enriquez
California State University, Chico
475 East 10th Avenue
Chico, California 95926

Michael J. Givens
University of California, Los Angeles
5731 Boelter Hall
Los Angeles, California 90095

Curtis B. Haselton
California State University, Chico
Department of Civil Engineering
475 East 10th Avenue
Chico, California 95926

Silvia Mazzoni
Degenkolb Engineers
235 Montgomery Street, Suite 500
San Francisco, California 94104

Erik Okstad
Rutherford & Chekene
55 Second Street, Suite 600
San Francisco, California 94105

Andreas Schellenberg
Rutherford & Chekene
55 Second Street, Suite 600
San Francisco, California 94105

Project Review Panel

Craig D. Comartin
CDComartin Inc.
7683 Andrea Avenue
Stockton, California 95207

Youssef Hashash
University of Illinois, Urbana-Champaign
Dept. of Civil and Environmental Engineering
205 North Mathews Avenue
Urbana, Illinois 61801

Annie M. Kammerer
U.S. Nuclear Regulatory Commission
Office of Nuclear Regulatory Research
Washington, D.C. 20555

Gyimah Kasali
Rutherford & Chekene
55 Second Street, Suite 600
San Francisco, California 94105

George Mylonakis
University of Patras, Greece
26500 Patras, Greece

Graham Powell
Graham H. Powell, Inc.
14710 Wolfgang Road
Truckee, California 96161

Workshop Participants

Peter Behnam
KPFF Consulting Engineers
6080 Center Drive, Suite 300
Los Angeles, California 90045

Lauren Carpenter
WHL Consulting Engineers, Inc.
350 South Figueroa Street, Suite 400
Los Angeles, California 90071

Michael Cochrane
Weidlinger Associates, Inc.
4551 Glencoe Avenue, Suite 350
Marina del Rey, California 90292

John Gavan
KPFF Consulting Engineers
6080 Center Drive, Suite 300
Los Angeles, California 90045

Tony Ghodsi
Englekirk Structural Engineers
925 Fort Stockton Drive, Suite 202
San Diego, California 92103

Christine Goulet
Pacific Earthquake Engineering Research Center
325 Davis Hall, University of California
Berkeley, California 94720

Robert D. Hanson
2926 Saklan Indian Drive
Walnut Creek, California 94595

Doug Hohbach
Hohbach-Lewin
260 Sheridan Avenue, Suite 150
Palo Alto, California 94306

Ben Hushmand
Hushmand Associates, Inc.
250 Goddard Road
Irvine, California 92618

Peter Lee
Skidmore, Owings & Merrill LLP
One Front Street, Suite 2500
San Francisco, California 94111

Anne Lemnitzer
University of California, Los Angeles
Dept. of Civil and Environmental Engineering
5731 Boelter Hall
Los Angeles, California 90095

Marshall Lew
MACTEC Engineering & Consulting, Inc.
5628 E. Slauson Avenue
Los Angeles, California 90040

Weian Liu
University of California, San Diego
Jacobs School of Engineering
9500 Gilman Drive, SERF 252
La Jolla, California 92093-0403

Michael Mahoney
Federal Emergency Management Agency
500 C Street, SW
Washington, D.C. 20472

David Mar
Tipping Mar
1906 Shattuck Avenue
Berkeley, California 94704

Neven Matasovic
Geosyntec Consultants
2100 Main Street, Suite 150
Huntington Beach, California 92648

Michael Mehrain
URS Corporation
915 Wilshire Boulevard, Suite 700
Los Angeles, California 90017

Navid Nastar
University of Southern California
Civil and Environmental Engineering
Kaprielian Hall, Room 225
3620 S. Vermont Avenue
Los Angeles, California 90089-2531

Patrick Smith
Fugro West, Inc.
4820 McGrath Street, Suite 100
Ventura, California 93003